Roles of Volatile Organic Compound Speciation in Winter Ozone Photochemistry, Long-Term Ozone Trends, and Secondary Carbonyl Formation in a Northwestern Chinese Industrial City

YANG JIN
PhD

The Hong Kong Polytechnic University
2026

The Hong Kong Polytechnic University

Department of Civil and Environmental Engineering

Roles of Volatile Organic Compound Speciation in Winter Ozone Photochemistry, Long-Term Ozone Trends, and Secondary Carbonyl Formation in a Northwestern Chinese Industrial City

YANG JIN

A thesis submitted in partial fulfillment of the requirements for the degree of Doctor of Philosophy

August 2026

Certificate of originality

I hereby declare that this thesis is my own work and that, to the best of my knowledge and belief, it reproduces no material previously published or written, nor material that has been accepted for the award of any other degree or diploma, except where due acknowledgement has been made in the text.

(Signed)

YANG JIN (Name of student)

Abstract

Volatile organic compounds (VOCs) are key precursors in the formation of secondary air pollutants, such as ozone (O_3) and carbonyls. Among VOCs, alkenes are particularly reactive and play a dominant role in secondary pollution formation, especially in industrial cities like Lanzhou, where high alkene concentrations are largely attributed to petrochemical activities. The unique VOC profile in these cities, characterized by alkene-rich emissions, raises important questions about their impact on urban air quality and secondary pollution formation. This thesis addresses these issues through three main studies: (1) investigating the mechanisms of wintertime O_3 formation in Lanzhou, (2) analyzing the long-term trends of O_3 in Lanzhou, and (3) exploring the formation and sources of secondary carbonyl compounds across five major Chinese cities. By integrating field measurements with advanced modelling, this work aims to elucidate the chemical processes, temporal variations, long-term trends, and source contributions of O_3 pollution driven by VOCs in northwestern Chinese industrial cities, thereby providing a scientific basis for more effective air quality management strategies.

The intensive field measurements in January 2018 revealed four O_3 episode days with maximum hourly concentrations exceeding 100 ppbv and peaking at 121 ppbv, despite cold temperatures and weak solar radiation. The average daytime concentration of total volatile organic compounds (VOCs) reached 153.4 ± 19.0 ppbv, with alkenes, mainly from the local petrochemical industry, comprising 82.3 ± 13.1 ppbv. Using a photochemical box model coupled with the Master Chemical Mechanism, it was found that the low temperatures and weak sunlight had minimal effect on VOC reactivity with OH radicals. Instead, the ozonolysis of alkenes generated Criegee intermediates, which rapidly decomposed into substantial ROx radicals (OH, HO_2, and RO_2) even without sunlight. This radical production led to the oxidation of VOCs, with alkene ozonolysis ultimately contributing to nearly 90 % of O_3 formation during these episodes. The mechanism was not active at night due to the NO titration effect. The study further showed that a reduction of alkenes by about 28.6 % or NO_x by 27.7 % in the early afternoon could significantly mitigate wintertime O_3 pollution. These findings challenge the traditional view that strong solar radiation is necessary for high O_3 production and highlight the importance of dark reactions in wintertime photochemistry. The results also suggest that alkene ozonolysis can be a major source, rather than a sink, of O_3 in heavily industrialized regions.

Except for the uniquely high O_3 concentration in winter, this research found that while concentrations of primary air pollutants such as $PM_{2.5}$, CO, SO_2, and NO_2 have declined significantly in recent years due to effective emission control measures, O_3 pollution in summer remains a persistent challenge. Although NO_2 and CO concentrations declined steadily, the effectiveness of VOC control was limited after the COVID-19 lockdown. Model simulations

revealed that O_3 formation in Lanzhou transitioned from a VOC-limited regime to a transitional regime from 2019 to 2023, largely driven by reductions in NO_x. The observed increase in O_3 levels during this period was mainly attributable to the decrease in NO_x concentrations. As the O_3 formation regime shifted from VOC-limited to a VOC-NO_x co-limited regime, it became evident that effective O_3 control now requires simultaneous management of both NO_x and VOC emissions. Alkenes were the primary contributors to O_3 formation throughout the decade, accounting for around 50–63 % of the total VOC contribution in Lanzhou. There was a notable contribution from reactive alkenes such as *trans/cis*-2-butene, ethene, and propene to O_3 formation. Source apportionment identified vehicle emissions, followed by petrochemical industry and solvent usage, as the major contributors to O_3 formation. These findings highlight the importance of targeted VOC controls, focusing not only on alkenes but also on specific aromatic compounds, to effectively mitigate O_3 pollution.

In addition to the significant impact of alkenes and aromatics on O_3, we also found the impact of carbonyls on O_3, by investigating the photochemical characteristics, sources, and joint O_3-carbonyl control strategies of formaldehyde, acetaldehyde, and acetone. These three carbonyls made up over 85 % of the total observed carbonyls, with the highest concentrations found in Beijing and Wuhan, indicating the impact of regional secondary pollution. Observations showed that Beijing (9.6 ± 0.1 ppbv) and Wuhan (5.2 ± 0.1 ppbv) exhibited the highest formaldehyde concentrations, followed by Shanghai, Chengdu, and Lanzhou. Model simulations revealed that anthropogenic alkenes accounted for over 50 % of formaldehyde formation in Beijing and Lanzhou, while isoprene contributed 10–20 % in other cities. Other VOC species contributed 1–2 % each, highlighting the complexity of VOC sources for formaldehyde production. In contrast, acetaldehyde and acetone were mainly produced from propene and α/β-pinene, respectively (about 50 % each), with the top ten VOCs accounting for around 90% of their formation. Furthermore, carbonyls were quantified for their role in O_3 formation across the cities, with the highest contribution observed in Beijing (33 %) and the lowest in Lanzhou (6 %). Comparison of their isopleths suggested that O_3 reduction strategies can also effectively reduce carbonyl concentrations. Finally, source apportionment combined with chemical mechanism analysis traced the sources of primary and secondary carbonyls, showing that vehicle emissions rich in alkenes were the largest contributors to secondary aldehyde formation in all five cities. Including their primary contributions, vehicles accounted for 40–50% of total aldehydes, followed by solvent usage. For acetone, biogenic sources dominated over anthropogenic ones. These findings deepen our understanding of carbonyl photochemistry and inform possible future mitigation strategies.

In summary, this thesis provides new insights into the mechanisms of O_3 and carbonyl pollution in urban China, especially in Lanzhou. The findings highlight the importance of considering

both traditional and non-traditional photochemical pathways, the need for targeted precursor controls, and the value of coordinated strategies for managing multiple secondary pollutants. The results fill important knowledge gaps in understanding O_3 and carbonyl pollution in Lanzhou. These findings offer a scientific basis for refining air quality management policies and can inform similar strategies in other cities facing persistent O_3 and carbonyl challenges. To ensure a comprehensive understanding and broader applicability of the findings, this thesis adopts a stepwise research framework. It begins with an in-depth case study of wintertime O_3 formation mechanisms in Lanzhou, followed by a long-term trend analysis in the same city, and ultimately expands to a multi-city comparative study of secondary carbonyl compounds. This progressive approach not only addresses the unique challenges faced in Lanzhou, but also facilitates the identification of common patterns and region-specific features across major Chinese cities.

The novelty of this study

This study makes several groundbreaking contributions to atmospheric chemistry and air pollution control, both in China and internationally. It represents the first comprehensive investigation of extremely high wintertime O_3 episodes in China, and, more significantly, is the first study worldwide to explore the causes of elevated O_3 concentrations under conditions of low sunlight and low temperatures. Through extensive field measurements and advanced modelling, this research uncovers the pivotal role of alkene ozonolysis, a pathway previously underestimated, in driving O_3 formation during winter. The discovery that alkene ozonolysis can dominate O_3 production under certain conditions challenges the conventional view that strong sunlight and high temperatures are prerequisites for severe O_3 pollution.

Furthermore, this work is the first to systematically document the long-term evolution of O_3 levels in Lanzhou, providing a detailed account of how O_3 formation mechanisms and radical chemistry have changed over the past decade. It offers clear evidence of the impact of emission reduction measures and changes in VOC composition on O_3 formation pathways and radical cycles, offering new perspectives on the effectiveness of air quality management in northwestern China.

In addition, this study is the first to conduct a detailed comparison of carbonyl photochemistry and sources across five major Chinese cities, utilizing simultaneous field observations and model simulations. By integrating the PBM-MCM and PMF models, the research quantitatively assesses both primary and secondary sources of carbonyls and their roles in O_3 formation. This comprehensive approach enables a more accurate understanding of the intricate relationships among VOC sources, carbonyl production, and O_3 generation. Moreover, the study pioneers the proposal and validation of joint control strategies targeting both O_3 and carbonyls, laying a scientific foundation for the coordinated management of multiple secondary pollutants. It also provides the first in-depth analysis of the photochemical behavior, sources, and joint control strategies for carbonyls in Lanzhou. These findings fill critical knowledge gaps and set a new benchmark for future research and policy development in air pollution control.

Publications

Publications as the first author:

1. **Yang J.**, Zeren Y., Guo H.*, Wang Y.*, Lyu X.P., Zhou B.N., Gao H., Yao D.W., Wang Z.X., Zhao S.Z., Li. J., Zhang G., 2024. Wintertime Ozone Surges: The Critical Role of Alkene Ozonolysis. Environmental Science and Ecotechnology, 22, 100477. (Impact factor: 14.0; Grade A)
2. **Yang J.**, Zeren Y., Guo H.*, Wang Y.*, Lyu X.P., Zeng L.W., Wang G.H., Zhang F., Liu X.F., Yao D.W., Wang F.W., 2026. Atmospheric formaldehyde, acetaldehyde, and acetone in five major Chinese cities: photochemical characteristics, sources, and joint ozone-carbonyl control strategies. Journal of Hazardous Materials, 502, 140600. (Impact factor: 11.3; Grade A)
3. **Yang J.**, Guo, H.*, Wang Y.*, Liu X.F., Zeng, L.W., Lyu, X.P., Zeren, Y.Z., Zhang, L. Long-term Trend of Ozone Formation and Radical Chemistry in Lanzhou. (in preparation)

Publications as co-author:

1. Zeng L.W., **Yang J.**, Guo H.*, Lyu X.P., 2022. Impact of NOx reduction on long-term surface ozone pollution in roadside and suburban Hong Kong: Field measurements and model simulations. Chemosphere, 302, 134816. (Impact factor: 7.086; Grade A)
2. Lyu X.P., Huo Y.X., **Yang J.**, Yao D.W., Li K.M., Lu H.X., Zeren Y.Z., Guo H.*, 2021.Real-time molecular characterization of air pollutants in a Hong Kong residence: implication of indoor source emissions and heterogeneous chemistry. Indoor Air, 1-13. (Impact factor: 4.739; Grade A)
3. Liu X.F., Guo H.*, Zeng L.W., Lyu X.P., Wang Y., Zeren Y.Z., **Yang J.**, Zhang L.Y., Zhao S.Z., Li J., Zhang G., 2021. Photochemical ozone pollution in five Chinese megacities in summer 2018. Science of the Total Environment 801, 149603. (Impact factor: 7.693; Grade A)
4. Zeng L., Li K., Guo H.*, Zhou B.N., Lyu X.P., Huo Y.X., Uhde E., **Yang J.**, Zeren Y.Z., Lu H., Yao D., 2023. Contributions of Indoor Household Activities to Inhalation Health

Risks Induced by Gaseous Air Pollutants in Hong Kong Home. Aerosol and Air Quality Research. (Impact factor: 4.0; Grade A)

Acknowledgements

Completing my doctoral studies at The Hong Kong Polytechnic University (PolyU) has been an incredibly meaningful and memorable chapter in my life. Throughout this journey, I have been fortunate to meet many talented and supportive individuals whose encouragement and guidance have been instrumental to both my academic and personal growth. I would like to take this opportunity to sincerely thank everyone who has contributed to my development during this time.

First and foremost, I am deeply grateful to my chief supervisor, Prof. GUO Hai. His unwavering support, profound expertise, and patient mentorship have had a significant impact on my research journey. Prof. GUO not only provided essential resources and insightful advice, but his trust and high expectations have continually motivated me, especially during the early stages when I was still adapting to research work. Words cannot fully express my appreciation for his guidance and encouragement.

I would also like to extend my heartfelt thanks to my past and present teammates and colleagues, whose collaboration and friendship have greatly enriched my experience at PolyU. In particular, I am thankful to Dr. WANG Yu for his generous assistance with the PBM-MCM model and for sharing his research skills. My gratitude also goes to all my teammates over the years: Dr. LYU Xiaopu, Dr. ZENG Lewei, Dr. ZEREN Yangzong, Dr. LIU Xufei, Dr. LU Haoxian, Dr. YAO Dawen, Dr. HUO Yunxi, Ms. ZHANG Luyao, Ms. ZHOU Beining, Ms. SHEK Kit Ying, Ms. SO Lok Kwan, Ms. GUO Peiwen, Mr. ZHANG Haonan, Ms. WU Min, and Mr. DENG Yuanhang. Their support has always been a source of motivation and friendship.

Finally, I owe my deepest thanks to my parents. Their constant love and encouragement have been my greatest strength. Their positive outlook and perseverance have inspired me to overcome difficulties and setbacks. I am truly fortunate to be their daughter and will always treasure the unconditional support they have given me.

To everyone who has been part of this journey, thank you for making it so special and unforgettable.

Contents

List of Figures

List of Tables

Chapter 1 Overview

1.1 Introduction

Tropospheric ozone (O_3) is a major secondary air pollutant, playing a pivotal role in atmospheric chemistry and exerting profound impacts on human health, ecosystems, and climate change (Ainsworth et al., 2012; Ashmore, 2005; Chameides et al., 1999; Liu et al., 2024; Simpson et al., 2014; Wang et al., 2007). O_3 formation in the lower atmosphere is mainly the result of intricate photochemical reactions involving its key precursors, i.e., nitrogen oxides (NO_x), volatile organic compounds (VOCs), and carbon monoxide (CO), alongside the influence of meteorological factors and regional transport (Cape, 2008; Collins, 2003; Jennifer, 1985; Liu et al., 2022; X. Lu et al., 2019). In recent decades, the rapid pace of urbanization and industrial development has resulted in increased emissions of O_3 precursors, leading to more frequent and severe O_3 pollution episodes, particularly in China's densely populated and heavily industrialized regions (S. Chen et al., 2020; Z. Chen et al., 2019; Gao et al., 2017; Hu et al., 2025; X.-B. Li et al., 2022; X. F. Liu et al., 2019; M. Wang et al., 2024; W. Wang, D. D. Parrish, et al., 2022; Y. Wang et al., 2022; L. Yang et al., 2019; X. Zhang et al., 2022).

As a result, O_3 pollution has become a major environmental issue in many of China's largest cities. This issue is particularly pronounced during the warmer months, when elevated temperatures and strong sunlight enhance the photochemical processes that drive O_3 formation. (Guo et al., 2009; Guo, Ling, Cheung, Jiang, et al., 2013; Guo et al., 2024; L. Li et al., 2016; Li et al., 2015; Lu et al., 2020; T. Wang et al., 2017; Y. Wang et al., 2017). As such, O_3 pollution events are generally concentrated in spring, summer, and autumn but rare in winter (Kgabi, 2012; N. Liu et al., 2019; Maji et al., 2019; Oltmans, 1994). However, a handful of studies have reported O_3 episode events (maximum hourly concentration exceeding 100 ppbv) in winter at specific locations with high surface albedo values and/or heavy precursor emissions (Edwards et al., 2014; Oltmans et al., 2014; Schnell et al., 2009; Singh et al., 1997). Notably, we found the unique high O_3 concentration in wintertime Lanzhou, which was quite rare in winter among China (Yang et al., 2024). And the O_3 formation mechanisms in winter have seldom been reported. Therefore, the underlying causes of the extremely high O_3

concentrations observed in cold weather and times of weak solar radiation are worth exploring during wintertime. Despite ongoing research, our understanding of the specific mechanisms behind O_3 formation remains incomplete, particularly regarding how O_3 precursors change during photochemical reactions and how these changes influence radical chemistry.

Most long-term studies on O_3 pollution have focused on regions such as the North China Plain (NCP), Yangtze River Delta (YRD), and Pearl River Delta (PRD), as well as major cities like Chengdu and Shanghai (S. Chen et al., 2020; Z. Chen et al., 2019; Gao et al., 2017; Hu et al., 2025; X.-B. Li et al., 2022; X. F. Liu et al., 2019; Mo et al., 2023; M. Wang et al., 2024; W. Wang, D. D. Parrish, et al., 2022; Y. Wang et al., 2022; L. Yang et al., 2019). These regions have been identified as O_3 hotspots, with rising O_3 concentrations documented over the past several decades (Lu et al., 2020). Lanzhou stands out as one of the earliest cities in China to recognize O_3 pollution, with records of photochemical smog dating back nearly 50 years (W. Guo et al., 2022; J. Li et al., 2020; Ta et al., 2004; Tang et al., 1985). Although the Clean Air Action (CAA) Plan was implemented in 2013 to curb air pollution through stricter emission controls and technological upgrades, Lanzhou continues to struggle with significant O_3 pollution (Du et al., 2020; Filonchyk & Yan, 2018; Zhao et al., 2021). This persistent challenge underscores the need for more effective and locally tailored control strategies. However, there remains a lack of research specifically focused on the trends and driving factors of O_3 pollution in Lanzhou. The city's unique environmental conditions and pollution sources make targeted studies essential for developing effective solutions.

Carbonyls are key components of atmospheric volatile organic compounds (VOCs) and play a significant role in air quality (Atkinson, 2000; Jenkin, 1997; W. Wang, B. Yuan, et al., 2022; Xue et al., 2016; Yang et al., 2018). These compounds can be emitted directly into the atmosphere or formed secondarily through complex photochemical reactions (Ling et al., 2017; Liu et al., 2009; Pang & Mu, 2006; Wu et al., 2023; Yang et al., 2017; Z. Yang et al., 2019; X. Zhang et al., 2022; Y. Zhang et al., 2019). Over the past few decades, global monitoring efforts have provided detailed information on the distribution of formaldehyde, acetaldehyde, and acetone (Ho et al., 2015; Liu et al., 2022; Liu et al., 2009; Lui et al., 2017; Yang et al., 2017;

X. Zhang et al., 2022; Y. Zhang et al., 2019). High concentrations of these carbonyls have been observed in many cities worldwide, particularly in East Asia (Liu et al., 2022). In China, especially in the North China Plain (NCP), Yangtze River Delta (YRD), and Pearl River Delta (PRD) regions, formaldehyde and acetaldehyde concentrations frequently exceed 20 and 10 ppbv, respectively (Y. Zhang et al., 2019). However, most previous studies focus on cities in the central/eastern regions and few research analyzed in western China (Cheng et al., 2010; Dai et al., 2025; Duan et al., 2008; Liu et al., 2022; Shen et al., 2021; C. Wang et al., 2017; W. Wang, B. Yuan, et al., 2022; Xue et al., 2016; Yang et al., 2018; P. Zeng et al., 2019; Zhang et al., 2021; J. Zhu et al., 2020). X. F. Liu et al. (2021) reported an achieved concurrent sampling in five Chinese megacities in summer 2018, but the concomitant high levels of carbonyls, as well as their sources, formation and transformation processes were not comprehensively characterized. More importantly, compared to most studies that concentrate on O_3 pollution control, few studies have examined control strategies for carbonyls. Given that the secondary formation of carbonyls also exhibits a nonlinear relationship with their precursors (Atkinson et al., 2006; J. Li et al., 2016; Liu et al., 2022; Luecken et al., 2012; Rosado-Reyes & Francisco, 2007; Wolfe et al., 2016; Zhang et al., 2021), it remains uncertain whether the current precursor reduction strategies for O_3 are equally applicable to carbonyls. As such, identifying the precursors of carbonyls and understanding their relationship is essential to provide better scientific guidance for the coordinated future reduction of secondary pollutants, including both O_3 and carbonyls.

To address these research gaps, this thesis integrates field measurements and advanced modeling techniques to systematically investigate O_3 and carbonyl photochemistry in Lanzhou. Specifically, the study combines long-term trend analysis, intensive campaigns, and multi-city concurrent sampling to: (1) evaluate the seasonal and chemical mechanisms driving O_3 pollution in Lanzhou, (2) investigate the long-term trend of O_3 formation and radical chemistry in Lanzhou, (3) quantify the formation and transformation pathways of major carbonyls in Lanzhou, and (4) evaluate the effectiveness of current and potential control strategies for both O_3 and carbonyls in Lanzhou. By employing the Photochemical Box Model coupled with the

Master Chemical Mechanism (PBM-MCM) and Positive Matrix Factorization (PMF) models, this work provides new insights into the complex interplay between O_3 and VOCs, especially carbonyls. The findings are expected to inform more effective air quality management and policy development for secondary pollution control in China and similar urban environments.

1.2 Scope of this study

This doctoral research aims to advance the understanding of O_3 and carbonyl photochemistry in urban China, with a particular focus on the unique challenges faced by northwestern cities such as Lanzhou. The scope of this study is defined by the following key objectives and research directions:

1. To provide the first comprehensive investigation of extremely high wintertime O_3 episodes in China, with a focus on Lanzhou as a representative city. Through intensive field measurements and advanced modeling, this study explores the underlying causes of O_3 pollution under low-sunlight and low-temperature conditions, a phenomenon that has been largely overlooked in previous research.
2. To elucidate the critical role of alkene ozonolysis in winter O_3 formation. By integrating observational data and photochemical box modeling, this work reveals how alkene ozonolysis, rather than traditional photochemical pathways, can dominate O_3 production during winter, fundamentally challenging the prevailing view that strong solar radiation and high temperatures are necessary for severe O_3 episode days.
3. To systematically analyze the long-term trends of O_3 formation and radical chemistry in Lanzhou. This thesis documents how O_3 formation mechanisms and radical cycles have evolved over more than a decade and assesses the impact of emission control measures and changes in VOC composition on O_3 regimes. The findings provide new insights into the effectiveness of air quality policies in northwestern China.
4. To conduct a detailed, multi-city comparison of carbonyl photochemistry and sources in five major Chinese cities. Using simultaneous field measurements and the combined application of the PBM-MCM and PMF models, this study quantitatively assesses both primary and secondary sources of carbonyls and their contributions to O_3 formation. This approach enables a more accurate evaluation of the complex interactions between VOC sources, carbonyl formation, and O_3 production across different urban environments.

   To propose and evaluate joint O_3–carbonyl control strategies. For the first time, this research develops and demonstrates coordinated management approaches for multiple

secondary pollutants, providing a scientific basis for integrated air quality control. The study also offers a comprehensive analysis of the photochemical characteristics, sources, and joint control strategies for carbonyls in Lanzhou.

Overall, this thesis aims to fill critical knowledge gaps in the understanding of O_3 and carbonyl photochemistry in China's urban areas, especially under atypical meteorological conditions and in regions with complex emission profiles. The findings are expected to inform future research, guide the development of more effective air pollution control policies, and serve as a reference for similar metropolitan and industrialized regions worldwide. To achieve these objectives, the research is structured to first focus on Lanzhou as a representative case, enabling detailed mechanistic and trend analyses under its unique meteorological and emission conditions. Building on the insights gained from Lanzhou, the study then broadens its scope to a comparative analysis across five major Chinese cities. This transition allows for the evaluation of the generalizability of the findings and the identification of both shared and distinct characteristics in O_3 and carbonyl photochemistry, thereby strengthening the overall scientific narrative and policy relevance of the thesis.

1.3 Outline of this thesis

To enhance the logical coherence and structural integration of the thesis, a clear research roadmap is established. As illustrated in Figure 1.1, the thesis is organized into three interconnected research components: (1) a mechanistic study of wintertime O_3 formation in Lanzhou, (2) a long-term trend analysis of O_3 and radical chemistry in Lanzhou, and (3) a multi-city comparative study of secondary carbonyl compounds. The rationale for this structure is to first gain a deep understanding of the processes and trends in a representative industrial city, and then extend these insights to a broader urban context through comparative analysis. This framework ensures that each research component builds upon the previous one, collectively addressing the overarching research objectives. This thesis is organized as follows:

1. **Chapter 1** introduces the research background, objectives and outline of this study.
2. **Chapter 2** reviews the literature on O_3 pollution, including O_3 and its precursors, O_3 photochemistry, and its long-term trends in China.
3. **Chapter 3** describes the methodology, including sampling sites, measurement techniques, and model configurations.
4. **Chapter 4** investigates the mechanisms of wintertime O_3 surges in Lanzhou, focusing on alkene ozonolysis and radical chemistry.
5. **Chapter 5** analyzes the long-term trends of O_3 formation and radical chemistry in Lanzhou.
6. **Chapter 6** examines the photochemical characteristics, sources, and joint control strategies of formaldehyde, acetaldehyde, and acetone in five Chinese megacities.
7. **Chapter 7** summarizes the main findings, discusses their implications, and provides suggestions for future research.

I participated in all sample analyses described in this thesis. All model simulations and data analyses were conducted by me.

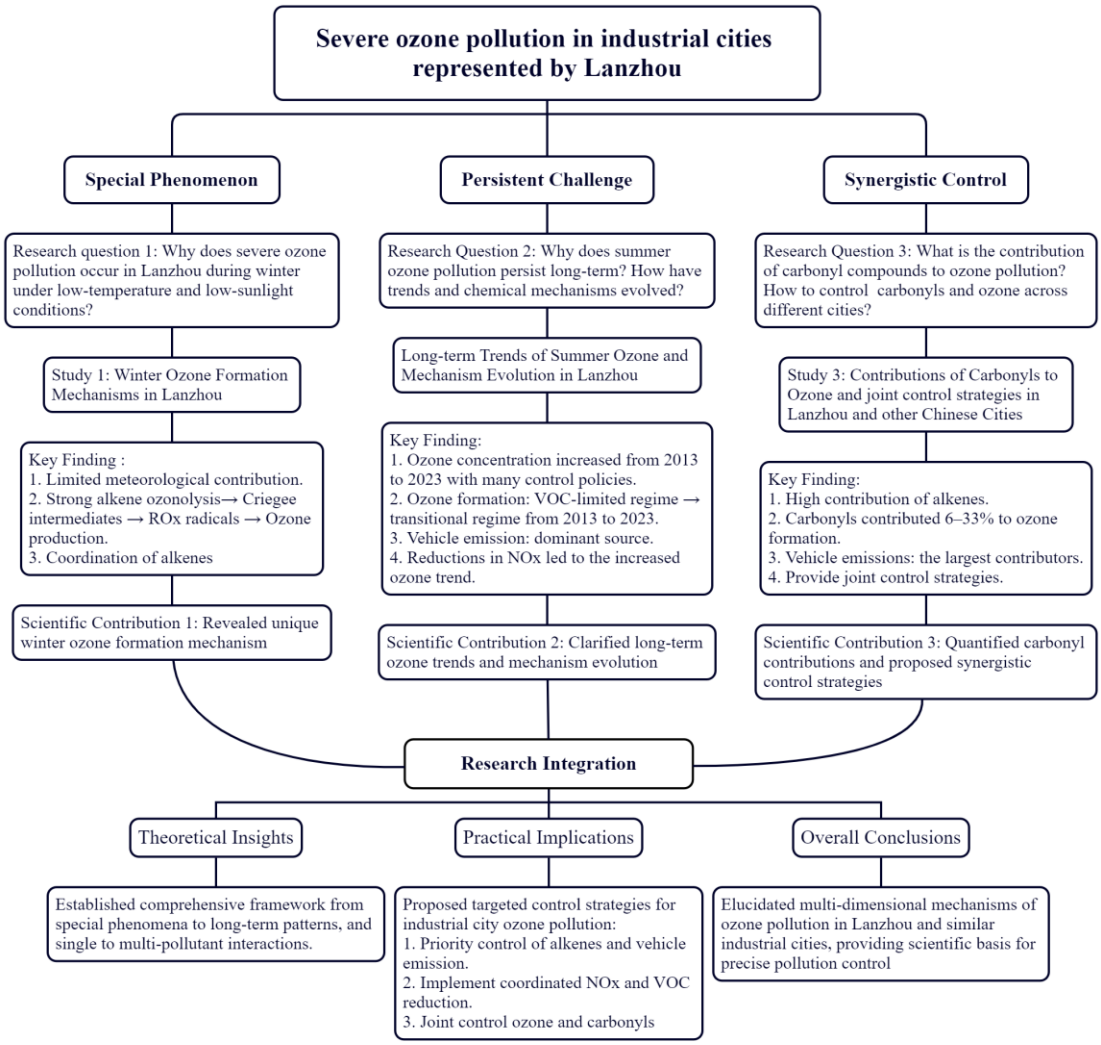

Figure 1.1. Technical roadmap of the three main research components in this thesis.

Chapter 2 Literature review

2.1 Overview of tropospheric O_3 pollution

O_3 is a trace atmospheric gas, with about 90 % located in the stratosphere, where it shields the Earth from harmful ultraviolet radiation (Fuhrer et al., 2016; Worden et al., 2008). About 10 % of atmospheric O_3 is present in the troposphere, where it acts as a secondary pollutant. Tropospheric O_3 is mainly generated through photochemical reactions involving VOCs, NO_x, and CO under sunlight (Cape, 2008; Collins, 2003; Jennifer, 1985; X. Lu et al., 2019). The negative impacts of tropospheric O_3 are well documented, as it can harm human health, damage vegetation, reduce crop yields, and influence the climate (Ainsworth et al., 2012; Ashmore, 2005; Chameides et al., 1999; Simpson et al., 2014; Wang et al., 2007). Long-term exposure to elevated O_3 levels has been linked to respiratory illnesses, cardiovascular problems, and a higher risk of premature death (Curtis et al., 2006; Liu et al., 2018; Manisalidis et al., 2020; Soares & Silva, 2022; J. J. Zhang et al., 2019). O_3 also threatens agricultural productivity by damaging plant tissues and suppressing photosynthesis, which can lead to significant economic losses for farmers (Emberson, 2020; Feng et al., 2015). Furthermore, O_3 contributes to climate change by altering the radiation balance and affecting interactions between the atmosphere and biosphere, thereby influencing temperature and weather patterns (X. Lu et al., 2019).

Since the mid-20th century, O_3 pollution had become a significant environmental concern in many urban and industrialized regions. The smog events in Los Angeles during the 1940s and 1950s marked the start of systematic O_3 research (Haagen-Smit, 1952). In the following decades, O_3 pollution was reported in various parts of the world, and long-term monitoring in North America and Europe showed that annual average O_3 concentrations at some sites doubled between the 1950s and 1990s (Chameides & Walker, 1973; Crutzen, 1974; Feister & Warmbt, 1987; Levy, 1971; Liu et al., 1987; Oltmans & Komhyr, 1986; Parrish et al., 2012). Since the 1990s, the implementation of stricter emission controls in developed countries has helped stabilize or even lower O_3 levels in North America and Europe (Chang et al., 2017; Lefohn et al., 2008; Oltmans et al., 2013; Simon et al., 2015).

However, O_3 pollution continues to worsen in many developing regions, especially in Asia. In countries like China and India, O_3 concentrations have kept rising (Gao et al., 2020; Guo et al., 2017; Lu et al., 2018; T. Wang et al., 2017; B. Zheng et al., 2018). Over the past thirty years, rapid industrialization and urbanization in China have led to increased emissions of O_3 precursors, particularly NO_x and VOCs. As a result, O_3 pollution has become more severe, especially in major urban clusters such as NCP, YRD, and PRD (Ding et al., 2008; Gao et al., 2017; K. Li et al., 2019; Qu et al., 2024; G. Yang et al., 2020; L. Zhang et al., 2023).

Lanzhou, located in a narrow river valley in northwestern China, is a typical industrial city with a long history of severe air pollution (W. Guo et al., 2022; Jia et al., 2016). Its industrial structure, dominated by petrochemical, metallurgical, and power generation sectors, combined with challenging meteorological and topographical conditions, has resulted in persistent air quality problems. Lanzhou was the site of China's earliest recorded photochemical smog events in the 1970s and 1980s, where local emissions of hydrocarbons and NO_x were identified as the main contributors (W. Guo et al., 2022; J. Li et al., 2020; Ta et al., 2004; Tang et al., 1985). High emissions of alkenes from the petrochemical industry, together with the city's valley terrain, often lead to severe O_3 pollution. The valley topography tends to trap pollutants near the surface, further deteriorating air quality (Cui et al., 2025; Du et al., 2020; W. Guo et al., 2022; Jia et al., 2016). Industrial activities, especially in the petrochemical sector, are major sources of O_3 precursors, including NO_x and VOCs (Dong et al., 2021; J. Liu et al., 2020; G. Y. Wang et al., 2020; Yan et al., 2021). As a result, O_3 pollution in Lanzhou is shaped by both chemical processes and local emissions, making it a complex issue to address. Despite the introduction of the CAA Plan in 2013, which aimed to reduce air pollution through stricter emission controls and technological upgrades, Lanzhou continues to struggle with O_3 pollution (Du et al., 2020; Filonchyk & Yan, 2018; Zhao et al., 2021). There is an urgent need for more comprehensive, long-term, and region-specific studies to better understand the evolving factors driving O_3 pollution in the city.

2.2 Influence of meteorological conditions on O_3

Meteorological conditions exert a profound influence on surface O_3 concentrations by modulating the chemical production, accumulation, and removal of O_3 and its precursors. Numerous studies have demonstrated that O_3 episode days are typically associated with a combination of high temperature, strong solar radiation, low relative humidity, weak wind, and reduced cloud cover (J. Liu et al., 2019; T. Ma et al., 2019; T. Wang et al., 2017; Yan et al., 2024). For instance, in North China, O_3 pollution events often coincide with surface high temperatures, low humidity, and anomalous southerly winds, and high-pressure systems in the mid-troposphere, which together create favourable conditions for O_3 accumulation (Gong & Liao, 2019). High temperatures not only accelerate the photochemical production of O_3 but also enhance the emission of biogenic volatile organic compounds (BVOCs), providing additional precursors for O_3 formation (Bloomer et al., 2009; X. Lu et al., 2019). However, under extreme heat, O_3 concentrations may be suppressed due to reduced BVOC emissions as vegetation stomata close (Steiner et al., 2010).

Relative humidity generally exhibits a negative correlation with O_3 levels. Increased humidity can weaken photochemical O_3 production by promoting the removal of excited-state oxygen atoms through reactions with water vapor, leading to the formation of hydroxyl radicals instead of O_3 (Jacob & Winner, 2009; Johnson et al., 1999). Observational studies in Chinese cities have shown that O_3 concentrations tend to decrease as relative humidity rises, with this effect being more pronounced at higher temperatures (Gong et al., 2021; Han, Gong, et al., 2019; Kavassalis & Murphy, 2017). Conversely, low humidity can reduce stomatal uptake of O_3 by vegetation, resulting in higher ambient O_3 concentrations (Gong et al., 2021).

Solar radiation is a key driver of O_3 photochemistry, as it provides the energy required for photolysis reactions, a critical step in O_3 formation (Jeong & Park, 2013; Qi et al., 2024). Reduced cloud cover increases the intensity of solar radiation at the surface, thereby accelerating O_3 production, while increased cloudiness can suppress O_3 formation by limiting photolytic activity (Jeong & Park, 2013; Zhao et al., 2020). Case studies in Shanghai and other

regions have confirmed that episodes of reduced cloud cover and enhanced solar radiation are often accompanied by elevated O_3 concentrations (Xu et al., 2021).

Wind speed and direction, as well as planetary boundary layer height (PBLH), play crucial roles in the transport, dispersion, and vertical mixing of O_3 and its precursors (Haman et al., 2014; He et al., 2017; Ma et al., 2020; Xu et al., 2018; Zhang et al., 2015). Strong winds can dilute local O_3 concentrations and facilitate pollutant removal, while stagnant conditions favor the accumulation of O_3 (Whaley et al., 2015; Zhang et al., 2015). The development of the boundary layer can promote the downward mixing of O_3-rich air from aloft, leading to higher surface O_3 levels, especially during the warm season (Haman et al., 2014; X. Lu et al., 2019). In some cases, cross-regional transport driven by prevailing winds has been shown to significantly elevate O_3 concentrations in downwind areas, as observed in both China and the Mediterranean (Adame & Sole, 2013; Gong et al., 2020; Tong et al., 2017).

On interannual and long-term timescales, meteorological variability has been identified as a significant contributor to observed O_3 trends in China. For example, meteorological conditions accounted for up to 37% of the summer O_3 increase in eastern China from 2013 to 2019 (K. Li et al., 2020), and similar contributions have been reported for other regions and periods (Han et al., 2020; Qian et al., 2022; Weng et al., 2022). In recent years, more humid and cooler conditions have helped reduce O_3 concentrations, but extreme heat events, such as those in 2022, have led to marked O_3 rebounds in several regions (Gao M. et al., 2023; Qiao et al., 2024). Furthermore, the impact of meteorological factors on O_3 pollution exhibits significant spatial heterogeneity, influenced by regional geography, emission patterns, and pollutant transport pathways (B. Li et al., 2023; Zhang et al., 2015).

Overall, the literature indicates that meteorological factors, including temperature, solar radiation, humidity, wind, boundary layer height, and cloud cover, interact in complex and regionally variable ways to influence O_3 mixing ratios. These interactions are not only critical for understanding the mechanisms of O_3 pollution formation but also for interpreting observed trends and developing effective air quality management strategies in China and other regions experiencing similar challenges (K. Li et al., 2020; X. Lu et al., 2019).

2.3 O_3 precursors and their sources in China

NO_x are crucial precursors in the formation of ground-level O_3, serving a dual function by both promoting and titrating O_3, which significantly affects O_3 photochemistry (Fu et al., 2019; Gao et al., 2017; K. Li et al., 2019). In China, NO_x emissions stem from a mix of human activities, such as fossil fuel combustion in vehicles, power plants, and industry, as well as natural sources like wildfires, lightning, and soil emissions (Wang et al., 2012). Over recent decades, rapid urbanization and industrial expansion have led to marked increases in NO_x emissions, with high concentrations frequently observed in major cities across the NCP, YRD, and PRD regions (Li et al., 2012; Ling & Guo, 2014; Liu et al., 2022; Ou et al., 2016; Ran et al., 2009; Shao et al., 2009; Zhang et al., 2014). In many areas, vehicle exhaust has become the leading source of NO_x, accounting for as much as 40–70 % of total emissions in the NCP and PRD, followed by coal combustion and power generation (Hao et al., 2001; Liu et al., 2017; H. Liu et al., 2020; Liu et al., 2022; X. F. Liu et al., 2019; Lu et al., 2013; Lyu et al., 2016b). The emission control policies in the 2010s resulted in a notable reduction in NO_x emissions nationwide, with a 21 % decrease reported in 48 cities between 2011 and 2015 (Liu et al., 2017). However, these reductions have had complex impacts on O_3 levels, as lower NO concentrations can reduce the titration effect, sometimes leading to higher O_3, especially in urban areas where O_3 formation is limited by VOCs (Fu et al., 2019; Gao et al., 2017; K. Li et al., 2019). This underscores the need to understand the interplay between NO_x and VOCs in local O_3 formation and highlights the importance of integrated control strategies.

VOCs are a diverse group of chemicals that play a central role in O_3 production through their reactions with NO_x under sunlight (Cape, 2008; Collins, 2003; Jennifer, 1985; X. Lu et al., 2019). The abundance and composition of VOCs in Chinese cities are shaped by both anthropogenic and biogenic sources (W. Guo et al., 2022; Henderson et al., 2010; Hua et al., 2023; X. F. Liu et al., 2021; X. F. Liu et al., 2019; Y. H. Liu et al., 2019; Lyu et al., 2016b; Song et al., 2018; P. Zeng et al., 2019). Major VOC species in urban areas include alkanes, aromatics, alkenes, and carbonyls, with their proportions varying according to local emission patterns and industrial activities (Huang et al., 2013; M. Z. Li et al., 2019; Louie et al., 2013).

For instance, alkanes and aromatics are often dominant in urban centers, while alkenes may be more prevalent in industrial zones (Cui et al., 2025; Du et al., 2020; W. Guo et al., 2022; Jia et al., 2016).

Among VOCs, carbonyls are particularly important due to their significant impact on air quality (Atkinson, 2000; Jenkin, 1997; W. Wang, B. Yuan, et al., 2022; Xue et al., 2016; Yang et al., 2018). These compounds can be directly emitted or formed secondarily through complex photochemical reactions (Ling et al., 2017; Liu et al., 2009; Pang & Mu, 2006; Wu et al., 2023; Yang et al., 2017; Z. Yang et al., 2019; X. Zhang et al., 2022; Y. Zhang et al., 2019). Formaldehyde, acetaldehyde, and acetone are the most abundant carbonyls in urban air. Notably, formaldehyde and acetaldehyde, because of their reactive carbonyl groups, act as key precursors for tropospheric O_3 formation (Guo, Ling, Cheung, Wang, et al., 2013; Yang et al., 2018; Zhang et al., 2021; Y. Zhang et al., 2019). The long-time exposure to high levels of formaldehyde and acetaldehyde, especially in urban or industrial settings, may pose health risks, including carcinogenicity and respiratory irritation (Bao et al., 2022; Ho et al., 2015; Lu et al., 2010; Z. Yang et al., 2019). Given the differences in emission sources and chemical processes across regions, it is essential to investigate the concentration patterns, primary sources, and secondary formation mechanisms of carbonyls in different cities to develop effective and targeted air pollution control policies.

The spatial and temporal distribution of formaldehyde, acetaldehyde, and acetone has been extensively documented through global monitoring over the past decades (Ho et al., 2015; Liu et al., 2022; Liu et al., 2009; Lui et al., 2017; Yang et al., 2017; X. Zhang et al., 2022; Y. Zhang et al., 2019). High concentrations of these carbonyls have been observed in cities worldwide, with particularly elevated levels in East Asia (Liu et al., 2022)**.** In China, regions such as the NCP, YRD, and PRD have reported especially high carbonyl concentrations, with formaldehyde and acetaldehyde often exceeding 20 and 10 ppbv, respectively (Y. Zhang et al., 2019). However, most previous studies were based on single-site sampling conducted over various periods, while simultaneous multi-city samplings, which eliminate uncertainty caused by time-separation and provide better intercomparison of specific secondary pollution across

cities for targeted air quality management, are scarce. X. F. Liu et al. (2021) reported an achieved concurrent sampling in five Chinese megacities in summer 2018, displaying the three major carbonyls ranked the first in Beijing with a mixing ratio of 24.3 ± 2.7 ppbv, accounting for 55 % of local total VOCs, followed by Wuhan (10.8 ± 1.5 ppbv), Lanzhou (7.6 ± 1.3 ppbv), Shanghai (6.8 ± 1.0 ppbv) and Chengdu (5.7 ± 2.0 ppbv). As the study focused on O_3 pollution, the concomitant high levels of carbonyls, as well as their sources, formation and transformation processes were not comprehensively characterized.

Furthermore, previous studies have extensively examined the contributions of primary and secondary sources of major carbonyls across cities (Bao et al., 2022; de Gouw et al., 2005; Ho et al., 2015; Li et al., 2010; Ling et al., 2017; Liu et al., 2022; Liu et al., 2009; Lui et al., 2017; Ma et al., 2016; Pang & Mu, 2006; Wang et al., 2015; Wu et al., 2023; Yang et al., 2017; Z. Yang et al., 2019). While specific proportions may vary depending on research methods, location, season, and the structure of local emission sources, primary sources of carbonyls, such as vehicle exhaust, industrial emissions, biogenic emission and biomass burning, generally contribute approximately 30-50 %, whereas secondary formation accounts for about 50-70 % (Guo, Ling, Cheung, Wang, et al., 2013; Hua et al., 2023; Liu et al., 2009; Pang & Mu, 2006; Rao et al., 2016). As the dominant part, the secondary formation of carbonyls mainly occurs through the reaction of VOCs with atmospheric oxidants, such as hydroxyl (OH) radicals. The following process generates alkyl (RO) radicals, which are subsequently decomposed into carbonyls (Anderson et al., 2017; Chen et al., 2022; Lin et al., 2012; Liu et al., 2022; Nussbaumer et al., 2021; Yang et al., 2018; Yang et al., 2023). Anthropogenic alkenes are the main precursors of formaldehyde and acetaldehyde (Ling et al., 2017; Yang et al., 2018), while isoprene emitted by plants can generate formaldehyde (Palmer et al., 2006; X. Yang et al., 2020). In contrast, C_3-C_5 alkanes and pinene are the main precursors of acetone (Guo, Ling, Cheung, Wang, et al., 2013; Ling et al., 2017; Lyu et al., 2024; Yang et al., 2018; X. Yang et al., 2020). However, most of these studies rely on sensitivity analyses or evaluate carbonyls changes by excluding precursors, quantitative assessments of precursor contributions through in-situ simulation remain limited (Chen et al., 2022; Ling et al., 2017; Lyu et al., 2024;

Yang et al., 2018; X. Yang et al., 2020), and even more challenging on tracing each VOC precursor through reaction pathways.

Especially in Lanzhou, most studies have focused on alkenes and have not fully explored the sources, secondary formation, and photochemical behavior of carbonyls (Dong et al., 2021; W. Guo et al., 2022; Jia et al., 2016; J. Liu et al., 2020; X. F. Liu et al., 2021; G. Y. Wang et al., 2020; Yan et al., 2021). There is a need for more comprehensive studies on carbonyls and their source in Lanzhou.

2.4 Contributions of carbonyls and their sources to O_3 formation

For carbonyls, more previous studies focused on their contribution to O_3 formation, mainly through the parameterized methods on calculating their O_3 formation potential (OFP) and OH reactivity (L_{OH}) (C. Wang et al., 2017); Yuan et al., 2024; (Bao et al., 2022; Huang et al., 2020; Hui et al., 2023; Z. Liu et al., 2021; Lyu et al., 2024; Shen et al., 2021; F. Wang et al., 2024; Yang et al., 2018; Yang et al., 2017; X. Yang et al., 2020; Zhang et al., 2021). Formaldehyde and acetaldehyde consistently rank among the top contributors in most OFP studies, qualitatively highlighting their importance in O_3 formation (Hui et al., 2023; F. Wang et al., 2024; X. Yang et al., 2020; Zhang et al., 2021); Yuan et al., 2024; (C. Wang et al., 2017). Based on the chemical mechanism, as intermediate products of VOC oxidation, formaldehyde and acetaldehyde are deeply involved in the radical cycle. The photolysis and oxidation of carbonyls produce hydroperoxyl (HO_2) and alkyl peroxy (RO_2) radicals (Edwards et al., 2014; Xue et al., 2016; Yang et al., 2018; Yang et al., 2017) These radicals then react with NO, facilitating the production of O_3 (Liu et al., 2012; Qu et al., 2021; Rao et al., 2016; Shen et al., 2021; W. Wang, B. Yuan, et al., 2022; Y. Xu et al., 2023; Y. Zhang et al., 2019). Compared to other approaches, in-situ simulations that incorporate detailed chemical mechanisms are better suited for quantitatively evaluating the contribution of carbonyls to radical generation and subsequent O_3 formation. For example, carbonyls were found to account for 21 %–70 % of the total radical RO_x (= OH + HO_2 + RO + RO_2) production in Beijing, Guangzhou and Hong Kong through in situ simulations (W. Wang, B. Yuan, et al., 2022; Xue et al., 2016; Yang et al., 2018; Zhang et al., 2021). Moreover, carbonyls were found influence 36.1-45.4 % in

Shanghai (J. Zhu et al., 2020), 13-31 % in Wuhan (P. Zeng et al., 2019), 31.5-55.9 % of O_3 formation in Beijing and Zibo in the North China Plain (Dai et al., 2025; Duan et al., 2008), and 23-37 % in Guangzhou, Shenzhen, and Shantou in the PRD regions (Cheng et al., 2010; Shen et al., 2021; C. Wang et al., 2017). While most current study focus on cities in the central/eastern regions, further investigation of other major city or city clusters, particularly in western China, where VOC profiles vary but also suffer from serous secondary pollutions was necessary.

More importantly, compared to most studies that concentrate on O_3 pollution control, few studies have examined control strategies for carbonyls. Given that the secondary formation of carbonyls also exhibits a nonlinear relationship with their precursors (Atkinson et al., 2006; J. Li et al., 2016; Liu et al., 2022; Luecken et al., 2012; Rosado-Reyes & Francisco, 2007; Wolfe et al., 2016; Zhang et al., 2021), it remains uncertain whether the current precursor reduction strategies for O_3 are equally applicable to carbonyls. As such, identifying the precursors of carbonyls and understanding their relationship is essential to provide better scientific guidance for the coordinated future reduction of secondary pollutants, including both O_3 and carbonyls.

2.5 O_3-precursor relationship and formation regimes

2.5.1 Long-term variation of O_3 formation regimes

Long-term changes in O_3 sensitivity to VOCs and NO_x have been observed in response to emission controls and evolving precursor ratios (Jin & Holloway, 2015; T. Wang et al., 2017; Wu et al., 2018). For example, reductions in NO_x emissions during the 12th Five-Year Plan slowed the transition to VOC-limited regimes in major city clusters, with some regions shifting to NO_x-limited or transitional regimes (T. Wang et al., 2017; Wu et al., 2018).

Lanzhou is among the first cities in China where O_3 pollution was recognized, with documented cases of photochemical smog dating back nearly half a century (W. Guo et al., 2022; J. Li et al., 2020; Ta et al., 2004; Tang et al., 1985). Although the CAA Plan was introduced in 2013 to address air pollution through stricter emission controls and technological improvements, Lanzhou continues to struggle with O_3 pollution (Du et al., 2020; Filonchyk & Yan, 2018; Zhao

et al., 2021). The CAA Plan included a range of measures, such as controlling industrial emissions, reducing dust pollution, managing scattered coal use, and regulating vehicle exhaust (Bureau, 2018; Government, 2013). In Lanzhou, the chemical formation of O_3 is particularly significant. High emissions of alkenes from the petrochemical industry, combined with the city's valley geography, frequently result in severe O_3 pollution. The valley setting tends to trap pollutants near the surface, further deteriorating air quality (Du et al., 2020; W. Guo et al., 2022; Jia et al., 2016). Industrial activities, especially those related to petrochemicals, are major contributors of O_3 precursors, including NO_x and VOCs (Dong et al., 2021; J. Liu et al., 2020; G. Y. Wang et al., 2020; Yan et al., 2021). Consequently, O_3 pollution in Lanzhou is influenced by both chemical reactions and local emissions, making it a complex problem to manage. Notably, Lanzhou also experiences significant wintertime O_3 pollution, a phenomenon that is uncommon in most other regions (Yang et al., 2024).

In contrast, much of the long-term research on O_3 in China has focused on regions such as the North China Plain (NCP), Yangtze River Delta (YRD), and Pearl River Delta (PRD), as well as major cities like Chengdu and Shanghai (S. Chen et al., 2020; Z. Chen et al., 2019; Gao et al., 2017; Hu et al., 2025; X.-B. Li et al., 2022; X. F. Liu et al., 2019; M. Wang et al., 2024; W. Wang, D. D. Parrish, et al., 2022; Y. Wang et al., 2022; L. Yang et al., 2019). These studies have provided valuable insights into O_3 trends and formation mechanisms. For instance, in the NCP, it has been observed that reducing NO_x emissions alone, especially during periods of high temperatures and strong sunlight, can sometimes lead to increased O_3 concentrations (S. Chen et al., 2020; Z. Chen et al., 2019; M. Wang et al., 2024; W. Wang, D. D. Parrish, et al., 2022). In the PRD region, an improper balance between NO_x and VOC controls and a weaker NO titration effect have also led to higher O_3 (X.-B. Li et al., 2022; L. Yang et al., 2019). Studies in Shanghai and Chengdu found that reducing NO_x could also increase O_3 (Gao et al., 2017; Y. Wang et al., 2022). And Lanzhou also found the O_3 formation transition from mainly controlled by NO_x in summer 2018 to a VOCs-dominated regime in summer 2019 (Y. Li et al., 2022). However, this study only analyzed transport from 2018 to 2019, during the overhaul of alkenes plant and heavy catalytic cracking unit in 2019 that was ever conducted in the history of Lanzhou petrochemical industry (Y. Li et al., 2022), which greatly increase the uncertainty

of this result. There remains a research gap in understanding the long-term O_3 trends and influencing factors specific to Lanzhou. The unique characteristics and pollution sources in Lanzhou necessitate targeted research to address its specific challenge.

In summary, although Lanzhou has a long history of O_3 research, most studies have focused on summer and on the effects of precursor controls. There is still a need for long-term studies that examine the evolution of O_3 formation regimes and the effectiveness of control measures in Lanzhou.

2.5.2 Seasonal and diurnal variation of O_3 formation regimes

The seasonal and diurnal variations of O_3 levels and their formation regimes have been widely studied in major city clusters across China (Jia et al., 2016; Y. Li et al., 2022; X. F. Liu et al., 2021; Lyu et al., 2016b; Xue, Wang, Gao, et al., 2014; P. Zeng et al., 2019; Zhang et al., 2014). In the NCP and YRD region, O_3 concentrations typically reach their highest levels during the summer months, whereas in the PRD region, peak O_3 values are more often observed in autumn (Ding et al., 2013; Ding et al., 2008; T. Wang et al., 2017; Zheng et al., 2010). In urban areas with elevated NO_x concentrations, O_3 formation is generally limited by the availability of VOCs. However, in suburban and industrial zones, the controlling regime can shift seasonally between VOC-limited and NO_x-limited conditions, especially when NO_x levels are lower (Jia et al., 2016; Li et al., 2012; Ran et al., 2009; Xue, Wang, Gao, et al., 2014; Zhang et al., 2014). Besides, the sudden changes in emissions can also alter O_3 sensitivity. For example, in Lanzhou, the overhaul of an alkenes plant and a heavy catalytic cracking unit in 2019 resulted in a shift in O_3 formation regime, from being primarily NO_x-controlled in the summer of 2018 to a VOCs-dominated regime in the summer of 2019 (Y. Li et al., 2022).

Typically, O_3 pollution peaks during the daytime when sunlight drives photochemical reactions (Steinfeld, 1998; T. Wang et al., 2017). In addition to the concentrations of O_3 precursors, the chemical formation of O_3 is highly related to meteorological conditions (i.e., temperature and solar radiation). High temperatures and strong solar radiation are conducive to the chemical production of O_3 (Guo et al., 2009; Guo, Ling, Cheung, Jiang, et al., 2013; L. Li et al., 2016; Li et al., 2015; Lu et al., 2020; T. Wang et al., 2017; Y. Wang et al., 2017). As such, O_3 pollution

events are generally concentrated in spring, summer, and autumn but rare in winter (Kgabi, 2012; N. Liu et al., 2019; Maji et al., 2019; Oltmans, 1994). However, a handful of studies have reported O_3 episode events (maximum hourly concentration exceeding 100 ppbv) in winter at specific locations with high surface albedo values and/or heavy precursor emissions (Edwards et al., 2014; Oltmans et al., 2014; Schnell et al., 2009; Singh et al., 1997). For example, in the winter of 1993, hourly O_3 peaks of 100–120 ppbv were discovered in Delhi, India, due to meteorological conditions favorable to the accumulation of air pollutants (Singh et al., 1997). In addition, in February 2008, O_3 pollution events occurred in a natural gas field in Wyoming, the United States of America (USA), (hourly maximum value attaining 140 ppbv) with a daily average temperature of −17 °C. These were attributed to high concentrations of O_3 precursors (i.e., alkanes) trapped by the shallow temperature inversion (Schnell et al., 2009). Moreover, in 2013, due to high snow albedo and strong carbonyl photolysis, severe O_3 pollution was found in the oil fields of Utah, USA, with a daily average temperature being −8 °C (Edwards et al., 2014; Oltmans et al., 2014).

In China, surprisingly, high O_3 values during cold weather have been widely observed in North China in recent years (K. Li et al., 2021; Yang et al., 2024). On the one hand, the reduction in NO_x emissions since 2013 has resulted in enhanced O_3 pollution in the NCP (K. Li et al., 2021). On the other hand, large O_3 precursor emissions from oil fields and/or petrochemical industrial areas have led to intensive production of O_3 in winter (S. Y. Chen et al., 2020; Edwards et al., 2014; Ma et al., 2012; Oltmans et al., 2014; Schnell et al., 2009). Specifically, several high O_3 days (maximum hourly values around 80 ppbv) in winter were observed in oil fields in the Yellow River Delta (YelRD) region, which were ascribed to heavy emissions of alkanes during oil extraction operations (T. Chen et al., 2020). In addition, highly reactive VOCs (i.e., ethene, propene, toluene, and xylene) emitted from industry sources, combined with favorable meteorological conditions for the accumulation of air pollutants, led to O_3 pollution (hourly maximum reaching 76 ppbv) in a city in North China during the winter (Zhan et al., 2023). It is particularly noteworthy that our study identified the highest O_3 concentrations in Lanzhou during winter, along with the greatest number of days exceeding high O_3 thresholds. Despite this, the underlying causes of these exceptional winter O_3 episode days have not been

thoroughly examined in previous research. Most existing studies in Lanzhou have concentrated on O_3 formation during the summer months, leaving the mechanisms responsible for elevated winter O_3 levels largely unexplored. Given Lanzhou's distinctive meteorological conditions and emission patterns in the colder seasons, further investigation is needed to clarify the processes contributing to these unusual wintertime O_3 events.

2.6 O_3 photochemistry and radical chemistry

The photochemical production of O_3 is governed by a complex interplay of reactions involving VOCs, NO_x, and CO, all driven by sunlight and regulated through radical cycling (Chameides & Walker, 1973; Crutzen, 1974; Levy, 1971). Over the years, several chemical mechanisms have been developed to simulate these processes, such as the Carbon Bond (CB4/05/6), Regional Atmospheric Chemical Mechanism (RACM1/2), and the Statewide Air Pollution Research Center mechanisms (SAPRC07/99), covering developments from the 1980s to the 2010s (Carter, 2000, 2010; Gery et al., 1988; Goliff et al., 2013; Stockwell et al., 1997; Yarwood et al., 2010; Yarwood & Rao, 2005; Yarwood et al., 2005).

The near-explicit Master Chemical Mechanism (MCM) has enabled more detailed studies of VOC oxidation and radical chemistry, offering deeper insights into the factors influencing O_3 formation (Jenkin, 2003; Jenkin, 1997; Lam et al., 2013; Saunders, 2003). The MCM (v3.3.1) encompasses around 17,000 reactions and 6,600 intermediate species, providing a comprehensive description of homogeneous gas-phase reactions in the atmosphere (X. F. Liu et al., 2019; Lyu et al., 2016a; Lyu et al., 2019; Y. Wang et al., 2018; Y. Wang et al., 2017). This model also incorporates parameters such as photolysis rates, dry deposition, boundary layer development, and vertical exchange. Site coordinates and observed solar radiation are used to calculate photolysis rates via the tropospheric ultraviolet and visible radiation module. The MCM has been widely applied in Chinese cities, demonstrating strong performance in simulating in situ photochemistry (X. F. Liu et al., 2019; Lyu et al., 2016a; Lyu et al., 2019; Y. Wang et al., 2018; Y. Wang et al., 2017).

A key metric for evaluating atmospheric photochemical activity is the net O_3 production rate, defined as the difference between O_3 production and destruction rates (X. F. Liu et al., 2019; Lyu et al., 2016a; Lyu et al., 2019; Y. Wang et al., 2018; Y. Wang et al., 2017; Yang et al., 2024). O_3 is primarily produced through reactions between NO and HO_2, as well as NO and RO_2, while its destruction involves reactions with OH and HO_2, O_3 photolysis, ozonolysis of alkenes, and the reaction between OH and NO_2 (X. F. Liu et al., 2019; Lyu et al., 2016a; Lyu et al., 2019; Y. Wang et al., 2018; Y. Wang et al., 2017; Yang et al., 2024). Radical chemistry, especially the cycling of RO_x radicals, is central to O_3 photochemistry and the oxidative capacity of the atmosphere (Heard, 2004; X. F. Liu et al., 2021; X. Ma et al., 2019; Slater et al., 2020; T. Wang et al., 2017; Y. Wang et al., 2023; Yang et al., 2024). The sources and cycling rates of these radicals vary by region, reflecting differences in precursor emissions, photolysis rates, and meteorological conditions (Lyu et al., 2016b; Wang et al., 2019; Y. Wang et al., 2018; Xue et al., 2016; J. X. Zhu et al., 2020).

Field measurements and modeling in Chinese cities have reported a wide range of net O_3 production rates, influenced by variations in precursor levels, weather, and local chemical regimes (X. F. Liu et al., 2021; K. Lu et al., 2019; Tan et al., 2019; Xue, Wang, Gao, et al., 2014). For example, in Beijing, the average daytime net O_3 production rate in summer was 25.8 ppbv h^{-1}, while in central China, rates ranged from 8.8 to 28 ppbv h^{-1} depending on location and season (Liu et al., 2012; Lu et al., 2017; Z. F. Tan et al., 2018; P. Zeng et al., 2019). Research on radical chemistry in China has mainly focused on cities like Beijing, Wuhan, Chengdu, Shanghai, and the PRD, highlighting the importance of VOC control and the distinct features of radical cycling in different urban environments (X. F. Liu et al., 2021; Liu et al., 2012; K. Lu et al., 2019; Lu et al., 2017; Tan et al., 2019; Z. F. Tan et al., 2018; Xue, Wang, Gao, et al., 2014; P. Zeng et al., 2019).

In Lanzhou, studies on O_3 photochemistry and radical chemistry have been conducted for the summer of 2018 by X. F. Liu et al. (2021) and Jia et al. (2018). However, there is still a lack of research on the long-term and wintertime characteristics of O_3 photochemistry and radical chemistry in the city.

In summary, while significant advances have been made in understanding O_3 photochemistry and its control in China, several important gaps remain. Most notably, research has largely concentrated on summer O_3 episode days, with limited attention to wintertime O_3 surges and their underlying mechanisms, particularly in northwestern cities such as Lanzhou (L. Li et al., 2016; Liu et al., 2012; Ran et al., 2011; Shao et al., 2009; She et al., 2024; Shu et al., 2020; Zeng et al., 2018). The observation of extremely high O_3 concentrations under low sunlight and low temperatures challenges the traditional view that strong solar radiation and high temperatures are necessary for severe O_3 pollution. There is also a lack of long-term, multi-city, and seasonally resolved studies on O_3 formation mechanisms, radical chemistry, and the effectiveness of emission control measures in Lanzhou. The distinct characteristics and emission sources found in cities like Lanzhou highlight the necessity for targeted research to address their unique air quality challenges. In particular, more work is needed to understand the secondary formation of carbonyls, their nonlinear interactions with precursors, and their influence on radical cycles and O_3 production in Lanzhou. Additionally, developing and testing integrated control strategies for both O_3 and carbonyls, as well as assessing their effectiveness across different urban settings, are important directions for future research.

For Lanzhou, there is a pressing need for comprehensive, long-term studies that integrate field observations, advanced modeling techniques, and seasonal analyses to gain a thorough understanding of O_3 and carbonyl photochemistry. Such efforts will provide a solid scientific foundation for improving air quality management and informing policy decisions in Lanzhou and other cities facing similar issues.

Chapter 3 Methodology

3.1 Sampling sites

In this study, field measurements were carried out at multiple sites across major city clusters in China during both the summer and winter of 2018. The selected sites represented five typical regions: the North China Plain (NCP), Sichuan Basin (SCB), northwestern China, the Yangtze River Delta (YRD), and central China, specifically including Beijing, Chengdu, Lanzhou, Shanghai, and Wuhan. Figure 3.1 illustrates the location of the sampling site in Lanzhou during the winter of 2018 and the summer of 2013, 2019-2023, while Figure 3.2 presents the locations of the sampling sites in Beijing, Chengdu, Lanzhou, Shanghai, and Wuhan during the summer of 2018. Lanzhou, recognized as one of the largest petrochemical centers in western China, hosted two key sampling sites. One site was established on the rooftop of the Lanyuan Hotel (LYH), and the other at the Atmospheric Composition Monitoring Superstation (LACMS). The LYH site (36°06′ N, 103°37′ E, 1695 m above sea level) is situated in a residential area associated with the PetroChina Lanzhou Petrochemical Company, approximately 0.7 km from the industrial zone and 2.2 km from the nearest highway (see Figure 3.1). This location is influenced by emissions from residential, industrial, and vehicular sources. Intensive sampling at the LYH site was conducted from January 1 to 31, 2018. Additional sampling campaigns were carried out at the LACMS site in August of 2013 and 2019-2023.

During the summer of 2018, sampling campaigns were conducted at the following locations: the Tower Branch of the Institute of Atmospheric Physics, Chinese Academy of Sciences in Beijing (39°58'28" N, 116°22'13" E); the Zi-Ka-Wei Observatory in Shanghai (31°11'27" N, 121°26'04" E); the Wuchang Culture and Sports Bureau in Wuhan (30°31'50" N, 114°18'28" E); the Sichuan Academy of Environmental Science in Chengdu (30°37'45" N, 104°03'50" E); and the Lanyuan Hotel in Xi Gu, Lanzhou (36°06'11" N, 103°37'48" E). Each site was carefully selected to represent typical urban environments and to ensure the representativeness of the data. Locations were chosen to minimize the influence of nearby emission sources (X. F. Liu et al., 2021).

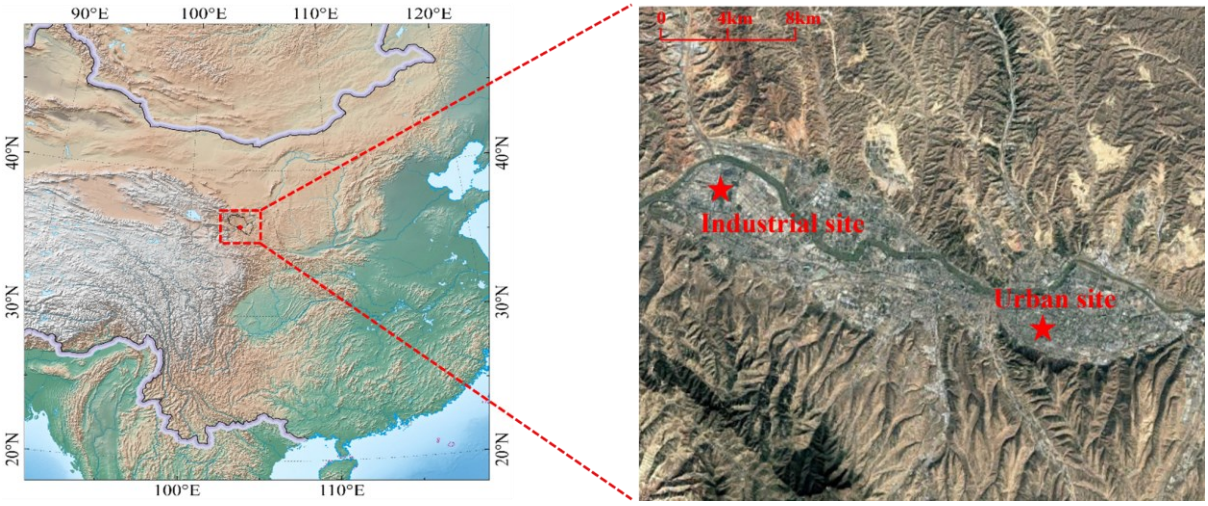

Figure 3.1 Maps showing the locations of the industrial and urban sites in Lanzhou.

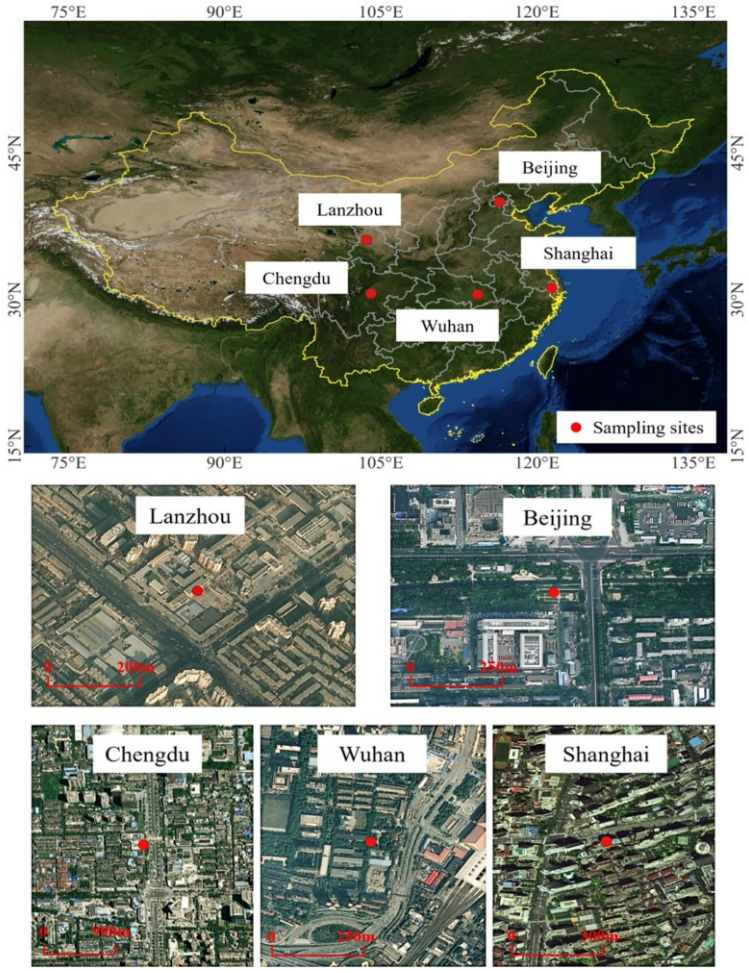

Figure 3.2 Maps showing the locations of the sampling site in Beijing, Chengdu, Lanzhou, Shanghai, and Wuhan in China.

3.2 Measurement techniques

3.2.1 Sampling campaign in Lanzhou in winter 2018

The hourly mixing ratios of O_3, NO, NO_2, CO, and SO_2 were obtained from the national monitoring site (https://www.cnemc.cn/), which was co-located with our sampling site. To measure volatile organic compounds (VOCs), an online gas chromatograph with photo ionization detector and flame ionization detector was employed, enabling the quantification of 60 VOC species, including 29 alkanes, 16 aromatics, 14 alkenes, and one alkyne (see Table 3.1). Detailed information regarding the instrument type, measurement techniques, detection limits, and time resolutions is provided in Table 3.2. Carbonyls were collected using silica cartridges impregnated with acidified 2,4-dinitrophenylhydrazine (DNPH). After sampling, the concentrations of 16 carbonyls species were determined by high-performance liquid chromatography (HPLC), as summarized in Table 3.3. An autonomous weather station was also operated at the sampling site to continuously monitor meteorological parameters, including relative humidity, temperature, solar radiation, wind speed, and wind direction. A total of 17 carbonyl samples were collected between January 6 and 11, 2018. Sampling was conducted during three-time intervals each day: 8:00–10:00, 12:00–14:00, and 16:00–18:00 local time (LT). It should be noted that the data collected from 12:00–14:00 on January 10 were excluded due to anomalies. During each sampling period, air was drawn through the DNPH cartridge for 120 minutes at a flow rate of 0.5 L min^{-1} using a calibrated pump. Following collection, the samples were analyzed using HPLC (PerkinElmer Series 2000, MA, USA) equipped with an ultraviolet detector. The instrument was calibrated with five gradient concentration standards, covering a wide range of carbonyl concentrations typically found in ambient air. In total, 16 carbonyl species were identified and quantified, all of which exhibited strong linear correlations between standard concentrations and instrument responses (R^2 > 0.999). The detection limits for all target carbonyls in this study were below 0.1 ppbv. Further details regarding the carbonyl sampling and analytical procedures can be found in our previous publication (X. F. Liu et al., 2021; X. F. Liu et al., 2019; Y. Wang et al., 2018).

Table 3.1 Descriptive statistics of VOC mixing ratios in winter Lanzhou. The 95 % C.I. and Max denote the 95 % confidence interval, and the maximum mixing ratio, respectively (Unit: ppbv). (# represents the VOC species used in the model simulations)

No.	Compounds	Mean	95 %C.I.	Max
	Alkanes and Alkyne			
1	**Ethane#**	6.80	0.53	64.59
2	**Propane#**	1.96	0.49	80.17
3	***i*-Butane#**	4.16	0.45	48.01
4	***n*-Butane#**	0.83	0.14	31.06
5	**Cyclopentane#**	0.92	0.11	11.07
6	***i*-Pentane#**	1.39	0.12	16.95
7	***n*-Pentane#**	2.12	0.25	37.30
8	**Cyclohexane#**	12.38	1.96	160.51
9	**Methylcyclopentane**	0.95	0.13	20.87
10	**2,2-**	1.69	0.19	36.98
11	**2,3-**	1.34	0.14	17.24
12	**2-Methylpentane#**	1.54	0.19	25.75
13	**3-Methylpentane#**	1.22	0.14	24.37
14	**2,4-**	0.53	0.10	23.43
15	**2,2-**	0.02	0.02	3.36
16	**2,3-**	0.86	0.16	21.09
17	**3-Methylhexane#**	0.08	0.02	5.99
18	**2,2,4-**	0.11	0.01	1.08
19	**Methylcyclohexane**	0.47	0.10	19.42
20	**2,3,4-**	0.65	0.12	17.81
21	**2-Methylheptane**	0.15	0.02	1.42
22	**3-Methylheptane**	0.06	0.01	2.16
23	***n*-Hexane#**	0.93	0.11	15.45
24	***n*-Heptane#**	0.24	0.13	21.28
25	***n*-Octane#**	0.32	0.07	9.27

26	***n*-Nonane[#]**	0.03	0.01	0.91
27	***n*-Decane[#]**	0.04	0.01	0.99
28	***n*-Undecane[#]**	1.20	0.21	21.51
29	***n*-Dodecane[#]**	1.93	0.16	19.95
30	**Ethyne[#]**	0.94	0.10	12.06
	Alkenes			
31	**Ethene[#]**	13.52	0.95	80.73
32	**Propene[#]**	25.18	2.51	188.95
33	***trans*-2-Butene[#]**	3.68	0.37	43.65
34	**1-Butene[#]**	1.00	0.13	14.10
35	***i*-Butene[#]**	0.72	0.10	10.19
36	***cis*-2-Butene[#]**	4.25	0.48	57.16
37	**1,3-Butadiene[#]**	1.18	0.11	15.76
38	***trans*-2-Pentene[#]**	0.63	0.09	12.67
39	**1-Pentene[#]**	4.37	0.52	59.20
40	***cis*-2-Pentene[#]**	1.27	0.11	17.85
41	**Isoprene[#]**	0.68	0.09	13.87
42	**2-methyl-1-**	0.19	0.04	5.48
43	**1-Hexene[#]**	0.34	0.06	10.61
44	***α*-Pinene[#]**	1.63	0.21	23.87
	Aromatics			
45	**Benzene[#]**	5.03	0.54	48.85
46	**Toluene[#]**	0.20	0.02	1.92
47	**Ethylbenzene[#]**	0.20	0.07	12.64
48	***m/p*-Xylenes[#]**	0.16	0.03	3.71
49	***o*-Xylene[#]**	0.26	0.10	26.64
50	**Styrene[#]**	0.01	0.01	0.80
51	***i*-Propylbenzene[#]**	0.12	0.05	11.20
52	***n*-Propylbenzene[#]**	2.75	0.56	75.52
53	***m*-Ethyltoluene[#]**	0.15	0.02	2.92

54	***p*-Ethyltoluene#**	0.31	0.04	5.38
55	***o*-Ethyltoluene#**	0.04	0.01	1.72
56	**1,3,5-**	1.90	0.13	12.81
57	**1,2,4-**	0.36	0.10	16.82
58	**1,2,3-**	0.07	0.01	1.82
59	***m*-Diethylbenzene**	0.43	0.05	4.19
60	***p*-Diethylbenzene**	0.07	0.02	2.97

Table 3.2 Information of instruments used for measuring trace gases and VOCs.

Species	Instrument	Measurement technique	Detection limit	Time resolution
O_3	API 400	UV photometry	0.6 ppbv	1 min
NO-NO_2-NO_x	API 200A	Chemiluminescence	0.4 ppbv	1 min
CO	API 300	Nondispersive infrared absorption with gas filter correlation	<0.05 ppmv	1 min
SO_2	API 100E	UV fluorescence	0.4 ppbv	1 min
VOCs	Syntech Spectras GC 955, Series 600/800	Online GC-PID/FID	0.002 – 0.056 ppbv	1 min
OVOCs	PerkinElmer series 2000, MA, USA	High-Performance Liquid Chromatograph (HPLC)	0.1 ppbv	60 min

Table 3.3 Descriptive statistics of OVOC mixing ratios in winter Lanzhou. The 95 % C.I. and Max denote the 95 % confidence interval, and the maximum mixing ratio, respectively (Unit: ppbv). (# represents the OVOC species used in the model simulations)

No.	Compounds	Mean	95 %C.I.	Max
1	**Formaldehyde#**	5.97	2.66	19.96
2	**Acetaldehyde#**	5.37	2.61	19.49
3	**Acetone#**	3.30	0.96	7.20
4	**Acrolein**	0.00	0.00	0.00

5	**Propionaldehyde**	0.18	0.25	2.27
6	**Crotonaldehyde**	0.05	0.02	0.14
7	**Methyl ethyl ketone**	0.72	0.46	4.12
8	**Iso- + n-**	0.15	0.09	0.63
9	**Benzaldehyde**	0.32	0.08	0.76
10	**Iso-pentanal/iso-**	0.35	0.10	0.79
11	**n-pentanal/n-**	0.08	0.05	0.36
12	**o-Tolualdehyde**	0.00	0.00	0.00
13	**m-Tolualdehyde**	0.00	0.00	0.00
14	**p-Tolualdehyde**	0.06	0.03	0.23
15	**n-hexaldehyde**	0.00	0.00	0.00
16	**2,5-**	0.00	0.00	0.00

3.2.2 Sampling campaigns in Lanzhou in August 2013, 2019-2023

The hourly mixing ratios of O_3, NO, NO_2, CO, and SO_2 from 2014 to 2024 (Figure 5.1) were obtained from the national monitoring site (https://www.cnemc.cn/), which is located near our sampling site. At the LACMS site, VOC measurements were conducted in August 2013 and from 2019 to 2023 using the EXPEC 2000 series analyzer, which quantified a total of 107 VOC species. Particulate matter (PM_{10} and $PM_{2.5}$) concentrations were determined using the 5030i SHARP PM synchronous mixed monitor. Trace gases, including NO_x, NO, NO_2, SO_2, O_3, and CO, were analyzed with Thermo Fisher Scientific online gas analyzers (models 42i, 43i, 49i, and 48i). Meteorological parameters such as air temperature, relative humidity, wind speed, and wind direction were measured using FWS500 sensors. Solar radiation was monitored with a Kipp & Zonen SMP22 analyzer, and visibility was assessed using a DNQ-2 analyzer. Detailed information on the measured VOC mixing ratios is provided in Table 5.5.

3.2.3 Sampling campaigns in five Chinese cities in summer 2018

Continuous monitoring of trace gases, including O_3, CO, and NO-NO_2-NO_x, was conducted at each selected site (see Table 3.4). To ensure precise and accurate measurements, a range of analyzers was employed across the sampling locations. In Beijing, Shanghai, Wuhan, and Lanzhou, O_3 concentrations were measured using a UV photometric analyzer (TEI Model TE49i), and the limit of detection (LOD) and precision for O_3 were 0.5 ppbv and ± 1.0 ppbv respectively. CO concentrations were determined with a nondispersive infrared analyzer (TEI Model 48iTL), featuring an LOD of 40 ppbv and a precision of ± 0.1 ppbv. NO-NO_2-NO_x levels were measured using a chemiluminescence analyzer (TEI Model 42iTL), and the LOD and precision were 0.05 ppbv and ± 0.4 ppbv respectively. SO_2 was measured using a pulsed UV fluorescence analyzer (TEI Model 43iTL), which offers an LOD of 0.05 ppbv and a precision of ± 0.2 ppbv. In Chengdu, the same measurement methods were applied, but different instrument models were used. O_3 was measured with an ECOTECH EC9810 UV photometric analyzer and the LOD and precision for O_3 were 0.4 ppbv and ± 1.0 ppbv

respectively. CO was measured with an ECOTECH EC9830 nondispersive infrared analyzer, which offers a LOD of 50 ppbv and a precision of ± 0.1 ppbv. NO-NO_2-NO_x was measured using a TEI Model T200U chemiluminescence analyzer with an LOD of 0.05 ppbv and a precision of ± 5.0 ppbv. SO_2 was measured with an ECOTECH EC9850 pulsed UV fluorescence analyzer, and the LOD and precision were 0.5 ppbv and ± 0.5 ppbv respectively. Meteorological parameters, including solar radiation, relative humidity, temperature, wind speed, and wind direction, were also recorded. At the Beijing and Shanghai sites, QS/T 1-2000 model weather stations were used, while HX-2000 model mini weather stations were deployed at the Wuhan, Chengdu, and Lanzhou sites. Detailed information is available in previous study(X. F. Liu et al., 2021; She et al., 2024).

Simultaneously, VOC samples were collected in pre-evacuated 2-L canisters at two-hour intervals from 08:00 to 20:00 local time. The VOC samples were analyzed using GC-MSD-ECD-FID, with detection limits ranging from 2 to 56 pptv. In total, 207 VOC samples were collected across the five cities. Carbonyl samples were collected using silica cartridges impregnated with acidified DNPH on selected days in five cities during August 2018. Sampling was conducted at six intervals each day: 08:00–10:00, 10:00–12:00, 12:00–14:00, 14:00–16:00, 16:00–18:00, and 18:00–20:00 local time. During each interval, air was drawn through the cartridges for 120 minutes at a flow rate of 0.5 L min^{-1}, resulting in a total of 209 carbonyl samples. After collection, all cartridges were stored at 4 °C until analysis. The carbonyl compounds trapped on the cartridges were eluted with acetonitrile and subsequently analyzed using HPLC equipped with an ultraviolet detector (PerkinElmer Series 2000, MA, USA). Sixteen carbonyl species were identified and quantified according to the USEPA Method TO-11A. All target compounds exhibited strong linear correlations between standard concentrations and instrument responses (R^2 > 0.999). The detection limits for the carbonyl species ranged from 1 to 6 pptv. Further details regarding the carbonyl sampling and analytical procedures can be found in our previous publication. (X. F. Liu et al., 2021; X. F. Liu et al., 2019; Y. Wang et al., 2018).

Table 3.4 Details of instruments used for trace gas observation at the five sampling sites (Unit for limit of detection (LOD) and precision: ppbv).

		Beijing	Chengdu	Lanzhou	Shanghai	Wuhan
O_3 analyzer	Model	TEI Model TE49i	ECOTECH EC9810	HJ 654-2013	TEI Model TE49i	HJ 654-2013
	LOD	0.5	0.4	2	0.5	2
	Precision	± 1.0	± 1.0	± 10	± 1.0	± 10
CO analyzer	Model	TEI Model 48iTL	ECOTECH EC9830	HJ 654-2013	TEI Model 48iTL	HJ 654-2013
	LOD	0.04	0.05	0.5	0.04	0.5
	Precision	± 0.1	± 0.1	± 1.0	± 0.1	± 1.0
NO-NO_2-NO_x analyzer	Model	TEI Model 42iTL	TEI Model T200U	HJ 654-2013	TEI Model 42iTL	HJ 654-2013
	LOD	0.05	0.05	2	0.05	2
	Precision	± 0.4	± 5.0	± 10	± 0.4	± 10
SO_2 analyzer	Model	TEI Model 43iTL	ECOTECH EC9850	HJ 654-2013	TEI Model 43iTL	HJ 654-2013
	LOD	0.05	0.5	2	0.05	2
	Precision	± 0.2	± 0.5	± 10	± 0.2	± 10

3.2.4 Chemical analysis of VOCs/Carbonyls

VOC analysis for the 2018 samples was conducted at The Hong Kong Polytechnic University (HKPolyU). The laboratory at HKPolyU utilized the same GC-MSD/FID/ECD system as the Rowland/Blake laboratory at the University of California, Irvine (UCI), which has been a leader in whole air VOC analysis since the 1970s (Colman et al., 2001; Simpson et al., 2010). A total of 59 individual VOCs were quantified from the canister samples using GC-MSD/FID/ECD system. Two separate gas chromatograph units were employed. In the first unit (GC-1), 250 mL of air from each canister was concentrated and then split into two streams: one analysed by the mass selective detector (MSD) and the other by the electron capture detector (ECD). In the second unit (GC-2), air samples were concentrated at low temperatures before analysis by the flame ionization detector (FID).

$$x_2\bar{x}\text{Audit Accuracy, \%} = \frac{\text{Spiked Value} - \text{Observed Value}}{\text{Spiked Value}} \times 100$$

The measure of replicate precision used in this study is the absolute value of the difference between replicate measurements of the sample divided by the average value and expressed as a percentage as follows:

$$\text{Percent difference} = \frac{|x_1 - x_2|}{\bar{x}} \quad (3.1)$$

where: x_1 = First measurement value.

x_2 = Second measurement value.

$\bar{x}$ = Average of the two values.

Performance criteria of replicate precision: within 25%.

A measure of analytical accuracy is the degree of agreement with audit standards. Audit accuracy is defined as the difference between the nominal concentration of the audit compound and the measured value divided by the audit value and expressed as a percentage, as illustrated in the following equation:

$$\text{Audit Accuracy, \%} = \frac{\text{Spiked Value} - \text{Observed Value}}{\text{Spiked Value}} \times 100 \quad (3.2)$$

Performance criteria of audit accuracy is within 30 percent for concentration normally expected in contaminated ambient air (0.5 to 25ppbv).

The method detection limit (MDL) is defined for each system by making seven replicate measurements of the compound of interest at a concentration near (within a factor of five) the expected detection limit, computing the standard deviation for the seven replicate concentrations, and multiplying this value by 3.14. Performance criteria of MDL is $\leq$ 0.5 ppbv.

The limit of detection (LOD) for each procedure was defined as the lowest amount of analyte that could be detected, though not necessarily quantified as an exact value. The noise level was estimated as the standard deviation of the blank, and both noise and signal were measured manually from the chromatogram printout. The LOD corresponded to a signal-to-noise ratio of 3.

Table 3.5 summarizes the MDL, precision, and accuracy for all 59 VOCs, which include 27 alkanes, 17 alkenes, 1 alkyne, and 14 aromatics. In this study, the precision was consistently below 8.24 %, and the accuracy was below 9.25 %. Carbonyl analysis for the 2018 samples was also conducted at HKPolyU using HPLC system. Table 3.6 presents the MDL and LOD for all 16 carbonyls; the LOD was consistently below 50 pptv, and the MDL was below 8 pptv.

Table 3.5 The method detection limit, precision and accuracy of 59 VOC species analyzed by GC-MSD/ECD/FID system.

Species	MDL(ppt)	Replicate Precision	Audit Accuracy
Alkanes			
Ethane	31.11	2.74 %	0.71 %
Propane	23.18	2.32 %	-3.26 %
***i*-Butane**	28.46	7.16 %	2.69 %
***i*-Pentane**	18.02	2.81 %	2.68 %
Methylcyclohexane	9.17	1.11 %	9.25 %
***n*-Butane**	55.77	4.57 %	3.14 %
***n*-Decane**	17.89	4.41 %	-7.12 %
***n*-Heptane**	10.71	2.17 %	-5.58 %
***n*-Hexane**	8.52	4.40 %	5.79 %
***n*-Nonane**	10.19	3.49 %	-0.74 %
***n*-Octane**	10.81	1.29 %	-2.72 %
***n*-Pentane**	10.54	2.54 %	2.97 %
2,2,4-Trimethylpentane	7.8	3.06 %	1.62 %
2,2-Dimethylbutane	18.88	2.79 %	2.28 %
2,3,4-Trimethylpentane	7.77	8.24 %	-8.88 %
2,3-Dimethylbutane	15.69	6.33 %	-8.29 %
2,3-Dimethylpentane	7.05	1.99 %	3.86 %
2,4-Dimethylpentane	10.75	1.76 %	4.43 %
2-methyl-2-Butene	8.89	6.87 %	0.00 %
2-Methylheptane	2.57	0.95 %	-8.78 %
2-Methylhexane	9.46	1.12 %	-3.03 %
2-Methylpentane	16.04	2.09 %	1.64 %
3-Methylheptane	6.58	0.88 %	-4.02 %
3-Methylhexane	16.21	0.23 %	-5.79 %
3-Methylpentane	16.84	3.03 %	2.28 %
Cyclohexane	8.31	0.62 %	-4.10 %

Cyclopentane	18.95	1.58 %	0.79 %
Alkenes and Alkynes			
Ethene	30.02	0.86 %	-3.11 %
Ethyne	34.12	2.41 %	3.11 %
Propene	53.78	5.79 %	2.70 %
1,3-Butadiene	18.97	6.41 %	-7.47 %
1-/*i*-Butene	36.39	5.71 %	4.53 %
1-Pentene	35.49	3.05 %	3.72 %
***trans*-2-Butene**	55.84	5.79 %	2.87 %
***trans*-2-Pentene**	9.4	5.48 %	-7.59 %
***cis*-2-Butene**	15.02	2.50 %	0.16 %
***cis*-2-Pentene**	15.59	3.25 %	3.54 %
Cyclopentene	20.44	1.27 %	2.58 %
2-methyl-1-Butene	22.91	0.44 %	-1.45 %
2-methyl-1-Pentene	13.14	1.66 %	2.39 %
3-methyl-1-Butene	21.21	2.80 %	1.93 %
4-methyl-1-Pentene	15.14	1.78 %	1.77 %
Isoprene	21	3.23 %	7.43 %
α-Pinene	13.16	4.17 %	-3.47 %
β-Pinene	13.07	2.70 %	2.68 %
Aromatics			
Benzene	18.14	0.08 %	3.56 %
Toluene	10.53	0.24 %	-6.58 %
***m/p*-Xylene**	17.79	1.67 %	-6.32 %
***o*-Xylene**	10.8	1.69 %	-4.16 %
Styrene	4.97	0.42 %	-2.15 %
Ethylbenzene	12.66	2.14 %	-3.85 %
***o*-Ethyltoluene**	15.19	6.05 %	-7.21 %
***m*-Ethyltoluene**	12.76	3.53 %	8.32 %
***p*-Ethyltoluene**	8.95	4.77 %	7.03 %

***i*-Propylbenzene**	12.2	6.49 %	-0.87 %
***n*-Propylbenzene**	16.96	3.66 %	-5.86 %
1,2,3-Trimethylbenzene	17.18	5.15 %	-4.50 %
1,2,4-Trimethylbenzene	15.12	4.49 %	8.77 %
1,3,5-Trimethylbenzene	14.42	5.30 %	8.34 %

Table 3.6 The method detection limit and limit of detection of 16 OVOC species analyzed by HPLC system.

Species	MDL(ppbv)	LOD(ppbv)
Formaldehyde	5.88	1.05
Acetaldehyde	7.02	8.46
Acetone	1.47	16.68
Acrolein	6.73	15.38
Propionaldehyde	6.95	17.90
Crotonaldehyde	0.72	23.22
2-butanone	4.37	39.82
i-+n-bBtyraldehyde	1.35	23.01
Benzaldehyde	0.47	25.65
i-Pentanal/i-Valeraldehyde	3.51	24.24
n-Pentanal/n-Valeraldehyde	1.33	21.19
o-TolBaldehyde	3.35	32.05
m-TolBaldehyde	4.83	30.43
p-TolBaldehyde	2.92	31.30
n-hexaldehyde	1.20	32.54
2,5-Dimethylbenzaldehyde	4.27	47.92

3.3 Model descriptions and configurations

3.3.1 Photochemical box model

3.3.1.1 Model description

A Photochemical Box Model coupled with the Master Chemical Mechanism (PBM-MCM) was employed to simulate O_3 photochemistry and assess the influence of meteorological conditions on the reaction rates of O_3 precursors. The MCM (v3.3.1) encompasses approximately 17,000 reactions and 6,600 intermediate species, providing a comprehensive description of homogeneous gas-phase reactions in the atmosphere (Jenkin, 2003; Jenkin, 1997; Lam et al., 2013; Saunders, 2003). In addition to chemical reactions, the model incorporates parameters such as photolysis rates, dry deposition rates, boundary layer development, and aloft exchange. The geographic coordinates of the sampling site and observed solar radiation were also input into the model, enabling calculation of photolysis rates via the tropospheric ultraviolet and visible radiation module (X. F. Liu et al., 2019; Lyu et al., 2016a; Lyu et al., 2019; Y. Wang et al., 2018; Y. Wang et al., 2017). The PBM-MCM has been widely applied in various Chinese cities, and its robust performance in simulating in situ photochemistry has been well documented (X. F. Liu et al., 2019; Lyu et al., 2016a; Lyu et al., 2019; Y. Wang et al., 2018; Y. Wang et al., 2017).

The heterogeneous uptake of HO_2 by aerosols was parameterized following the approaches described in previous studies (Tan et al., 2020; Yang et al., 2022). The loss rate of HO_2 due to aerosol uptake was calculated as:

$$L_{(HO_2)het} = 0.25\,\gamma_{eff} v_{HO_2} ASA [HO_2] \tag{3.3}$$

where γ_{eff} is the effective uptake coefficient, parametrizes the influence of both physical and chemical processes and varies in the highly uncertain range of 0-1 (Song et al., 2021). In this study, we adopted a γ values of 0.08, which have been used in the previous study (Li et al., 2025; Tan et al., 2020; Yang et al., 2022), to evaluate the impact of HO_2 uptake on radical

concentrations. ν_{HO2} is the mean molecular velocity of HO_2, and in this study, ν_{HO2} was calculated by temperature and we applied the value of 4.44×10^5 cm s^{-1} at 25 °C, consistent with the value used in previous study (Tan et al., 2020). ASA is the aerosol surface area concentration. In the absence of direct ASA measurements, ASA was estimated by multiplying the mass concentration of $PM_{2.5}$ by 20, as suggested by previous studies (X. Chen et al., 2019; Tan et al., 2020; X. Wang et al., 2017; Yang et al., 2022).

The index of agreement (IOA) is commonly used to evaluate model performance, with values ranging from 0 to 1. A higher IOA value indicates better model performance (X. F. Liu et al., 2021; X. F. Liu et al., 2019; Lyu et al., 2016c; Lyu et al., 2019; Y. Wang et al., 2018; Y. Wang et al., 2017). The calculation equation is shown below:

$$\mathrm{IOA} = 1 - \frac{\sum_{i=1}^{n}(O_i - S_i)^2}{\sum_{i=1}^{n}(|O_i - \tilde{O}| + |S_i - \tilde{O}|)^2} \quad (3.4)$$

where S_i and O_i are simulated and observed values, respectively; $\tilde{O}$ represents the averages of all observed values, and n is the number of samples.

The net O_3 production rate (P_{O_3-NO}) is defined as the difference between gross production rate of O_3 (G_{O_3-NO}) and destruction rate of O_3 (D_{O_3-NO}) (Equation 3.5). G_{O_3-NO} is produced by the reactions of HO_2 + NO and RO_2 + NO (Equation 3.6). D_{O_3-NO} is formed by the reactions of HO_2 + O_3, OH + O_3, $O(^1D)$ + H_2O, OH + NO_2, and alkenes + O_3 (Equation 3.7). The k values represent the reactions rates, $O(^1D)$, NO, and NO_2 are assumed to be at the instantaneous steady state.

$$P_{O_3-NO} = G_{O_3-NO} - D_{O_3-NO} \quad (3.5)$$

$$G_{O_3-NO} = k_{HO_2+NO}[HO_2][NO] + \sum k_{RO_2+NO}[RO_2][NO] \quad (3.6)$$

$$D_{O_3-NO} = k_{HO_2+O_3}[HO_2][O_3] + k_{OH+O_3}[OH][O_3] + k_{O(^1D)+H_2O}[O(^1D)][O_3] + k_{OH+NO_2}[OH][NO_2] + k_{alkenes+O_3}[alkenes][O_3] \quad (3.7)$$

In this study, the sources of RO_x were identified as follows: photolysis of HONO (HONO + *hv*), photolysis of O_3 ($O(^1D)$ + H_2O), photolysis of H_2O_2, photolysis of OVOCs (including HCHO + *hv* and other OVOCs + *hv*), and ozonolysis of alkenes (O_3 + alkenes). (Ling et al., 2014). Criegee intermediates (CIs), generated from the reaction between O_3 and alkenes, can rapidly decompose into OH and HO_2, serving as a significant source of radicals. To assess the contribution of CIs to RO_x formation, the simulated reaction rates of the CI pathway and other intermediate pathways were extracted from the model results for further analysis.

The PBM-MCM model was also employed to simulate the production and destruction pathway rates of formaldehyde, acetaldehyde, and acetone. The net production rate of formaldehyde was determined by subtracting the total destruction rate from the gross production rate, as described in Equation 3.8. The gross production rate of formaldehyde was calculated as the sum of the oxidation rates of CH_3O and other RO, the reaction rates of carbonyls with OH, the oxidation rates of carbonyls, the reaction rates of alkenes with O_3, and other radical reactions, including those involving RO_2, RCO_3, Criegee intermediates, and chloride (as listed in Table 3.7), as shown in Equation 3.9. Conversely, the total destruction rate of formaldehyde was determined by summing the rates of formaldehyde photolysis, its reaction with OH, and its reaction with NO_3, as outlined in Equation 3.10. The production and destruction pathway rates for acetaldehyde and acetone are presented in Equations 3.11 to 3.16.

$$P_{HCHO} = G_{HCHO} - D_{HCHO} \tag{3.8}$$

$$G_{HCHO} = k_{CH_3O+O_2}[CH_3O][O_2] + \sum k_{RO+O_2}[RO][O_2] + \sum k_{OVOCs+OH}[Carbonyls][OH] + \sum k_{hv+OVOCs}[OVOCs] + \sum k_{Alkenes+O_3}[Alkenes][O_3] + Others \tag{3.9}$$

$$D_{HCHO} = k_{hv+HCHO}[HCHO] + k_{HCHO+OH}[HCHO][OH] + k_{HCHO+NO_3}[HCHO][NO_3] \tag{3.10}$$

$$P_{CH3CHO} = G_{CH3CHO} - D_{CH3CHO} \tag{3.11}$$

$$G_{CH3CHO} = \sum k_{RO+O_2}[RO][O_2] + \sum k_{Carbonyls+OH}[OVOCs][OH] + \sum k_{hv+Carbonyls}[Carbonyls] + \sum k_{Alkenes+O_3}[Alkenes][O_3] + Others \tag{3.12}$$

$$D_{CH3CHO} = k_{hv+CH3CHO}[CH3CHO] + k_{CH3CHO+OH}[CH3CHO][OH] + k_{CH3CHO+NO_3}[CH3CHO][NO_3] \quad (3.13)$$

$$P_{CH3COCH3} = G_{CH3COCH3} - D_{CH3COCH3} \quad (3.14)$$

$$G_{CH3COCH3} = \sum k_{RO+O_2}[RO][O_2] + \sum k_{Carbonyls+OH}[Carbonyls][OH] + \sum k_{hv+Carbonyls}[Carbonyls] + \sum k_{Alkenes+O_3}[Alkenes][O_3] + Others \quad (3.15)$$

$$D_{CH3COCH3} = k_{hv+CH3COCH3}[CH3COCH3] + k_{CH3COCH3+OH}[CH3COCH3][OH] \quad (3.16)$$

The relative incremental reactivity (RIR) values were defined as the relative change in the net O_3 production rate resulting from variations in the concentrations of O_3 precursors. (Cardelino & Chameides, 1995; Lyu et al., 2016a; Y. Wang et al., 2018; Y. Wang et al., 2017; Xue, Wang, Louie, et al., 2014). These values were used to assess the sensitivity of O_3 production to its precursors. The RIR value is calculated as follows:

$$\mathrm{RIR(X)} = \frac{[\mathrm{P_{O_3}(X) - P_{O_3}(X - \Delta X)}]/\mathrm{P_{O_3}(X)}}{\frac{\Delta \mathrm{S(x)}}{\mathrm{S(x)}}} \quad (3.17)$$

where X represents a specific O_3 precursor (*i.e.*, individual VOC species, NO_x, or CO), S(X) stands for the measured concentration of X, and ΔS(X) is hypothetical change in the concentration of X. In the study, we applied 10 % S(X) as the hypothetical change, $\mathrm{P_{O_3}(X)}$ and $\mathrm{P_{O_3}(X - \Delta X)}$ denote the O_3 production in base run and scenario with ΔS(X) for X species, respectively (X. F. Liu et al., 2021; X. F. Liu et al., 2019; Lyu et al., 2016c; Lyu et al., 2019; Y. Wang et al., 2018; Y. Wang et al., 2017).

Table 3.7 Detailed reactions of other production pathways of carbonyls.

No.	Reactions	Constant	No.	Reactions	Constant
	Other production pathways of HCHO			**Other production pathways of CH3CHO**	
1	CH3O2=HCHO	2*KCH3O2*RO2*0.5*(1-7.18*EXP(-885/TEMP))	**1**	C2H5O2=CH3CHO	2*(KCH3O2*6.4D-14)@0.5*RO2*0.2
2	GLYOOB=HCHO	KDEC*0.20	**2**	C3DBCO3+HO2=CH3CHO+HO2+CO+OH	KAPHO2*0.44
3	CH3C2H2O2=HCHO+CH3O2+CO	KDEC*0.65	**3**	C3DBCO3+NO=CH3CHO+HO2+CO+NO2	KAPNO
4	HOCH2CO3=HCHO+HO2	1.00D-11*0.7*RO2	**4**	C3DBCO3+NO3=CH3CHO+HO2+CO+NO2	KRO2NO3*1.74
5	CH2OO+CO=HCHO	1.20D-15	**5**	C3DBCO3=CH3CHO+HO2+CO	1.00D-11*RO2*0.7
6	CH2OO+NO=HCHO+NO2	1.00D-14	**6**	CH3CHOHCO3+HO2=CH3CHO+HO2+OH	KAPHO2*0.44
7	CH2OO+NO2=HCHO+NO3	1.00D-15	**7**	CH3CHOHCO3+NO=CH3CHO+HO2+NO2	KAPNO
8	CH2OO+SO2=HCHO+SO3	7.00D-14	**8**	CH3CHOHCO3+NO3=CH3CHO+HO2+NO2	KRO2NO3*1.74
9	CH2OO=HCHO+H2O2	6.00D-18*H2O	**9**	CH3CHOHCO3=CH3CHO+HO2	1.00D-11*RO2
10	GLYOOA=HCHO	KDEC*0.125	**10**	C4NO3COOOH+NO3=CH3CHO+GLYOX	KNO3AL*4.0
11	CNO3OCL=HCHO+NO2+CO+CL	J<15>	**11**	CH3CHOO+CO=CH3CHO	1.20D-15
12	CH2OHCOCL=HCHO+HO2+CL+CO	J<15>	**12**	CH3CHOO+NO=CH3CHO+NO2	1.00D-14
13	NO3CH2CO3+HO2=HCHO+NO2+OH	KAPHO2*0.44	**13**	CH3CHOO+NO2=CH3CHO+NO3	1.00D-15
14	NO3CH2CO3+NO=HCHO+NO2+NO2	KAPNO	**14**	CH3CHOO+SO2=CH3CHO+SO3	7.00D-14
15	NO3CH2CO3+NO3=HCHO+NO2+NO2	KRO2NO3*1.74	**15**	CH3CHOO=CH3CHO+H2O2	6.00D-18*H2O

16	NO3CH2CO3=HCHO+NO2	1.00D-11*0.7*RO2	**16**	MGLOOB=CH3CHO	KDEC*0.125
17	CH3C2H2O2=CH3CO3+HCHO	KDEC*0.35	**17**	MGLOOA=CH3CHO	KDEC*0.20
18	MACROOA=CH3CO3+HCHO+HO2	KDEC*0.095	**18**	PRNO3CO3+HO2=CH3CHO+NO2+OH	KAPHO2*0.44
19	MVKOOA=CH3O2+HCHO+CO+HO2	KDEC*0.095	**19**	PRNO3CO3+NO=CH3CHO+NO2+NO2	KAPNO
20	HOCH2CO3+HO2=HO2+HCHO+OH	KAPHO2*0.44	**20**	PRNO3CO3+NO3=CH3CHO+NO2+NO2	KRO2NO3*1.74
21	MGLOOA=CH3CO3+HCHO+HO2	KDEC*0.20	**21**	PRNO3CO3=CH3CHO+NO2	1.00D-11*0.7*RO2
22	ISOPBO2=MVK+HCHO+OH	1.04D11*EXP(-9746/TEMP)	**Other production pathways of CH3COCH3**		
23	ISOPDO2=MACR+HCHO+OH	1.88D11*EXP(-9752/TEMP)	**1**	MBOOOA=CH3COCH3+HO2+CO+OH	KDEC*0.36
24	C524O2=HMACR+HCHO+OH	1.88D11*EXP(-9752/TEMP)	**2**	MBOOOA=CH3COCH3+HO2+HO2	KDEC*0.20
25	C3NO3COO=NO3CH2CO3+HCHO	KDEC	**3**	IC3H7O2=CH3COCH3	2*(KCH3O2*1.6D-12*EXP(-2200/TEMP)*0.5*RO2*0.2
26	HMACO3+HO2=HOCH2CO3+HCHO+OH	KAPHO2*0.44	**4**	IPRHOCO3+HO2=CH3COCH3+HO2+OH	KAPHO2*0.44
27	HMACO3+NO=HOCH2CO3+HCHO+NO2	KAPNO	**5**	IPRHOCO3+NO=CH3COCH3+HO2+NO2	KAPNO
28	HMACO3+NO3=HOCH2CO3+HCHO+NO2	KRO2NO3*1.74	**6**	IPRHOCO3+NO3=CH3COCH3+HO2+NO2	KRO2NO3*1.74
29	HMACO3=HOCH2CO3+HCHO	1.00D-11*RO2*0.7	**7**	IPRHOCO3=CH3COCH3+HO2	1.00D-11*RO2*0.7
30	C5COCHOO=CHOC2CO3+HCHO	KDEC	**8**	CH3CCH3OO+CO=CH3COCH3	1.20D-15

31	C6135COO=CHOC3COCO3+HCHO	KDEC	**9**	CH3CCH3OO+NO=CH3COCH3+NO2	1.00D-14
32	CHOC3COO=HCOCH2CO3+HCHO	KDEC	**10**	CH3CCH3OO+NO2=CH3COCH3+NO3	1.00D-15
33	C5124COO=C312COCO3+HCHO	KDEC	**11**	CH3CCH3OO+SO2=CH3COCH3+SO3	7.00D-14
34	C522CO3+HO2=CHOC2CO3+HCHO+OH	KAPHO2*0.44	**12**	CH3CCH3OO=CH3COCH3+H2O2	6.00D-18*H2O
35	C522CO3+NO=CHOC2CO3+HCHO+NO2	KAPNO	**13**	CO2C3OOA=CH3COCH3	KDEC*0.2
36	C522CO3+NO3=CHOC2CO3+HCHO+NO2	KRO2NO3*1.74	**14**	MPRBNO3CO3+HO2=CH3COCH3+NO2+OH	KAPHO2*0.44
37	C522CO3=CHOC2CO3+HCHO	1.00D-11*RO2*0.7	**15**	MPRBNO3CO3+NO=CH3COCH3+NO2+NO2	KAPNO
38	C46CO3+HO2=HOC2H4CO3+HCHO+OH	KAPHO2*0.44	**16**	MPRBNO3CO3+NO3=CH3COCH3+NO2+NO2	KRO2NO3*1.74
39	C46CO3+NO=HOC2H4CO3+HCHO+NO2	KAPNO	**17**	MPRBNO3CO3=CH3COCH3+NO2	1.00D-11*0.7*RO2
40	C46CO3+NO3=HOC2H4CO3+HCHO+NO2	KRO2NO3*1.74	**18**	MEK2OOA=CH3COCH3	KDEC*0.255
41	C46CO3=HOC2H4CO3+HCHO	1.00D-11*RO2*0.7	**19**	MIBK3COO=CH3COCH3+CH3CO3+CO	KDEC
42	ACO3+HO2=HO2+CO+HCHO+OH	KAPHO2*0.44	**20**	C3ME3CHOO=HCOCH2O2+CH3COCH3	KDEC
43	ACO3+NO=HO2+CO+HCHO+NO2	KAPNO			
44	ACO3+NO3=HO2+CO+HCHO+NO2	KRO2NO3*1.74			
45	ACO3=HO2+CO+HCHO	1.00D-11*0.7*RO2			
46	ACROOA=HO2+CO+HCHO+CO+OH	KDEC*0.08			
47	ACROOA=HO2+CO+HCHO+HO2	KDEC*0.34			
48	HOCH2CO3+NO=NO2+HO2+HCHO	KAPNO			
49	HOCH2CO3+NO3=NO2+HO2+HCHO	KRO2NO3*1.74			

50	NAOOA=HO2+NO2+HCHO	KDEC*0.125
51	GAOOA=HO2+HO2+HCHO	KDEC*0.125
52	MACROOA=OH+CO+CH3CO3+HCHO	KDEC*0.25
53	NAOOA=OH+NO2+CO+HCHO	KDEC*0.57
54	GAOOA=OH+HO2+CO+HCHO	KDEC*0.57

3.3.1.2 Photochemical box model validation in Lanzhou in winter 2018

For the study of wintertime air quality in Lanzhou in 2018, temperature, relative humidity, O_3, NO, NO_2, CO, SO_2, VOCs, and carbonyls data collected at the sampling site in January 2018 were interpolated to a time resolution of 600 seconds and subsequently input into the model to simulate O_3 formation mechanisms. The VOC and carbonyl species included in the model are listed in Tables 3.1 and 3.3; concentrations of other species in these tables were below detection limits. Due to the lack of direct HONO measurements, average diurnal profiles of nitrous acid (HONO) from previous studies in Lanzhou were used in the model simulations, the diurnal profile of HONO used in this work presented in Figure 3.3 (W. Li et al., 2021; N. Wang et al., 2018; W. Zhang et al., 2019; Xinran Zhang et al., 2022).

To quantify the impact of HONO uncertainty on O_3 and OH production and destruction rates, sensitivity tests were conducted by comparing three scenarios: the base scenario (using observed HONO concentrations), the first intervention scenario (doubling HONO concentrations), and the second intervention scenario (excluding HONO). As shown in Figure 3.4a, the net O_3 production rate increased by approximately 8 % in the first intervention scenario compared to the base scenario, while a slight decrease (~7 %) was observed in the second intervention scenario. Photolysis of HONO is a key source of OH radicals (Acker et al., 2006; Czader et al., 2012; Hendrick et al., 2014; Su et al., 2008). Doubling HONO concentrations led to a 4.3 % increase in the daytime average OH production rate (4.4×10^6 molecules cm^{-3} s^{-1}) and a 1.4 % increase in the maximum OH production rate (4.8×10^6 molecules cm^{-3} s^{-1}) compared to the base case. In contrast, omitting HONO resulted in a 2.9 % decrease in the daytime average OH production rate (2.9×10^6 molecules cm^{-3} s^{-1}) and a 1.0 % decrease in the maximum OH production rate (3.5×10^6 molecules cm^{-3} s^{-1}). Overall, the uncertainty in HONO concentrations had a limited impact (less than 5 %) on OH production and destruction, and these uncertainties were quantitatively analysed (Figure 3.4).

The model results indicated that radical concentrations reached statistical equilibrium within 18 hours (Figure 3.5). Therefore, a one-day spin-up period prior to the study period was used to ensure equilibrium in the simulations. Model performance was evaluated by comparing simulated and observed hourly O_3 mixing ratios from January 1 to 31, 2018 (Figure 3.6). The simulated O_3 agreed well with observations, with IOA values of 0.89 on O_3 episode days and 0.86 on non-episode days, consistent with the range reported in previous studies (0.74–0.89)

(X. F. Liu et al., 2021; X. F. Liu et al., 2019; Lyu et al., 2016c; Lyu et al., 2019; Y. Wang et al., 2018; Y. Wang et al., 2017). The model performed better on episode days, likely due to stronger photochemical activity and more intensive O_3 production. The high IOA values suggest that wintertime O_3 pollution in Lanzhou is primarily driven by local formation (Figure 3.6). Some overestimation of simulated daytime O_3 on non-episode days was observed, which can be attributed to the limited consideration of physical processes such as horizontal and vertical dispersion, advection, and mixing in the photochemical box model (X. F. Liu et al., 2021; X. F. Liu et al., 2019; Lyu et al., 2016c; Lyu et al., 2019; Y. Wang et al., 2018; Y. Wang et al., 2017). Additionally, stronger chemical production of O_3 on episode days contributed to the improved model performance in reproducing O_3 concentrations compared to non-episode days.

To assess uncertainties associated with observed alkanes, alkenes, aromatics, carbonyls, and NO_x, sensitivity tests were performed using model simulations (Figures 3.7–3.11). The sensitivities of net O_3 production rates, the percentage contributions of O_3 production and destruction pathways, and RIR values to 15 % changes in alkanes, alkenes, aromatics, and NO_x were calculated, with the percentage change determined by the uncertainty levels of the observed species (Table 4.2). Overall, only limited changes were observed in these parameters, and the diurnal patterns of net O_3 production rates, pathway contributions, and RIR values remained consistent. The increase in daily maximum net O_3 production rate was greatest for a 15 % increase in alkenes (5.30 ppbv h^{-1}), compared to alkanes (3.90 ppbv h^{-1}) and aromatics (4.01 ppbv h^{-1}), indicating that alkenes have the largest impact on O_3 production. Furthermore, the O_3 formation mechanism remained VOC-limited regardless of increases or decreases in VOCs and NO_x.

Due to the limited number of carbonyl samples, the average diurnal variation of carbonyls (including data points at 08:00–10:00, 12:00–14:00, and 16:00–18:00 LT) on O_3 non-episode days was used in the model simulation. Figure 3.11 illustrates the impact of carbonyl uncertainty on simulated O_3 production and destruction rates and RIR values. Scenarios with a 100 % increase in carbonyl concentrations, without carbonyl constraint, and the base scenario were considered. The 100 % increase threshold was chosen because the average O_3 concentration nearly doubled from non-episode (22.7 ± 1.8 ppbv) to episode days (43.1 ± 11.2 ppbv). Generally, doubling carbonyl concentrations increased the maximum daytime net O_3 production rate by only 8.4 % (approximately 4.5 ppbv h^{-1}). The proportions of O_3 formation

and destruction pathways changed by less than 4 % and 1 %, respectively, under the increased and unconstrained carbonyl scenarios. Additionally, the RIR pattern remained unchanged across all scenarios, indicating that O_3 formation remained VOC-limited under these carbonyl variations.

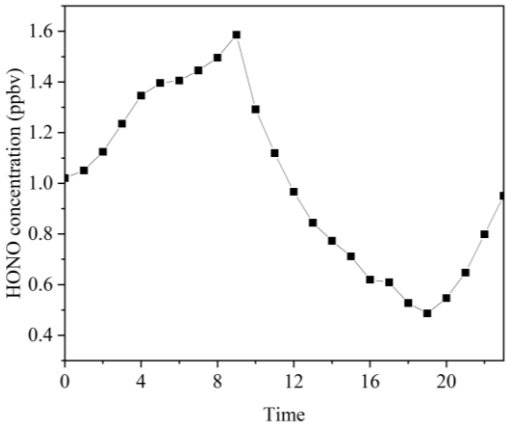

Figure 3.3. Diurnal profile of HONO in Lanzhou

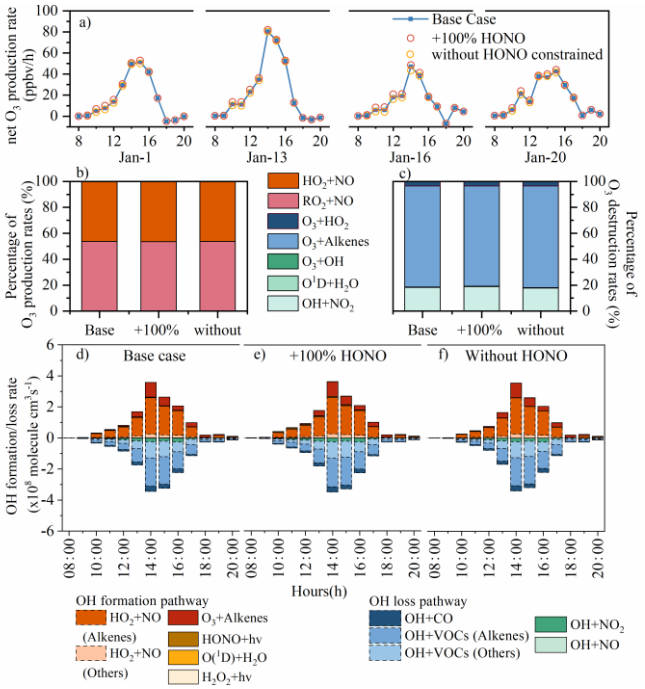

Figure 3.4. Sensitivity test of (a) net O_3 production rates, (b) contribution percentages of O_3 production rates and (c) contribution percentages of O_3 destruction rates, (d) OH

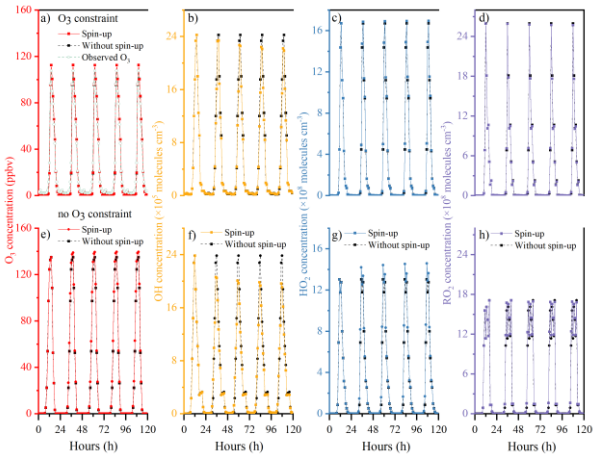

Figure 3.5. The 5-day spin-up simulations of (a) O_3, (b) OH, (c) HO_2, (d) RO_2 concentrations with O_3 constraint and (e) O_3, (f) OH, (g) HO_2, (h) RO_2 concentrations without O_3 constraint on O_3 episode day.

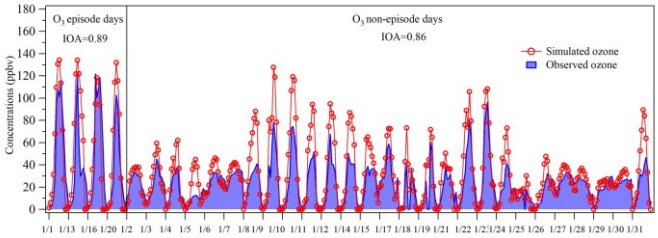

Figure 3.6. Hourly mixing ratios of simulated and observed O_3 in January 2018.

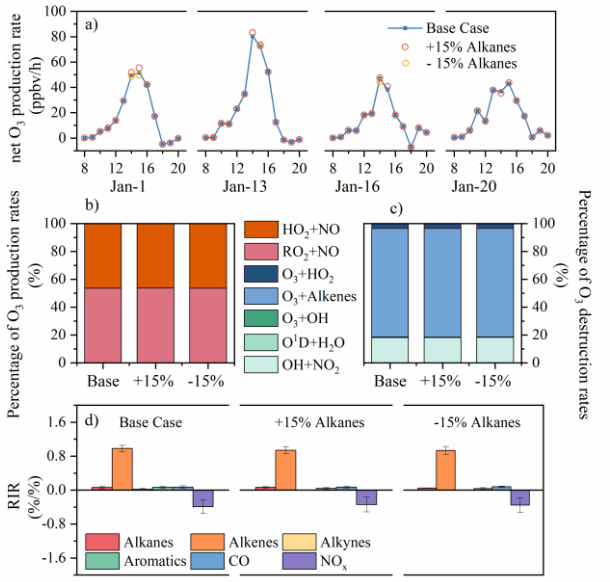

Figure 3.7. Sensitivities of (a) net O_3 production rates, (b) contributions of O_3 production and (c) destruction pathways, (d) RIR values to increase and decrease of 15 % alkanes.

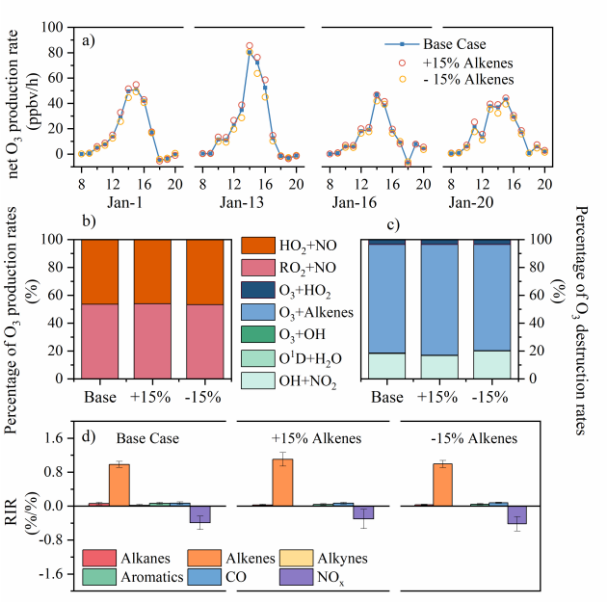

Figure 3.8. Sensitivities of (a) net O_3 production rates, (b) contributions of O_3 production and (c) destruction pathways, (d) RIR values to increase and decrease of 15 % alkenes.

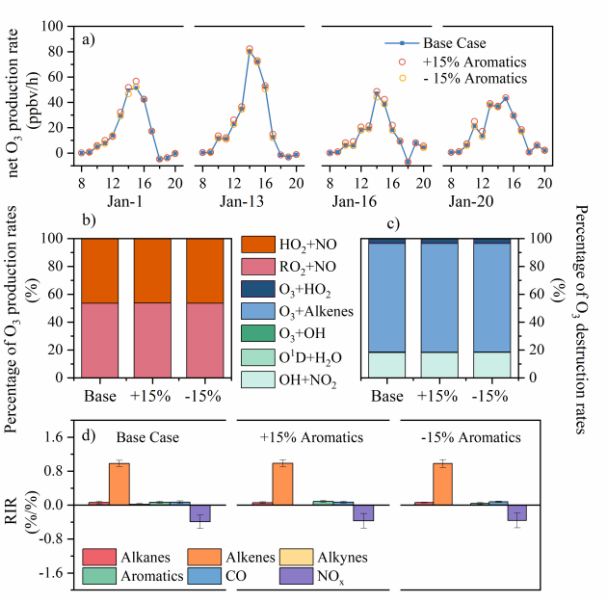

Figure 3.9. Sensitivities of (a) net O_3 production rates, (b) O_3 production rates and (c) O_3 destruction pathways, (d) RIR values to increase and decrease of 15 % aromatics.

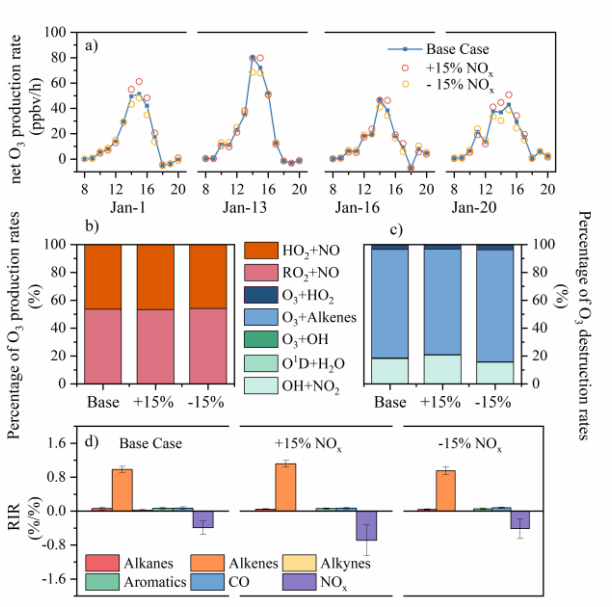

Figure 3.10. Sensitivities of (a) net O_3 production rates, (b) contributions of O_3 production and (c) destruction pathways, (d) RIR values to increase and decrease of 15 % NO_x.

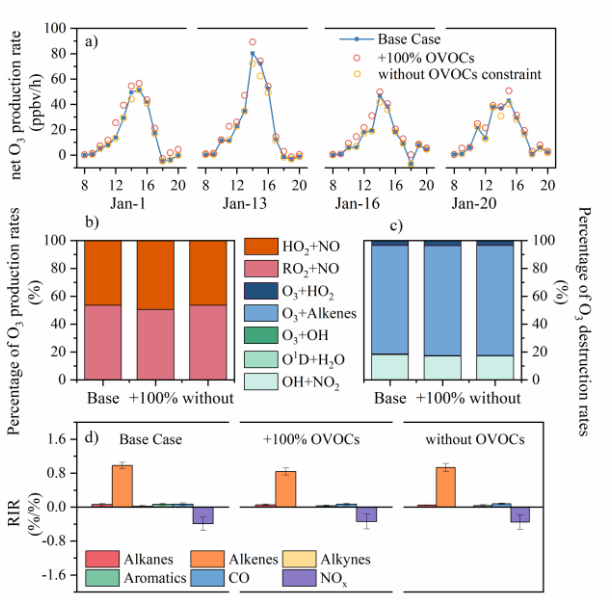

Figure 3.11. Uncertainty test of (a) net O_3 production rates, (b) O_3 production rates and (c) O_3 destruction pathways, (d) RIR values on four O_3 episode days with base case, 2 times carbonyls concentrations, and without carbonyls constraint.

3.3.1.3 Photochemical box model validation in Lanzhou in summer 2013, and 2019-2023

Recognizing that previous analyses of O_3 precursor trends were insufficient to fully explain the observed O_3 variations in Lanzhou during the summers of 2013 and 2019–2023, this study employed the PBM-MCM model to simulate O_3 concentrations under various conditions. Hourly observational data, including temperature, relative humidity, trace gases, and 50 VOCs (comprising 19 alkanes, 15 alkenes, 1 alkyne, and 15 aromatics), were interpolated to a time resolution of 600 seconds and used as model inputs. To ensure the reliability of the simulation results, the IOA was adopted as a performance metric. The IOA values in this study ranged from 0.81 to 0.91, indicating strong agreement between the modeled and observed O_3 concentrations (Figure 3.8 and Table 3.11)

Table 3.8. The IOA information in all days and O_3 episode days in Lanzhou in August 2013, and 2019-2023

	2013	**2019**	**2020**	**2021**	**2022**	**2023**
All	0.90	0.91	0.83	0.85	0.88	0.85
O_3	0.81	0.88	0.85	0.83	0.88	0.83

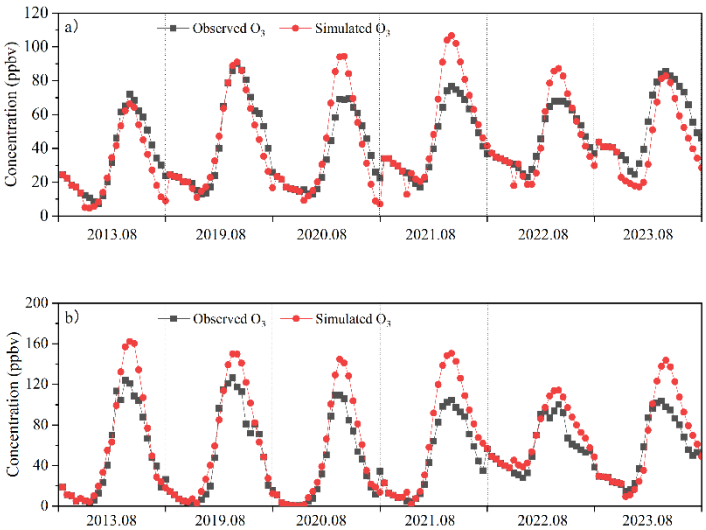

Figure 3.11. The model performance in a) all days and b) O_3 episode days in Lanzhou in August 2013, and 2019-2023.

3.3.1.4 Photochemical box model validation in five cities in summer 2018

Hourly observational data, including temperature, relative humidity, trace gases, 50 VOCs (comprising 19 alkanes, 15 alkenes, 1 alkyne, and 15 aromatics), as well as 3 carbonyls (formaldehyde, acetaldehyde, and acetone), were input into the model. These data were interpolated to a time resolution of 600 seconds. Photolysis parameters were parameterized based on photon fluxes calculated using the Tropospheric Ultraviolet and Visible (TUV) radiation module, while dry deposition module accounted for the removal of air pollutants, with deposition rates averaged over the mixed layer height (MLH), which was set to range from 300 m at night to 1400 m during the day (Lam et al., 2013; X. F. Liu et al., 2019; Lyu et al., 2016a; Lyu et al., 2019; Y. Wang et al., 2018; Y. Wang et al., 2017). To ensure the reliability of the simulation results, the IOA was adopted as a performance metric. The IOA values in this study ranged from 0.79 to 0.91, indicating strong agreement between the modeled and observed O_3 concentrations (Figure 3.11). As radical concentrations typically reach statistical equilibrium within two days (Figure 3.12), a 2-day spin-up period was used prior to the study period to ensure the equilibrium in the model simulations. The model has been extensively applied across many cities in China, and its effectiveness in simulating in-situ photochemistry has been consistently demonstrated (X. F. Liu et al., 2019; Lyu et al., 2016a; Lyu et al., 2019; Y. Wang et al., 2018; Y. Wang et al., 2017).

The simulation results for O_3 closely matched the observed diurnal patterns, with peak concentrations occurring at noon and lower levels in the morning and evening. The IOA values for Beijing, Wuhan, Chengdu, and Lanzhou ranged from 0.74 to 0.88, demonstrating the reliability of the model simulations. Further details can be found in Liu et al. (2021a). The PBM-MCM model was also applied to simulate the production and destruction pathway rates of formaldehyde, acetaldehyde, and acetone, with detailed methodologies provided in Section 3.3.1.1.

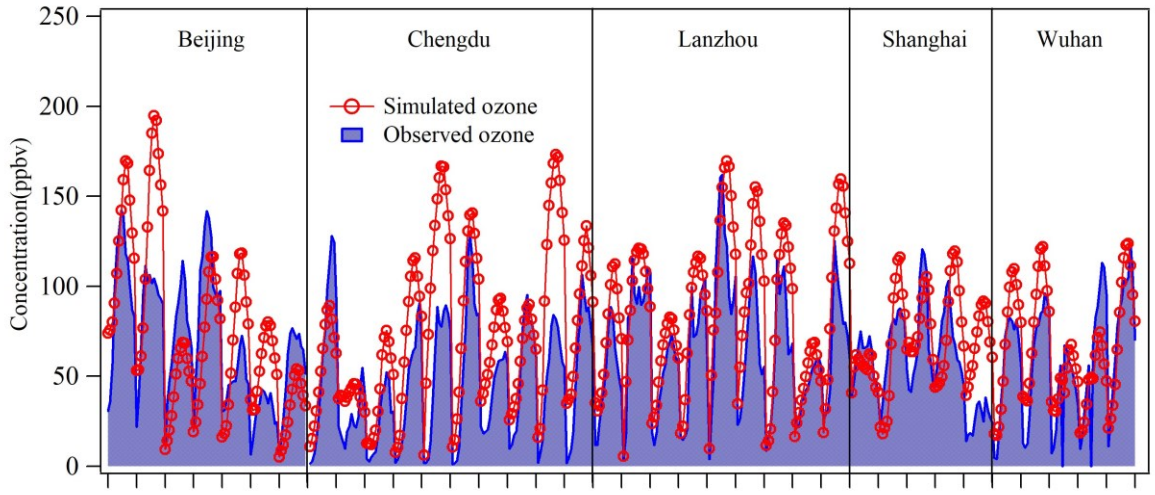

Figure 3.12. The model performance in the five sampling cities.

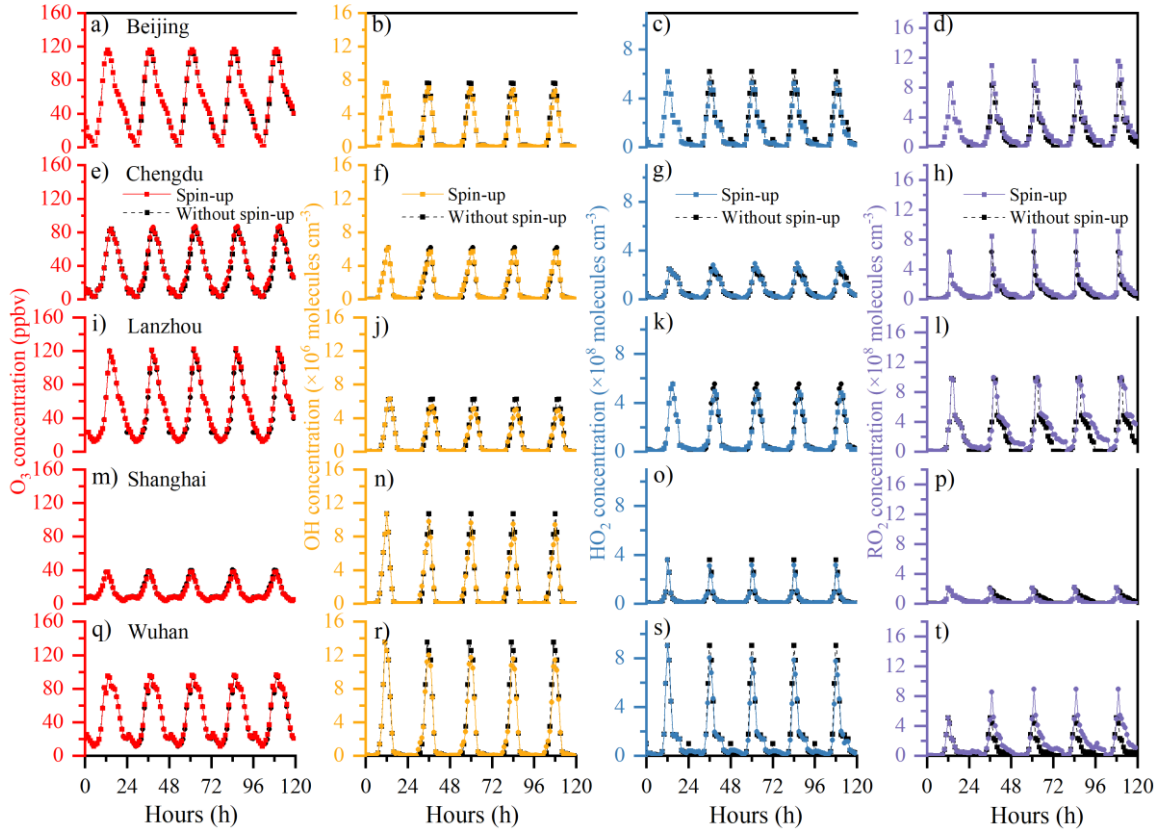

Figure 3.13. The 5-day spin-up simulations of O_3, OH, HO_2, and RO_2 concentrations with O_3 constraint in the five sampling cities.

3.3.2 Positive matrix factorization model

The dataset was analyzed using a receptor model, specifically, the Positive Matrix Factorization (PMF) model 5.0 developed by USEPA. This multivariate factor analysis tool is widely used for receptor-based source apportionment (USEPA, 2017).

The mass balance equation for the PMF model is presented in Equation 3.17 (Ling et al., 2014; Paatero, 1997). The model resolves the matrices of source contributions (G) and source profiles (F) by minimizing the objective function Q, as shown in Equation 3.17:

$$X_{ij} = \Sigma_{k=1}^{p} g_{ik} f_{kj} + e_{ij} \quad (3.17)$$

where x_{ij} means the concentration of species j in sample i, g_{ik} represents the concentration of factor k contribute in sample i, f_{kj} indicates the mass percentage of species j in source k, with p stands for the number of sources of pollution and e_{ij} explains the residual for species j in sample i.

$$Q = \Sigma_{i=1}^{n} \Sigma_{j=1}^{m} \left(\frac{X_{ij} - \Sigma_{k=1}^{p} g_{ik} f_{kj}}{u_{ij}} \right)^2 \quad (3.18)$$

where m and n are the number of species and samples respectively, u_{ij} represents the uncertainty of j species in i sample. Q_{robust} would automatically exclude the points not fit to the model in the calculation, the optimum solution selects by the lowest Q value while Q_{true} would include all the points (Hua et al., 2023; X. F. Liu et al., 2021; X. F. Liu et al., 2019; Y. H. Liu et al., 2019; Lyu et al., 2016b; Song et al., 2018; P. Zeng et al., 2019).

The concentration and uncertainty (unc) files for VOCs were required as input for the PMF model. The uncertainty values can be determined either from observations or calculated using specific equations. In this study, uncertainties were calculated according to Equations 3.19 and 3.20 in the USEPA guidelines:

$$u = \frac{5}{6} \times MDL \ (C \leq MDL) \quad (3.19)$$

$$unc = \sqrt{(Error\ fraction \times concentration)^2 + (0.5 \times MDL)^2} (C > MDL) \quad (3.20)$$

where C means the concentration of VOCs and MDL represents the method detection limit. 10 % error fraction was selected (Hua et al., 2023; X. F. Liu et al., 2021; X. F. Liu et al., 2019; Y. H. Liu et al., 2019; Lyu et al., 2016b; Song et al., 2018; P. Zeng et al., 2019).

As the contributions of different VOC species to carbonyl formation have been quantified by the PBM-MCM model, these results can be integrated with the VOC species profiles of each primary source identified by PMF. This approach allows for the estimation of the contribution of VOCs from each primary source to the secondary carbonyl formation.

C_j indicates the total contribution of VOC species in source *j* to the carbonyl formation, which can be calculated through Equation 3.21.

$$C_j = \sum_i (C_i \times f_{i,j}) \quad (3.21)$$

where C_i means the percentage contribution of VOC species *i* to the carbonyl formation from PBM-MCM results, $f_{i,j}$ denotes the percentage fraction of VOC species *i* in source *j* from PMF source profile.

Based on the PMF results, C_j^{pri} represents the primary contribution of source *j* to carbonyls, while C_{sec} means the total secondary source contribution. Then the contribution of source *j* to the secondary formation of carbonyl compound, as shown in the C_j^{sec}, can be calculated by C_j divided by C_{sec} (Equation 3.22). Therefore, the total contribution of source *j* to carbonyls, C_j^{total}, can be obtained by summing C_j^{pri} and C_j^{sec} (Equation 3.23).

$$C_j^{sec} = C_j \times C_{sec} \quad (3.22)$$

$$C_j^{total} = C_j^{pri} + C_j^{sec} \quad (3.23)$$

The primary and secondary sources of carbonyls can be calculated based on Equations 3.19-21. For example, according to the PMF results for formaldehyde in Beijing in Table 6.8, the industrial source contributes 12.9 %, and the secondary source contributes 43.8 %. The primary contribution of the industrial source to formaldehyde is denoted as C_j^{pri}, while its secondary contribution is extracted from the 43.8 % secondary source (C_{sec}).

Based on the MCM results, propene contributes 20.9 % to formaldehyde formation in Beijing, and according to PMF, 28.5 % of propene originates from the industrial source. Therefore, the contribution of propene from the industrial source to formaldehyde is calculated as 20.9 % × 28.5 %. Similarly, the contributions of other VOC species from the industrial source to formaldehyde formation are calculated in the same method. The total contribution of all VOCs from the industrial source to formaldehyde is calculated using Equation 3.19 ($C_j = \sum_i (C_i \times f_{i,j})$), resulting in 16.9 %.

The secondary contribution of the industrial source to formaldehyde is then calculated using Equation 3.20 ($C_j^{sec} = C_j \times C_{sec}$), which is 16.9 % multiplied by 43.8 %, resulting in 7.4 %.

Therefore, the total contribution of the industrial source to formaldehyde, including both primary and secondary sources, is calculated using Equation 3.21 ($C_j^{total} = C_j^{pri} + C_j^{sec}$), which is 12.9 % plus 7.4 %, resulting in 20.3 %.

3.3.3 Multiple linear regression model

In the atmosphere, compounds originating from similar or identical sources often exhibit strong correlations in their concentrations, consequently, the source apportionment model can be established through multiple linear regression analysis (Friedfeld et al., 2002; Garcia et al., 2006; F. Wang et al., 2024). To evaluate the relative contributions of primary and secondary sources to the observed carbonyl concentrations, this study uses ethyne (C_2H_2) and O_3 as tracers for primary and secondary sources, respectively. C_2H_2 is chosen as a specific tracer for primary sources due to its long lifetime and predominant origin from combustion emissions (Cheng et al., 2024; Yang et al., 2017; L. Zhang et al., 2024). The statistical similarity between carbonyl compounds and acetylene can thus represent the primary contribution to the measured carbonyl concentrations. O_3, as an indicator of photochemical smog, is considered a typical secondary compound in the atmosphere. The contributions of primary and secondary sources to carbonyls can be estimated using a multiple linear regression model, as shown below:

$$[\text{Carbonyl}]=\beta_0+\beta_1 [C_2H_2]+\beta_2 [O_3] \quad (3.24)$$

In this equation, [Carbonyl], [C_2H_2], and [O_3] represent the concentrations of the target carbonyls, C_2H_2, and O_3, respectively. The coefficients β_0, β_1, and β_2 are the regression coefficients of the model. According to this formula, the carbonyl concentration can be divided into three components: background concentration (β_0), primary source contribution (β_1 [C_2H_2]), and secondary production (β_2 [O_3]) (Bao et al., 2022; Friedfeld et al., 2002; Garcia et al., 2006; Li et al., 2014; Li et al., 2010; Lui et al., 2017; Wang et al., 2015; Wu et al., 2023; Yang et al., 2017; Z. Yang et al., 2019).

In the five cities studied, O_3 was used as a tracer for secondary formation, while C_2H_2 served as a tracer of primary emissions. The relative contributions of primary emissions, secondary formation, and background levels in these cities are shown in Table 6.9.

Chapter 4 Wintertime Ozone Surges: The Critical Role of Alkene Ozonolysis

4.1 Introduction

Ground-level ozone (O_3) pollution has attracted public attention in the past decades due to its detrimental impacts on human health, vegetation growth, and climate change (Ainsworth et al., 2012; Ashmore, 2005; Chameides et al., 1999; Simpson et al., 2014; Wang et al., 2007). Tropospheric O_3 concentrations are influenced by photochemical reactions among O_3 precursors (i.e., nitrogen oxides(NO_x = NO + NO_2), volatile organic compounds (VOCs), and carbon monoxide (CO), as well as by regional transport and stratosphere–troposphere exchange (Cape, 2008; Collins, 2003; Jennifer, 1985; X. Lu et al., 2019). In addition to the concentrations of O_3 precursors, the chemical formation of O_3 is highly related to meteorological conditions (i.e., temperature and solar radiation). High temperatures and strong solar radiation are conducive to the chemical production of O_3 (Guo et al., 2009; Guo, Ling, Cheung, Jiang, et al., 2013; L. Li et al., 2016; Li et al., 2015; Lu et al., 2020; T. Wang et al., 2017; Y. Wang et al., 2017). As such, O_3 pollution events are generally concentrated in spring, summer, and autumn but rare in winter (Kgabi, 2012; N. Liu et al., 2019; Maji et al., 2019; Oltmans, 1994). However, a handful of studies have reported O_3 episode events (maximum hourly concentration exceeding 100 ppbv) in winter at specific locations with high surface albedo values and/or heavy precursor emissions (Edwards et al., 2014; Oltmans et al., 2014; Schnell et al., 2009; Singh et al., 1997). For example, in the winter of 1993, hourly O_3 peaks of 100–120 ppbv were discovered in Delhi, India, due to meteorological conditions favorable to the accumulation of air pollutants (Singh et al., 1997). In addition, in February 2008, O_3 pollution events occurred in a natural gas field in Wyoming, the United States of America (USA), (hourly maximum value attaining 140 ppbv) with a daily average temperature of −17 °C. These were attributed to high concentrations of O_3 precursors (i.e., alkanes) trapped by the shallow temperature inversion (Schnell et al., 2009). Moreover, in 2013, due to high snow albedo and strong

carbonyl photolysis, severe O_3 pollution was found in the oil fields of Utah, USA, with a daily average temperature being −8 °C (Edwards et al., 2014; Oltmans et al., 2014).

In China, surprisingly, high O_3 values during cold weather have been widely observed in North China in recent years (Figure 4.1). On the one hand, the reduction in NO_x emissions since 2013 has resulted in enhanced O_3 pollution in the North China Plain (K. Li et al., 2021). On the other hand, large O_3 precursor emissions from oil fields and/or petrochemical industrial areas have led to intensive production of O_3 in winter (S. Y. Chen et al., 2020; Edwards et al., 2014; Ma et al., 2012; Oltmans et al., 2014; Schnell et al., 2009). Specifically, several high O_3 days (maximum hourly values around 80 ppbv) in winter were observed in oil fields in the Yellow River Delta (YelRD) region, which were ascribed to heavy emissions of alkanes during oil extraction operations (T. Chen et al., 2020). In addition, highly reactive VOCs (i.e., ethene, propene, toluene, and xylene) emitted from industry sources, combined with favorable meteorological conditions for the accumulation of air pollutants, led to O_3 pollution (hourly maximum reaching 76 ppbv) in a city in North China during the winter (Zhan et al., 2023). Moreover, it is notable that the highest O_3 concentration was discovered in Lanzhou during winter (Figure 4.1 and Table 4.1), which also experienced the highest frequency of days with high O_3 levels (Figure 4.1b). However, the driving factors of this unique O_3 episode event have not yet been explored.

Lanzhou is a typical industrial city in northwestern China, where the first discovery of photochemical smog dates back to the mid-1970s (Wenkai Guo et al., 2022; X. F. Li et al., 2017; Tang et al., 1985). Apart from the dense air pollutants emitted from the local petrochemical industry (Dong et al., 2021; J. Liu et al., 2020; G. Y. Wang et al., 2020; Yan et al., 2021), Lanzhou's basin topography contributes to poor air quality by creating unfavorable conditions for the diffusion of air pollutants (W. Guo et al., 2022; Jia et al., 2016). Previous research on O_3 pollution in Lanzhou has mainly focused on the relationships between O_3 and its precursors. For example, it was found that the O_3 formation regime at an industrial site in Lanzhou transferred from a NO_x-limited regime to a transitional one in the summer (W. Guo et al., 2022; Jia et al., 2016; X. F. Liu et al., 2021; Xue, Wang, Gao, et al., 2014). In addition, the

contributions of VOCs to O_3 production have been quantified (W. Guo et al., 2022; Jia et al., 2016; X. F. Liu et al., 2021). Specifically, alkenes, especially C_4 alkenes emitted from the petrochemical industry, were identified as the most important contributors to O_3 formation (W. Guo et al., 2022; Henderson et al., 2010). However, these studies solely focused on O_3 formation in the summer, mainly due to the frequent occurrence of high O_3 days under intense solar radiation and high temperatures. On the contrary, the O_3 formation mechanisms in winter have seldom been reported. Therefore, the underlying causes of the extremely high O_3 concentrations observed in cold weather and times of weak solar radiation are worth exploring during wintertime. Furthermore, there is a lack of detailed information about the O_3 formation mechanisms, such as the evolution of O_3 precursors during photochemical reactions and their impacts on radical chemistry.

To fill these knowledge gaps, an intensive sampling campaign of O_3, its precursors, and meteorological parameters was conducted in Lanzhou during the winter of 2018. A photochemical box model incorporating a Master Chemical Mechanism (PBM-MCM) was employed to investigate the relationship between O_3 and weather conditions. More importantly, critical photochemical reactions were studied, including the evolution of VOCs and their contributions to O_3 production. Based on the results, emission control suggestions have been devised for O_3 mitigation in Lanzhou. The findings of this study will draw public attention to winter O_3 pollution and provide new insights into photochemistry with intensive alkene emissions.

Table 4.1. Monthly average O_3, DM8A O_3, number of O_3 episode days (daily maximum O_3 greater than 80 ppbv), temperature, relative humidity, and solar radiation in winter 2015-2022.

Parameter	Value in	Value in
Monthly	18.9 ±	19.7 ±
Average	36.3 ±	37.6 ±
Number of	5	4.5 ±
Monthly	-4.4 ±	-3.1 ±
Monthly	49.3 ±	43.3 ±
Monthly	365.7 ±	408.4

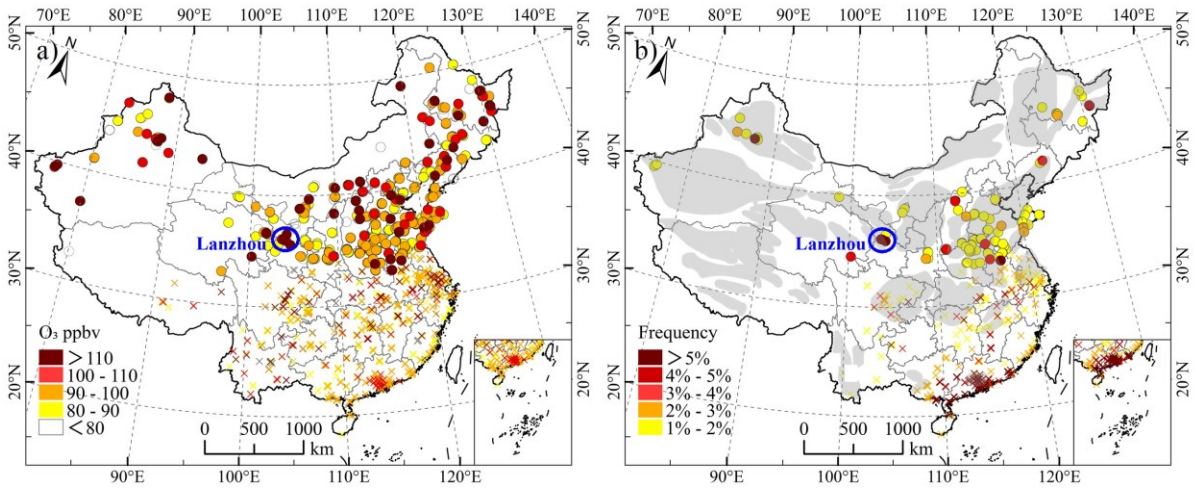

Figure 4.1. (a) Daily maximum O_3 averages (greater than 80 ppbv) and (b) Frequencies of O_3 pollution days (daily maximum O_3 larger than 80 ppbv) in winter days of 2015-2020 in China. Note: dots and crosses represent the sites in North China and South China, respectively; grey shaded areas denote the distribution of oil fields

4.2 Overview of O_3 pollution in winter

4.2.1 Winter O_3 pollution in China

Figure 4.1a presents the daily maximum average O_3 concentrations (>80 ppbv) recorded in winter (defined as December, January, and February) at 1,590 monitoring stations in China during 2015–2020. Surprisingly, 76.3 % of the monitoring stations (1,213 sites) recorded high concentrations of O_3, which sharply contrasts with the traditional understanding that O_3 pollution mainly occurs in the warmer season. Among these stations, 59.6 % were in South China (crossed). The remaining 40.4 % that witnessed high O_3 concentrations were located in North China (dotted), where the meteorological conditions were considered unfavorable for O_3 pollution (i.e., low temperatures and weak solar radiation) (J. Liu et al., 2019; T. Ma et al., 2019; T. Wang et al., 2017; Yan et al., 2024). In addition, 37 % of the stations (452 sites) recorded a frequency of O_3 pollution days (hourly O_3 concentration > 80 ppbv) of more than 1 % during the winter days between 2015 and 2020 (Figure 4.1b). Analyzing the environment surrounding those sites revealed that rural sites were primarily near oil fields (gray-shaded areas) and that the urban sites were generally distributed in cities with petrochemical industries. Notably, Lanzhou experienced the highest frequency of O_3 pollution days (17.8 %). Thus, Lanzhou is an ideal place to investigate the mechanisms underlying winter O_3 pollution.

4.2.2 Winter O_3 pollution in Lanzhou

Figure 4.2 shows a time series of the concentrations of trace gases and VOCs recorded in January 2018. Four O_3 episode days (January 1, 13, 16, and 20, shaded in red) were recorded, with an average daily maximum of 115 ± 8.5 ppbv, despite cold weather and weak solar radiation. The daytime average concentrations of NO and NO_2 were 16.0 ± 4.0 and 31.4 ± 3.4 ppbv, respectively, which were higher than those recorded in other cities in China (Chu et al., 2020; Fu et al., 2020; Gao et al., 2016; K. Li et al., 2021; R. Li et al., 2017), indicating a strong effect of NO titration. Furthermore, there were four more days (January 9–10, 12, and 23, shaded in blue) when the hourly maximum concentration of O_x (O_3 + NO_2) exceeded 100 ppbv.

Overall, the O_3 pollution was severe in Lanzhou that winter, which may have resulted from local photochemical reactions due to high concentrations of O_x.

The concentrations of air pollutants and meteorological conditions recorded on O_3 episode days and non-episode days are compared in Figure 4.3. The average daytime temperature on O_3 episode days (−1.7 ± 1.3 °C) was higher than that on O_3 non-episode days (−5.7 ± 0.5 °C, *t*-test, $p < 0.05$), while the relative humidity on O_3 episode days was lower than that on O_3 non-episode days ($p < 0.05$) (Table 4.2). The solar radiation, wind speed, and planetary boundary layer height (PBLH) levels were comparable ($p > 0.05$). Notably, concentrations of O_3 precursors, including CO, NO, NO_2, and total non-methane volatile organic compounds (TVOCs) were higher on O_3 episode days than on O_3 non-episode days ($p < 0.05$). In particular, the concentration of alkenes was almost 1.5 times that on O_3 non-episode days, and the diurnal pattern of alkene concentration showed an elevated concentration at 14:00 local time (LT) on O_3 episode days, which was significantly higher than that on O_3 non-episode days. However, no such difference was found in meteorological parameters. Thus, it can be speculated that the increase in the alkene concentration was related to local emissions. At relatively high temperatures and low relative humidity levels on O_3 episode days, the large amounts of O_3 precursors might have accelerated O_3 production (Belan & Savkin, 2019; Duan et al., 2008; M. Li et al., 2021; Pusede et al., 2015).

In this study, the average daytime concentration of TVOCs on O_3 episode days was 153.4 ± 19.0 ppbv, which was considerably higher than that recorded at other industrial sites in China, such as Xi'an (85.3 ± 60.6 ppbv), Jiyuan (54.3 ± 27.5 ppbv), Wuhan (44.1 ppbv), Taiwan (64 ppbv), and Guanzhong Plain (42.4–74.3 ppbv) (Hui et al., 2018; J. H. Li et al., 2022; Sun et al., 2020; Tsai et al., 2008; Z. B. Wang et al., 2020). It was even comparable to that recorded at other oilfield sites around the world; for example, the YelRD region (171.2 ± 527.2 ppbv), Junggar Basin (213 ± 97.7 ppbv), Upper Green River Basin (230 ppbv), and Denver-Julesburg Basin (97 ppbv) (T. Chen et al., 2020; Field et al., 2015; Gilman et al., 2013; H. Zheng et al., 2018). Figure 4.4a shows the percentage of VOC groups and the average daytime concentrations of the top 20 VOC species on O_3 episode days. It is worth noting that alkenes

(82.3 ± 13.1 ppbv) accounted for the largest proportion (53.7 ± 8.5 %) of TVOCs, which was different from the results found in other oilfields where alkanes comprised the largest proportion (Figure 4.4b). Specifically, propene (35.2 ± 9.8 ppbv), ethene (25.1 ± 6.5 ppbv), and *trans*/*cis*-2-butene (7.8 ± 3.6 ppbv) accounted for the largest proportion of alkenes. Although the high reactivity of alkenes makes them suitable for involvement in strong photochemical reactions, the low temperatures and weak solar radiation levels of winter were not triggering factors for intensive O_3 production. Hence, the O_3 formation mechanism was elaborated in the following sections with the aid of PBM-MCM model simulations.

Table 4.2 Daytime (8:00-20:00 LT) average of meteorological and chemical parameters on O_3 episode and non-episode days in Lanzhou.

	Winter Episodes	**Winter Non-episodes**	**Summer Episodes**	**Summer Non-episodes**
Relative humidity (%)	38.3 ± 3.8	52.4 ± 1.9	55.5 ± 4.8	57.2 ± 4.1
Solar radiation (W m^{-}	263.6 ± 60.7	255.3 ± 23.0	438.8 ± 63.2	328.3 ± 64.6
Wind speed (m s^{-1})	1.5 ± 0.2	1.5 ± 0.1	0.4 ± 0.1	0.5 ± 0.1
Temperature (℃)	-1.7 ± 1.3	-5.7 ± 0.5	24.5 ± 1.0	24.0 ± 1.0
Planetary boundary layer height (m)	366.3 ± 65.8	382.2 ± 30.8	1432.7 ± 86.4	1005.7 ± 47.9
NO (ppbv)	16.0 ± 4.0	13.6 ± 1.6	2.0 ± 0.5	2.3 ± 0.9
NO_2 (ppbv)	31.4 ± 3.4	25.6 ± 1.7	17.6 ± 2.4	12.5 ± 1.7
CO (ppmv)	2.0 ± 0.2	1.4 ± 0.1	0.6 ± 0.03	0.5 ± 0.03
O_3 (ppbv)	43.1 ± 11.2	22.7 ± 1.8	81.2 ± 8.1	57.3 ± 7.3
Maximum O_3 (ppbv)	121.8	96.1	161.9	88.6
TVOC (ppbv)	153.4 ± 19.0	115.1 ± 7.2	79.0 ± 8.5	66.3 ± 6.7
Alkanes (ppbv)	55.7 ± 9.8	41.9 ± 3.8	41.2 ± 3.4	30.5 ± 2.1
Alkenes (ppbv)	82.3 ± 13.1	60.5 ± 4.9	27.8 ± 2.1	25.3 ± 2.2
Alkynes (ppbv)	1.3 ± 0.5	0.9 ± 0.1	1.5 ± 0.3	1.1 ± 0.1
Aromatics (ppbv)	14.1 ± 2.7	11.8 ± 1.1	12.7 ± 1.5	7.3 ± 0.9

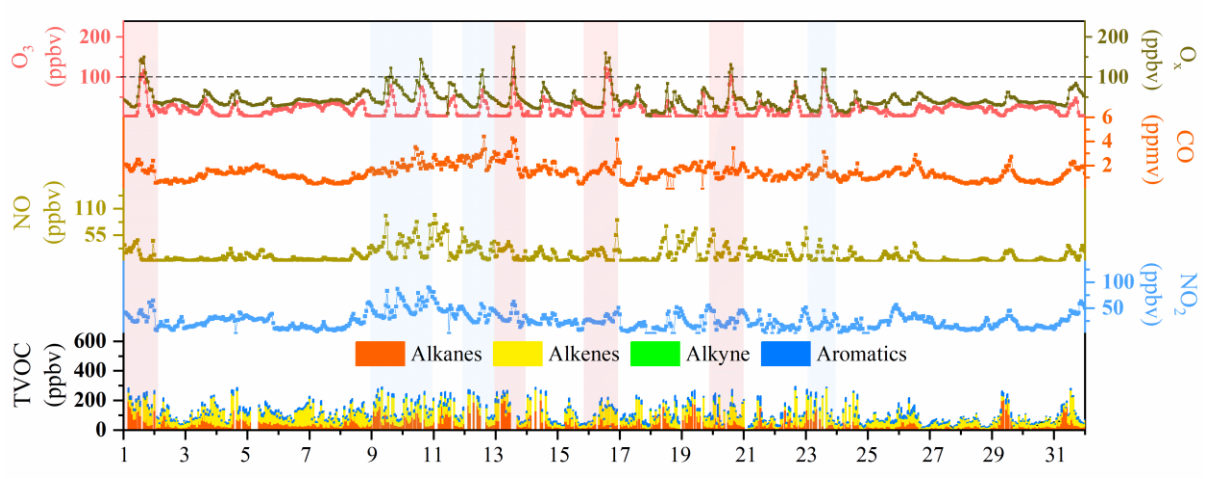

Figure 4.2. Time series of trace gases and VOCs in January 2018. O_3 episode days (hourly maximum concentration of O_3 exceeded 100 ppbv) are shaded in red. Ox days (hourly maximum concentration of O_x exceeded 100 ppbv) are shaded in blue.

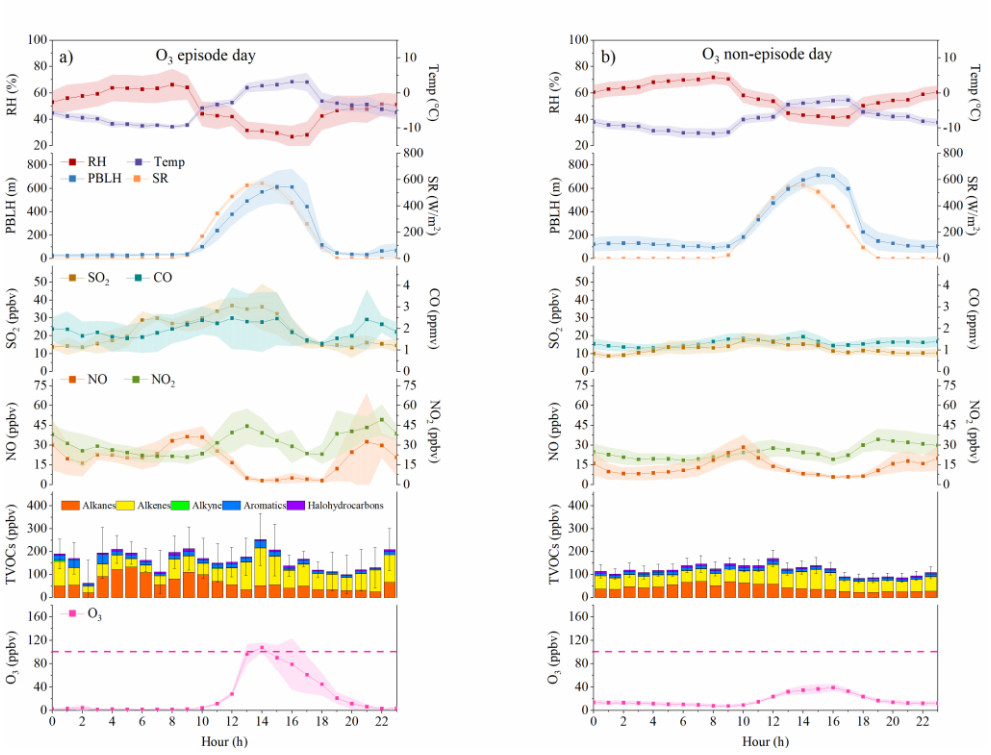

Figure 4.3. Diurnal profiles of meteorological parameters, trace gases and VOCs on (a) O_3 episode days and (b) non-episode days.

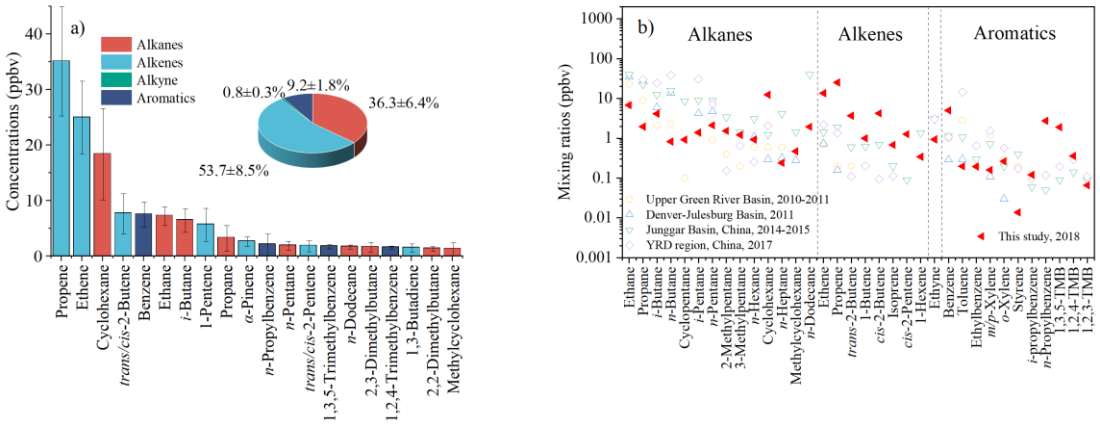

Figure 4.4. (a) Compositions of VOCs and daytime average concentrations of top 20 VOC species on O_3 episode days. (b) Comparison of VOCs concentrations in winter among different sites (T. Chen et al., 2020; Field et al., 2015; Gilman et al., 2013; Z. B. Wang et al., 2020).

4.3 Influence of meteorological conditions on winter O_3 formation

We compared the meteorological conditions and air pollutant concentrations in winter and summer (Table 4.2). The reduced PBLH in winter corresponded to higher levels of O_3 precursors than in summer. This might have resulted from weaker mixing and diffusion processes under the shallower PBLH in winter (L. Liu et al., 2021; Shen et al., 2024; Yin et al., 2019). Notably, the relative humidity and temperature were much lower, and the solar radiation was weaker on the winter O_3 episode days compared to summer ones. Although previous studies have demonstrated that lower relative humidity leads to higher O_3 concentrations in the temperature range of 30 to −30 °C (Belan & Savkin, 2019), the effects of temperature and solar radiation remain unclear. In Figure 4.5, panel (a) shows the effects of temperature on VOC reactivity with OH, while panel (b) displays the effect of solar radiation on simulated OH concentration. Weak solar radiation decreased the OH concentration, which could further inhibit O_3 formation. In contrast, an increase in temperature reduced the VOC reactivity of *trans/cis*-2-butene, while the VOC reactivity of 1,3,5-trimethylbenzene (135TMB) was stable during temperature changes due to the value of the fixed constant *k* of 135TMB and OH (Figure 4.5a). Additionally, the reactivity of cyclohexane and OH slightly increased with increasing temperature.

To further investigate the impacts of temperature and solar radiation on O_3 formation, the reaction rates of alkanes, alkenes, and aromatics with OH were simulated under changes in temperature and solar radiation during the most active photochemical reaction period (13:00–16:00 LT, hereinafter the peak period) on O_3 episode days (Figure 4.6a). The relationships between the reaction rates of VOCs and solar radiation were close to linear regressions, with slopes of 0.1, 2.0, and 0.1 ppbv h^{-1} per 100 W m^{-2} for alkanes, alkenes, and aromatics, respectively. In addition, the reaction rates of alkenes increased with increasing temperature below 10 °C and decreased slightly when the temperature exceeded 10 °C (Figure 4.6b). The reaction rate of alkenes on winter O_3 episode days was only approximately 15 % lower than that on summer O_3 episode days. It was lower than those of alkanes and aromatics (~30 %). Upon further investigation of the alkene species, it was found that the reaction rate of *trans*/*cis*-

2-butene increased slowly above 0 °C (Supplementary Material Figure 4.5c). In general, low temperatures and weak solar radiation in winter reduced the reactivity of VOCs with OH to a certain extent but had a limited impact on the reaction rates of alkenes with OH.

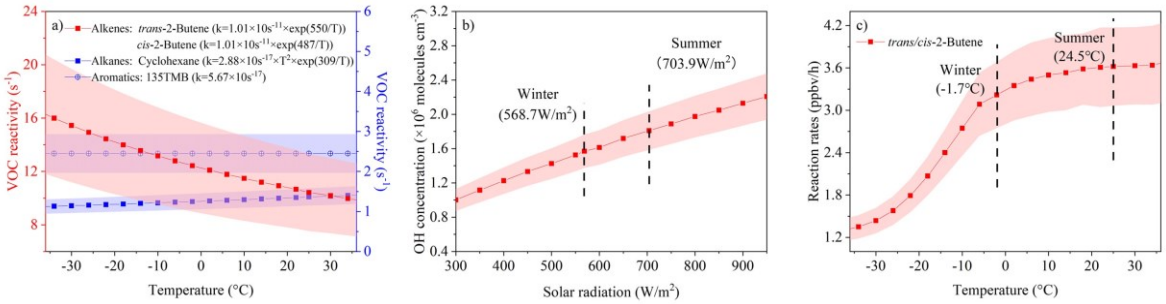

Figure 4.5. (a) VOC reactivity with OH during the peak period (13:00-16:00 LT) under different temperatures. (b) Average concentrations of simulated OH during the peak period (13:00-16:00 LT) under different solar radiation (c) Reaction rates of *trans/cis*-2-Butene with OH during the peak period (13:00-16:00 LT) under different temperatures. (Black dotted lines stand for the daytime average of temperature on O_3 episode days in winter and summer, respectively).

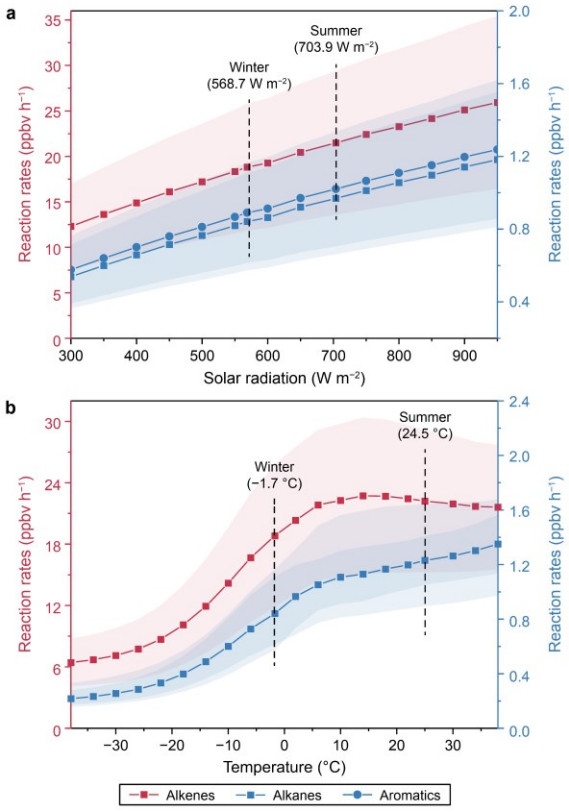

Figure 4.6. Reaction rates of VOC groups with OH during the peak period (13:00-16:00 LT) under different (a) solar radiations and (b) temperatures. (Black dotted lines stand for the daily maximum average solar radiation and daytime average temperature on O_3 episode days in winter and summer, respectively. O_3 episode days in winter include 1, 13, 16, and 20 January 2018).

Note: dots and crosses represent the sites in North China and South China, respectively; grey shaded areas denote the distribution of oil fields.

4.4 Photochemical mechanisms underlying winter O_3 pollution

As shown in Figure 4.7, OH plays a vital role in the RO_x (OH + HO_2 + RO + RO_2) cycle in photochemical reactions through initially oxidizing VOCs, which subsequently leads to O_3 formation (T. Wang et al., 2017). In general, OH concentrations are much lower in winter compared to summer due to the aggravated OH sink caused by higher concentrations of NO_2 (i.e., the reaction of OH and NO_2) (Table 4.3), and the reduced photolysis sources (i.e., photolysis of O_3 and HONO) when solar radiation is weak in winter. Such processes could suppress O_3 formation regardless of the abundance of VOCs. In this study, although the average daytime OH concentration on the winter O_3 episode days ([0.8 ± 0.1] × 10^6 molecules cm^{-3}) was lower than that on summer O_3 episode days ([2.0 ± 0.3] × 10^6 molecules cm^{-3}) (Table 4.4) (X. F. Liu et al., 2021), the average OH concentration during the peak period still reached (2.0 ± 0.1) × 10^6 molecules cm^{-3}, which was significantly higher than that found in previous studies (Heard, 2004; X. Ma et al., 2019; Slater et al., 2020). This high concentration of OH attracted our attention; therefore, we further explored the radical chemistry associated with OH formation.

4.4.1 Sources of OH

Figure 4.8a depicts the contributions of initial sources to OH, HO_2, and RO_2 on O_3 episode days. It was found that the ozonolysis of alkenes made an extraordinary contribution to OH formation, accounting for 90.9 ± 17.6 % of the OH sources. As the second contributor, photolysis of HONO accounted for 8.7 ± 0.1 % of the OH sources, and the remaining sources contributed a total of 0.4 ± 0.1 %. Therefore, O_3–alkene reactions were discovered to be the predominant sources of OH. Furthermore, alkene ozonolysis can occur in a dark environment (Alam et al., 2013; Ariya et al., 2000). A handful of studies have shown that O_3 + alkenes contribute to OH formation. For example, it was reported that the maximum daily average contribution of O_3 + alkenes to OH was (0.3 ± 0.05) × 10^7 molecules cm^{-3} s^{-1} in Shanghai in the summer of 2018 (X. F. Liu et al., 2021). The value at a mountainous background site in South China (Nanling site) was found to be (0.03 ± 0.01) × 10^7 molecules cm^{-3} s^{-1} (Y. Wang et al., 2023). The contribution level reported at both urban and background sites in the literature

is significantly lower than the (2.1 ± 0.7) × 10^7 molecules cm^{-3} s^{-1} determined in this study (Figure 4.9). The reactions involving O_3 + alkenes were neglected in previous work due to their minor contributions to OH formation. To investigate the sources of OH further, we compared the simulated results with and without OH radicals generated by Criegee intermediates (CIs) via model simulations. The results indicated that 31.0 ± 6.3 % of the OH was reduced when OH radicals produced by CIs were excluded (Figure 4.10). CIs generated by the ozonolysis of alkenes can rapidly decompose into OH, HO_2, and RO_2 (e.g., *trans*-2-butene, 4.1) and were determined to be one of the major sources of radicals in this study (Emmerson et al., 2005; Hatakeyama, 1994; Jacob, 1999; Osborn & Taatjes, 2015; Y. Wang et al., 2018). Specifically, *trans*/*cis*-2-butenes accounted for 63 % of OH initiation (Figure 4.8a). CH_3CHOOB, a CI species generated from *trans*/*cis*-2-butene/pentene, was the largest contributor to OH, contributing to a daytime average of (1.63 ± 0.31) × 10^7 molecules cm^{-3} s^{-1} of OH on O_3 episode days (Table 4.5). Table 4.6 compares the average daytime reaction rates between alkenes with OH and alkenes with O_3. It was found that the reaction rates of *trans*/*cis*-2-butene/pentene with O_3 were higher than those with OH. However, the reaction rates of OH with other alkenes, particularly propene, were found to be greater (Figure 4.9b). This indicated that *trans*/*cis*-2-butene/pentenes tended to react with O_3 and thus promote the initiation of OH, which, in turn, enhanced VOC oxidation and participated in -radical cycling, ultimately leading to significant O_3 production (Figure 4.9a).

Table 4.3. Daytime (8:00-20:00 LT) average of meteorological and chemical parameters on O_3 episode and non-episode days in Lanzhou.

	Winter		Summer	
	Winter Episodes	**Non-episodes**	**Summer Episodes**	**Non-episodes**
Relative humidity (%)	38.3 ± 3.8	52.4 ± 1.9	55.5 ± 4.8	57.2 ± 4.1
Solar radiation (W m^{-2})	263.6 ± 60.7	255.3 ± 23.0	438.8 ± 63.2	328.3 ± 64.6
Wind speed (m s^{-1})	1.5 ± 0.2	1.5 ± 0.1	0.4 ± 0.1	0.5 ± 0.1
Temperature (℃)	-1.7 ± 1.3	-5.7 ± 0.5	24.5 ± 1.0	24.0 ± 1.0
Planetary boundary layer height (m)	366.3 ± 65.8	382.2 ± 30.8	1432.7 ± 86.4	1005.7 ± 47.9
NO (ppbv)	16.0 ± 4.0	13.6 ± 1.6	2.0 ± 0.5	2.3 ± 0.9
NO_2 (ppbv)	31.4 ± 3.4	25.6 ± 1.7	17.6 ± 2.4	12.5 ± 1.7
CO (ppmv)	2.0 ± 0.2	1.4 ± 0.1	0.6 ± 0.03	0.5 ± 0.03
O_3 (ppbv)	43.1 ± 11.2	22.7 ± 1.8	81.2 ± 8.1	57.3 ± 7.3
Maximum O_3 (ppbv)	121.8	96.1	161.9	88.6
TVOC (ppbv)	153.4 ± 19.0	115.1 ± 7.2	79.0 ± 8.5	66.3 ± 6.7
Alkanes (ppbv)	55.7 ± 9.8	41.9 ± 3.8	41.2 ± 3.4	30.5 ± 2.1
Alkenes (ppbv)	82.3 ± 13.1	60.5 ± 4.9	27.8 ± 2.1	25.3 ± 2.2
Alkynes (ppbv)	1.3 ± 0.5	0.9 ± 0.1	1.5 ± 0.3	1.1 ± 0.1

Aromatics (ppbv)	14.1 ± 2.7	11.8 ± 1.1	12.7 ± 1.5	7.3 ± 0.9

Table 4.4. Daytime (08:00–20:00 LT) average concentrations of OH, HO_2, RO_2, and contributions pathways to production & destruction rates of OH, HO_2 and RO_2.

		Episodes in winter	**Non-episodes in winter**	**In summer (X. F. Liu et al., 2021)**
OH concentration ($\times10^6$ molecules cm^{-3})		0.8 ± 0.1	0.7 ± 0.1	2.0 ± 0.3
HO_2 concentration ($\times10^8$ molecules cm^{-3})		4.8 ± 0.7	1.3 ± 0.2	/
RO_2 concentration ($\times10^8$ molecules cm^{-3})		8.4 ± 1.3	5.1 ± 0.9	/
OH formation pathways ($\times10^7$molecules cm^{-3} s^{-1})	HO_2 + NO	7.9 ± 1.0	3.8 ± 0.0	3.9 ± 0.8
	HONO + *hv*	0.2 ± 0.0	0.2 ± 0.0	0.1 ± 0.0
	$O^1D + H_2O$	0.0 ± 0.0	0.0 ± 0.0	0.1 ± 0.0
	O_3 + Alkenes	2.1 ± 0.7	0.6 ± 0.1	0.3 ± 0.1
	H_2O_2 + *hv*	0.0 ± 0.0	0.0 ± 0.0	0.0 ± 0.0
OH loss pathways ($\times10^7$molecules cm^{-3} s^{-1})	OH + CO	-1.0 ± 0.2	-0.5 ± 0.0	-0.6 ± 0.1
	OH + VOCs	-8.8 ± 1.2	-3.7 ± 0.4	-3.3 ± 0.6
	OH + NO	-0.1 ± 0.0	-0.1 ± 0.0	-0.1 ± 0.0
	OH + NO_2	-1.0 ± 0.1	-0.4 ± 0.0	-0.5 ± 0.1

HO_2 formation pathways ($\times10^7$molecules cm^{-3} s^{-1})	RO_2 + NO	9.1 ± 1.3	3.8 ± 0.4	/
	OH + CO	1.0 ± 0.2	0.5 ± 0.1	/
	HCHO + *hv*	0.1 ± 0.0	0.1 ± 0.0	/
	OVOCs + *hv*	0.1 ± 0.0	0.1 ± 0.0	/
	O_3 + Alkenes	0.7 ± 0.1	0.3 ± 0.1	/
	OH + HCHO	0.1 ± 0.0	0.1 ± 0.0	/
HO_2 loss pathways ($\times10^7$molecules	HO_2 + NO	-7.9 ± 1.0	-3.8 ± 0.4	/
	HO_2 + RO_2	-1.6 ± 0.3	-0.2 ± 0.0	/
	HO_2 + HO_2	-0.6 ± 0.1	-0.8 ± 0.2	/
	HO_2 + O_3	-0.2 ± 0.0	-0.0 ± 0.0	
RO_2 formation pathways	OH + VOCs	8.8 ± 1.2	3.7 ± 0.4	/
	O_3 + Alkenes	2.4 ± 0.4	0.7 ± 0.1	/
	OVOCs + *hv*	0.1 ± 0.0	0.1 ± 0.0	/
RO_2 loss pathways	RO_2 + NO	-9.1 ± 1.3	-3.8 ± 0.4	/
	HO_2 + RO_2	-1.6 ± 0.3	-0.2 ± 0.0	/

Table 4.5. Daytime (08:00-20:00 LT) average formation rates of OH, HO_2, RO_2 contributed by the decomposition of Criegee intermediates on O_3 episode days.

CI Species	**Precursors**	**Reactions of CI decomposition**	**OH formation rate ($\times 10^7$ molecules cm^{-3} s^{-1})**	**HO_2 formation rate ($\times 10^7$ molecules cm^{-3} s^{-1})**	**RO_2 formation rate ($\times 10^7$ molecules cm^{-3} s^{-1})**
CH_2OOA	Ethene	$CH_2OOA = HO_2 + CO + OH$	0.01 ± 0.00	0.01 ± 0.00	/
CH_3CHOOA	Propene	$CH_3CHOOA = CH_3O_2 + CO + OH$ $CH_3CHOOA = CH_3O_2 + HO_2$	0.15 ± 0.03	0.08 ± 0.01	0.23 ± 0.04
CH_2OOB	Propene 1-Butene 1-Pentene	$CH_2OOB = HO_2 + CO + OH$	0.17 ± 0.03	0.17 ± 0.03	/
C_2H_5CHOOA	1-Butene	$C_2H_5CHOOA = C_2H_5O_2 + CO + OH$ $C_2H_5CHOOA = C_2H_5O_2 + HO_2$	0.00 ± 0.00	0.00 ± 0.00	0.00 ± 0.00
CH_3CHOOB	*trans*/*cis*-2-Butene trans/cis-2-Pentene	$CH_3CHOOB = CH_3O_2 + CO + OH$ $CH_3CHOOB = CH_3O_2 + HO_2$	1.63 ± 0.31	0.36 ± 0.07	1.98 ± 0.38
C_2H_5CHOOB	*trans*/*cis*-2-Pentene	$C_2H_5CHOOB = C_2H_5O_2 + CO + OH$ $C_2H_5CHOOB = C_2H_5O_2 + HO_2$	0.16 ± 0.04	0.03 ± 0.01	0.19 ± 0.05
CH_2OOD	1,3-Butadiene	$CH_2OOD = HO_2 + CO + OH$	0.00 ± 0.00	0.00 ± 0.00	/
ACROOA	1,3-Butadiene	$ACROOA = HO_2 + 2CO + HCHO + OH$ $ACROOA = HO_2 + CO + HCHO + HO_2$	0.00 ± 0.00	0.01 ± 0.00	/

C_3H_7CHOOA	1-Pentene	$C_3H_7CHOOA = NC_3H_7O_2 + CO + OH$ $C_3H_7CHOOA = NC_3H_7O_2 + HO_2$	0.02 ± 0.00	0.01 ± 0.00	0.04 ± 0.01

Table 4.6. Daytime (08:00-20:00 LT) average reaction rates of alkenes with OH/O_3 on O_3 episode days.

Alkenes	Reactions	Reaction rate (ppbv h^{-1})
Ethene + OH	$C_2H_4 + OH = HOCH_2CH_2O_2$	0.80 ± 0.13
Ethene + O_3	$C_2H_4 + O_3 = HCHO + CH_2OOA$	0.11 ± 0.02
Propene + O_3	$C_3H_6 + O_3 = CH_2OOB + CH_3CHO$	0.59 ± 0.10
Propene + O_3	$C_3H_6 + O_3 = CH_3CHOOA + HCHO$	0.59 ± 0.10
Propene + OH	$C_3H_6 + OH = HYPROPO_2$	3.86 ± 0.64
Propene + OH	$C_3H_6 + OH = IPROPOLO_2$	0.58 ± 0.10
1-Butene + O_3	$BUT1ENE + O_3 = C_2H_5CHOOA + HCHO$	0.01 ± 0.00
1-Butene + O_3	$BUT1ENE + O_3 = CH_2OOB + C_2H_5CHO$	0.01 ± 0.00
1-Butene + OH	$BUT1ENE + OH = HO_3C_4O_2$	0.01 ± 0.00
1-Butene + OH	$BUT1ENE + OH = NBUTOLAO_2$	0.08 ± 0.01
***trans*-2-Butene + O_3**	$TBUT2ENE + O_3 = CH_3CHO + CH_3CHOOB$	2.78 ± 0.70
***trans*-2-Butene + OH**	$TBUT2ENE + OH = BUT2OLO_2$	1.09 ± 0.25
***cis*-2-Butene + O_3**	$CBUT2ENE + O_3 = CH_3CHO + CH_3CHOOB$	0.98 ± 0.26

***cis*-2-Butene + OH**	CBUT2ENE + OH = $BUT2OLO_2$	0.59 ± 0.16
1,3-Butadiene + O_3	$C_4H_6 + O_3$ = ACR + CH_2OOD	0.01 ± 0.00
1,3-Butadiene + O_3	$C_4H_6 + O_3$ = HCHO + ACROOA	0.01 ± 0.00
1,3-Butadiene + OH	C_4H_6 + OH = $BUTDAO_2$	0.08 ± 0.02
1,3-Butadiene + OH	C_4H_6 + OH = $BUTDBO_2$	0.24 ± 0.06
1,3-Butadiene + OH	C_4H_6 + OH = $BUTDCO_2$	0.05 ± 0.01
1-Pentene + O_3	PENT1ENE + O_3 = C_3H_7CHOOA + HCHO	0.09 ± 0.02
1-Pentene + O_3	PENT1ENE + O_3 = CH_2OOB + C_3H_7CHO	0.09 ± 0.02
1-Pentene + OH	PENT1ENE + OH = $PE1ENEAO_2$	0.48 ± 0.10
1-Pentene + OH	PENT1ENE + OH = $PE1ENEBO_2$	0.07 ± 0.02
***trans*-2-Pentene + O_3**	TPENT2ENE + O_3 = C_2H_5CHOOB + CH_3CHO	0.15 ± 0.06
***trans*-2-Pentene + O_3**	TPENT2ENE + O_3 = CH_3CHOOB + C_2H_5CHO	0.15 ± 0.06
***trans*-2-Pentene + OH**	TPENT2ENE + OH = $PE2ENEAO_2$	0.05 ± 0.02
***trans*-2-Pentene + OH**	TPENT2ENE + OH = $PE2ENEBO_2$	0.05 ± 0.02
***cis*-2-Pentene + O_3**	CPENT2ENE + O_3 = C_2H_5CHOOB + CH_3CHO	0.25 ± 0.05
***cis*-2-Pentene + O_3**	CPENT2ENE + O_3 = CH_3CHOOB + C_2H_5CHO	0.25 ± 0.05
***cis*-2-Pentene + OH**	CPENT2ENE + OH = $PE2ENEAO_2$	0.08 ± 0.01
***cis*-2-Pentene + OH**	CPENT2ENE + OH = $PE2ENEBO_2$	0.08 ± 0.01

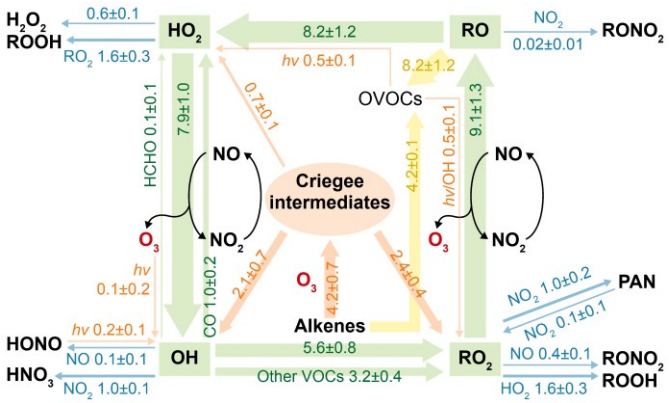

Figure 4.7. Daytime (08:00–20:00 LT) average budget of RO_x on O_3 episode days (1, 13, 16, and 20 January 2018). (unit: $\times 10^7$molecules cm^{-3} s^{-1}) The orange, blue and green arrows indicate the initiation, termination, and recycling pathways of radicals, respectively, and the yellow arrows denote reactions related to OVOCs.

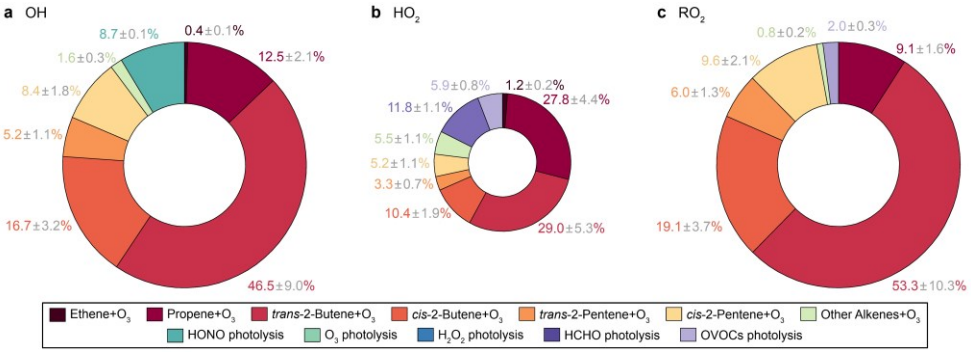

Figure 4.8. Daytime (08:00–20:00 LT) average contributions of initial sources to (a) OH, (b) HO_2, and (c) RO_2 on O_3 episode days (1, 13, 16, and 20 January 2018).

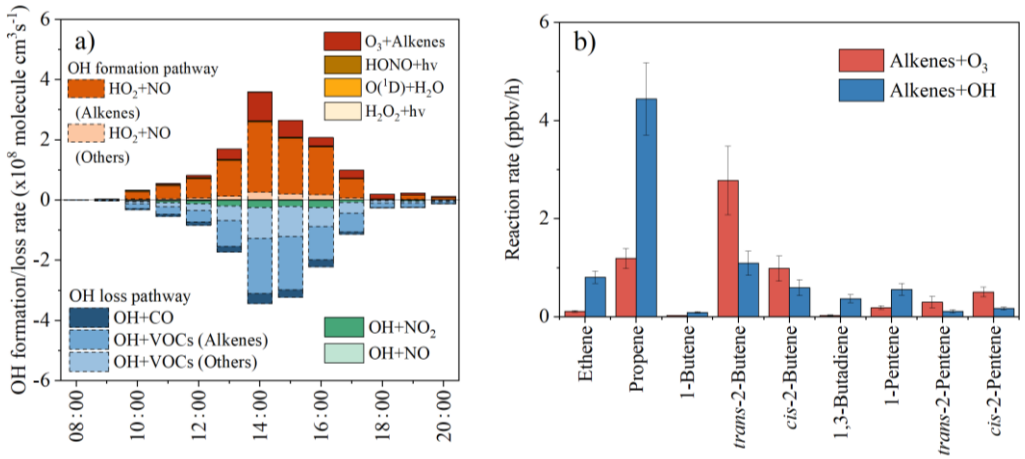

Figure 4.9. (a) Diurnal cycles of pathway contributions to OH production and destruction rates on O_3 episode days (08:00–20:00 LT); (b) Comparison of reaction rates between alkenes + O_3 and alkenes + OH.

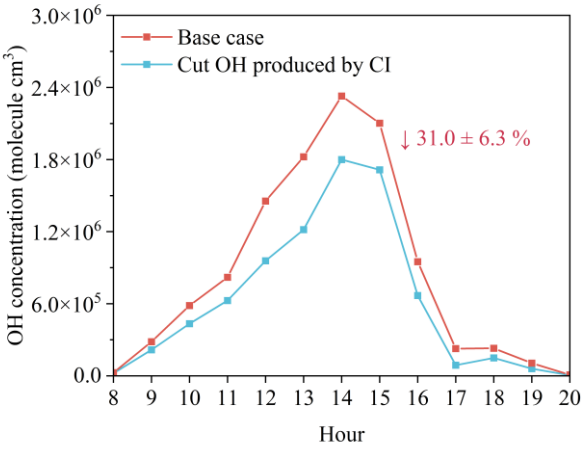

Figure 4.10. Average diurnal concentrations of OH by base scenario and scenario without OH generated by Criegee intermediates.

4.4.2 Sources of HO_2 and RO_2

In addition to OH, CIs can be decomposed into HO_2 and RO_2, which also play important roles in radical cycling (Emmerson et al., 2005; Hatakeyama, 1994; Ling et al., 2014; Osborn & Taatjes, 2015; Z. Tan et al., 2018). Figures 4.8b and 4.8c show the predominant initiations of HO_2 and RO_2 on O_3 episode days, respectively. Alkene ozonolysis accounted for 82.4 ± 14.7 % and 98.0 ± 19.1 % of the initiated HO_2 and RO_2, respectively, which was in sharp contrast to the findings of previous studies that showed the photolysis of OVOCs was the main source of HO_2 and RO_2 (Ling et al., 2014). As shown in Figure 4.7, HO_2 and RO_2 promoted OH formation by accelerating RO_x cycling, resulting in more VOCs participating in the propagation reactions. As shown in Figure 4.9a, the reaction of HO_2 with NO dominated OH formation. In addition, the large contribution of ozonolysis of alkenes to OH during the peak period (13:00–16:00 LT) cannot be ignored. Criegee intermediates generated by the ozonolysis of alkenes can rapidly decompose into OH, HO_2, and RO_2. The example reaction (e.g., trans-2-butene, 4.1) is shown below. The reactions of VOCs were the main pathway for OH loss. Due to the balance of formation and loss rates, the additional OH formation generated by alkene-O_3 reactions would oxidate VOCs, and subsequently participate in the RO_x cycle. Furthermore, the RO_2 produced by the alkene-O_3 reactions facilitated HO_2 formation through the transformation of RO_2 - RO - HO_2 (Figure 4.11a). The following reactions of HO_2/RO_2 and NO accelerated the RO_x cycle, continuously promoting OH formation, and resulting in more VOCs participating in the RO_x cycle. Therefore, HO_2 and RO_2 were identified as one of important driving factors for the O_3 pollution in this study.

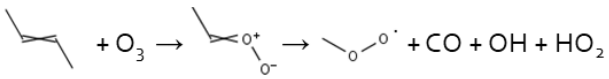

(4.1)

Moreover, HO_2 and RO_2 generated by the ozonolysis of alkenes reacted directly with NO, subsequently producing O_3 (Figure 4.7). This was different from previous studies, where O_3 formation was mainly achieved through the OH-initiated oxidation of VOCs (X. F. Liu et al., 2021). The average daytime reaction rates of RO_2 and HO_2 produced from O_3 + alkenes were

$(2.4 \pm 0.4) \times 10^7$ and $(0.7 \pm 0.1) \times 10^7$ molecules cm^{-3} s^{-1}, respectively, which were the largest contributors excluding OH + VOCs and RO_2 + NO (Table 4.4), suggesting a crucial role for alkene ozonolysis in RO_2 and HO_2 initiations. Furthermore, methyl peroxy radical (CH_3O_2) accounted for the vast majority of RO_2 species produced by alkene–O_3 reactions (72.4 ± 14.0 %, Figure 4.8c); it was mainly generated from *trans*/*cis*-2-butene/pentenes (Table 4.5). Therefore, the abovementioned peroxy radicals boosted the production of O_3 by directly reacting with NO and accelerating the RO_x cycling. Overall, despite the lower temperatures and weaker solar radiation levels in winter, a large amount of alkenes emitted from the local petrochemical industry could still enter the radical cycling by reacting with O_3. Alkene ozonolysis dominated the massive O_3 production by generating OH, which subsequently promoted the oxidation of VOCs and formed RO_2 and HO_2, accelerating RO_x cycling and directly producing O_3 via reactions with NO

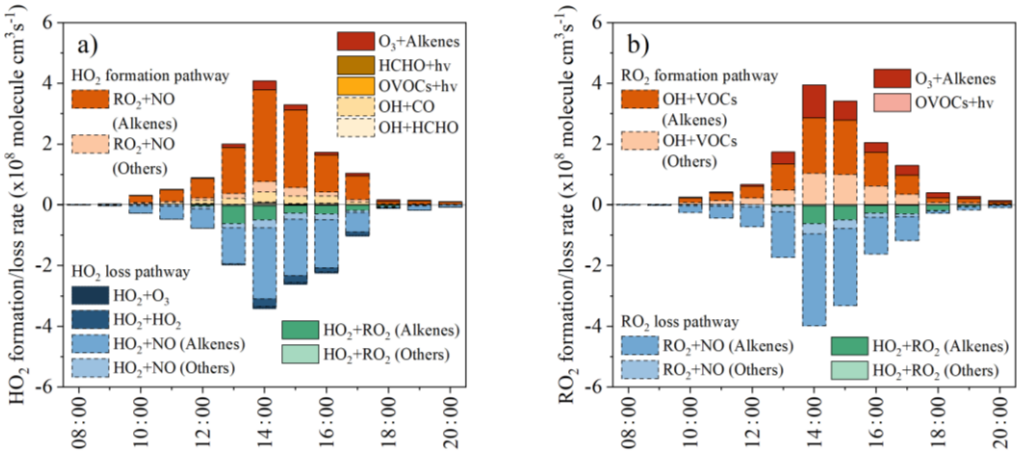

Figure 4.11. Diurnal (08:00–20:00 LT) cycles of pathway contributions to simulated (a) HO_2 and (b) RO_2 production and destruction rates on O_3 episode days.

4.4 Quantification of O_3 formation

4.4.1 O_3 production and destruction

Figure 4.12a shows the average diurnal profiles of simulated O_3 production and destruction rates on O_3 episode days in winter, compared to those on O_3 non-episode days in winter and summer (Table 4.7). The average daytime net O_3 production rate was significantly higher on O_3 episode days in winter (17.0 ± 2.3 ppbv h^{-1}) compared to that in summer (8.9 ± 1.7 ppbv h^{-1}) ($p > 0.05$) (X. F. Liu et al., 2021). Meanwhile, the maximum O_3 production rate (53.4 ppbv h^{-1}) during winter O_3 episode days was greater than that during summer O_3 episode days (~21 ppbv h^{-1}) (X. F. Liu et al., 2021). In addition, we found that compared to other Chinese cities in summer, O_3 production was more intensive in Lanzhou, which was considered more conducive to O_3 formation. The rates recorded in other cities include 4.6–7.0 ppbv h^{-1} (Wuhan), 3.4–4.6 ppbv h^{-1} (Chengdu), 5.1–7.7 ppbv h^{-1} (Beijing), and 2.1–3.5 ppbv h^{-1} (Shanghai) (X. F. Liu et al., 2021).

The HO_2 + NO and RO_2 + NO pathways dominated O_3 production. Specifically, 90.8 ± 8.5 % and 88.4 ± 9.7 % of the two respective pathways were related to alkenes via the donation of peroxy radicals. The contributions of alkene species to the HO_2 and RO_2 + NO pathways were quantified in Section 4.4.2. Furthermore, 78.0 ± 11.5 % of O_3 destruction resulted from the reactions of alkenes with O_3, which was different from the main reaction of NO_2 with OH in Lanzhou during summer and in other regions in China (X. F. Liu et al., 2021). Although O_3 was destructed by reactions with alkenes, the radicals generated from these pathways produced more than twice the amount of O_3 through radical initiation compared to the O_3 loss, especially for the butene isomers (Figure 4.12b). These findings showed that the reactions of alkenes with O_3 governed O_3 production and destruction and thus further indicated the pivotal role that alkenes play in O_3 pollution.

Table 4.7. Daytime (08:00–20:00 LT) averages of main pathways' contributions to O_3 production and destruction rates (unit: ppbv h^{-1}).

		Episodes in winter	Non-episodes in winter	In summer (X. F. Liu et al., 2021)
	Net P(O_3) production rate	17.0 ± 2.3	8.6 ± 1.1	8.9 ± 1.7
P	HO_2 + NO	11.5 ± 1.5	5.5 ± 0.6	5.5 ± 1.1
r	RO_2 + NO	13.3 ± 1.8	5.5 ± 0.6	5.0 ± 0.9
D	OH + NO_2	-1.4 ± 0.2	-0.7 ± 0.1	-0.7 ± 0.2
e	O_3 + Alkenes	-6.0 ± 1.0	-1.7 ± 0.2	-0.5 ± 0.1
s	O^1D + H_2O	-0.0 ± 0.0	-0.0 ± 0.0	-0.2 ± 0.0
t	O_3 + OH	-0.0 ± 0.0	-0.0 ± 0.0	-0.0 ± 0.0
r	O_3 + HO_2	-0.3 ± 0.0	-0.0 ± 0.0	-0.2 ± 0.0

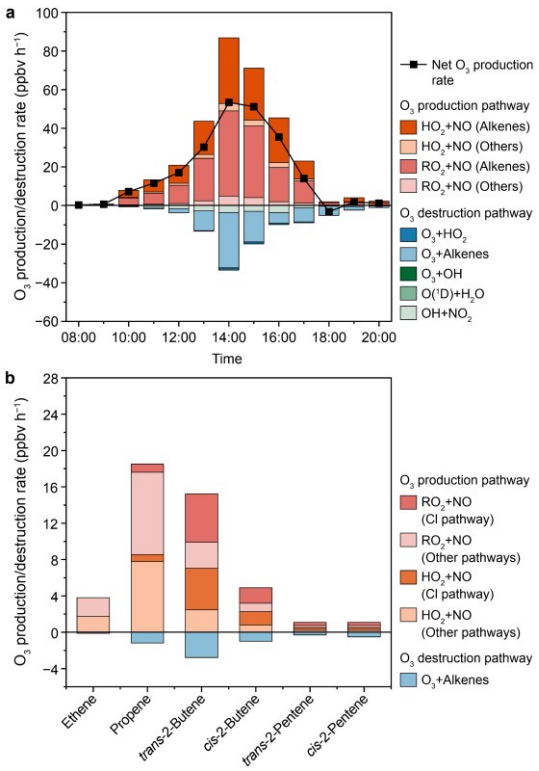

Figure 4.12 (a) Daytime (08:00–20:00 LT) average profiles of simulated O_3 production and destruction rates of main pathways on O_3 episode days. (b) Daytime average pathway contributions of major alkenes to O_3 production and destruction rates on O_3 episode days. O_3 episode days include 1, 13, 16, and 20 January 2018.

4.4.2 Contributions of alkenes to O_3 production

Figure 4.13 presents the detailed evolution of major alkene species and their contributions to O_3 production during the peak period (13:00–16:00 LT) on O_3 episode days. The O_3 production was dominated by the RO_2 + NO and HO_2 + NO pathways (Figure 4.12a), responsible for 54.3 ± 5.0 % and 45.6 ± 4.0 %, respectively.

When we analyzed the origin of RO_2 in the RO_2 + NO pathway, three radicals were found to account for most of the reactions with NO: propyl peroxy radical ($HYPROPO_2$), CH_3O_2, and 2-hydroxy butyl peroxy radical ($BUT2OLO_2$). These radicals explained 30.9 ± 2.9 %, 27.9 ± 3.8 %, and 11.5 ± 1.7 % of the RO_2 + NO pathway, respectively. $HYPROPO_2$ and $BUT2OLO_2$ were mainly generated by the OH-initiated oxidation of propene and *trans*/*cis*-2-butene, respectively (Figure 4.13). In addition, 2-hydroxy ethyl peroxy radical ($HOCH_2CH_2O_2$) and 2-hydroxy pentyl peroxy radicals ($PE2ENEAO_2$ and $PE2ENEBO_2$) originated from the OH-initiated oxidation of ethene and *trans*/*cis*-2-pentene, responsible for 6.5 ± 0.7 % and 1.5 ± 0.3 % of RO_2 in the RO_2 + NO pathway, respectively. Unlike the abovementioned radicals, CH_3O_2 was mainly produced by the ozonolysis of alkenes, and 87.8 ± 16.5 % of it was derived from CH_3CHOOB, which was one of the CIs. More specifically, 91.8 ± 18.5 % of CH_3CHOOB was produced by the ozonolysis of *trans*/*cis*-2-butene, and the remainder was generated by the ozonolysis of propene (8.2 ± 2.7 %). Additionally, 10.7 ± 1.4 % of CH_3O_2 evolved from CH_3CHOOA, another CI produced by the ozonolysis of propene. Finally, 1.0 ± 0.1 % of RO_2 in the RO_2 + NO pathway was ethyl peroxy radical ($C_2H_5O_2$), which was derived from a CI (C_2H_5CHOOB) produced by the ozonolysis of *trans*/*cis*-2-pentene.

Regarding the HO_2 + NO pathway, HO_2 was found to be derived from alkyl peroxy radicals, which followed the evolution of $RO_2 \rightarrow RO \rightarrow HO_2$. Thus, the sources of HO_2 in the HO_2 + NO pathway were similar to those of RO_2 in the RO_2 + NO pathway. Specifically, radicals including propyl radical (HYPROPO), methyl radical (CH_3O), 2-hydroxy butyl radical (BUT2OAO), and 2-hydroxy ethoxy radical ($HOCH_2CH_2O$) provided 31.2 ± 3.5 %, 27.8 ± 4.6 %, 11.2 ± 2.0 %, and 6.6 ± 1.4 % of HO_2, respectively, in this pathway. The remaining alkenes contributed 6.0 ± 1.4 % of HO_2. In addition, formaldehyde (HCHO) generated from

HYPROPO and CH_3O radicals contributed 2.4 ± 0.3 % of HO_2 in the HO_2 + NO pathway. Furthermore, a small HO_2 contribution (2.9 ± 0.4 %) was provided by C_1–C_3 aldehydes produced from either alkenes or their alkyl radicals.

Overall, 89.6 ± 8.7 % of O_3 production on the O_3 episode days was attributed to alkenes. The four largest contributors were *trans*/*cis*-2-butene (34.8 ± 3.7 % of the total O_3 production), propene (34.5 ± 5.3 %), ethene (6.6 ± 0.8 %), and *trans*/*cis*-2-pentene (4.7 ± 0.9 %). Other VOC groups only contributed 10.4 ± 9.5 % of O_3 production.

Given the dominant role that alkenes were found to play in O_3 production, we evaluated a series of O_3 control strategies related to alkenes, as shown in Figure 4.14a. It was found that a reduction of approximately 84.2 % propene or 80.7 % *trans/cis*-2-butene could prevent the hourly maximum O_3 concentration from exceeding 100 ppbv. However, mitigation strategies were found to be less effective for other single alkene species. As discussed in Section 4.4.2, butene isomers and propene were the two most important sources of O_3 production. Notably, if total alkenes were reduced by 26.4 %, the hourly maximum O_3 concentration would be lower than 100 ppbv (Figure 4.14b) due to the combined effect of butene isomers and propene. Moreover, if the reduction was solely performed in the early afternoon (i.e., 28.6 % reduction in alkenes between 13:00 and 16:00 LT), excessive O_3 concentrations (>100 ppbv) could be prevented (Figure 4.14b)

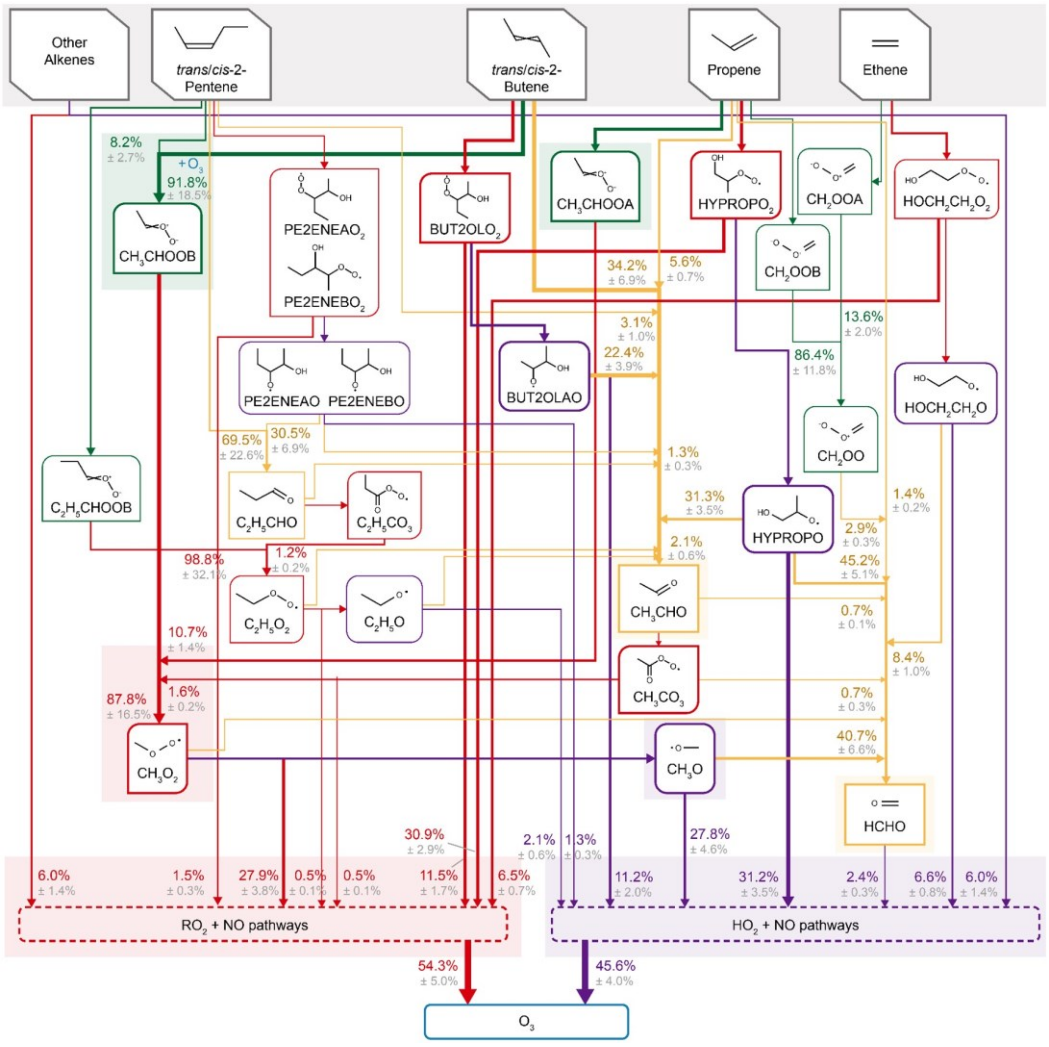

Figure 4.13. Evolution processes of alkenes and their contributions to O_3 formation during the peak period (13:00-16:00 LT) on O_3 episode days (1, 13, 16, and 20 January 2018).

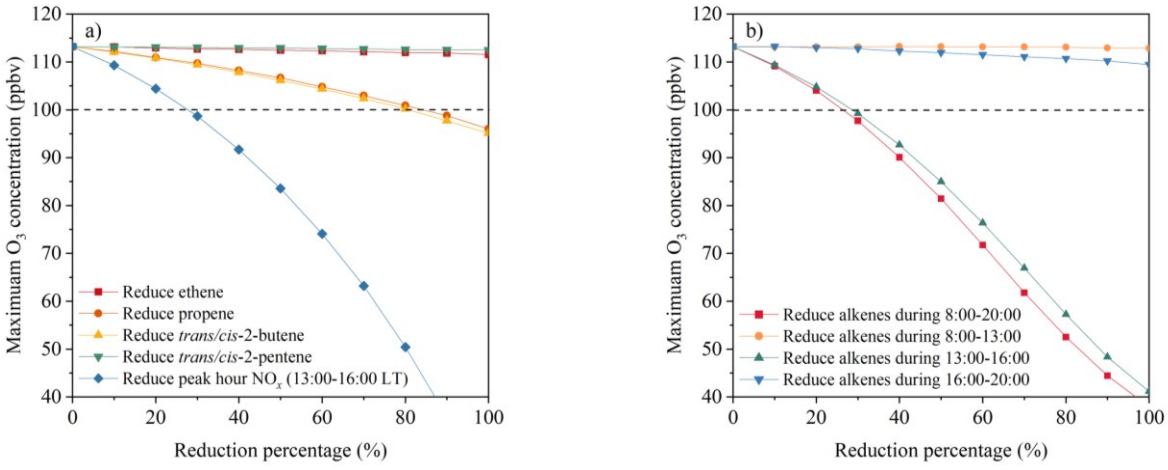

Figure 4.14. Hourly maximum O_3 concentrations under (a) different reduction scenarios of alkene species and NO_x, (b) different alkenes reduction time periods.

4.5 Impact of NO_x

Despite the considerable influence of alkenes, the impact of NO_x cannot be ignored. The NO concentration increased from 17:00 to 21:00 LT and remained relatively high until 10:00 LT the next day, resulting in the nighttime O_3 concentration being close to zero due to the NO titration effect (Figure 4.3a). Subsequently, it hindered the ozonolysis of alkenes after 17:00 LT and before 10:00 LT (Figure 4.15c). In addition, RIR values were calculated to determine the relationship between O_3 and its precursors. Overall, the average daytime RIR values of NO_x were negative, suggesting an inhibitory effect on O_3 formation (Figure 4.16a). Specifically, the negative hourly RIR values of NO_x were mainly concentrated in the mornings and evenings (Figure 4.16b). This was attributed to the NO titration effect, which inhibited the ozonolysis of alkenes and subsequently restricted the reactions of HO_2 and RO_2 with NO. However, the hourly RIR values of NO_x were positive from 12:00 to 17:00 LT (Figure 4.16b), indicating that O_3 formation was co-limited by VOCs and NO_x during this period, consistent with that in summer (X. F. Liu et al., 2021). After sunrise, as NO_2 photolysis increased, more O_3 was produced and participated in reactions with alkenes (Figure 4.15c). Furthermore, the RIR values of NO_x were higher than those of alkenes from 14:00 to 17:00 LT (Figure 4.16b), implying that O_3 formation inclined into a NO_x-limited regime. Therefore, it was found that a 27.7 % reduction in NO_x during the period of 13:00–16:00 LT could effectively maintain the O_3 concentration below 100 ppbv (Figure 4.14a).

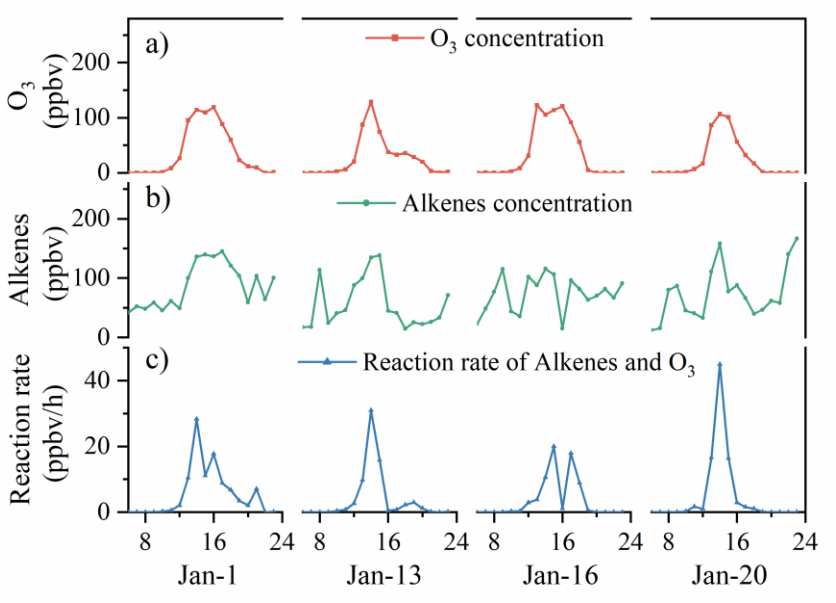

Figure 4.15. Diurnal variations of hourly (a) O_3, (b) alkenes, and (c) reaction rate of alkenes with O_3 on episode days.

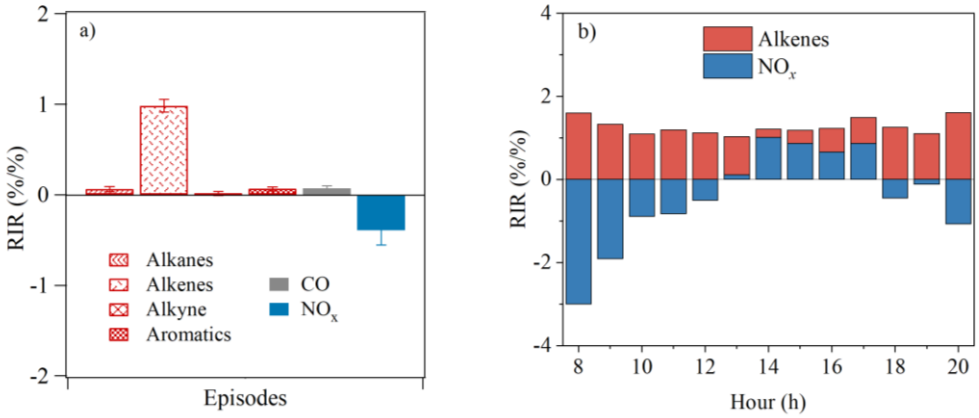

Figure 4.16. (a) Daytime (08:00–20:00 LT) average RIR values of O_3 precursors. (b) Hourly RIR values of alkenes and NO_x on O_3 episode days.

4.6 Summary

Contrary to the consensus that O_3 pollution mainly occurs in warm weather with strong solar radiation, we discovered through intensive sampling that O_3 concentrations in Lanzhou were extremely high in winter. Using observation-based box model simulations, we found that large amounts of alkenes emitted from the local petrochemical industry reacted with O_3 and produced Criegee intermediates, which further decomposed into substantial amounts of RO_x and ultimately accelerated O_3 production. The *trans*/*cis*-2-butene, propene, ethene, and *trans*/*cis*-2-pentene were identified as the top four alkenes, accounting for more than 80 % of O_3 production. We also discovered that temperature changes had a limited impact on the ozonolysis of alkenes, which can also occur in dark environments. Our findings provide new information that challenges the consensus, showing that warm weather and strong solar radiation are not indispensable factors for intensive photochemical reactions and that dark reactions in photochemistry could surpass photolysis reactions and trigger intense O_3 production. Moreover, our findings challenge the understanding that alkene ozonolysis mainly leads to the destruction of O_3; in this study, it was the culprit responsible for severe O_3 pollution. Given the increased industrialization and elevated demand for olefin products worldwide, paying serious attention to alkene-related air pollution is essential. Furthermore, high snow albedo could intensify the RO_x cycling and O_3 production processes identified in this study. The findings of this study emphasize the importance of recognizing O_3 pollution in locations with cold weather and weak sunlight and provide a reference for studying atmospheric oxidation reactions and free radical chemistry in petrochemical industrial environments. The control measures proposed in this study are also applicable to similar regions.

Chapter 5 Long-term Trend of Ozone Formation and Radical Chemistry in Lanzhou

5.1 Introduction

Ozone (O_3) pollution poses serious health and environmental challenges worldwide. As a major air pollutant at ground level, O_3 has been associated with a variety of adverse health effects, including respiratory illnesses, cardiovascular diseases, and an increased risk of premature death (Curtis et al., 2006; Liu et al., 2018; Manisalidis et al., 2020; Soares & Silva, 2022; J. J. Zhang et al., 2019). In addition to its impact on human health, O_3 damages vegetation and reduces agricultural yields by harming plant tissues and inhibiting photosynthesis, resulting in substantial economic losses in the agricultural sector (Emberson, 2020; Feng et al., 2015). O_3 also contributes to climate change by altering the radiation balance and affecting interactions between the atmosphere and biosphere, which can influence temperature and weather patterns (X. Lu et al., 2019). Despite ongoing mitigation efforts, O_3 pollution remains a persistent problem in many regions, driven by both natural processes and human activities. Understanding long-term trends in O_3 pollution is therefore crucial for developing effective control strategies.

Lanzhou stands out as one of the earliest cities in China where O_3 pollution was documented, with records of photochemical smog dating back nearly five decades (W. Guo et al., 2022; J. Li et al., 2020; Ta et al., 2004; Tang et al., 1985). Although the Clean Air Action (CAA) Plan was launched in 2013 to tackle air pollution through stricter emission controls and technological upgrades, Lanzhou continues to face significant O_3 pollution challenges (Du et al., 2020; Filonchyk & Yan, 2018; Zhao et al., 2021). The CAA Plan included a range of measures, such as controlling industrial emissions, reducing dust pollution, managing scattered coal use, and regulating vehicle exhaust (Bureau, 2018; Government, 2013). In Lanzhou, the chemical formation of O_3 is particularly important. High emissions of alkenes from the petrochemical industry, combined with the city's valley topography, frequently result in severe

O_3 pollutions. The valley setting tends to trap pollutants near the ground, further worsening air quality (Du et al., 2020; W. Guo et al., 2022; Jia et al., 2016). Industrial activities, especially in the petrochemical sector, are major sources of O_3 precursors, including nitrogen oxides (NO_x) and volatile organic compounds (VOCs) (Dong et al., 2021; J. Liu et al., 2020; G. Y. Wang et al., 2020; Yan et al., 2021). As a result, O_3 pollution in Lanzhou is influenced by both complex chemical processes and substantial local emissions, making it a particularly challenging issue to manage. Notably, Lanzhou also experiences significant wintertime O_3 pollution —a phenomenon uncommon in most other regions (Yang et al., 2024).

In China, much of the long-term research on O_3 pollution has focused on regions such as the North China Plain (NCP), Yangtze River Delta (YRD), and Pearl River Delta (PRD), as well as major cities like Chengdu and Shanghai (S. Chen et al., 2020; Z. Chen et al., 2019; Gao et al., 2017; Hu et al., 2025; X.-B. Li et al., 2022; X. F. Liu et al., 2019; M. Wang et al., 2024; W. Wang, D. D. Parrish, et al., 2022; Y. Wang et al., 2022; L. Yang et al., 2019). These studies have provided important insights into O_3 trends and formation mechanisms. For instance, in the NCP, it has been observed that reducing NO_x emissions alone, particularly during periods of high temperatures and strong sunlight, can sometimes lead to increased O_3 concentrations (S. Chen et al., 2020; Z. Chen et al., 2019; M. Wang et al., 2024; W. Wang, D. D. Parrish, et al., 2022). In the PRD, an imbalance between NO_x and VOC controls, along with a weaker NO titration effect, has also contributed to elevated O_3 levels (X.-B. Li et al., 2022; L. Yang et al., 2019). Studies in Shanghai and Chengdu also found that reducing NO_x could increase O_3 (Gao et al., 2017; Y. Wang et al., 2022). In Lanzhou, a shift in O_3 formation was observed —from being mainly NO_x-controlled in summer 2018 to a VOCs-dominated regime in summer 2019 (Y. Li et al., 2022). However, this finding was based on analysis of only the 2018—2019 period, during which major overhauls of the alkenes plant and heavy catalytic cracking unit took place —an unprecedented event in the history of Lanzhou's petrochemical industry (Y. Li et al., 2022). These unique circumstances introduce considerable uncertainty to the results.

Consequently, there remains a significant research gap in understanding the long-term trends and influencing factors of O_3 pollution specific to Lanzhou.

Previous studies have demonstrated that O_3 formation regimes can shift over time and that the effectiveness of control measures may vary accordingly (K. Li et al., 2019; T. Wang et al., 2017). Long-term monitoring and modeling are therefore essential for capturing these dynamic changes. Mechanistic studies using the Photochemical Box Model coupled with the Master Chemical Mechanism (PBM-MCM) have provided valuable insights into local O_3 formation pathways and the impacts of precursor controls (X. F. Liu et al., 2019; Lyu et al., 2016a; Lyu et al., 2019; Y. Wang et al., 2018; Y. Wang et al., 2017). Additionally, Positive Matrix Factorization (PMF) has been widely applied to identify the primary sources of VOCs and other O_3 precursors in Chinese cities (Hua et al., 2023; X. F. Liu et al., 2021; X. F. Liu et al., 2019; Y. H. Liu et al., 2019; Lyu et al., 2016b; Song et al., 2018; P. Zeng et al., 2019). Given the current lack of long-term studies on O_3 pollution in Lanzhou, this research examines O_3 trends and their driving factors in the city from 2013 to 2023. By employing both the PBM-MCM and PMF models, this study aims to uncover the mechanisms underlying O_3 variation in Lanzhou. The analysis provides a comprehensive understanding of the factors influencing O_3 levels and assesses the impact of the CAA Plan. The results will offer scientific guidance for future policy development and air quality management in Lanzhou and other cities facing similar challenges.

.

5.2 Long-term trends in O_3 and other air pollutant levels

Figures 5.1 presents the trends in daytime (07:00–19:00 LT) average concentrations of major air pollutants, i.e., $PM_{2.5}$, CO, SO_2, NO_2, and O_3, in Lanzhou from 2014 to 2024. From 2019 to 2024, CO, SO_2, and NO_2 showed significant declines, indicating the effectiveness of emission reduction measures implemented during this period. In contrast, O_3 levels presented an upward trend of 0.56 ppbv yr^{-1}, highlighting the persistent challenge of O_3 pollution despite overall improvements in air quality. From 2014 to 2018, NO_2 concentrations increased at an annual rate of 1.54 ppbv yr^{-1}, while $PM_{2.5}$, CO, and SO_2 levels declined at rates of –1.69 μg m^{-3} yr^{-1}, -0.02 ppmv yr^{-1}, and -0.19 ppbv yr^{-1}, respectively. Notably, O_3 concentrations continued to rise steadily during this period, with an annual increase of 0.97 ppbv yr^{-1}, almost double the rate observed in 2019–2024. A range of measures such as stricter control of industrial emissions, dust pollution prevention, scattered coal treatment, and coordinated vehicle exhaust regulation, were implemented to combat air pollution (Bureau, 2018; Government, 2013). Significant reductions in CO and SO_2 concentrations reflect the positive impact of improved vehicle emission standards and targeted sulfur emission policies. Changes in NO_2 levels are likely the result of strengthened traffic management measures. These trends are in line with observations in other major Chinese cities (Maji & Sarkar, 2020; Zheng et al., 2024).

Table 5.1 summarizes the daytime (07:00–19:00 LT) average concentrations of pollutants on O_3 episode days and all days, as well as the number of O_3 episode days in Lanzhou from 2014 to 2024. Between 2014 and 2018, both the daytime average O_3 concentrations on episode days (defined as days when the daily maximum O_3 exceeds 100 ppbv) and on all days showed an upward trend, reaching their highest values in 2016 at 63.99 ± 1.01 ppbv and 29.47 ± 1.64 ppbv, respectively. From 2019 to 2024, average O_3 concentrations increased for both O_3 episode days and all days, reaching their highest values in 2022 at 67.38 ± 1.96 ppbv and 35.55 ± 1.50 ppbv, respectively. The number of O_3 episode days peaked at 16 and 11 days in 2016 and 2018, respectively, and then dropped from 7 days in 2019 to 1 day by 2024. Although the frequency of extreme O_3 pollution events has been significantly reduced, overall O_3 pollution levels remain relatively high. This suggests that current control measures are more effective at

mitigating O_3 episode days but have limited impact on reducing the general O_3 background level. Therefore, further comprehensive strategies targeting O_3 precursors are needed to achieve broader improvements in O_3 pollution.

Seasonal characteristics of O_3 pollution are detailed in Table 5.2, with the four seasons defined as spring (March–May), summer (June–August), autumn (September–November), and winter (December–February). O_3 concentrations were highest in summer, followed by spring, autumn, and winter, with average values on all days reaching 44.86 ± 0.75 ppbv, respectively. This seasonal pattern highlighted the influence of higher temperatures and stronger solar radiation on O_3 formation during the summer months. Table 5.2 also shows that the majority of O_3 episode days occurred in summer (61 days), compared to only 0-5 days in other seasons. Notably, the rate of O_3 increase during summer was markedly higher than in other seasons for both periods, with values of 2.50 ppbv yr^{-1} from 2014 to 2018 and 1.70 ppbv yr^{-1} from 2019 to 2024. To more effectively evaluate the O_3 control plan in Lanzhou, our analysis focused on the summer season, when O_3 pollution is most severe.

Table 5.3 shows the number of O_3 episode days and the average concentrations of O_3 and meteorological parameters for all days during summertime in Lanzhou from 2014 to 2024. While June, July, and August all experience elevated O_3 levels, separate analysis of these months offers limited additional insight, as August shares similar meteorological characteristics with June and July and is representative of summer O_3 pollution. Therefore, August was selected for detailed analysis of summer O_3 pollution in this study.

Table 5.1. Daytime (07:00–19:00 LT) average concentration of O_3 on O_3 episode days and all days, and the number of O_3 episode days and high O_x days in Lanzhou from 2014 to 2024.

Year	Daytime (07:00–19:00 LT) average concentration of O_3 on O_3 episode days (ppbv)	Daytime (07:00–19:00 LT) average concentration of O_3 on all days (ppbv)	Number of O_3 episode days (daily maximum O_3>100 ppbv)
2014	/	24.13 ± 1.35	/
2015	61.21 ± 3.40	24.11 ± 1.35	1
2016	63.99 ± 1.01	29.47 ± 1.64	16
2017	59.68 ± 1.32	29.33 ± 1.58	9
2018	62.34 ± 1.23	28.63 ± 1.56	11
2019	50.71 ± 1.46	29.32 ± 1.52	7
2020	57.76 ± 1.77	33.60 ± 1.48	6
2021	59.88 ± 1.57	30.47 ± 1.53	7
2022	67.38 ± 1.96	35.55 ± 1.50	4
2023	59.96 ± 1.87	33.57 ± 1.68	5
2024	62.47 ± 3.60	33.56 ± 1.67	1

Table 5.2. Summary of daytime (07:00–19:00 LT) average concentration of O_3 on all days, the number of O_3 episode days, and the increased rate of daily average O_3 concentration by season in different seasons of Lanzhou from 2014 to 2024.

Seasons	Daytime (07:00–19:00 LT) average O_3 concentration (ppbv)	Number of O_3 episode days	Increased rate of daily average O_3 concentration from 2014 to 2018 (ppbv yr^{-1})	Increased rate of daily average O_3 concentration from 2019 to 2024 (ppbv yr^{-1})
Spring	36.30 ± 0.63	5	1.85 ($p < 0.05$)	0.46 ($p < 0.05$)
Summer	44.86 ± 0.75	61	2.50 ($p < 0.05$)	1.70 ($p < 0.05$)
Autumn	23.36 ± 0.67	1	0.51 ($p < 0.05$)	0.71 ($p < 0.05$)
Winter	16.34 ± 0.57	0	0.19 ($p > 0.05$)	-0.33 ($p > 0.05$)

Table 5.3. Daytime (07:00–19:00 LT) average values of O_3 and meteorological parameters for all days of summertime Lanzhou from 2014 to 2024.

Month	O_3 (ppbv)	Temperature (°C)	RH (%)	Wind speed ($m\ s^{-1}$)	Solar radiation ($W\ m^{-2}$)
201406	32.76 ± 2.80	21.40 ± 0.43	45.38 ± 1.87	2.24 ± 0.12	341.09 ± 22.35
201407	29.83 ± 3.42	24.01 ± 0.51	45.97 ± 1.91	1.87 ± 0.10	395.21 ± 24.92
201408	29.30 ± 2.97	21.06 ± 0.42	53.13 ± 1.78	1.82 ± 0.11	339.31 ± 23.32
201506	37.06 ± 3.59	21.42 ± 0.40	40.29 ± 1.97	2.21 ± 0.12	360.06 ± 23.30
201507	39.22 ± 3.44	24.13 ± 0.52	39.07 ± 1.89	1.89 ± 0.11	423.89 ± 24.59
201508	36.77 ± 1.91	22.95 ± 0.42	39.82 ± 1.82	1.96 ± 0.12	394.58 ± 24.34
201606	44.11 ± 3.62	23.15 ± 0.44	35.35 ± 1.65	2.01 ± 0.12	416.27 ± 24.00
201607	52.04 ± 4.80	24.74 ± 0.45	45.06 ± 1.95	2.03 ± 0.13	407.99 ± 24.62
201608	44.87 ± 4.19	24.87 ± 0.50	52.77 ± 1.88	2.17 ± 0.11	328.98 ± 22.35
201706	45.98 ± 3.99	21.77 ± 0.43	40.17 ± 1.95	1.89 ± 0.10	400.79 ± 23.82
201707	50.51 ± 4.37	26.53 ± 0.50	37.54 ± 1.98	2.45 ± 0.13	424.23 ± 23.75
201708	46.06 ± 4.85	20.53 ± 0.52	60.64 ± 2.00	1.60 ± 0.08	293.55 ± 23.57
201806	45.52 ± 3.35	23.39 ± 0.47	36.46 ± 1.65	2.14 ± 0.12	387.35 ± 23.20
201807	39.22 ± 4.33	23.44 ± 0.47	55.25 ± 1.86	1.83 ± 0.10	350.38 ± 24.13
201808	39.97 ± 4.19	22.47 ± 0.33	63.52 ± 1.46	1.70 ± 0.09	326.69 ± 21.83
201906	38.96 ± 3.22	20.66 ± 0.38	49.24 ± 2.12	1.97 ± 0.10	356.97 ± 23.65
201907	45.87 ± 3.24	22.90 ± 0.40	46.65 ± 1.59	1.56 ± 0.09	408.98 ± 23.71
201908	43.01 ± 3.30	21.75 ± 0.47	51.12 ± 2.03	1.71 ± 0.11	318.25 ± 24.45
202006	51.48 ± 3.31	22.13 ± 0.42	37.82 ± 1.68	2.25 ± 0.14	386.22 ± 23.58
202007	47.55 ± 4.17	23.11 ± 0.41	48.17 ± 1.88	1.96 ± 0.10	382.73 ± 23.21
202008	47.69 ± 3.48	21.38 ± 0.46	55.43 ± 1.71	1.83 ± 0.10	324.62 ± 22.94
202106	44.79 ± 3.18	22.52 ± 0.45	37.17 ± 1.70	2.27 ± 0.12	376.23 ± 23.31
202107	51.28 ± 2.85	26.20 ± 0.45	37.97 ± 1.67	1.85 ± 0.10	440.59 ± 24.25
202108	47.77 ± 3.76	22.96 ± 0.46	42.40 ± 1.89	2.11 ± 0.14	362.47 ± 23.58
202206	52.94 ± 2.63	24.31 ± 0.48	32.36 ± 1.81	2.37 ± 0.12	424.09 ± 24.80
202207	57.44 ± 3.41	25.29 ± 0.50	41.34 ± 1.95	1.99 ± 0.13	415.51 ± 25.39

202208	53.75 ± 3.81	23.77 ± 0.55	57.79 ± 1.52	1.76 ± 0.11	309.10 ± 22.40
202306	51.44 ± 2.64	22.82 ± 0.49	35.01 ± 1.61	2.07 ± 0.13	416.20 ± 24.18
202307	52.26 ± 4.22	25.04 ± 0.48	38.13 ± 1.61	2.02 ± 0.10	414.06 ± 24.17
202308	49.69 ± 3.11	24.19 ± 0.46	40.61 ± 1.63	2.14 ± 0.13	385.82 ± 24.24
202406	54.02 ± 2.47	22.24 ± 0.45	42.14 ± 1.81	1.91 ± 0.11	405.03 ± 24.03
202407	50.77 ± 3.04	24.80 ± 0.39	45.19 ± 1.52	1.96 ± 0.10	374.31 ± 22.84
202408	50.08 ± 2.40	24.54 ± 0.44	49.11 ± 1.86	1.82 ± 0.09	367.60 ± 23.86

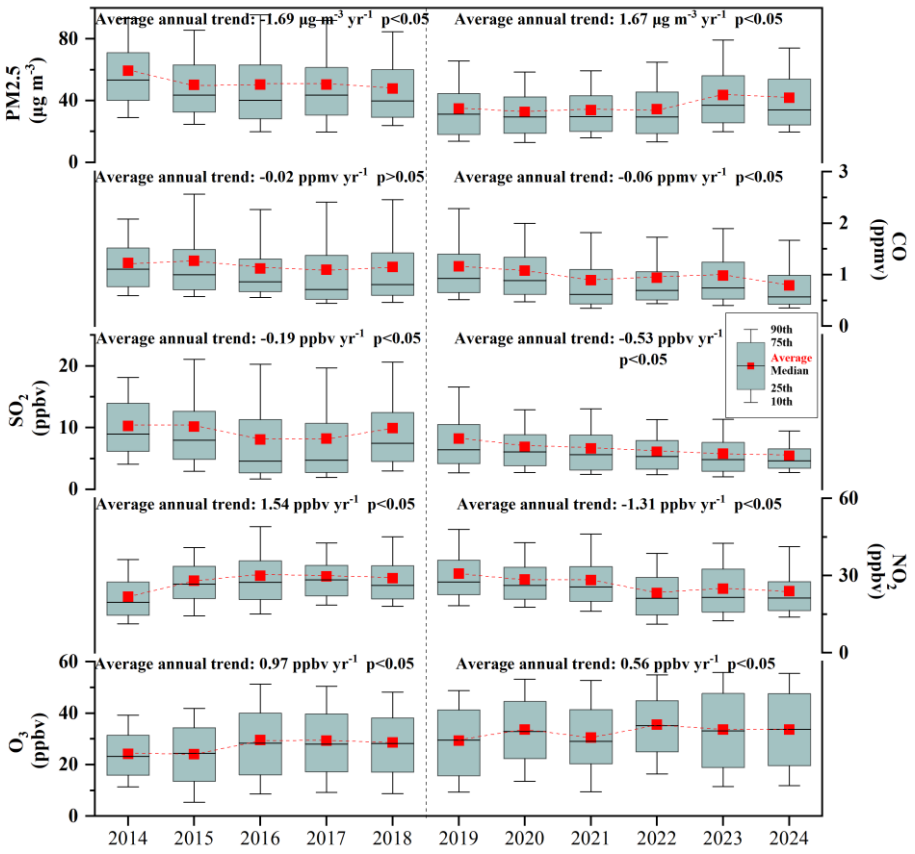

Figure 5.1. Long-term trend of daytime (07:00–19:00 LT) average concentrations of air pollutants in Lanzhou from 2014 to 2024.

5.3 Long-term trends of meteorological parameters and O_3 precursors in Lanzhou from August 2013 to 2024

Figure 5.2 illustrates the long-term trends in daytime (07:00–19:00 LT) average concentrations of O_3, meteorological parameters, and O_3 precursors in Lanzhou from August 2013 to 2023. During this period, the daily average O_3 concentration exhibited a steady upward trend, increasing at a rate of 2.55 ppbv yr^{-1} from 2013 to 2018, and 1.45 ppbv yr^{-1} from 2019 to 2023 ($p<0.05$). Meteorological conditions, such as temperature and solar radiation, significantly influenced average O_3 levels. Additionally, the complex mechanisms of O_3 formation, driven by interactions between precursors such as NO_x and VOCs, as well as meteorological factors, meant that reductions in precursor emissions do not always result in lower O_3 concentrations. Thus, the following sections of this chapter will explore the factors contributing to the increase in O_3 concentrations from both meteorological and chemical perspectives and provide recommendations for effective O_3 pollution control.

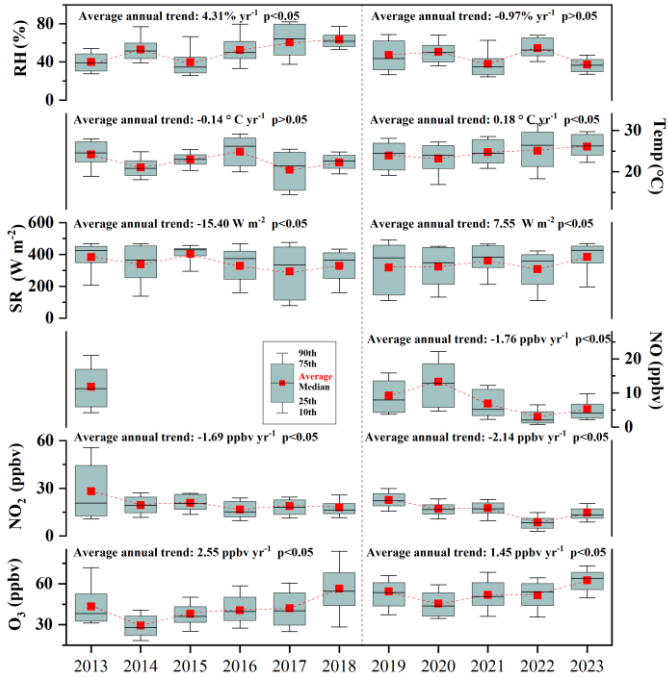

Figure 5.2. Long-term trends in daytime (07:00–19:00 LT) average concentrations of O_3, meteorological parameters, and O_3 precursors in Lanzhou during August for the years 2013 and 2019–2023.

5.3.1 Meteorological influences

Meteorological parameters exhibited distinct trends across the two periods. During daytime hours (07:00–19:00 LT), average relative humidity (RH) increased significantly from 2013 to 2018 at a rate of 4.31 % yr^{-1}, followed by a slight, statistically insignificant decrease of 0.97 % yr^{-1} from 2019 to 2023. Solar radiation (SR) showed significant declines in the first period, decreasing 15.40 W m^{-2} yr^{-1} ($p < 0.05$), while Temperature (Temp) presented an insignificant decline trend with a rate of 0.14°C yr^{-1} ($p > 0.05$). In contrast, from 2019 to 2023, Temp and SR exhibited increases of 0.18°C yr^{-1} and 7.55 W m^{-2} yr^{-1}, and these changes were statistically significant ($p < 0.05$). These meteorological variations likely reflect regional climate variability and local weather patterns. Importantly, the observed changes in meteorological factors do not align with the trends in average O_3 concentrations, suggesting that meteorological conditions alone cannot fully explain O_3 variability. This inconsistency indicates that chemical processes may play a more substantial role in O_3 formation, warranting further investigation.

5.3.2 Chemical influences

According to Figures 5.2, trace gas data from 2013 to 2023 indicate that daytime (07:00–19:00 LT) average concentrations of NO_2 and CO exhibited declining trends during summer, with more pronounced decreases observed from 2019 to 2023 compared to 2013 to 2018. Specifically, the daytime average concentration of NO_2 decreased at a rate of 1.69 ppbv yr^{-1} from 2013 to 2018, accelerating to 2.14 ppbv yr^{-1} from 2019 to 2023 ($p < 0.05$). For NO and VOCs, data were available for August 2013 and August 2019–2023, as shown in Figures 5.2-5.3 and Table 5.4. The daytime average concentration of NO decreased significantly from 2019 to 2023 at a rate of 1.76 ppbv yr^{-1} ($p < 0.05$). Among VOC groups, alkanes, alkenes, and alkynes exhibited similar trends between 2013 and 2019. The concentration of alkanes decreased significantly from 29.15 ± 1.02 ppbv to 13.41 ± 1.09 ppbv ($p < 0.05$), while alkenes and aromatics decreased significantly from 7.73 ± 0.43 ppbv to 2.60 ± 0.23 ppbv and 8.74 ± 0.60 ppbv to 2.78 ± 0.25 ppbv, respectively ($p < 0.05$). From 2013 to 2019, TVOC showed significant decreases ($p < 0.05$). However, from 2019 to 2023, VOC concentrations

experienced considerable fluctuations, largely influenced by the COVID-19 lockdown measures. During the initial phase (2019–2020), the concentrations of alkenes, alkynes, and aromatics increased significantly. In contrast, from 2020 to 2022, all VOC groups exhibited marked decreases, which can be attributed to the strict lockdown restrictions that limited anthropogenic emissions. Following the lifting of lockdown measures (2022–2023), the concentrations of alkanes, alkenes, and TVOCs rebounded rapidly, with 2023 levels surpassing those observed in 2019. The significantly lower NO_x and VOC levels observed in 2022 compared to other years can be attributed to three main factors. First, abnormal meteorological conditions occurred in August 2022, including five rainstorm warnings, with relative humidity 35% higher than in other years and precipitation in August accounting for 40% of the annual total, which greatly enhanced the removal of pollutants through wet deposition. Second, the main district in Lanzhou was under lockdown from July to August 2022, resulting in a substantial reduction in anthropogenic emissions. Third, strict control policies were implemented, with real-time emissions from key industries monitored 24 hours a day, and six key industries required to meet emission standards for all pollutants. These combined factors led to a significant decrease in NO_x and VOC concentrations in 2022

These results suggest that while NO_x control measures have had a sustained and significant impact, the overall effectiveness of VOC control remains limited. The significant decrease in VOC concentrations from 2013 to 2019 indicates substantial progress in VOC control, whereas the marked increase from 2022 to 2023 highlights the need for further attention. Therefore, future pollution control strategies should prioritize the coordinated management of different VOC types to achieve more effective air quality improvements.

Figure 5.4 further illustrate the daytime (07:00–19:00 LT) proportions of different VOC groups in Lanzhou during August 2013, 2016, and 2019–2023. Alkanes remained the dominant group from 2013 to 2023, comprising approximately 57–70 % of total VOCs, indicating their substantial contribution to the overall VOC composition. During this period, alkenes accounted for about 11–21 %, while aromatics contributed 14–23 % from August 2013 to 2020, and decreased to 4.3 ± 0.7 % in August 2023.

To better understand the nonlinear relationship between O_3 and its precursors, we simulated daily maximum O_3 concentrations in August 2013 and from 2019 to 2023 under varying NO_x and VOC concentrations, ranging from 0 % to 200 % of baseline values (Figure 5.5). The results indicate that during the summers of 2013 and 2019–2022 in Lanzhou, O_3 formation was primarily VOC-limited and decreasing NO_x concentrations led to an increase in O_3 concentration, with the fluctuated VOC concentrations. From 2019 to 2023, Lanzhou experienced a transition from a VOC-limited regime to a transitional regime, where both VOCs and NO_x influenced O_3 formation. When VOC concentrations remained stable and the regime shifted from VOC-limited to a VOC-NO_x co-limited regime between 2019 and 2023, reductions in NO_x alone contributed to persistently high average O_3 concentrations. These findings highlight that effective O_3 mitigation in Lanzhou requires substantial and coordinated reductions in both NO_x and VOC emissions. Therefore, focusing on VOC emission reductions in the short term, followed by prioritizing NO_x reductions in the long term, is an effective strategy for improving summertime O_3 air quality in Lanzhou. To further assess the individual impacts of different VOC species on O_3 formation, the PBM-MCM model was employed to investigate the mechanisms of O_3 production, radical chemistry, and the specific contributions of various VOC species (Section 5.4).

Table 5.4. Daytime (07:00-19:00 LT) average values of O_3 and O_3 precursors in Lanzhou in August 2013, and 2019-2023.

	2013	**2019**	**2020**	**2021**	**2022**	**2023**
O_3 (ppbv)	43.13 ± 3.22	55.89 ± 4.45	45.24 ± 2.72	51.84 ± 2.84	51.51 ± 2.23	62.48 ± 2.75
NO (ppbv)	11.44 ± 1.45	9.39 ± 1.31	13.28 ± 1.40	6.87 ± 0.96	3.10 ± 0.49	5.25 ± 0.71
NO_2 (ppbv)	28.13 ± 2.25	22.86 ± 1.08	17.18 ± 0.93	17.51 ± 1.01	8.68 ± 0.63	14.67 ± 0.93
CO (ppmv)	0.60 ± 0.09	1.04 ± 0.07	1.00 ± 0.06	0.72 ± 0.04	0.85 ± 0.02	0.70 ± 0.04
TVOCs(ppbv)	38.32 ± 2.05	19.39 ± 1.70	21.52 ± 1.59	15.23 ±2.36	10.79 ± 0.97	21.16 ± 4.02
Alkanes (ppbv)	29.15 ± 1.02	13.41 ± 1.09	12.25 ± 0.86	10.22 ± 1.85	6.59 ± 0.55	14.87 ± 2.46
Alkenes (ppbv)	7.73 ± 0.43	2.60 ± 0.23	3.64 ± 0.35	2.53 ± 0.26	1.93 ± 0.24	4.41 ± 1.31
Alkyne (ppbv)	/	0.60 ± 0.13	2.26 ± 0.14	1.26 ± 0.11	1.24 ± 0.09	0.96 ± 0.11
Aromatics (ppbv)	8.74 ± 0.60	2.78 ± 0.25	3.37 ± 0.25	1.22 ± 0.14	1.03 ± 0.09	0.92 ± 0.14

Table 5.5. Daytime (07:00-19:00 LT) average values of VOC species in Lanzhou in August 2013, and 2019-2023 (Unit: ppbv). ($^{\#}$ represents the VOC species used in the model simulations)

Compounds	**2013**	**2019**	**2020**	**2021**	**2022.**	**2023**
Ethane$^{\#}$	/	2.72 ± 0.14	2.48 ± 0.11	2.28 ± 0.11	2.00 ± 0.14	2.49 ± 0.29
Propane$^{\#}$	3.40 ± 0.30	2.62 ± 0.19	1.89 ± 0.12	1.01 ± 0.11	1.29 ± 0.13	0.90 ± 0.26
***i*-Butane$^{\#}$**	2.43 ± 0.04	0.91 ± 0.06	0.90 ± 0.07	0.60 ± 0.05	0.45 ± 0.04	1.03 ± 0.21

***n*-Butane[#]**	1.75 ± 0.01	1.39 ± 0.20	2.04 ± 0.22	1.10 ± 0.13	0.99 ± 0.11	1.72 ± 0.27
***i*-Pentane[#]**	1.57 ± 0.08	1.40 ± 0.50	1.87 ± 0.16	0.87 ± 0.08	0.78 ± 0.09	0.95 ± 0.18
***n*-Pentane[#]**	0.88 ± 0.03	0.20 ± 0.05	0.86 ± 0.10	0.41 ± 0.05	0.39 ± 0.05	0.53 ± 0.19
Cyclopentane	0.63 ± 0.02	3.34 ± 0.49	0.14 ± 0.02	0.09 ± 0.04	0.04 ± 0.00	0.27 ± 0.19
***n*-Hexane[#]**	0.55 ± 0.01	0.27 ± 0.04	0.75 ± 0.08	0.55 ± 0.13	0.27 ± 0.03	0.69 ± 0.27
2,2-Dimethylbutane[#]	0.45 ± 0.01	0.05 ± 0.02	0.03 ± 0.00	0.16 ± 0.10	0.01 ± 0.00	0.08 ± 0.07
2,3-Dimethylbutane[#]	0.34 ± 0.01	0.31 ± 0.02	0.29 ± 0.02	0.23 ± 0.09	0.08 ± 0.01	0.19 ± 0.07
2-Methylpentane[#]	0.34 ± 0.01	0.41 ± 0.05	0.24 ± 0.03	0.24 ± 0.09	0.20 ± 0.02	0.31 ± 0.13
3-Methylpentane[#]	0.43 ± 0.04	0.21 ± 0.02	0.38 ± 0.04	0.27 ± 0.09	0.14 ± 0.02	0.17 ± 0.09
2-Methylheptane	1.49 ± 0.01	0.05 ± 0.01	0.03 ± 0.00	0.16 ± 0.11	0.01 ± 0.00	0.07 ± 0.07
3-Methylheptane	0.10 ± 0.01	0.04 ± 0.01	0.03 ± 0.00	0.12 ± 0.09	0.01 ± 0.00	0.04 ± 0.05
Methylcyclopentane	0.22 ± 0.06	0.12 ± 0.01	0.24 ± 0.02	0.16 ± 0.08	0.08 ± 0.01	0.11 ± 0.09
Cyclohexane[#]	2.95 ± 0.07	0.24 ± 0.02	0.03 ± 0.00	0.44 ± 0.18	0.04 ± 0.00	0.94 ± 0.41
***n*-Heptane[#]**	0.13 ± 0.01	0.05 ± 0.01	0.06 ± 0.01	0.26 ± 0.13	0.04 ± 0.01	0.60 ± 0.42
2,3-Dimethylpentane	0.19 ± 0.02	0.08 ± 0.01	0.02 ± 0.00	0.35 ± 0.09	0.02 ± 0.01	0.64 ± 0.12
2,4-Dimethylpentane	0.08 ± 0.01	0.01 ± 0.00	0.01 ± 0.00	0.15 ± 0.11	0.01 ± 0.00	0.06 ± 0.07
2-Methylhexane[#]	1.97 ± 0.05	0.14 ± 0.01	0.05 ± 0.00	0.12 ± 0.08	0.04 ± 0.01	0.09 ± 0.08
3-Methylhexane[#]	0.27 ± 0.01	0.09 ± 0.01	0.07 ± 0.01	0.15 ± 0.09	0.04 ± 0.00	0.1 ± 0.09
Methylcyclohexane	0.16 ± 0.01	0.05 ± 0.01	0.04 ± 0.00	0.15 ± 0.10	0.04 ± 0.01	0.06 ± 0.03

2,2,4-Trimethylpentane	0.10 ± 0.01	0.04 ± 0.00	0.08 ± 0.01	0.14 ± 0.09	0.02 ± 0.00	0.07 ± 0.08
2,3,4-Trimethylpentane	0.26 ± 0.06	0.04 ± 0.01	0.02 ± 0.00	0.12 ± 0.09	0.01 ± 0.00	0.08 ± 0.10
***n*-Octane**[#]	0.58 ± 0.13	0.09 ± 0.01	0.04 ± 0.00	0.11 ± 0.07	0.03 ± 0.01	0.06 ± 0.06
***n*-Nonane**[#]	0.29 ± 0.01	0.03 ± 0.01	0.03 ± 0.00	0.22 ± 0.12	0.01 ± 0.00	0.56 ± 0.08
***n*-Decane**[#]	0.16 ± 0.01	0.03 ± 0.00	0.03 ± 0.00	0.13 ± 0.09	0.01 ± 0.00	1.38 ± 1.39
***n*-Undecane**[#]	0.03 ± 0.01	0.05 ± 0.01	0.03 ± 0.00	0.12 ± 0.08	0.01 ± 0.00	0.12 ± 0.07
***n*-Dodecane**[#]	0.10 ± 0.02	0.05 ± 0.01	0.05 ± 0.00	0.11 ± 0.07	0.01 ± 0.00	0.60 ± 0.33
Ethyne[#]	/	0.60 ± 0.13	2.26 ± 0.14	1.26 ± 0.11	1.24 ± 0.09	0.94 ± 0.11
Ethene[#]	/	1.24 ± 0.12	2.20 ± 0.21	1.41 ± 0.16	1.18 ± 0.18	1.78 ± 0.37
Propene[#]	2.43 ± 0.10	0.32 ± 0.10	0.57 ± 0.09	0.23 ± 0.04	0.29 ± 0.05	1.12 ± 0.34
1-Butene[#]	1.15 ± 0.09	0.12 ± 0.01	0.10 ± 0.02	0.09 ± 0.02	0.09 ± 0.01	0.12 ± 0.10
***cis*-2-Butene**[#]	2.59 ± 0.12	0.08 ± 0.00	0.09 ± 0.02	0.05 ± 0.02	0.05 ± 0.00	0.22 ± 0.20
***trans*-2-Butene**[#]	0.55 ± 0.04	0.11 ± 0.01	0.10 ± 0.02	0.09 ± 0.03	0.05 ± 0.00	0.28 ± 0.20
1-Pentene[#]	0.35 ± 0.02	0.34 ± 0.01	0.00 ± 0.00	0.13 ± 0.03	0.15 ± 0.00	0.17 ± 0.10
***cis*-2-Pentene**[#]	0.23 ± 0.04	0.02 ± 0.00	0.04 ± 0.02	0.05 ± 0.03	0.02 ± 0.00	0.19 ± 0.17
***trans*-2-Pentene**[#]	0.20 ± 0.01	0.14 ± 0.02	0.07 ± 0.02	0.04 ± 0.00	0.04 ± 0.00	0.30 ± 0.14
1-Hexene[#]	0.07 ± 0.01	0.64 ± 0.09	0.03 ± 0.00	0.10 ± 0.02	0.01 ± 0.00	0.01 ± 0.00
1,3-Butadiene[#]	/	0.07 ± 0.02	0.15 ± 0.02	0.10 ± 0.04	0.05 ± 0.01	0.08 ± 0.02
Isoprene[#]	0.16 ± 0.00	0.09 ± 0.02	0.32 ± 0.03	0.30 ± 0.04	0.10 ± 0.02	0.15 ± 0.12

Benzene[#]	1.94 ± 0.01	0.82 ± 0.07	1.12 ± 0.11	0.39 ± 0.04	0.28 ± 0.03	0.20 ± 0.03
Toluene[#]	1.01 ± 0.01	0.93 ± 0.08	0.92 ± 0.07	0.35 ± 0.03	0.36 ± 0.03	0.22 ± 0.03
Ethylbenzene[#]	0.56 ± 0.01	0.40 ± 0.03	0.21 ± 0.01	0.14 ± 0.02	0.07 ± 0.01	0.09 ± 0.02
Styrene[#]	0.18 ± 0.01	0.46 ± 0.07	0.16 ± 0.02	0.03 ± 0.01	0.02 ± 0.00	0.03 ± 0.01
***m/p*-Xylene[#]**	0.85 ± 0.03	0.03 ± 0.00	0.47 ± 0.03	0.10 ± 0.01	0.15 ± 0.02	0.09 ± 0.01
***o*-Xylene[#]**	0.38 ± 0.01	0.13 ± 0.02	0.23 ± 0.02	0.15 ± 0.02	0.07 ± 0.01	0.01 ± 0.00
***i*-Propylbenzene[#]**	1.12 ± 0.01	0.01 ± 0.00	0.01 ± 0.00	0.01 ± 0.00	0.00 ± 0.00	0.02 ± 0.00
***n*-Propylbenzene[#]**	0.24 ± 0.15	0.02 ± 0.00	0.02 ± 0.00	0.01 ± 0.00	0.01 ± 0.00	0.01 ± 0.01
***m*-Ethyltoluene[#]**	0.54 ± 0.22	0.03 ± 0.00	0.04 ± 0.00	0.03 ± 0.01	0.01 ± 0.00	0.04 ± 0.01
***p*-Ethyltoluene[#]**	0.52 ± 0.07	0.04 ± 0.01	0.02 ± 0.00	0.01 ± 0.00	0.01 ± 0.00	0.01 ± 0.00
***o*-Ethyltoluene[#]**	0.96 ± 0.02	0.02 ± 0.00	0.02 ± 0.00	0.01 ± 0.00	0.01 ± 0.00	0.01 ± 0.01
1,3,5-Trimethylbenzene[#]	0.07 ± 0.01	0.03 ± 0.01	0.03 ± 0.00	0.03 ± 0.01	0.01 ± 0.00	0.04 ± 0.01
1,2,4-Trimethylbenzene[#]	0.09 ± 0.01	0.02 ± 0.00	0.06 ± 0.00	0.01 ± 0.00	0.02 ± 0.00	0.02 ± 0.01
1,2,3-Trimethylbenzene[#]	0.20 ± 0.01	0.03 ± 0.01	0.02 ± 0.00	0.01 ± 0.00	0.01 ± 0.00	0.02 ± 0.01
***m*-Diethylbenzene**	0.03 ± 0.01	0.04 ± 0.01	0.02 ± 0.00	0.01 ± 0.00	0.00 ± 0.00	0.03 ± 0.01
***p*-Diethylbenzene**	0.05 ± 0.01	0.01 ± 0.00	0.02 ± 0.00	0.01 ± 0.01	0.00 ± 0.00	0.02 ± 0.01

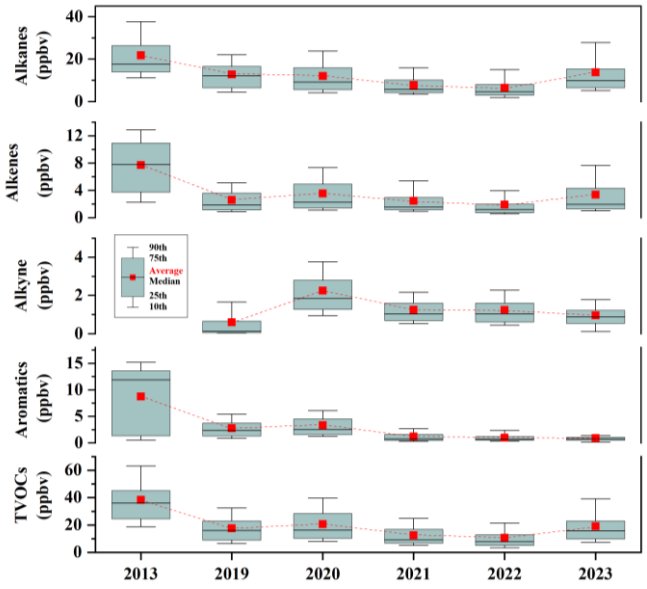

Figure 5.3. Daytime (07:00–19:00 LT) concentrations of different VOC groups in Lanzhou during August of 2013 and 2019-2023.

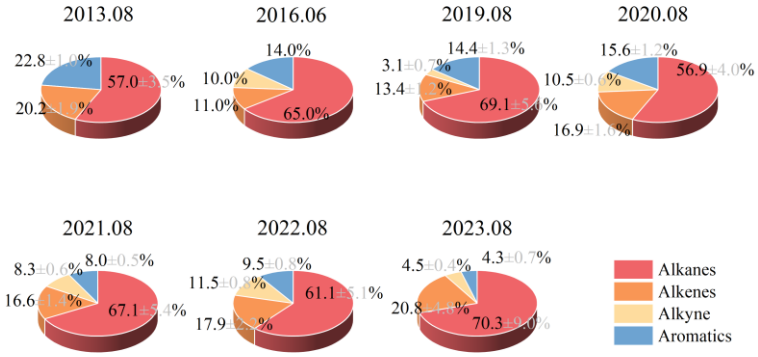

Figure 5.4. Daytime (07:00–19:00 LT) proportions of VOC groups in Lanzhou in August 2013, June 2016, and August 2019-2023. Data for June 2016 are sourced from Wu (2019).

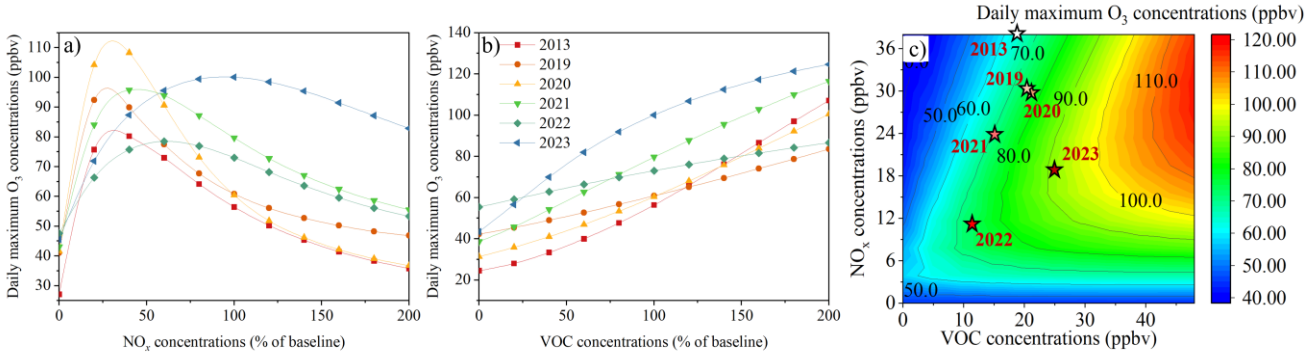

Figure 5.5. Simulated daily maximum O_3 concentrations under different conditions in Lanzhou in August 2013, and 2019-2023.

5.4 Radical chemistry and VOC contributions

5.4.1 O_3 formation mechanism

Figure 5.6 shows the simulated daytime (07:00–19:00 LT) O_3 production and destruction pathways for all days and O_3 episode days in 2013 and 2019-2023, while Table 5.6 list the average reaction rates for different pathways during the same daytime (07:00–19:00 LT) period. From 2019 to 2023, the net O_3 production rate in Lanzhou during summer ranged from 6.0 to 9.0 ppbv h^{-1}, consistent with both observed O_3 concentration trends and findings from a previous study in 2018 (X. F. Liu et al., 2021). In 2013, the net O_3 production rate was 5.2 ± 0.4 ppbv h^{-1}, which is 1.5 ppbv h^{-1} lower than the rate simulated for 2019 ($p < 0.05$). From 2019 to 2023, although an increasing trend was observed, the increase was not statistically significant ($p = 0.06$).

The dominant O_3 production pathway was HO_2 + NO, with reaction rates remaining stable between 5.3 and 6.7 ppbv h^{-1} from 2019 to 2023 ($p > 0.05$). The RO_2 + NO pathway also maintained rates between 2.8 and 4.8 ppbv h^{-1} during this period ($p > 0.05$). Compared to 2013, the rates of both the HO_2 + NO and RO_2 + NO pathways in 2019 were higher ($p < 0.05$). For O_3 destruction, the main pathway was OH + NO_2, which showed a significant decreasing trend from 2019 to 2023 ($p < 0.05$), while the reaction rate in 2013 was smaller than in 2019 ($p < 0.05$). Other destruction pathways, such as O_3 + alkenes, showed smaller rates from 2019 to 2023 compared to those in 2013 ($p < 0.05$), likely due to higher alkene concentrations in 2013 (Table 5.4). These findings suggested that reductions in NO_x and alkene concentrations have led to decreased O_3 consumption in summer in Lanzhou through titration reactions and alkene ozonolysis, potentially diminishing the effectiveness of air pollution control policies in managing O_3 levels.

Table 5.6. Daytime (07:00-19:00 LT) average reaction rates of production and destruction pathways of O_3 on all days in Lanzhou in August 2013, 2019-2023.

		2013	2019	2020	2021	2022	2023
Observed O_3 concentration (ppbv)		43.13 ± 3.22	55.89 ± 4.45	45.24 ± 2.72	51.84 ± 2.84	51.51 ± 2.23	62.48 ± 2.75
Net production rate (ppbv h^{-1})		6.14 ± 0.50	7.82 ± 0.64	6.23 ± 0.53	7.65 ± 0.69	6.01 ± 0.48	9.02 ± 0.97
Total production rate (ppbv h^{-1})		9.27 ± 0.63	11.57 ± 0.93	8.15 ± 0.66	9.77 ± 0.82	8.22 ± 0.63	11.33 ± 1.08
Total destruction rate (ppbv h^{-1})		-3.14 ± 0.14	-3.75 ± 0.30	-1.92 ± 0.13	-2.12 ± 0.15	-2.22 ± 0.16	-2.30 ± 0.14
Production rate (ppbv h^{-1})	HO_2 + NO	5.20 ± 0.36	6.72 ± 0.53	5.34 ± 0.43	5.91 ± 0.48	5.97 ± 0.46	6.50 ± 0.61
	RO_2 + NO	4.08 ± 0.27	4.85 ± 0.40	2.81 ± 0.23	3.85 ± 0.34	4.25 ± 0.17	4.83 ± 0.47
Destruction rate (ppbv h^{-1})	OH + NO_2	-1.92 ± 0.11	-2.77 ± 0.22	-1.43 ± 0.10	-1.61 ± 0.11	-1.42 ± 0.10	-1.40 ± 0.10
	O_3 + Alkenes	-1.02 ± 0.04	-0.17 ± 0.01	-0.10 ± 0.00	-0.08 ± 0.00	-0.09 ± 0.00	-0.42 ± 0.04
	O^1D + H_2O	-0.14 ± 0.02	-0.73 ± 0.08	-0.32 ± 0.03	-0.34 ± 0.03	-0.58 ± 0.06	-0.32 ± 0.03
	O_3 + OH	-0.02 ± 0.00	-0.05 ± 0.01	-0.03 ± 0.00	-0.04 ± 0.00	-0.07 ± 0.00	-0.04 ± 0.00
	O_3 + HO_2	-0.04 ± 0.00	-0.03 ± 0.00	-0.04 ± 0.00	-0.06 ± 0.01	-0.05 ± 0.00	-0.12 ± 0.01

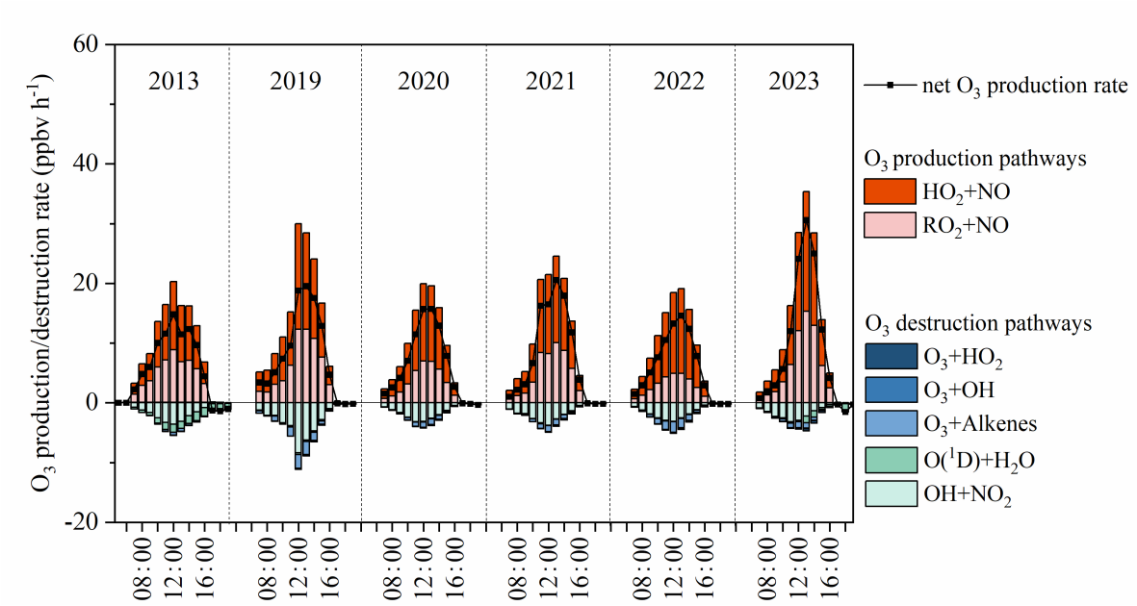

Figure 5.6. Simulated O_3 production and destruction rates on all days in Lanzhou in August 2013, 2019-2023.

5.4.2 Radical chemistry

Figures 5.7-5.9 present the OH, HO_2, and RO_2 formation and loss pathways on O_3 episode and non-episode days from 2013 to 2023, while Table 5.7 list the daytime average reaction rates for these pathways. From 2019 to 2023, OH concentrations remained stable at around 2×10^6 molecules cm^{-3}, comparable to levels observed in 2013, indicating no significant trend ($p > 0.05$). These simulated OH concentrations in 2013, 2019-2023 were consistent with previous findings for summertime Lanzhou in 2018 (X. F. Liu et al., 2021). The dominant OH production pathway was the reaction between HO_2 and NO, with production rates ranging from (3.6-4.7) $\times 10^7$ molecules cm^{-3} s^{-1} in both 2013 and 2019-2023. The main OH destruction pathway was OH + VOCs, with rates stable between (1.8-3.9) $\times 10^7$ molecules cm^{-3} s^{-1} across the same periods, followed by OH+CO and $OH+NO_2$. The rates of OH+CO and $OH+NO_2$ were similar in 2013 and 2019-2023, at (0.5-1.8) $\times 10^7$ and (1.0-1.9) $\times 10^7$ molecules cm^{-3} s^{-1} respectively. For HO_2 and RO_2 radicals, the simulated average concentrations remained stable at (1.0-2.4) $\times 10^7$ and (4.3-7.2) $\times 10^7$ molecules cm^{-3}, respectively in 2013 and 2019-2023. The main production pathway for HO_2 was RO_2 + NO, with rates of (1.9-3.3) $\times 10^7$ molecules cm^{-3} in both periods. The dominant loss pathway for HO_2 was HO_2 + NO, accounting for over 90 % of total HO_2 loss. For RO_2 radicals, average concentrations fluctuated between 4.3×10^8 and 7.2×10^8 molecules cm^{-3}, with OH + VOCs and RO_2 + NO serving as the main production and loss pathways, respectively, each contributing over 90 % to RO_2 formation and loss.

Table 5.7. Daytime (07:00-19:00 LT) average concentrations of OH, HO_2, RO_2, and production & destruction rates of OH, HO_2, and RO_2 on all days in Lanzhou in August 2013, 2019-2023.

		2013	2019	2020	2021	2022	2023
OH concentration ($\times10^6$ molecules cm^{-3})		1.83 ± 0.11	2.02 ± 0.24	1.95 ± 0.23	2.22 ± 0.24	2.01 ± 0.30	2.30 ± 0.18
HO_2 concentration ($\times10^8$ molecules cm^{-3})		1.30 ± 0.11	1.56 ± 0.10	1.00 ± 0.08	1.31 ± 0.10	1.25 ± 0.10	2.37 ± 0.23
RO_2 concentration ($\times10^8$ molecules cm^{-3})		5.38 ± 1.28	6.19 ± 1.17	5.31 ± 0.63	5.44 ± 0.64	5.28 ± 0.60	7.20 ± 1.54
OH formation pathways ($\times10^7$molecules cm^{-3} s^{-1})	HO_2 + NO	3.56 ± 0.10	4.61 ± 0.40	3.66 ± 0.36	4.05 ± 0.40	4.10 ± 0.39	4.45 ± 0.50
	HONO + *hv*	0.62 ± 0.05	1.34 ± 0.15	0.75 ± 0.6	0.94 ± 0.07	1.61 ± 0.13	0.79 ± 0.06
	$O^1D + H_2O$	0.20 ± 0.02	0.99 ± 0.13	0.44 ± 0.05	0.46 ± 0.05	0.80 ± 0.09	0.44 ± 0.05
	O_3 + Alkenes	0.70 ± 0.03	0.12 ± 0.00	0.07 ± 0.00	0.05 ± 0.00	0.06 ± 0.00	0.29 ± 0.03
	H_2O_2 + *hv*	0.01 ± 0.00	0.01 ± 0.00	0.01 ± 0.00	0.01 ± 0.00	0.01 ± 0.00	0.01 ± 0.00
OH loss pathways ($\times10^7$molecules	OH + CO	-0.48 ± 0.04	-1.75 ± 0.16	-1.22 ± 0.11	-1.13 ± 0.09	-1.63 ± 0.18	-0.95 ± 0.09
	OH + VOCs	-2.96 ± 0.20	-2.63 ± 0.29	-1.78 ± 0.19	-2.88 ± 0.32	-2.69 ± 0.16	-3.91 ± 0.32
	OH + NO	-0.30 ± 0.03	-0.72 ± 0.07	-0.33 ± 0.03	-0.34 ± 0.03	-0.50 ± 0.05	-0.18 ± 0.02
	OH + NO_2	-1.11 ± 0.09	-1.90 ± 0.19	-0.98 ± 0.08	-1.10 ± 0.09	-1.94 ± 0.17	-0.96 ± 0.08
	RO_2 + NO	2.80 ± 0.23	2.66 ± 0.27	1.92 ± 0.19	2.64 ± 0.28	2.54 ± 0.14	3.31 ± 0.40
	OH + CO	0.48 ± 0.04	1.75 ± 0.16	1.43 ± 0.12	1.13 ± 0.09	1.63 ± 0.18	0.95 ± 0.09
	HCHO + *hv*	0.20 ± 0.02	0.34 ± 0.04	0.20 ± 0.02	0.21 ± 0.02	0.16 ± 0.02	0.21 ± 0.02

HO_2 formation pathways	OVOCs + *hv*	0.04 ± 0.00	0.05 ± 0.00	0.02 ± 0.00	0.02 ± 0.00	0.01 ± 0.00	0.03 ± 0.00
	O_3 + Alkenes	0.70 ± 0.03	0.12 ± 0.00	0.07 ± 0.00	0.05 ± 0.00	0.06 ± 0.00	0.29 ± 0.03
	OH + HCHO	0.25 ± 0.02	0.30 ± 0.04	0.27 ± 0.03	0.28 ± 0.06	0.27 ± 0.03	0.30 ± 0.04
HO_2 loss pathways ($\times10^7$molecules	HO_2 + NO	-3.56 ± 0.30	-4.61 ± 0.40	-3.66 ± 0.36	-4.05 ± 0.40	-4.10 ± 0.39	-4.45 ± 0.50
	HO_2 + RO_2	-0.15 ± 0.03	-0.07 ± 0.01	-0.07 ± 0.01	-0.06 ± 0.01	-0.03 ± 0.00	-0.22 ± 0.03
	HO_2 + HO_2	-0.02 ± 0.00	0.00 ± 0.00	-0.02 ± 0.00	-0.02 ± 0.00	-0.02 ± 0.00	-0.09 ± 0.01
	HO_2 + O_3	-0.03 ± 0.00	-0.02 ± 0.00	-0.03 ± 0.00	-0.04 ± 0.00	-0.04 ± 0.00	-0.09 ± 0.01
RO_2 formation pathways ($\times10^7$molecules	OH + VOCs	2.96 ± 0.23	2.63 ± 0.29	2.09 ± 0.22	2.88 ± 0.32	2.69 ± 0.16	3.91 ± 0.32
	O_3 + Alkenes	0.70 ± 0.03	0.12 ± 0.00	0.07 ± 0.00	0.05 ± 0.00	0.06 ± 0.00	0.29 ± 0.03
	OVOCs + *hv*	0.04 ± 0.00	0.05 ± 0.00	0.02 ± 0.00	0.02 ± 0.00	0.01 ± 0.00	0.04 ± 0.00
RO_2 loss pathways	RO_2 + NO	-2.80 ± 0.23	-2.66 ± 0.27	-1.92 ± 0.19	-2.64 ± 0.28	-2.54 ± 0.14	-3.31 ± 0.40
	HO_2 + RO_2	-0.15 ± 0.03	-0.07 ± 0.01	-0.07 ± 0.01	-0.06 ± 0.01	-0.03 ± 0.00	-0.22 ± 0.03

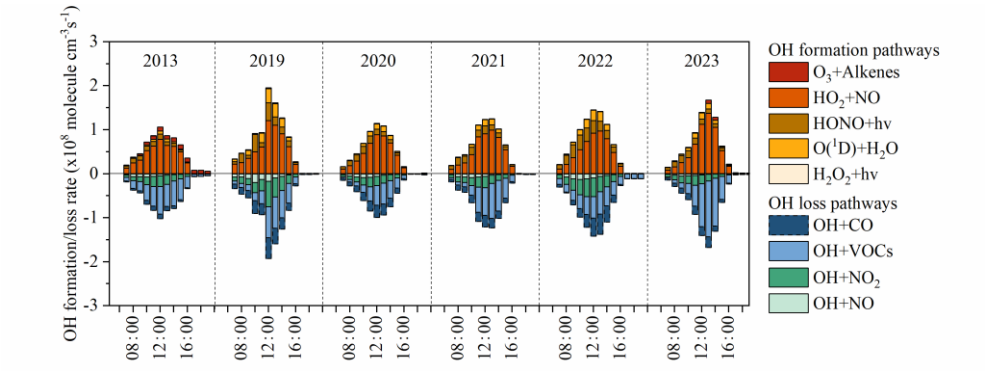

Figure 5.7. Simulated OH formation and loss rates on all days in Lanzhou in August 2013, 2019-2023.

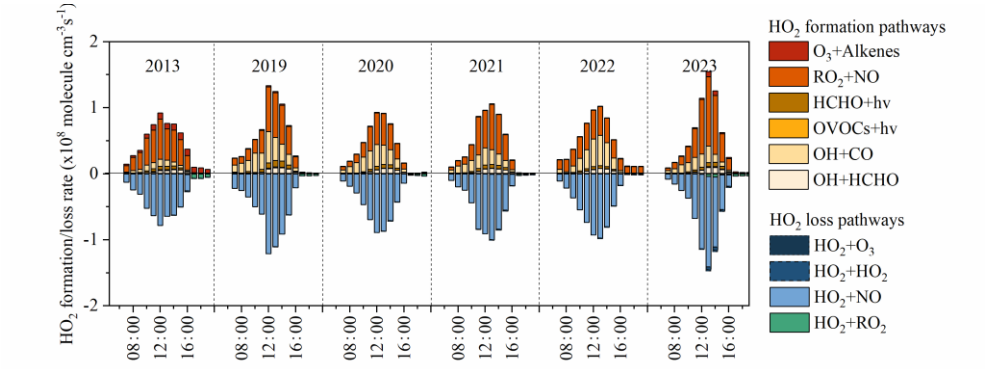

Figure 5.8. Simulated HO_2 formation and loss rates on all days in Lanzhou in August 2013, 2019-2023.

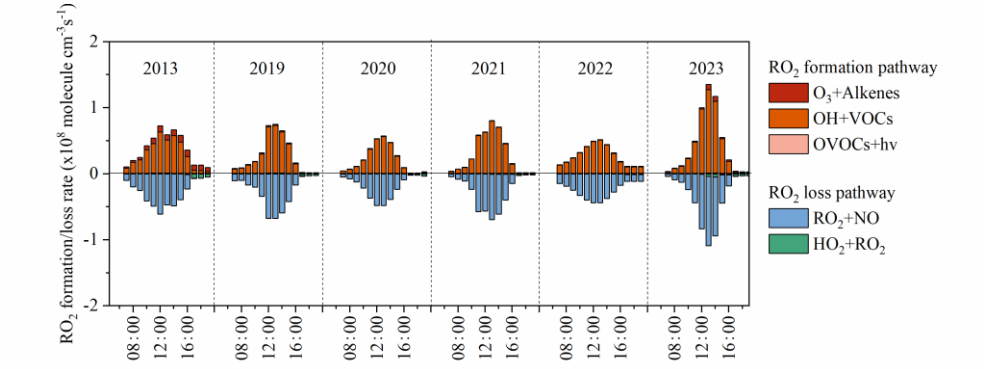

Figure 5.9. Simulated RO_2 formation and loss rates on all days in Lanzhou in August 2013, 2019-2023.

5.4.3 VOC contributions to O_3 formation

Table 5.8 summarize the average contributions of VOC groups and individual species to O_3 formation during the peak period (12:00–15:00 LT) on all days and O_3 episode days in Lanzhou for August 2013 and 2018–2023. As shown in Table 5.8, alkenes were the predominant contributors to O_3 formation in 2013 and 2019–2022, together accounting for 50-63 % of the total VOC contribution, followed by aromatics, alkanes and alkyne. Alkanes and aromatics ranged from 8-30 % and alkynes consistently below 1 %. Among the individual VOC species listed in Table 5.9, alkenes such as *trans/cis*-2-butene, propene, and ethene exhibited the highest contributions to O_3 formation, while aromatics including *m/p/o*-xylene and toluene also made substantial contributions. For example, in 2013, *cis*-2-butene was the dominant VOC, accounting for 18.5 ± 0.9 % of the total measured VOCs, while propene and *trans*-2-butene contributed 14.0 ± 0.6 % and 5.3 ± 0.4 %, respectively. From 2019 to 2023, ethene and propene continued to contribute significantly, accounting for approximately 10-19 % and 6-17 %, respectively, while *trans/cis*-2-butene comprised around 5-9 %. Among aromatics, *m/p/o*-xylene and toluene contributed 2-13 % and 1-7 %, respectively, from 2019 to 2023. Overall, the data indicate a markable contribution from alkenes throughout 2013 and 2019-2023. These findings highlight the necessity for targeted VOC control strategies to effectively mitigate O_3 pollution.

Table 5.8. Average contributions of VOC groups to O_3 formation during peak hours (12:00–15:00 LT) on all days in Lanzhou in August 2013, 2019-2023.

	2013	**2019**	**2020**	**2021**	**2022**	**2023**
Alkanes	18.71 ± 0.70 %	18.26 ± 1.52 %	17.66 ± 3.54 %	28.77 ± 7.11 %	21.49 ± 0.55 %	28.54 ± 6.95 %
Alkenes	**51.50 ± 2.86 %**	**53.13 ± 6.06 %**	**50.44 ± 7.08 %**	**51.31 ± 5.43 %**	**55.88 ± 1.52 %**	**63.19 ± 9.29 %**
Alkyne	/	0.14 ± 0.04 %	0.25 ± 0.14 %	0.43 ± 0.03 %	0.59 ± 0.04 %	0.06 ± 0.02 %
Aromatics	29.79 ± 2.95 %	28.48 ± 3.44 %	31.64 ± 6.80 %	19.49 ± 2.50 %	22.04 ± 1.02 %	8.07 ± 1.32 %

Table 5.9. Average contributions of VOC species to O_3 formation during peak hours (12:00–15:00 LT) on all days in Lanzhou in August 2013, 2019-2023.

Species	**2013**	**2019**	**2020**	**2021**	**2022**	**2023**
Ethane	/	0.34 ± 0.07 %	0.26 ± 0.14 %	0.54 ± 0.02 %	0.65 ± 0.02 %	0.37 ± 0.04 %
Propane	0.68 ± 0.06 %	1.58 ± 0.07 %	0.62 ± 0.24 %	0.87 ± 0.09 %	1.53 ± 0.03 %	0.48 ± 0.14 %
***i*-Butane**	2.00 ± 0.03 %	2.14 ± 0.15 %	1.61 ± 0.16 %	2.14 ± 0.16 %	2.21 ± 0.09 %	2.29 ± 0.47 %
***n*-Butane**	1.00 ± 0.01 %	2.05 ± 0.33 %	2.22 ± 0.55 %	2.73 ± 0.30 %	3.39 ± 0.09 %	2.66 ± 0.42 %
***i*-Pentane**	1.51 ± 0.08 %	2.50 ± 0.21 %	4.22 ± 0.58 %	3.63 ± 0.31 %	4.49 ± 0.05 %	2.47 ± 0.47 %
***n*-Pentane**	0.81 ± 0.03 %	0.58 ± 0.04 %	1.47 ± 0.48 %	1.61 ± 0.18 %	2.12 ± 0.05 %	1.31 ± 0.47 %
2,2-Dimethylbutane	0.53 ± 0.01 %	0.18 ± 0.04 %	0.03 ± 0.02 %	0.81 ± 0.46 %	0.07 ± 0.00 %	0.25 ± 0.22 %
2,3-Dimethylbutane	0.48 ± 0.01 %	1.23 ± 0.04 %	0.68 ± 0.25 %	1.42 ± 0.51 %	0.68 ± 0.03 %	0.73 ± 0.27 %

2-Methylpentane	0.49 ± 0.01 %	2.00 ± 0.12 %	1.05 ± 0.15 %	1.49 ± 0.51 %	1.71 ± 0.04 %	1.21 ± 0.50 %
3-Methylpentane	0.58 ± 0.05 %	1.09 ± 0.06 %	1.82 ± 0.26 %	1.58 ± 0.48 %	1.13 ± 0.05 %	0.62 ± 0.33 %
***n*-Hexane**	0.59 ± 0.01 %	1.08 ± 0.08 %	2.63 ± 0.28 %	2.55 ± 0.55 %	1.73 ± 0.03 %	2.01 ± 0.78 %
Cyclohexane	5.31 ± 0.13 %	1.82 ± 0.13 %	0.05 ± 0.03 %	3.43 ± 0.28 %	0.43 ± 0.01 %	4.57 ± 0.99 %
2-Methylhexane	2.97 ± 0.08 %	0.55 ± 0.04 %	0.23 ± 0.16 %	0.78 ± 0.48 %	0.36 ± 0.01 %	0.37 ± 0.33 %
3-Methylhexane	0.44 ± 0.02 %	0.39 ± 0.08 %	0.43 ± 0.13 %	1.06 ± 0.58 %	0.39 ± 0.01 %	0.44 ± 0.04 %
***n*-Heptane**	0.14 ± 0.01 %	0.18 ± 0.01 %	0.13 ± 0.04 %	1.18 ± 0.54 %	0.25 ± 0.01 %	1.70 ± 0.19 %
***n*-Octane**	0.52 ± 0.12 %	0.25 ± 0.03 %	0.11 ± 0.02 %	0.43 ± 0.25 %	0.16 ± 0.00 %	0.14 ± 0.04 %
***n*-Nonane**	0.44 ± 0.02 %	0.09 ± 0.01 %	0.02 ± 0.01 %	1.43 ± 0.72 %	0.09 ± 0.00 %	2.28 ± 0.33 %
***n*-Decane**	0.19 ± 0.01 %	0.09 ± 0.01 %	0.04 ± 0.02 %	0.66 ± 0.42 %	0.07 ± 0.00 %	4.37 ± 0.40 %
***n*-Undecane**	0.03 ± 0.01 %	0.13 ± 0.01 %	0.03 ± 0.02 %	0.43 ± 0.27 %	0.05 ± 0.00 %	0.27 ± 0.16 %
***n*-Dodecane**	0.00 ± 0.00 %	0.00 ± 0.00 %	0.00 ± 0.00 %	0.00 ± 0.00 %	0.00 ± 0.00 %	0.00 ± 0.00 %
Ethyne	/	0.14 ± 0.04 %	0.25 ± 0.14 %	0.43 ± 0.03 %	0.59 ± 0.04 %	0.20 ± 0.02 %
Ethene	**/**	**10.20 ± 0.5 %**	**16.69 ± 1.60 %**	**16.36 ± 1.70 %**	**18.91 ± 0.08 %**	**12.89 ± 1.68 %**
Propene	**14.04 ± 0.58 %**	**8.75 ± 0.44 %**	**13.23 ± 1.16 %**	**5.75 ± 0.92 %**	**10.00 ± 0.07 %**	**17.47 ± 1.30 %**
1-Butene	5.29 ± 0.41 %	2.55 ± 0.23 %	1.62 ± 0.15 %	1.79 ± 0.36 %	2.47 ± 0.08 %	1.49 ± 0.24 %
***trans*-2-Butene**	**5.27 ± 0.38 %**	**6.68 ± 0.68 %**	**4.64 ± 0.22 %**	**3.73 ± 0.14 %**	**2.86 ± 0.30 %**	**7.24 ± 0.17 %**
***cis*-2-Butene**	**18.49 ± 0.86 %**	**2.88 ± 0.36 %**	**2.13 ± 0.26 %**	**1.54 ± 0.57 %**	**2.13 ± 0.14 %**	**4.24 ±0.85 %**
1,3-Butadiene	/	2.09 ± 0.19 %	3.64 ± 0.70 %	2.87 ± 0.05 %	1.98 ± 0.09 %	1.43 ± 0.36 %

1-Pentene	2.42 ± 0.14 %	6.39 ± 0.68 %	3.07 ± 0.06 %	3.89 ± 0.82 %	6.19 ± 0.21 %	3.17 ± 0.87 %
***trans*-2-Pentene**	1.21 ± 0.06 %	6.11 ± 0.59 %	1.40 ± 0.22 %	1.05 ± 0.00 %	1.45 ± 0.09 %	4.92 ± 0.30 %
***cis*-2-Pentene**	1.99 ± 0.35 %	1.01 ± 0.03 %	0.77 ± 0.31 %	1.87 ± 0.03 %	1.03 ± 0.04 %	4.43 ± 0.96 %
1-Hexene	0.54 ± 0.08 %	2.34 ± 0.05 %	0.56 ± 0.23 %	3.33 ± 0.61 %	0.46 ± 0.02 %	0.21 ± 0.00 %
Isoprene	2.25 ± 0.00 %	4.13 ± 0.31 %	2.69 ± 0.17 %	9.13 ± 0.23 %	8.40 ± 0.40 %	5.70 ± 0.56 %
Benzene	1.56 ± 0.01 %	0.95 ± 0.20 %	1.38 ± 0.13 %	1.35 ± 0.13 %	1.34 ± 0.21 %	0.43 ± 0.06 %
Toluene	**2.18 ± 0.02 %**	**6.79 ± 0.72 %**	**6.97 ± 1.15 %**	**3.27 ± 0.26 %**	**4.64 ± 0.22 %**	**1.28 ± 0.17 %**
Ethylbenzene	1.84 ± 0.03 %	3.37 ± 0.35 %	1.63 ± 0.29 %	1.99 ± 0.26 %	1.37 ± 0.08 %	0.80 ± 0.18 %
***m/p*-Xylene**	**7.37 ± 0.26 %**	**6.76 ± 0.07 %**	**8.01 ± 1.91 %**	**3.75 ± 0.34 %**	**7.76 ± 0.17 %**	**2.11 ± 0.23 %**
***o*-Xylene**	**3.15 ± 0.08 %**	**2.12 ± 0.45 %**	**4.78 ± 1.20 %**	**5.37 ± 0.66 %**	**3.46 ± 0.13 %**	**0.22 ± 0.00 %**
Styrene	0.74 ± 0.04 %	3.01 ± 0.78 %	2.26 ± 0.53 %	0.53 ± 0.16 %	0.49 ± 0.04 %	0.33 ± 0.11 %
***i*-Propylbenzene**	1.13 ± 0.01 %	0.08 ± 0.01 %	0.05 ± 0.03 %	0.04 ± 0.00 %	0.06 ± 0.01 %	0.05 ± 0.00 %
***n*-Propylbenzene**	0.32 ± 0.20 %	0.22 ± 0.06 %	0.24 ± 0.13 %	0.06 ± 0.00 %	0.08 ± 0.01 %	0.04 ± 0.00 %
***m*-Ethyltoluene**	4.52 ± 1.84 %	0.64 ± 0.05 %	0.84 ± 0.29 %	1.09 ± 0.33 %	0.50 ± 0.04 %	0.90 ± 0.23 %
***p*-Ethyltoluene**	1.13 ± 0.15 %	0.64 ± 0.05 %	0.31 ± 0.11 %	0.09 ± 0.00 %	0.13 ± 0.01 %	0.06 ± 0.00 %
***o*-Ethyltoluene**	3.38 ± 0.07 %	0.31 ± 0.04 %	0.37 ± 0.12 %	0.15 ± 0.00 %	0.21 ± 0.01 %	0.09 ± 0.01 %
1,3,5-Trimethylbenzene	0.63 ± 0.09 %	1.75 ± 0.37 %	1.42 ± 0.34 %	1.17 ± 0.36 %	0.54 ± 0.04 %	0.98 ± 0.04 %
1,2,4-Trimethylbenzene	0.87 ± 0.10 %	0.87 ± 0.06 %	2.79 ± 0.37 %	0.42 ± 0.00 %	1.16 ± 0.05 %	0.52 ± 0.26 %
1,2,3-Trimethylbenzene	0.97 ± 0.05 %	0.96 ± 0.21 %	0.59 ± 0.21 %	0.21 ± 0.00 %	0.29 ± 0.02 %	0.26 ± 0.03 %

5.5 VOC sources and their contributions to O_3 formation

5.5.1 Source apportionment

To investigate the sources of various O_3 precursors, 21 VOCs and 3 trace gases were selected as inputs for the PMF model to perform source apportionment. A total of 3,622 samples collected in Lanzhou in 2013 and from 2019 to 2023 were analyzed, with the results presented in Figure 5.10. Factor 1 was identified as solvent usage, based on the significant contributions of aromatics, particularly toluene, ethylbenzene, and *m/p/o*-xylene (Ling & Guo, 2014; Shao et al., 2016). Factor 2 was characterized by high levels of C_2–C_3 alkanes and alkenes, such as ethane, ethene, propane, and propene, along with notable amounts of NO_x and CO, and was therefore attributed to diesel exhaust (X. F. Liu et al., 2021; Lyu et al., 2019). Factor 3 exhibited substantial amounts of *i/n*-butane, along with moderate quantities of NO_x, and CO, leading to its identification as LPG usage (Guo, Ling, Cheung, Wang, et al., 2013; Ho, 2009; Ling & Guo, 2014; X. F. Liu et al., 2021; X. F. Liu et al., 2019; Lyu et al., 2019; Lyu et al., 2017). Factor 4 was marked by significant contributions from long-chain alkanes, notably *i/n*-pentane, *n*-hexane, *n*-heptane, *n*-octane, *n*-nonane, and *n*-decane, as well as some NO_x and CO, and was thus classified as gasoline usage (Ho, 2009; Ling & Guo, 2014; Lyu et al., 2019). Factor 5 was recognized as biogenic emission due to the dominant presence of isoprene (Qian et al., 2019; Zhou et al., 2019). Finally, Factor 6 was identified as the petrochemical industry, given the prominent contributions of 1,3-butadiene and styrene (Knighton et al., 2012; X. F. Liu et al., 2021).

5.5.2 Source contributions to O_3 production

The percentages of different sources contributing to O_3 formation from 2013 to 2023 are presented in Figure 5.10. Using the PBM-MCM model, we quantified the roles of individual VOC species in O_3 formation (see Table 5.9), while the distributions of VOC species from different sources were identified by the PMF model (see Figure 5.10). The source contributions to O_3 formation were evaluated by integrating the results of the PMF and PBM-MCM models.

Several key sources played significant roles in contributing to O_3 levels throughout this period. As both gasoline and diesel exhaust are categorized as vehicle emissions, they are treated as a single source in the following discussion.

Based on Figure 5.11a, vehicle emissions consistently accounted for around 60 % of the total VOC concentration in Lanzhou from 2013 and 2019-2023, followed by LPG usage and petrochemical industry. Regarding O_3 formation, the contribution of vehicle emissions remained between 32 % and 45 % during 2013 and 2019-2023, while the petrochemical industry contributed steadily, accounting for about 20 % to 28 % in both periods (Figure 5.11b). The contribution from solvent usage remained at approximately 15 % to 22 %, whereas LPG usage and biogenic emissions both showed limited contributions, accounting for about 7-10 % and 4-10 % respectively. The notable contribution from vehicle emissions highlights the need for stricter control measures targeting this source. Meanwhile, the stable contributions from the petrochemical industry and solvent usage underscore the importance of regulating VOC emissions from these sectors.

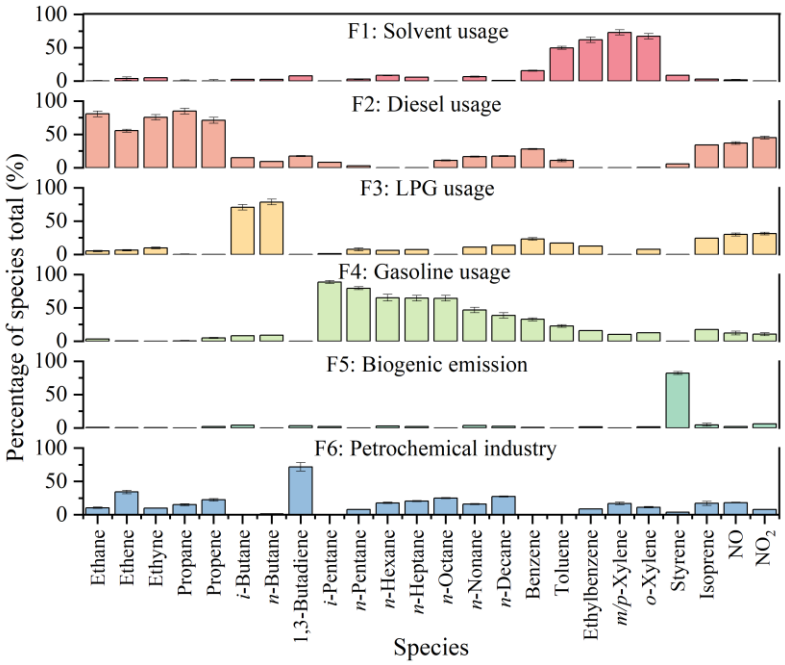

Figure 5.10. Average profiles of the O_3 precursor sources in Lanzhou.

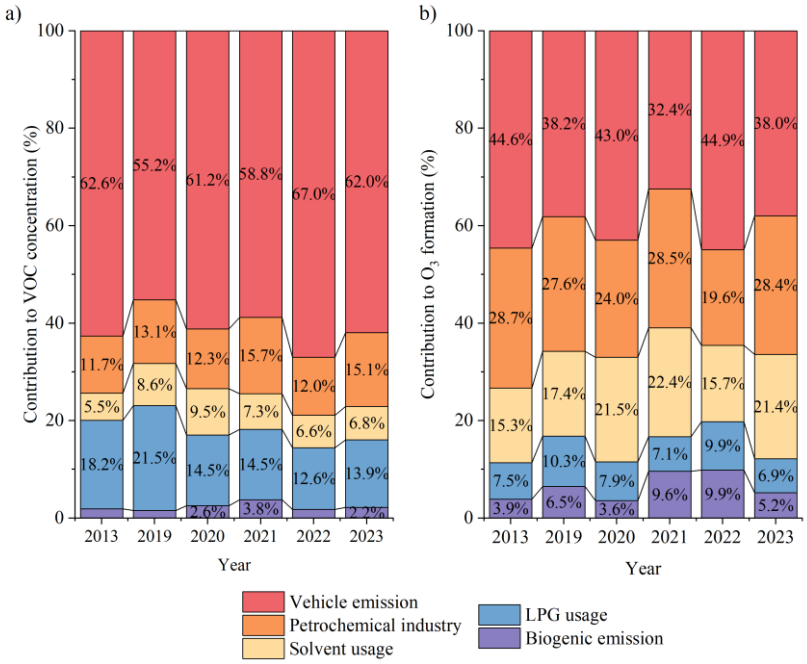

Figure 5.11 Percentage of source contribution to on a) VOC concentration, b) O_3 formation in 2013, and 2019 to 2023 in Lanzhou.

5.6 Summary

This study systematically examined the long-term trends, chemical mechanisms, and source contributions of O_3 pollution in Lanzhou from 2013 to 2023, with particular emphasis on the summertime period when O_3 levels peak. The results showed that, although concentrations of primary air pollutants such as $PM_{2.5}$, CO, SO_2, and NO_2 have declined significantly in recent years due to effective emission control measures, O_3 concentrations exhibited a continuous upward trend during 2013–2023, indicating that O_3 pollution remains a persistent challenge. While NO_2 and CO concentrations decreased steadily, the effectiveness of VOC control measures was comparatively limited.

Model simulations further revealed a shift in O_3 formation regimes in Lanzhou. In 2013, O_3 formation was primarily VOC-limited; however, from 2019 to 2023, a transition occurred from a VOC-limited regime to a transitional regime, largely driven by reductions in NO_x. The observed increase in O_3 levels during this period was mainly attributable to the decrease in NO_x concentrations. As the O_3 formation regime shifted from VOC-limited to VOC-NO_x co-limited, it became clear that effective O_3 control now requires simultaneous management of both NO_x and VOC emissions.

Alkenes were identified as the dominant contributors to O_3 formation in Lanzhou throughout the decade, accounting for approximately 50–63% of the total VOC contribution. Ethene, propene, and *trans/cis*-2-butene made particularly significant contributions. Six major sources of O_3 precursors were identified, with vehicular emissions being the largest contributor to ambient VOCs, followed by the petrochemical industry and solvent usage. This highlights the need for additional efforts to reduce emissions from these sources.

Overall, these findings provide a robust scientific basis for refining O_3 pollution control policies in Lanzhou and may offer valuable guidance for developing similar strategies in other cities facing persistent O_3 challenges.

Chapter 6 Atmospheric formaldehyde, acetaldehyde, and acetone in five Chinese megacities: photochemical characteristics, sources, and joint ozone-carbonyl control strategies

6.1 Introduction

Carbonyls are important components of atmospheric volatile organic compounds (VOCs) and have a significant impact on air quality (Atkinson, 2000; Jenkin, 1997; W. Wang, B. Yuan, et al., 2022; Xue et al., 2016; Yang et al., 2018). They enter the atmosphere both through direct emissions and secondary formation via complex photochemical reactions (Ling et al., 2017; Liu et al., 2009; Pang & Mu, 2006; Wu et al., 2023; Yang et al., 2017; Z. Yang et al., 2019; Y. Zhang et al., 2019). Among these carbonyls, formaldehyde, acetaldehyde, and acetone are most abundant in urban environments. Formaldehyde and acetaldehyde, in particular, act as key precursors for tropospheric ozone (O_3) formation due to their reactive carbonyl groups (Guo, Ling, Cheung, Wang, et al., 2013; Yang et al., 2018; Zhang et al., 2021; Y. Zhang et al., 2019). Prolonged exposure to high concentrations of formaldehyde and acetaldehyde, which is common in urban or industrial areas, poses health risks, including carcinogenicity and respiratory irritation (Bao et al., 2022; Ho et al., 2015; Lu et al., 2010; Z. Yang et al., 2019). Given regional differences in emission sources and chemical processes, understanding the concentration levels, primary sources, and secondary formation mechanisms of carbonyl compounds in various cities is crucial for formulating effective, targeted air pollution control strategies.

The spatiotemporal distribution of formaldehyde, acetaldehyde, and acetone has been extensively documented through global observations over recent decades (Ho et al., 2015; Liu et al., 2022; Liu et al., 2009; Lui et al., 2017; Yang et al., 2017; X. Zhang et al., 2022; Y. Zhang et al., 2019), which reveals high mixing ratios of these carbonyls in cities worldwide, especially in East Asia **(Liu et al., 2022).** In China, regions such as the North China Plain (NCP), Yangtze River Delta (YRD), and Pearl River Delta (PRD) have reported elevated carbonyl levels, with

formaldehyde and acetaldehyde often exceeding 20 and 10 ppbv, respectively (Y. Zhang et al., 2019). However, most previous studies relied on single-site sampling over various periods, thereby limiting direct intercity comparisons and introducing uncertainties due to time separation. Simultaneous multi-city sampling, which enables more accurate assessment of secondary pollution and supports targeted air quality management, remains rare. For example, one previous study conducted concurrent sampling in five major Chinese cities during the summer of 2018, finding the highest carbonyl concentrations in Beijing (24.3 ± 2.7 ppbv, 55 % of total VOCs), followed by Wuhan (10.8 ± 1.5 ppbv), Lanzhou (7.6 ± 1.3 ppbv), Shanghai (6.8 ± 1.0 ppbv), and Chengdu (5.7 ± 2.0 ppbv) (X. F. Liu et al., 2021). However, as that study focused on O_3 pollution, the sources, formation, and transformation processes of carbonyls were not comprehensively characterized.

Previous studies have extensively examined the contributions of primary and secondary sources to major carbonyl compounds across various cities (Bao et al., 2022; de Gouw et al., 2005; Ho et al., 2015; Li et al., 2010; Ling et al., 2017; Liu et al., 2009; Lui et al., 2017; Ma et al., 2016; Pang & Mu, 2006; Wang et al., 2015; Wu et al., 2023; Yang et al., 2017; Z. Yang et al., 2019). While the exact proportions vary depending on methodology, location, season, and local emission profiles, primary sources, such as vehicle exhaust, industrial emissions, biogenic emissions, and biomass burning, typically account for 30–50 % of carbonyls, with secondary formation contributing 50–70 % (Guo, Ling, Cheung, Wang, et al., 2013; Hua et al., 2023; Liu et al., 2009; Pang & Mu, 2006; Rao et al., 2016). Secondary formation, the dominant pathway, mainly occurs through VOC reactions with atmospheric oxidants such as hydroxyl (OH) radicals, producing alkyl (RO) radicals that decompose into carbonyls (Anderson et al., 2017; Chen et al., 2022; Lin et al., 2012; Liu et al., 2022; Nussbaumer et al., 2021; Yang et al., 2018; Yang et al., 2023). Anthropogenic alkenes are key precursors for formaldehyde and acetaldehyde (Ling et al., 2017; Yang et al., 2018), while plant-emitted isoprene generates formaldehyde (Palmer et al., 2006; X. Yang et al., 2020). Acetone is primarily formed from C_3-C_5 alkanes and pinene (Guo, Ling, Cheung, Wang, et al., 2013; Ling et al., 2017; Lyu et al., 2024; Yang et al., 2018; X. Yang et al., 2020). However, most research relies on sensitivity

analyses or precursor exclusion to infer contributions, with few studies providing quantitative assessments through in-situ simulation. Tracing the contributions of individual VOC precursors via reaction pathways remains particularly challenging (Chen et al., 2022; Ling et al., 2017; Lyu et al., 2024; Yang et al., 2018; X. Yang et al., 2020).

Apart from investigating carbonyl sources, many studies have focused on their role in O_3 formation, mainly using parameterized methods such as O_3 formation potential (OFP) and OH reactivity (L_{OH}) calculation (Bao et al., 2022; Huang et al., 2020; Hui et al., 2023; Z. Liu et al., 2021; Lyu et al., 2024; Shen et al., 2021; C. Wang et al., 2017; F. Wang et al., 2024; Yang et al., 2018; Yang et al., 2017; X. Yang et al., 2020; Zhang et al., 2021). Formaldehyde and acetaldehyde consistently rank among the top contributors in OFP studies, qualitatively highlighting their importance in O_3 formation (Hui et al., 2023; F. Wang et al., 2024; X. Yang et al., 2020; Yuan et al., 2024; Zhang et al., 2021). Mechanistically, as intermediate products of VOC oxidation, formaldehyde and acetaldehyde are deeply involved in the radical cycle. Their photolysis or oxidation produces hydroperoxyl (HO_2) and alkyl peroxy (RO_2) radicals (Edwards et al., 2014; Xue et al., 2016; Yang et al., 2018; Yang et al., 2017), which react with NO to promote O_3 formation (Liu et al., 2012; Qu et al., 2021; Rao et al., 2016; Shen et al., 2021; W. Wang, B. Yuan, et al., 2022; Y. Xu et al., 2023; Y. Zhang et al., 2019). Compared to parameterized approaches, in situ simulations that incorporate detailed chemical mechanisms can quantitatively assess carbonyl contributions to peroxy radicals and O_3 formation. For example, in situ modeling has shown that carbonyls promote 21 %–70 % of total RO_x (= OH + HO_2 + RO + RO_2) radical production in cities like Beijing, Guangzhou, and Hong Kong (W. Wang, B. Yuan, et al., 2022; Xue et al., 2016; Yang et al., 2018; Zhang et al., 2021). Their influence on O_3 formation has also been quantified as 36–45 % in Shanghai (J. Zhu et al., 2020), 13-31 % in Wuhan (P. Zeng et al., 2019), 32-56 % in Beijing and Zibo in the NCP (Dai et al., 2025; Duan et al., 2008), and 23-37 % in Guangzhou, Shenzhen, and Shantou in the PRD region (Cheng et al., 2010; Shen et al., 2021; C. Wang et al., 2017), indicating a wide range of contributions. In contrast, simulations based on simultaneous multi-city sampling data offer more comparable assessments of contributions and better capture the diversity of

photochemical processes across different urban environments (Bao et al., 2022; W. Guo et al., 2022; X. F. Liu et al., 2021; Song et al., 2018; Yang et al., 2024). Importantly, while O_3 pollution control has been widely studied, few investigations have addressed control strategies specifically for carbonyls. Given the nonlinear relationship between carbonyl secondary formation and their precursors (Atkinson et al., 2006; J. Li et al., 2016; Liu et al., 2022; Luecken et al., 2012; Rosado-Reyes & Francisco, 2007; Wolfe et al., 2016; Zhang et al., 2021), it remains unclear whether current O_3 precursor reduction strategies are equally effective for carbonyls. Therefore, identifying carbonyl precursors and understanding their interaction mechanisms is essential for developing coordinated strategies to reduce both O_3 and carbonyl pollution.

To address the research gaps related to carbonyl compounds, this study utilized data from a concurrent sampling campaign conducted in Beijing, Chengdu, Lanzhou, Shanghai, and Wuhan during the summer of 2018. A photochemical box model incorporating the Master Chemical Mechanism (PBM-MCM) was employed to investigate the photochemistry of formaldehyde, acetaldehyde, and acetone in these five representative Chinese cities. Specifically, the study quantified the degradation processes from VOCs to the three carbonyls, clarified the detailed reaction pathways through which carbonyls promote peroxy radical and O_3 formation, and assessed the effectiveness of O_3 control strategies on carbonyl concentrations. Furthermore, based on the quantitative results from the PBM-MCM, a positive matrix factorization (PMF) model was applied to further explore the source contributions of both primary and secondary carbonyls. These findings are expected to enhance the understanding of carbonyl photochemistry and provide a theoretical basis for more effective secondary pollution control strategies across diverse environments.

6.2 Spatial distribution characteristics of carbonyls

Figure. 6.1 illustrates the daytime (07:00–19:00 LT) variations and proportion of carbonyls in the five sampled cities during August 2018. The mean concentrations of carbonyls observed in each city, along with comparisons to values reported in previous studies, are summarized in Table 6.1. Among the carbonyls, formaldehyde, acetone, and acetaldehyde were the most abundant species, collectively accounting for over 85 % of the total carbonyls in all five cities. In Beijing and Wuhan, formaldehyde was the predominant carbonyl, with concentrations of 9.6 ± 0.1 ppbv and 5.2 ± 0.1 ppbv, respectively, representing nearly or more than 40 % of the total carbonyls. Based on previous O_3 study in five cities, it is known that the total oxidant (O_x = O_3 + NO_2) levels in Beijing, Wuhan, and Lanzhou were higher during the sampling period, indicating more intense photochemical activity in these three cities (X. F. Liu et al., 2021) . Further comparison with data from national monitoring sites within 25 km around revealed that O_x levels were consistently high at these sites in both Beijing and Wuhan, suggesting the formation of city-scale regional pollution (shown in Figure 6.2). Although formaldehyde has a relatively short lifetime, it may still accumulate at the city scale, which could contribute to the higher levels observed in Beijing and Wuhan. The higher proportion of formaldehyde relative to acetone in these cities is consistent with previous findings (Huang et al., 2020; Qian et al., 2019; Yang et al., 2018; Z. Yang et al., 2019), and observations in other cities such as Guangzhou, Shenzhen, Xiamen, and Xi'an (Ho et al., 2014; Ho et al., 2015; Lu et al., 2010). In contrast, acetone was the most abundant carbonyl in Shanghai, Chengdu, and Lanzhou, where the proportion of formaldehyde was lower (<30 %) and its concentrations were around 2 ppbv, aligning with findings from previous studies (Ho et al., 2015).

Acetaldehyde was the third most abundant carbonyl compound measured. The highest concentration was observed in Beijing at 7.2 ± 0.1 ppbv, while concentrations in the other four cities ranged from 1.0 to 1.7 ppbv (Table 6.1). Notably, the ratio of formaldehyde to acetaldehyde varied considerably among the five cities. In Beijing and Lanzhou, formaldehyde and acetaldehyde concentrations were comparable, whereas in Shanghai and Chengdu,

formaldehyde levels were approximately twice those of acetaldehyde. In Wuhan, this ratio exceeded three. These variations can be attributed to differences in primary carbonyl emissions, regional influences, and VOC compositions among the cities, with the latter likely playing a more significant role due to its impact on the secondary formation of carbonyls (de Gouw et al., 2005; Friedfeld et al., 2002; Ling et al., 2017; Liu et al., 2009; Lui et al., 2017; Wu et al., 2023; Yang et al., 2017; Z. Yang et al., 2019). From the perspective of secondary formation, the precursor of acetaldehyde, propene, was relatively high in both Beijing and Lanzhou (>2.5 ppbv) (X. F. Liu et al., 2021), which may have resulted in a stronger acetaldehyde formation capacity and thus a closer ratio of formaldehyde to acetaldehyde in these two cities. Additionally, the relatively high concentration of acetaldehyde in Beijing may also be attributed to local regional accumulation. In contrast, propene levels in the other three cities were all below 0.5 ppbv, indicating a weaker capacity for acetaldehyde formation. Considering the higher formaldehyde levels in Wuhan, the ratio of formaldehyde to acetaldehyde in Wuhan was correspondingly larger. Details regarding the characteristics of observed VOC components can be found in Figure 6.2 and our previous study (X. F. Liu et al., 2021). According to Table 6.1 and Figure 6.2, Beijing recorded the highest concentration of carbonyls at 24.3 ± 2.7 ppbv, followed by Wuhan at 10.8 ± 1.5 ppbv. The other three cities (i.e., Lanzhou, Shanghai, and Chengdu) showed similar concentrations of 7.6 ± 1.3 ppbv, 6.8 ± 1.0 ppbv, and 5.7 ± 2.0 ppbv, respectively. The carbonyl concentrations observed in Beijing were among the highest reported in China, with carbonyls comprising more than half of the total VOCs (TVOCs) at 55.0 ± 6.1 %. These findings underscore the significant role of carbonyls in the VOC profile and their substantial contribution to O_3 formation processes (Bao et al., 2022; Ho et al., 2015; Huang et al., 2020; Hui et al., 2023; Mo et al., 2022; Z. Xu et al., 2023; X. Yang et al., 2020; Z. Yang et al., 2019; X. Zhang et al., 2022). In Wuhan and Shanghai, carbonyls contributed similarly to the TVOCs, at 35.9 ± 5.0 % and 35.6 ± 5.2 %, respectively, which is consistent with proportions reported in previous studies (Han, Huang, et al., 2019; Hui et al., 2023; Y. H. Liu et al., 2019; Mo et al., 2022; W. Wang et al., 2023). In contrast, carbonyls comprised less than 20 % of the TVOCs in both Chengdu and Lanzhou (Bao et al., 2022; Ho et al., 2015; Yang et al., 2018; Z.

Yang et al., 2019), a result attributed to the high proportion of alkanes, which made up nearly half of the TVOCs in these cities. Additionally, Lanzhou exhibited elevated levels of alkenes (26.1 ± 4.1 %), consistent with its profile as an industrial city (B. Li et al., 2021; Liu et al., 2023; Z. Zhang et al., 2023), further influencing the TVOC profile. Overall, these findings indicate that carbonyls play a significant role in shaping the VOC composition and secondary pollution in major central and eastern Chinese cities (Beijing, Wuhan, and Shanghai) during the summer.

Moreover, the formation processes and contributions of VOC species to carbonyls, along with their potential sources, will be elucidated through modeling and discussed in the following sections.

Table 6.1. Daytime (07:00–19:00LT) average concentrations of formaldehyde, acetaldehyde, acetone and total carbonyls in this study and previous studies (unit: ppbv).

Location	Formaldehyde	Acetaldehyde	Acetone	Carbonyls	References
Beijing-urban site	9.57 ± 0.09	7.21 ± 0.08	6.60 ± 0.07	24.34 ± 2.72	This study
Chengdu-urban site	2.07 ± 0.27	1.03 ± 0.16	2.63 ± 0.60	5.70 ± 2.04	This study
Lanzhou-urban site	1.84 ± 0.08	1.70 ± 0.08	3.25 ± 0.08	7.56 ± 1.27	This study
Shanghai-urban site	2.27 ± 0.05	1.41 ± 0.04	2.45 ± 0.07	6.82 ± 1.03	This study
Wuhan-urban site	5.17 ± 0.06	1.66 ± 0.02	3.46 ± 0.08	10.80 ± 1.52	This study
Beijing-urban site	11.17 ± 5.32	5.27 ± 2.24	6.98 ± 3.01	28.49 ± 10.64	(Yang et al., 2018)
Beijing-urban site	6.31 ± 2.79	2.90 ± 1.36	4.16 ± 1.44	/	(Huang et al., 2020)
Beijing-urban site	8.49 ± 2.11	2.97 ± 0.79	6.72 ± 1.58	21.05 ± 4.99	(Qian et al., 2019)
Beijing-urban site	8.35 ± 3.34	3.05 ± 0.99	/	13.8 ± 4.61	(Ho et al., 2015)
Beijing-urban site	8.3	5.38	12.09	/	(Zhang et al., 2012)
Chengdu-urban site	9.86 ± 4.41	3.57 ± 2.19	4.41 ± 2.32	20.38 ± 9.24	(Bao et al., 2022)
Chengdu-urban site	11.4 ± 3.80	3.09 ± 1.05	/	17.7 ± 5.49	(Ho et al., 2015)
Fujian-urban site	4.96 ± 2.13	1.74 ± 0.81	3.05 ± 1.20	12.15 ± 2.53	(X. Zhang et al., 2022)
Guangzhou-urban site	11.2	5.89	7.21	/	(Lu et al., 2010)
Guangzhou-urban site	/	2.54	4.39	/	(X.-B. Li, B. Yuan, S. Wang, et al., 2022)

Guangzhou-urban site	6.69 ± 1.98	2.28 ± 0.77	/	11.0 ± 3.23	(Ho et al., 2015)
Guangzhou-urban site	9.84	5.28	10.93	/	(Lyu et al., 2020)
Guiyang-urban site	3.91	3.16	2.15	/	(Pang & Lee, 2010)
Nanning-urban site	5.53	8.77	2.29	/	(Guo et al., 2016)
Qinghai Lake-rural site	3.90 ± 1.12	1.97 ± 0.77	/	6.93 ± 2.23	(Ho et al., 2015)
Qinzhou-urban site	5.46	4.46	1.03	/	(Guo et al., 2014)
Shanghai-urban site	5.53 ± 1.46	4.55 ± 1.06	4.04 ± 1.77	/	(Huang et al., 2009)
Shanghai-suburban site	1.54 ± 0.51	0.29 ± 0.07	/	2.16 ± 0.63	(Ho et al., 2015)
Shenzhen-urban site	1.60 ± 0.86	1.16 ± 0.90	2.31 ± 1.32	/	(Huang et al., 2020)
Shenzhen-urban site	/	1.98	3.78	/	(Zhu et al., 2019)
Shenzhen-urban site	/	2.05	4.49	/	(Huang et al., 2019)
Shenzhen-urban site	4.24	1.96	2.93	/	(Z. Ma et al., 2019)
Wuhan-urban site	4.90 ± 2.36	2.35 ± 0.94	2.88 ± 1.66	11.29 ± 3.85	(Z. Yang et al., 2019)
Wuhan-urban site	4.69 ± 2.33	1.72 ± 0.94	/	8.29 ± 4.02	(Ho et al., 2015)
Wuhan-suburban site	3.37 ± 1.99	1.85 ± 0.80	2.54 ± 1.72	8.72 ± 3.75	(Z. Yang et al., 2019)
Xiamen-urban site	1.72 ± 0.18	0.87 ± 0.18	/	3.33 ± 0.56	(Ho et al., 2015)
Xi'an-urban site	5.31	2.89	3.11	/	(Ho et al., 2014)
Yantai-urban site	7.43 ± 4.14	3.82 ± 2.19	/	15.4 ± 8.08	(Ho et al., 2015)
Hok Tsui, Hong Kong -background site	/	2.14 ± 0.16	4.20 ± 0.26	/	(Lyu et al., 2024)

Hok Tsui, Hong Kong-background site	2.00 ± 1.04	0.59 ± 0.28	/	2.80 ± 1.35	(X. Yang et al., 2020)
Hok Tsui, Hong Kong-background site	0.93 ± 0.39	1.72 ± 0.88	3.37 ± 1.55	/	(Yuan et al., 2024)
Hok Tsui, Hong Kong-rural site	2.04 ± 0.82	0.55 ± 0.17	/	/	(Lui et al., 2017)
Tsuen Wan, Hong Kong-urban site	2.93 ± 0.16	2.17 ± 0.22	4.17 ± 0.59	/	(Guo, Ling, Cheung, Wang, et al., 2013)
Tung Chung, Hong Kong-urban site	3.75 ± 0.65	1.27 ± 0.22	/	/	(Lui et al., 2017)
Nan'ao, Hong Kong-background site	/	1.62	1.8	/	(Huang et al., 2019)
Yuen Long, Hong Kong-urban site	4.23 ± 0.81	1.55 ± 0.33	/	/	(Lui et al., 2017)
Hong Kong-urban site	/	/	10.59 ± 3.50	/	(F. Wang et al., 2024)
Hong Kong-roadside site	/	/	11.40 ± 3.34	/	(F. Wang et al., 2024)
Hong Kong-suburban site	/	4.07 ± 2.81	3.28 ± 1.40	/	(Hui et al., 2023)
Lasa-rural site	0.83 ± 0.31	0.32 ± 0.13	/	1.27 ± 0.46	(Ho et al., 2015)
Mt. Tai-mountain site	3.48	1.27	/	/	(Yang et al., 2017)
Mt. Tai Mo Shan, Hong Kong-mountain site	2.69 ± 0.16	1.39 ± 0.11	3.62 ± 0.29	/	(Guo, Ling, Cheung, Wang, et al., 2013)
Mt. Waliguan-mountain site	3.42 ± 1.55	2.36 ± 1.84	0.85 ± 0.36	/	(Mu et al., 2007)

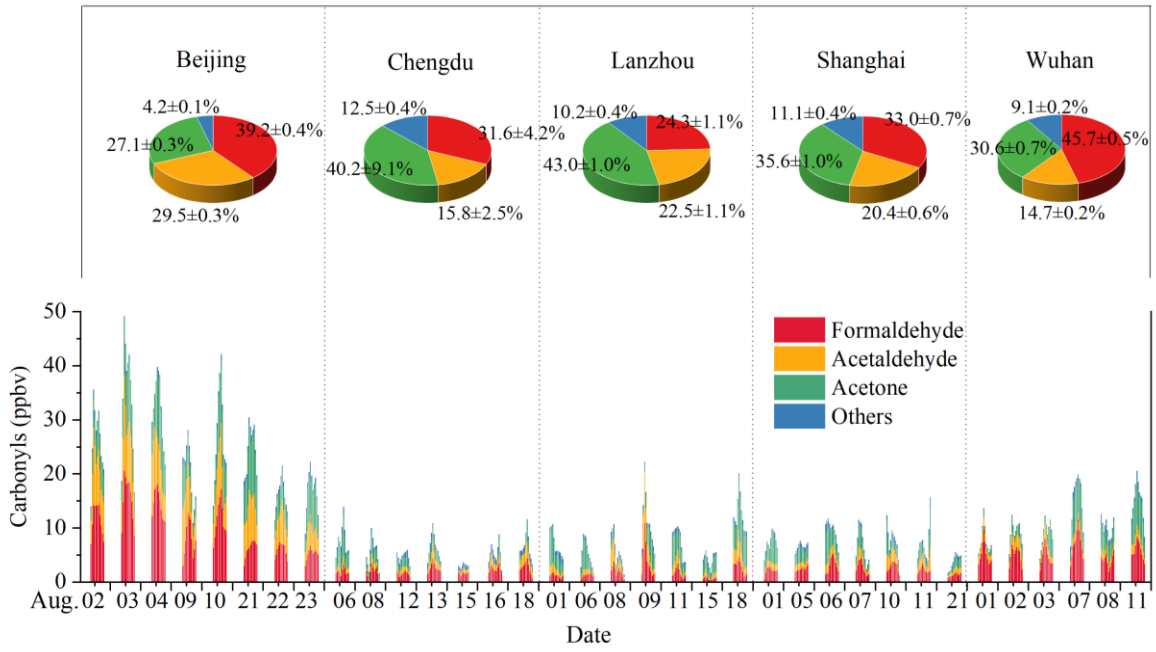

Figure 6.1. Daytime (07:00–19:00 LT) temporal variations and spatial distributions of carbonyls in the five sampling cities.

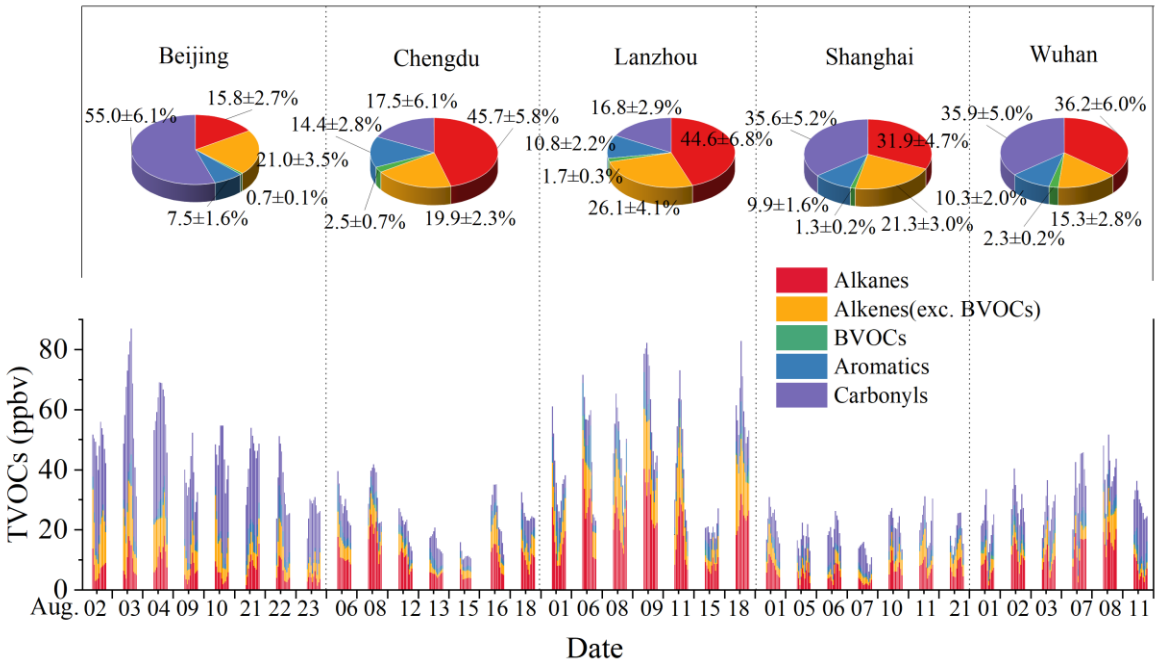

Figure 6.2. Daytime (07:00–19:00LT) temporal variations and spatial distributions of TVOCs in the five sampling cities.

6.3 Formation mechanism of carbonyls

6.3.1 Formaldehyde

Figure 6.3 depicts the daytime (07:00–19:00 LT) production and destruction pathways of formaldehyde in the five cities, with detailed reaction rates for each pathway provided in Table 6.2. As illustrated in Figure 6.3, formaldehyde production in all five cities was primarily driven by the decomposition of RO radicals (RO + O_2). In contrast, formaldehyde destruction was mainly governed by its reactions with OH radicals and by photolysis, with both processes contributing to a similar extent. All five cities exhibited positive net production rates of formaldehyde, consistent with previous studies in Beijing, Wuhan, and the YRD region (Wu et al., 2023; Yang et al., 2018; X. Yang et al., 2020; P. Zeng et al., 2019; Zhang et al., 2021). Among the five cities, Beijing had the highest daytime average production rate of 6.4 ± 1.0 ppbv h^{-1}, followed by Wuhan at 5.3 ± 0.7 ppbv h^{-1}, reflecting strong secondary formation capabilities in both cities. Additionally, the elevated concentrations of formaldehyde observed in Beijing and Wuhan result in more intense destruction processes via both OH oxidation and photolysis. Consequently, Beijing, Lanzhou and Wuhan showed comparable net production rates of approximately 3-4 ppbv h^{-1}, with Chengdu following. Shanghai recorded the lowest net production rate, at 1.7 ± 0.3 ppbv h^{-1}.

The pie charts in Figure 6.3 further illustrate the proportions of various RO decomposition pathways, showing that the six dominant RO species contributed over 70 % of formaldehyde production in all five cities. The methyl radical (CH_3O), extensively produced from a wide range of VOCs, was the predominant RO radical, accounting for 25–43 % of formaldehyde formation across the cities. The 2-oxoethoxy radical ($HCOCH_2O$), mainly generated from *α/β*-pinene, ethane, and toluene, ranked second, contributing approximately 11–16 %. Notably, other RO radicals exhibited distinct city-specific features. The 2-hydroxy ethoxy radical ($HOCH_2CH_2O$), primarily derived from ethene, played a significant role (~16 %) in Beijing and Lanzhou. In contrast, the 1-hydroxypropane-2-yloxy radical (HYPROPO), mainly formed from propene, contributed substantially to formaldehyde production in Wuhan, accounting for

around 15 %. The 1-methyl-1-vinyl-2-hydroxyethoxy radical (ISOPBO), a typical isoprene-derived radical, contributed most prominently (~5 %) in Chengdu. Additional minor formation pathways are detailed in Tables 3.7 and 6.2. These findings highlight the diversity of VOCs involved in formaldehyde production and underscore the complexity of its formation mechanisms, which are strongly influenced by the distinct VOC profiles of each city.

To further quantify the parent VOCs contributing to formaldehyde formation, Table 6.4 presents the average contributions of various VOC species across the five cities, while Table 6.3 provides a detailed proportional breakdown for each city. As shown in Table 6.4, alkenes were the predominant contributors to formaldehyde production, accounting for an average of 62 % across all cities. Anthropogenic alkenes, including ethene, propene, 1-butene, and 1,3-butadiene, contributed more than 30 % overall, with their share exceeding 50 % in Beijing and Lanzhou (Table 6.3). In contrast, biogenic alkenes such as isoprene and *α/β*-pinene played a significant role in Chengdu and Wuhan, comprising 28 % and 24 % of formaldehyde formation, respectively. These results are consistent with previous sensitivity analyses, which have identified specific species such as ethene, propene, and isoprene as major contributors to formaldehyde formation (Chen et al., 2022; Ling et al., 2017; Lyu et al., 2024; Yang et al., 2018; X. Yang et al., 2020).

However, quantitative analysis reveals that the combined contribution of these well-studied, typical VOC species accounted for less than or around 50 % of formaldehyde formation in the five cities. As shown in Table 6.4, aside from the prominent alkene species, individual VOC species each contributed approximately 1–2 % to formaldehyde production. This suggests that nearly every VOC can generate formaldehyde through oxidation and degradation processes, reflecting the previously discussed diversity of formaldehyde formation pathways. The top ten VOC species together contributed less than 60 % of formaldehyde formation in Beijing, Chengdu, Shanghai, and Wuhan, while in Lanzhou, their combined contribution was around 70 % (as illustrated in Figure 6.4). These results suggest that previous studies relying on sensitivity analyses may have overemphasized the role of typical alkene species, potentially

underestimating the contributions of other VOCs in urban environments. Therefore, while prioritizing alkene control is important, its overall impact on formaldehyde reduction is limited. Effective mitigation of formaldehyde formation requires comprehensive control of the entire spectrum of VOCs.

Notably, in Lanzhou, anthropogenic alkenes dominated formaldehyde formation, accounting for 58.2 ± 0.8 % (Table 6.3). Ethene and propene were particularly significant contributors, representing 14.8 ± 0.1 % and 19.2 ± 0.3 % of formaldehyde formation, respectively, followed by α-pinene (11.2 ± 0.3 %), 1,3-butadiene (8.6 ± 0.3 %), and 1-butene (6.8 ± 0.1 %). The elevated contribution of alkenes is attributed to the high ambient levels of these compounds (12.6 ± 2.0 ppbv), primarily emitted from the petrochemical industry in Lanzhou (W. Guo et al., 2022; Jia et al., 2016; X. F. Liu et al., 2021; Yang et al., 2024), which more accurately reflects the characteristics of formaldehyde formation in industrial cities. Additionally, isoprene exerted a considerable influence on formaldehyde formation in Chengdu, contributing 20.7 ± 0.2 %. This is due to the higher isoprene levels observed in Chengdu (0.6 ± 0.1 ppbv), whereas isoprene concentrations in the other cities were only half to a quarter of those in Chengdu (X. F. Liu et al., 2021). This further underscores the significant role of isoprene in formaldehyde formation in areas with high biogenic emissions.

Table 6.2. Daytime (07:00–19:00 LT) reaction rates of production and destruction pathways of formaldehyde, acetaldehyde and acetone.

	Reaction rate (ppbv h^{-1})	Beijing	Chengdu	Lanzhou	Shanghai	Wuhan
Formaldehyde	Net production rate	3.53 ± 0.49	2.16 ± 0.25	3.46 ± 0.38	1.71 ± 0.28	3.39 ± 0.29
	Total production rate	6.43 ± 0.97	2.54 ± 0.31	3.71 ± 0.42	2.69 ± 0.48	5.34 ± 0.69
	Total destruction rate	-2.90 ± 0.52	-0.38 ± 0.06	-0.24 ± 0.04	-0.98 ± 0.20	-1.95 ± 0.41
	Pr Alkenes + O_3	0.20 ± 0.02	0.08 ± 0.01	0.29 ± 0.03	0.03 ± 0.00	0.10 ± 0.01
	Other RO + O_2	3.32 ± 0.52	1.36 ± 0.18	2.37 ± 0.30	1.45 ± 0.27	2.99 ± 0.42
	Other carbonyls + OH/*hv*	0.17 ± 0.02	0.15 ± 0.02	0.18 ± 0.02	0.10 ± 0.01	0.23 ± 0.02
	CH_3O + O_2	2.58 ± 0.41	0.83 ± 0.10	0.69 ± 0.07	0.99 ± 0.18	1.75 ± 0.23
	Other production pathways	0.16 ± 0.02	0.11 ± 0.01	0.17 ± 0.02	0.12 ± 0.02	0.27 ± 0.03
	De HCHO + *hv*	-1.54 ± 0.26	-0.23 ± 0.04	-0.15 ± 0.03	-0.54 ± 0.10	-1.01 ± 0.18
	HCHO + OH	-1.36 ± 0.26	-0.14 ± 0.03	-0.09 ± 0.02	-0.44 ± 0.10	-0.94 ± 0.23
	HCHO + NO_3	-0.01 ± 0.01	-0.01 ± 0.01	0.01 ± 0.01	0.01 ± 0.01	-0.01 ± 0.01
Acetaldehyde	Net production rate	0.30 ± 0.13	0.39 ± 0.04	1.33 ± 0.16	0.19 ± 0.03	0.42 ± 0.04
	Total production rate	2.03 ± 0.29	0.51 ± 0.05	1.46 ± 0.18	0.59 ± 0.10	0.90 ± 0.12
	Total destruction rate	-1.72 ± 0.32	-0.12 ± 0.02	-0.13 ± 0.02	-0.39 ± 0.08	-0.47 ± 0.11
	Alkenes + O_3	0.35 ± 0.04	0.09 ± 0.01	0.48 ± 0.05	0.05 ± 0.01	0.14 ± 0.01
	RO + O_2	1.60 ± 0.25	0.40 ± 0.05	0.93 ± 0.14	0.50 ± 0.09	0.71 ± 0.10

	P	Other carbonyls + OH/*hv*	0.06 ± 0.01	0.02 ± 0.002	0.02 ± 0.01	0.03 ± 0.01	0.04 ± 0.01
	r	Other production pathways	0.02 ± 0.002	0.01 ± 0.001	0.02 ± 0.01	0.01 ± 0.01	0.01 ± 0.01
	D	CH_3CHO + *hv*	-0.06 ± 0.01	-0.01 ± 0.001	-0.01 ± 0.01	-0.02 ± 0.003	-0.02 ± 0.01
	e	CH_3CHO + OH	-1.66 ± 0.31	-0.12 ± 0.02	-0.12 ± 0.02	-0.38 ± 0.08	-0.45 ± 0.10
	s	CH_3CHO + NO_3	-0.01 ± 0.01	-0.01 ± 0.01	-0.01 ± 0.01	0.01 ± 0.01	-0.01 ± 0.01
Acetone	Net production rate		0.41 ± 0.05	0.22 ± 0.03	0.44 ± 0.05	0.15 ± 0.02	0.77 ± 0.08
	Total production rate		0.44 ± 0.05	0.23 ± 0.03	0.45 ± 0.05	0.16 ± 0.03	0.79 ± 0.08
	Total destruction rate		-0.03 ± 0.01	-0.01 ± 0.001	-0.01 ± 0.01	-0.01 ± 0.01	-0.02 ± 0.01
	P	Alkenes + O_3	0.05 ± 0.01	0.01 ± 0.01	0.04 ± 0.01	0.01 ± 0.01	0.02 ± 0.01
	r	RO + O_2	0.36 ± 0.04	0.20 ± 0.03	0.37 ± 0.04	0.15 ± 0.02	0.50 ± 0.05
	o	Other carbonyls + OH/*hv*	0.02 ± 0.01	0.01 ± 0.01	0.03 ± 0.05	0.01 ± 0.01	0.05 ± 0.01
	d	Other production pathways	0.01 ± 0.01	0.01 ± 0.01	0.04 ± 0.01	0.01 ± 0.01	0.03 ± 0.01
	D	CH_3COCH_3 + *hv*	-0.01 ± 0.01	-0.01 ± 0.01	-0.01 ± 0.01	-0.01 ± 0.01	-0.01 ± 0.01
	e	CH_3COCH_3 + OH	-0.02 ± 0.01	-0.01 ± 0.01	-0.01 ± 0.01	-0.01 ± 0.01	-0.01 ± 0.01

Table 6.3. Contribution of VOC species to formaldehyde formation during peak hours (11:00–14:00 LT).

	Beijing	**Chengdu**	**Lanzhou**	**Shanghai**	**Wuhan**
Alkanes	**20.80 ± 0.19 %**	**19.13 ± 0.21 %**	**13.30 ± 0.21 %**	**23.51 ± 0.53 %**	**20.74 ± 0.22 %**

Ethane	1.01 ± 0.01 %	0.90 ± 0.01 %	0.57 ± 0.01 %	2.77 ± 0.11 %	0.95 ± 0.01 %
Propane	1.01 ± 0.01 %	0.89 ± 0.01 %	0.56 ± 0.01 %	0.94 ± 0.01 %	1.00 ± 0.01 %
***i*-Butane**	1.01 ± 0.01 %	0.99 ± 0.01 %	0.63 ± 0.01 %	0.96 ± 0.01 %	1.03 ± 0.01 %
***n*-Butane**	1.05 ± 0.01 %	1.04 ± 0.02 %	0.63 ± 0.01 %	1.20 ± 0.04 %	1.15 ± 0.01 %
***i*-Pentane**	1.04 ± 0.01 %	1.01 ± 0.01 %	0.59 ± 0.01 %	1.06 ± 0.01 %	1.18 ± 0.01 %
***n*-Pentane**	1.05 ± 0.01 %	1.28 ± 0.02 %	0.82 ± 0.01 %	1.44 ± 0.06 %	1.41 ± 0.04 %
2,2-Dimethylbutane	1.01 ± 0.01 %	0.91 ± 0.01 %	0.58 ± 0.01 %	0.95 ± 0.01 %	1.01 ± 0.01 %
2,3-Dimethylbutane	1.01 ± 0.01 %	0.89 ± 0.01 %	0.57 ± 0.01 %	0.95 ± 0.01 %	1.00 ± 0.01 %
2-Methylpentane	1.18 ± 0.01 %	1.08 ± 0.01 %	0.82 ± 0.01 %	1.04 ± 0.01 %	1.09 ± 0.01 %
3-Methylpentane	1.15 ± 0.01 %	1.22 ± 0.01 %	0.72 ± 0.01 %	1.11 ± 0.01 %	1.10 ± 0.01 %
***n*-Hexane**	1.19 ± 0.01 %	1.20 ± 0.01 %	1.13 ± 0.02 %	2.50 ± 0.15 %	1.24 ± 0.01 %
Cyclohexane	1.10 ± 0.01 %	0.95 ± 0.01 %	0.68 ± 0.02 %	1.25 ± 0.03 %	1.11 ± 0.01 %
2-Methylhexane	1.03 ± 0.01 %	1.00 ± 0.01 %	0.85 ± 0.01 %	1.08 ± 0.01 %	1.11 ± 0.01 %
3-Methylhexane	1.04 ± 0.01 %	0.91 ± 0.01 %	0.59 ± 0.01 %	0.99 ± 0.01 %	1.03 ± 0.01 %
***n*-Heptane**	1.14 ± 0.01 %	0.97 ± 0.01 %	0.78 ± 0.01 %	1.02 ± 0.01 %	1.04 ± 0.01 %
***n*-Octane**	1.17 ± 0.01 %	1.03 ± 0.01 %	0.61 ± 0.01 %	1.08 ± 0.01 %	1.08 ± 0.01 %
***n*-Nonane**	1.45 ± 0.01 %	0.98 ± 0.01 %	0.92 ± 0.01 %	1.09 ± 0.01 %	1.08 ± 0.01 %
***n*-Decane**	1.17 ± 0.01 %	0.98 ± 0.01 %	0.69 ± 0.01 %	1.12 ± 0.01 %	1.13 ± 0.01 %
Undecane	1.01 ± 0.01 %	0.89 ± 0.01 %	0.57 ± 0.01 %	0.95 ± 0.01 %	1.00 ± 0.01 %

Alkenes (Anthropogenic)	**50.78 ± 0.24 %**	**31.69 ± 0.40 %**	**58.21 ± 0.84 %**	**39.01 ± 0.64 %**	**35.46 ± 0.20 %**
Ethene	13.43 ± 0.03 %	11.18 ± 0.15 %	14.81 ± 0.14 %	15.26 ± 0.49 %	16.53 ± 0.06 %
Propene	20.94 ± 0.05 %	4.58 ± 0.04 %	19.15 ± 0.25 %	7.78 ± 0.04 %	5.93 ± 0.03 %
1-Butene	4.24 ± 0.04 %	5.06 ± 0.07 %	6.84 ± 0.05 %	4.32 ± 0.01 %	2.58 ± 0.01 %
***trans*-2-Butene**	1.06 ± 0.01 %	0.94 ± 0.01 %	0.72 ± 0.02 %	0.97 ± 0.01 %	1.03 ± 0.01 %
***cis*-2-Butene**	1.04 ± 0.01 %	0.92 ± 0.01 %	0.66 ± 0.01 %	0.96 ± 0.01 %	1.02 ± 0.01 %
1,3-Butadiene	1.57 ± 0.01 %	1.65 ± 0.02 %	8.58 ± 0.25 %	2.01 ± 0.02 %	1.39 ± 0.02 %
1-Pentene	1.57 ± 0.01 %	2.25 ± 0.02 %	3.54 ± 0.03 %	1.51 ± 0.01 %	1.14 ± 0.01 %
3-Methyl-1-butene	1.39 ± 0.01 %	0.96 ± 0.01 %	0.72 ± 0.01 %	1.05 ± 0.01 %	1.16 ± 0.01 %
2-Methyl-1-butene	2.19 ± 0.01 %	1.13 ± 0.01 %	1.15 ± 0.03 %	2.26 ± 0.01 %	1.54 ± 0.01 %
***trans*-2-Pentene**	1.01 ± 0.01 %	0.92 ± 0.01 %	0.59 ± 0.01 %	0.96 ± 0.01 %	1.01 ± 0.01 %
***cis*-2-Pentene**	1.03 ± 0.01 %	0.92 ± 0.01 %	0.62 ± 0.01 %	0.95 ± 0.01 %	1.00 ± 0.01 %
2-Methyl-2-butene	1.32 ± 0.04 %	1.19 ± 0.04 %	0.82 ± 0.03 %	0.98 ± 0.01 %	1.14 ± 0.01 %
Alkenes (Biogenic)	**10.24 ± 0.07 %**	**28.42 ± 0.55 %**	**15.49 ± 0.38 %**	**18.03 ± 0.22 %**	**24.14 ± 0.35 %**
Isoprene	4.95 ± 0.03 %	20.68 ± 0.16 %	2.94 ± 0.04 %	13.69 ± 0.09 %	12.41 ± 0.21 %
α-Pinene	2.91 ± 0.02 %	4.55 ± 0.25 %	11.17 ± 0.31 %	1.57 ± 0.02 %	6.78 ± 0.09 %
β-Pinene	2.39 ± 0.02 %	3.19 ± 0.14 %	1.37 ± 0.03 %	2.77 ± 0.11 %	4.95 ± 0.05 %
Aromatics	**15.97 ± 0.15 %**	**18.59 ± 0.26 %**	**11.70 ± 0.27 %**	**17.14 ± 0.20 %**	**17.43 ± 0.16 %**
Benzene	1.02 ± 0.01 %	1.01 ± 0.01 %	0.60 ± 0.01 %	0.97 ± 0.01 %	1.04 ± 0.01 %

Toluene	1.34 ± 0.01 %	3.01 ± 0.10 %	0.81 ± 0.01 %	1.97 ± 0.04 %	1.72 ± 0.01 %
Ethylbenzene	1.09 ± 0.01 %	1.27 ± 0.01 %	0.95 ± 0.01 %	1.34 ± 0.01 %	1.48 ± 0.01 %
***m/p*-Xylene**	1.80 ± 0.02 %	3.25 ± 0.04 %	2.39 ± 0.11 %	2.28 ± 0.04 %	2.14 ± 0.02 %
***o*-Xylene**	1.27 ± 0.01 %	1.58 ± 0.01 %	1.12 ± 0.04 %	1.37 ± 0.01 %	1.43 ± 0.02 %
Styrene	1.01 ± 0.01 %	0.89 ± 0.01 %	0.57 ± 0.01 %	0.95 ± 0.01 %	1.00 ± 0.01 %
Isopropylbenzene	1.05 ± 0.01 %	0.90 ± 0.01 %	0.63 ± 0.01 %	0.98 ± 0.01 %	1.04 ± 0.01 %
***n*-Propylbenzene**	1.09 ± 0.01 %	0.91 ± 0.01 %	0.65 ± 0.01 %	0.97 ± 0.01 %	1.02 ± 0.01 %
***m*-Ethyltoluene**	1.02 ± 0.01 %	0.95 ± 0.01 %	0.60 ± 0.01 %	0.96 ± 0.01 %	1.02 ± 0.01 %
***p*-Ethyltoluene**	1.07 ± 0.01 %	0.95 ± 0.01 %	0.71 ± 0.01 %	1.04 ± 0.01 %	1.10 ± 0.01 %
***o*-Ethyltoluene**	1.04 ± 0.01 %	0.92 ± 0.01 %	0.61 ± 0.01 %	1.01 ± 0.01 %	1.05 ± 0.01 %
1,3,5-Trimethylbenzene	1.06 ± 0.01 %	0.94 ± 0.01 %	0.68 ± 0.01 %	1.00 ± 0.01 %	1.09 ± 0.01 %
1,2,4-Trimethylbenzene	1.03 ± 0.01 %	1.05 ± 0.01 %	0.71 ± 0.01 %	1.17 ± 0.01 %	1.20 ± 0.01 %
1,2,3-Trimethylbenzene	1.08 ± 0.01 %	0.97 ± 0.01 %	0.68 ± 0.01 %	1.11 ± 0.01 %	1.11 ± 0.01 %
Alkyne	**1.18 ± 0.01 %**	**1.26 ± 0.02 %**	**0.67 ± 0.02 %**	**1.36 ± 0.04 %**	**1.21 ± 0.01 %**
Ethyne	1.18 ± 0.01 %	1.26 ± 0.02 %	0.67 ± 0.02 %	1.36 ± 0.04 %	1.21 ± 0.01 %

Table 6.4 Average contributions of VOC species to formaldehyde formation during peak hours (11:00–14:00LT) in five cities.

Alkanes	**19.5 %**	**Alkenes**	**62.3 %**	**Aromatics**	**16.16 %**

Ethane	1.24 %	**(Anthropogenic)**		Benzene	0.93 %
Propane	0.88 %	Ethene	**14.24 %**	Toluene	1.77 %
***i*-Butane**	0.92 %	Propene	**11.68 %**	Ethylbenzene	1.22 %
***n*-Butane**	1.01 %	1-Butene	**4.61 %**	*m*-Xylene	2.37 %
***i*-Pentane**	0.98 %	*trans*-2-Butene	0.94 %	*p*-Xylene	
***n*-Pentane**	1.20 %	*cis*-2-Butene	0.92 %	*o*-Xylene	1.35 %
2,2-Dimethylbutane	0.89 %	1,3-Butadiene	**3.04 %**	Styrene	0.88 %
2,3-Dimethylbutane	0.88 %	1-Pentene	2.00 %	*i*-Propylbenzene	0.92 %
2-Methylpentane	1.04 %	3-Methyl-1-butene	1.06 %	*n*-Propylbenzene	0.93 %
3-Methylpentane	1.06 %	2-Methyl-1-butene	1.65 %	*m*-Ethyltoluene	0.91 %
***n*-Hexane**	1.45 %	*trans*-2-Pentene	0.90 %	*p*-Ethyltoluene	0.97 %
Cyclohexane	1.02 %	*cis*-2-Pentene	0.90 %	*o*-Ethyltoluene	0.93 %
2-Methylhexane	1.01 %	2-Methyl-2-butene	1.09 %	1,3,5-Trimethylbenzene	0.95 %
3-Methylhexane	0.91 %	**Alkenes**		1,2,4-Trimethylbenzene	1.03 %
***n*-Heptane**	0.99 %	**(Biogenic)**		1,2,3-Trimethylbenzene	0.99 %
***n*-Octane**	1.00 %	Isoprene	**10.93 %**	**Alkyne**	**1.14 %**
***n*-Nonane**	1.11 %	α-Pinene	**5.40 %**	Ethyne	1.14 %
***n*-Decane**	1.02 %	β-Pinene	2.93 %		
Undecane	0.88 %				

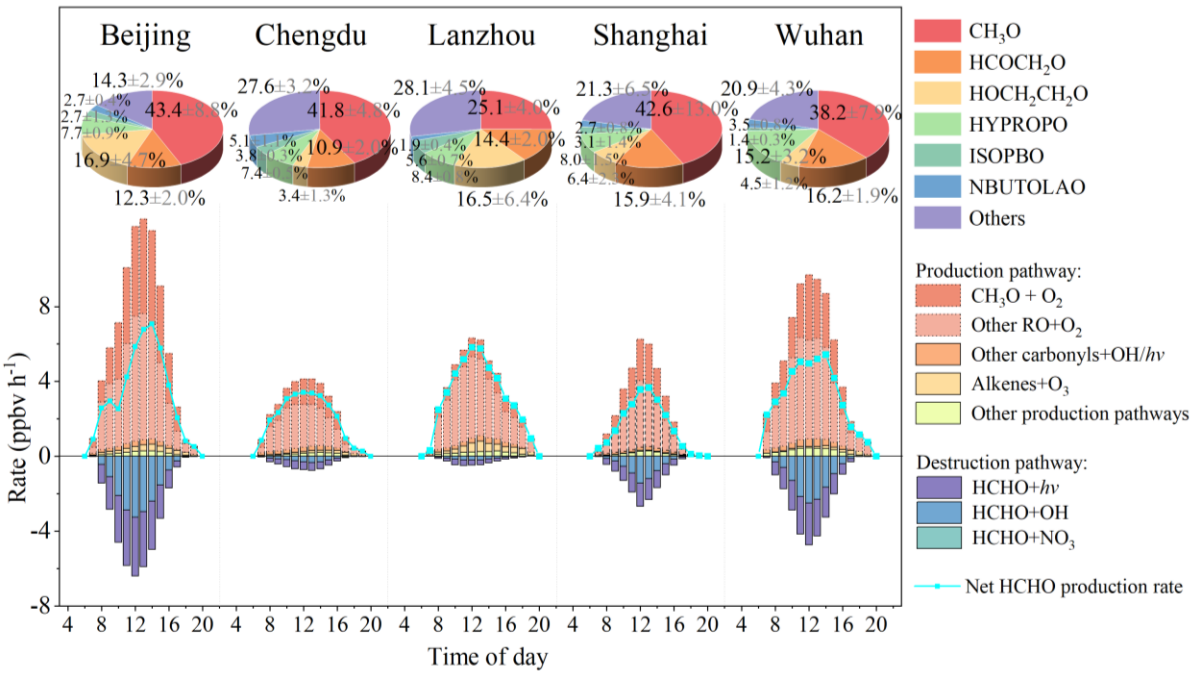

Figure 6.3. Diurnal variations of simulated production and destruction pathways of formaldehyde (HCHO) in the five cities. The pie charts illustrate the proportions of the main RO species contributing to the RO decomposition pathways for each city.

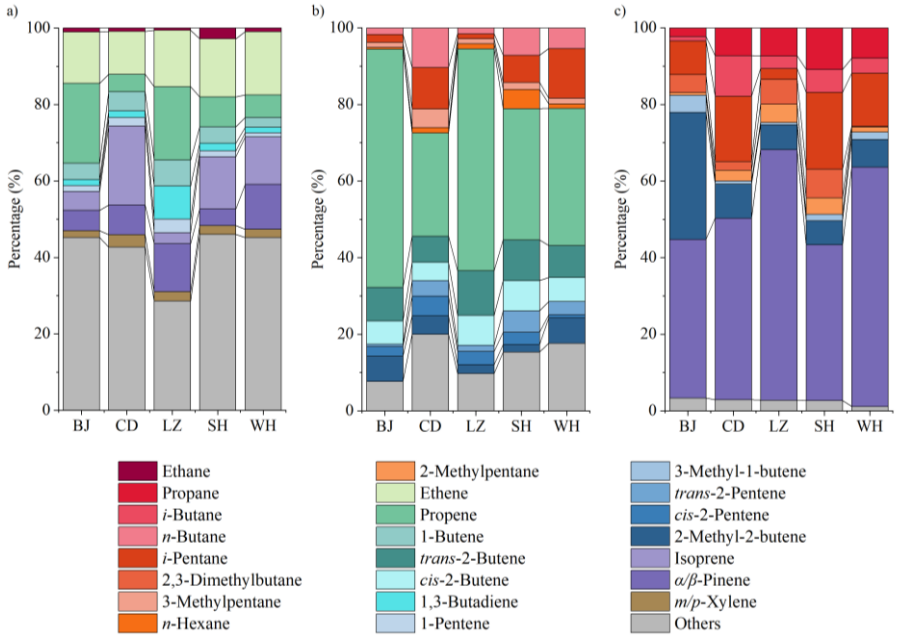

Figure 6.4. The top 10 contributed VOC species and their proportions to a) formaldehyde, b) acetaldehyde, and c) acetone formation during the peak hours (11:00-14:00 LT) in Beijing (BJ), Chengdu (CD), Lanzhou (LZ), Shanghai (SH) and Wuhan (WH).

6.3.2 Acetaldehyde

Figure 6.5 illustrates the simulated production and destruction pathways of acetaldehyde in the five cities. As with formaldehyde, acetaldehyde production was predominantly governed by the decomposition of RO radicals. However, unlike formaldehyde, the destruction of acetaldehyde was dominated by its reaction with OH radicals. Net production of acetaldehyde was observed in all five cities, with Lanzhou exhibiting the highest net production rate at 1.3 ± 0.2 ppbv h^{-1}. The other cities showed considerably lower net production rates, ranging from approximately 0.2 to 0.4 ppbv h^{-1}. Although Beijing had a high acetaldehyde production rate, its substantial destruction rate, mainly due to OH oxidation, led to a lower net production rate.

Furthermore, the pie charts in Figure 6.5 show that the top six RO species accounted for approximately 70–80 % of RO decomposition, leading to acetaldehyde formation in the five cities. The propene-derived HYPROPO radical was the most abundant in all cities except Chengdu, representing around 60 % of RO decomposition in Lanzhou and Beijing. In contrast, the ethyl radical (C_2H_5O), mainly produced from alkanes, was most significant in Chengdu (~35 %) and also played a vital role in Shanghai and Wuhan, contributing about 23-27 %. Additionally, the 2-hydroxy-2-methylpropoxy radical (BUT_2OLAO), produced from *trans/cis*-2-butene, exerted a considerable influence in Shanghai, Lanzhou, and Wuhan. Notably, the ozonolysis of certain alkenes (such as propene) directly produces acetaldehyde, making this pathway a major contributor in Beijing and Lanzhou, where propene concentrations (3.1 ± 0.1 ppbv and 2.6 ± 0.1 ppbv, respectively) were about ten times higher than in the other three cities. These findings indicate that acetaldehyde formation is governed by distinct parent VOC species, with their relative contributions closely linked to the unique VOC composition characteristics of each city.

Table 6.5 presents the VOC contribution profiles to acetaldehyde formation in the five cities. Anthropogenic alkenes were the dominant VOC group, contributing nearly 90 % in Beijing and Lanzhou, and around 60 % in Chengdu, Shanghai, and Wuhan. In these latter three cities, alkanes also played a significant role, accounting for over 25 % of acetaldehyde production. Figure 6.4b highlights the top ten VOC species contributing to acetaldehyde formation in the

five cities. Propene emerged as the predominant contributor in all cities, particularly in Beijing and Lanzhou, where it accounted for 62 % and 58 % of acetaldehyde production, respectively. The important role of propene in acetaldehyde formation in Beijing has also been documented in previous research (Yang et al., 2018). Additionally, *trans/cis*-2-butene made a substantial contribution, accounting for approximately 10–20 % across the five cities. Its significant role has been reported at background sites such as Hong Kong (Lyu et al., 2024). Pentene isomers also contributed about 10 % to acetaldehyde formation in all cities. Furthermore, C_4–C_6 alkanes, mainly *n*-butane and *i*-pentane, contributed over 20 % to acetaldehyde production in Chengdu, Shanghai, and Wuhan. Notably, 3-methylpentane and *n*-hexane were particularly significant in Chengdu and Shanghai, each accounting for about 5 %, highlighting the specificity in VOC composition among the cities. Despite these differences, the control strategies for reducing acetaldehyde formation remain consistent across all cities: targeting propene emissions can significantly reduce acetaldehyde production, followed by the control of C_4–C_5 alkenes.

Table 6.5. Contribution of VOC species to acetaldehyde formation during peak hours (11:00–14:00 LT).

	Beijing	Chengdu	Lanzhou	Shanghai	Wuhan
Alkanes	**9.04 ± 0.48 %**	**35.27 ± 1.25 %**	**9.26 ± 0.41 %**	**26.99 ± 1.18 %**	**27.81 ± 1.47 %**
Ethane	0.89 ± 0.09 %	2.50 ± 0.18 %	0.70 ± 0.02 %	1.43 ± 0.12 %	2.11 ± 0.29 %
Propane	0.01 ± 0.01 %	0.04 ± 0.01 %	0.03 ± 0.01 %	0.07 ± 0.01 %	0.25 ± 0.03 %
***i*-Butane**	0.00 ± 0.00 %	0.08 ± 0.01 %	0.01 ± 0.01 %	0.02 ± 0.01 %	0.03 ± 0.01 %
***n*-Butane**	1.70 ± 0.02 %	**10.35 ± 0.40 %**	1.55 ± 0.07 %	**7.15 ± 0.13 %**	**5.44 ± 0.09 %**
***i*-Pentane**	2.05 ± 0.18 %	**10.84 ± 0.21 %**	1.28 ± 0.08 %	**7.05 ± 0.47 %**	**12.92 ± 0.69 %**
***n*-Pentane**	0.12 ± 0.01 %	1.96 ± 0.07 %	0.67 ± 0.03 %	1.23 ± 0.02 %	1.66 ± 0.07 %
2,2-Dimethylbutane	0.03 ± 0.01 %	0.11 ± 0.01 %	0.04 ± 0.01 %	0.04 ± 0.01 %	0.04 ± 0.01 %
2,3-Dimethylbutane	0.01 ± 0.01 %	0.02 ± 0.01 %	0.01 ± 0.01 %	0.04 ± 0.01 %	0.01 ± 0.01 %
2-Methylpentane	0.15 ± 0.01 %	0.38 ± 0.01 %	0.27 ± 0.01 %	0.15 ± 0.01 %	0.17 ± 0.01 %
3-Methylpentane	1.39 ± 0.06 %	**4.90 ± 0.22 %**	1.32 ± 0.03 %	1.86 ± 0.07 %	1.50 ± 0.08 %
***n*-Hexane**	0.39 ± 0.02 %	1.39 ± 0.06 %	1.33 ± 0.06 %	**5.03 ± 0.17 %**	1.13 ± 0.05 %
Cyclohexane	0.00 ± 0.00 %	0.00 ± 0.00 %	0.00 ± 0.00 %	0.01 ± 0.00 %	0.00 ± 0.00 %
2-Methylhexane	0.01 ± 0.01 %	0.11 ± 0.01 %	0.14 ± 0.01 %	0.14 ± 0.01 %	0.14 ± 0.01 %
3-Methylhexane	0.38 ± 0.01 %	0.41 ± 0.01 %	0.26 ± 0.01 %	0.67 ± 0.01 %	0.53 ± 0.01 %
***n*-Heptane**	0.43 ± 0.01 %	0.78 ± 0.01 %	0.25 ± 0.02 %	0.60 ± 0.02 %	0.45 ± 0.02 %
***n*-Octane**	0.42 ± 0.01 %	0.63 ± 0.01 %	0.49 ± 0.01 %	0.58 ± 0.06 %	0.50 ± 0.05 %

***n*-Nonane**	0.71 ± 0.01 %	0.30 ± 0.01 %	0.62 ± 0.01 %	0.37 ± 0.02 %	0.34 ± 0.02 %
***n*-Decane**	0.35 ± 0.01 %	0.47 ± 0.01 %	0.28 ± 0.01 %	0.56 ± 0.03 %	0.57 ± 0.02 %
Undecane	0.00 ± 0.00 %	0.00 ± 0.00 %	0.00 ± 0.00 %	0.00 ± 0.00 %	0.00 ± 0.00 %
Alkenes (Anthropogenic)	**89.10 ± 0.70 %**	**58.07 ± 1.39 %**	**88.74 ± 1.66 %**	**66.39 ± 0.77 %**	**63.7 ± 0.56 %**
Ethene	0.00 ± 0.00 %	0.00 ± 0.00 %	0.00 ± 0.00 %	0.00 ± 0.00 %	0.00 ± 0.00 %
Propene	**62.24 ± 0.08 %**	**26.90 ± 0.13 %**	**57.93 ± 0.15 %**	**34.26 ± 0.16 %**	**35.84 ± 0.09 %**
1-Butene	0.92 ± 0.02 %	2.22 ± 0.25 %	1.71 ± 0.09 %	1.25 ± 0.11 %	1.22 ± 0.04 %
***trans*-2-Butene**	**8.79 ± 0.23 %**	**6.85 ± 0.08 %**	**11.68 ± 0.55 %**	**10.65 ± 0.07 %**	**8.35 ± 0.04 %**
***cis*-2-Butene**	**5.99 ± 0.11 %**	**4.77 ± 0.09 %**	**7.77 ± 0.44 %**	**7.90 ± 0.10 %**	**6.26 ± 0.07 %**
1,3-Butadiene	0.00 ± 0.00 %	0.00 ± 0.00 %	0.00 ± 0.00 %	0.00 ± 0.00 %	0.00 ± 0.00 %
1-Pentene	0.46 ± 0.05 %	2.65 ± 0.13 %	1.78 ± 0.07 %	0.8 ± 0.08 %	0.27 ± 0.05 %
3-Methyl-1-butene	0.05 ± 0.01 %	0.03 ± 0.01 %	0.01 ± 0.01 %	0.02 ± 0.01 %	0.06 ± 0.01 %
2-Methyl-1-butene	0.87 ± 0.05 %	0.65 ± 0.12 %	0.47 ± 0.09 %	0.78 ± 0.03 %	0.79 ± 0.05 %
***trans*-2-Pentene**	0.68 ± 0.01 %	4.04 ± 0.35 %	1.63 ± 0.16 %	5.57 ± 0.16 %	3.48 ± 0.06 %
***cis*-2-Pentene**	2.51 ± 0.04 %	5.18 ± 0.15 %	3.44 ± 0.08 %	3.22 ± 0.04 %	0.82 ± 0.04 %
2-Methyl-2-butene	6.58 ± 0.10 %	4.78 ± 0.08 %	2.34 ± 0.02 %	1.93 ± 0.01 %	6.61 ± 0.11 %
Alkenes (Biogenic)	**0.06 ± 0.01 %**	**0.42 ± 0.07 %**	**0.03 ± 0.01 %**	**0.18 ± 0.02 %**	**0.35 ± 0.03 %**
Isoprene	0.06 ± 0.01 %	0.42 ± 0.07 %	0.03 ± 0.01 %	0.18 ± 0.02 %	0.35 ± 0.03 %
***α*-Pinene**	0.00 ± 0.00 %	0.00 ± 0.00 %	0.00 ± 0.00 %	0.00 ± 0.00 %	0.00 ± 0.00 %

***β*-Pinene**	0.00 ± 0.00 %	0.00 ± 0.00 %	0.00 ± 0.00 %	0.00 ± 0.00 %	0.00 ± 0.00 %
Aromatics	**1.80 ± 0.11 %**	**6.23 ± 0.24 %**	**1.97 ± 0.25 %**	**6.43 ± 0.48 %**	**8.14 ± 0.38 %**
Benzene	0.00 ± 0.00 %	0.00 ± 0.00 %	0.00 ± 0.00 %	0.00 ± 0.00 %	0.00 ± 0.00 %
Toluene	0.00 ± 0.00 %	0.01 ± 0.01 %	0.00 ± 0.00 %	0.01 ± 0.01 %	0.01 ± 0.01 %
Ethylbenzene	0.31 ± 0.02 %	1.27 ± 0.09 %	0.43 ± 0.08 %	2.33 ± 0.27 %	3.17 ± 0.19 %
***m/p*-Xylene**	0.32 ± 0.01 %	1.84 ± 0.01 %	0.46 ± 0.01 %	1.03 ± 0.01 %	0.91 ± 0.01 %
***o*-Xylene**	0.08 ± 0.01 %	0.29 ± 0.01 %	0.05 ± 0.01 %	0.07 ± 0.01 %	0.12 ± 0.01 %
Styrene	0.00 ± 0.00 %	0.00 ± 0.00 %	0.00 ± 0.00 %	0.00 ± 0.00 %	0.00 ± 0.00 %
Isopropylbenzene	0.00 ± 0.00 %	0.00 ± 0.00 %	0.00 ± 0.00 %	0.01 ± 0.00 %	0.01 ± 0.00 %
***n*-Propylbenzene**	0.08 ± 0.01 %	0.03 ± 0.01 %	0.03 ± 0.01 %	0.05 ± 0.01 %	0.04 ± 0.01 %
***m*-Ethyltoluene**	0.12 ± 0.01 %	0.49 ± 0.02 %	0.14 ± 0.02 %	0.18 ± 0.02 %	0.39 ± 0.01 %
***p*-Ethyltoluene**	0.14 ± 0.01 %	0.12 ± 0.01 %	0.10 ± 0.02 %	0.40 ± 0.07 %	0.59 ± 0.07 %
***o*-Ethyltoluene**	0.18 ± 0.01 %	0.18 ± 0.01 %	0.13 ± 0.02 %	0.62 ± 0.04 %	0.58 ± 0.02 %
1,3,5-Trimethylbenzene	0.19 ± 0.01 %	0.42 ± 0.01 %	0.21 ± 0.01 %	0.61 ± 0.01 %	0.57 ± 0.01 %
1,2,4-Trimethylbenzene	0.18 ± 0.01 %	1.32 ± 0.05 %	0.30 ± 0.05 %	0.87 ± 0.02 %	1.42 ± 0.03 %
1,2,3-Trimethylbenzene	0.18 ± 0.01 %	0.26 ± 0.01 %	0.10 ± 0.02 %	0.24 ± 0.01 %	0.32 ± 0.01 %
Alkyne	**0.00 ± 0.00 %**	**0.00 ± 0.00 %**	**0.00 ± 0.00 %**	**0.00 ± 0.00 %**	**0.00 ± 0.00 %**
Ethyne	0.00 ± 0.00 %	0.00 ± 0.00 %	0.00 ± 0.00 %	0.00 ± 0.00 %	0.00 ± 0.00 %

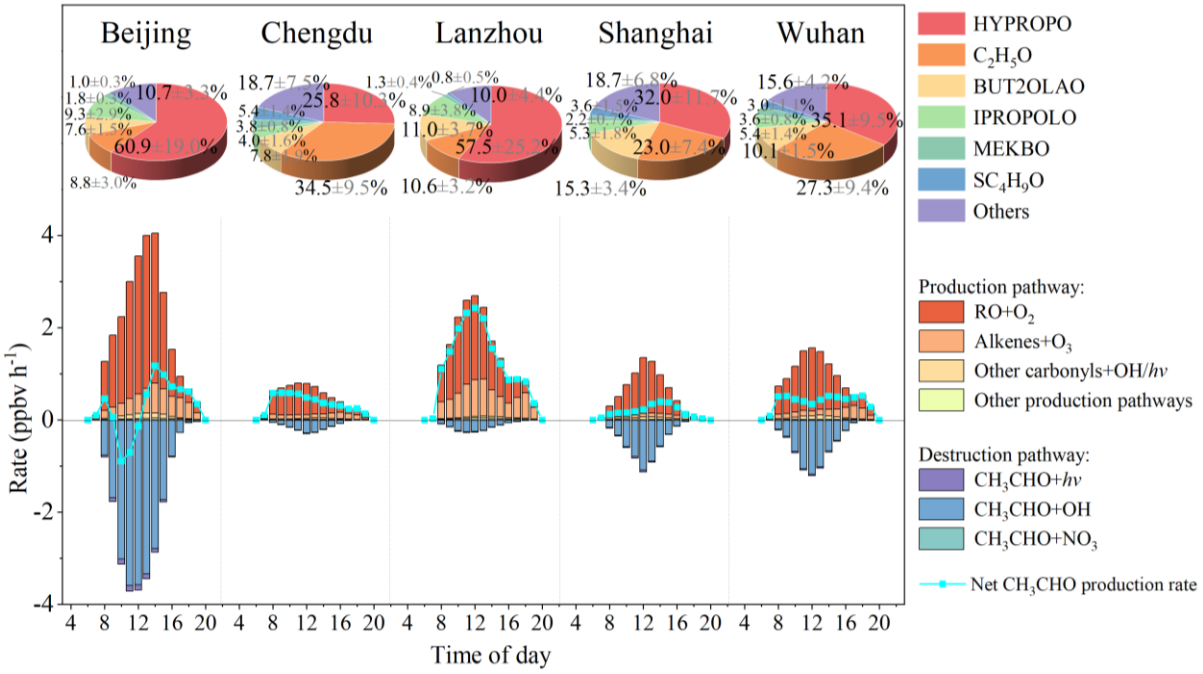

Figure 6.5. Diurnal variations of simulated production and destruction pathways of acetaldehyde (CH_3CHO). The pie charts illustrate the proportions of the main RO species contributing to the RO decomposition pathways for each city.

6.3.3 Acetone

Figure 6.6 illustrates the simulated production and destruction pathways of acetone in the five cities. Acetone was primarily produced through RO decomposition. In contrast to aldehydes, its destruction via reaction with OH radicals was negligible, highlighting acetone's atmospheric stability and its tendency to accumulate to high concentrations. Net acetone production rate was highest in Wuhan, reaching 0.8 ± 0.1 ppbv h^{-1}, followed by Beijing and Lanzhou at approximately 0.4 ppbv h^{-1}. The lowest net production rate was calculated in Shanghai, at 0.2 ± 0.02 ppbv h^{-1}**.** The higher mixing ratios of acetaldehyde and acetone observed in summer in Beijing, compared to the other four cities, despite the fact that their production rates are lower than those in Lanzhou and Wuhan, respectively. This can be mainly attributed to two factors. First, the concentrations of carbonyls are influenced not only by secondary formation but also by primary emissions and regional transport. In Beijing, primary emissions play a significant role, accounting for 55–70% of carbonyl concentrations, much higher than in Lanzhou and Wuhan, where simulated net production rates are higher. Second, regional transport contributes substantially to pollutant levels in Beijing. Previous studies have shown that Beijing is significantly affected by the regional transport of air pollutants from surrounding provinces, especially Hebei, which contributes 37–42% of $PM_{2.5}$, 31% of O_3 pollution, and 36–50% of VOC concentrations (C. Li et al., 2022; Panagi et al., 2025; P. Wang et al., 2020; Z. Zhang et al., 2024). These factors together explain the elevated carbonyl mixing ratios in Beijing

The pie charts in Figure 6.6 reveal that the top six RO species accounted for only about 50 % of the total RO radicals contributing to acetone formation in the five cities, indicating a considerable diversity of RO sources. Radicals derived from *α/β*-pinene (*i.e.*, C98O, C919O, C106O, and C108O, as designated in the MCM) contributed approximately 15-50 % to acetone formation across the cities. In addition, the isopropoxy radical (IC_3H_7O), mainly produced from propane and 2,3-dimethylbutene, and the 1,1-

dimethylpropoxy radical (IPECO), formed from the degradation of *i*-pentane, also played significant roles, with their contributions varying among the cities. Notably, alkene ozonolysis, particularly the reaction between 2-methyl-2-butene and O_3, made a more substantial contribution to acetone formation in Beijing.

Figure 6.4c displays the top ten VOC species contributing to acetone formation in the five cities, with detailed contributions for each species listed in Table 6.6. Collectively, these top ten VOCs accounted for over 95 % of acetone formation in all cities. *α/β*-pinene emerged as dominant contributor, responsible for over 60 % of acetone formation in Lanzhou and Wuhan, and around 40 % in Beijing, Chengdu, and Shanghai. This underscores the significant role of biogenic sources in acetone production, consistent with findings from the Hok Tsui site in Hong Kong (Lyu et al., 2024). Notably, in Lanzhou, *α/β*-pinene was primarily emitted from industrial sources rather than biogenic sources, highlighting the importance of anthropogenic pinene emissions in industrial cities (Cheng et al., 2018; Dai et al., 2010; Rouvière et al., 2006; H. Wang et al., 2022)**.** In Shanghai, alkanes were identified as the most significant contributors to acetone formation ($p < 0.05$), accounting for 51 % of the total contribution, a similarly high alkane contribution was also observed in Hong Kong (Guo, Ling, Cheung, Wang, et al., 2013). In Beijing, 2-methyl-2-butene contributed over 30 % to acetone formation, while in the other four cities, its contribution was around 6–7 %. Additionally, *i*-pentane made a substantial impact on acetone formation in the remaining four cities, followed by propane and *i*-butane**.**

Table 6.6. Contribution of VOC species to acetone formation during peak hours (11:00–14:00LT).

	Beijing	**Chengdu**	**Lanzhou**	**Shanghai**	**Wuhan**
Alkanes	**20.04 ± 0.82 %**	**42.65 ± 0.42 %**	**27.23 ± 0.84 %**	**50.50 ± 0.70 %**	**27.87 ± 0.72 %**
Ethane	0.00 ± 0.00 %	0.00 ± 0.00 %	0.00 ± 0.00 %	0.00 ± 0.00 %	0.00 ± 0.00 %
Propane	2.24 ± 0.22 %	**7.26 ± 0.17 %**	**7.30 ± 0.42 %**	**10.87 ± 0.30 %**	**7.94 ± 0.49 %**
***i*-Butane**	1.14 ± 0.02 %	**10.58 ± 0.05 %**	3.34 ± 0.08 %	**5.97 ± 0.07 %**	3.89 ± 0.08 %
***n*-Butane**	0.00 ± 0.00 %	0.00 ± 0.00 %	0.00 ± 0.00 %	0.00 ± 0.00 %	0.00 ± 0.00 %
***i*-Pentane**	**8.82 ± 0.17 %**	**17.06 ± 0.03 %**	2.77 ± 0.03 %	**20.06 ± 0.03 %**	**13.86 ± 0.08 %**
***n*-Pentane**	0.00 ± 0.00 %	0.00 ± 0.00 %	0.00 ± 0.00 %	0.00 ± 0.00 %	0.00 ± 0.00 %
2,2-Dimethylbutane	0.17 ± 0.01 %	0.29 ± 0.01 %	0.17 ± 0.01 %	0.20 ± 0.01 %	0.06 ± 0.01 %
2,3-Dimethylbutane	**4.71 ± 0.34 %**	2.30 ± 0.06 %	**6.48 ± 0.24 %**	**7.48 ± 0.26 %**	0.20 ± 0.03 %
2-Methylpentane	2.25 ± 0.05 %	2.37 ± 0.02 %	2.36 ± 0.04 %	1.62 ± 0.02 %	0.56 ± 0.01 %
3-Methylpentane	0.00 ± 0.00 %	0.00 ± 0.00 %	0.00 ± 0.00 %	0.00 ± 0.00 %	0.00 ± 0.00 %
***n*-Hexane**	0.00 ± 0.00 %	0.00 ± 0.00 %	0.00 ± 0.00 %	0.00 ± 0.00 %	0.00 ± 0.00 %
Cyclohexane	0.00 ± 0.00 %	0.00 ± 0.00 %	0.00 ± 0.00 %	0.00 ± 0.00 %	0.00 ± 0.00 %
2-Methylhexane	0.67 ± 0.01 %	2.76 ± 0.08 %	4.80 ± 0.02 %	4.30 ± 0.01 %	1.35 ± 0.02 %
3-Methylhexane	0.00 ± 0.00 %	0.00 ± 0.00 %	0.00 ± 0.00 %	0.00 ± 0.00 %	0.00 ± 0.00 %
***n*-Heptane**	0.00 ± 0.00 %	0.00 ± 0.00 %	0.00 ± 0.00 %	0.00 ± 0.00 %	0.00 ± 0.00 %

***n*-Octane**	0.00 ± 0.00 %	0.00 ± 0.00 %	0.00 ± 0.00 %	0.00 ± 0.00 %	0.00 ± 0.00 %
***n*-Nonane**	0.00 ± 0.00 %	0.00 ± 0.00 %	0.00 ± 0.00 %	0.00 ± 0.00 %	0.00 ± 0.00 %
***n*-Decane**	0.00 ± 0.00 %	0.00 ± 0.00 %	0.00 ± 0.00 %	0.00 ± 0.00 %	0.00 ± 0.00 %
Undecane	0.00 ± 0.00 %	0.00 ± 0.00 %	0.00 ± 0.00 %	0.00 ± 0.00 %	0.00 ± 0.00 %
Alkenes (Anthropogenic)	**37.65 ± 0.23 %**	**9.73 ± 0.09 %**	**7.12 ± 0.07 %**	**7.97 ± 0.11 %**	**9.16 ± 0.22 %**
Ethene	0.00 ± 0.00 %	0.00 ± 0.00 %	0.00 ± 0.00 %	0.00 ± 0.00 %	0.00 ± 0.00 %
Propene	0.00 ± 0.00 %	0.00 ± 0.00 %	0.00 ± 0.00 %	0.00 ± 0.00 %	0.00 ± 0.00 %
1-Butene	0.00 ± 0.00 %	0.00 ± 0.00 %	0.00 ± 0.00 %	0.00 ± 0.00 %	0.00 ± 0.00 %
***trans*-2-Butene**	0.00 ± 0.00 %	0.00 ± 0.00 %	0.00 ± 0.00 %	0.00 ± 0.00 %	0.00 ± 0.00 %
***cis*-2-Butene**	0.00 ± 0.00 %	0.00 ± 0.00 %	0.00 ± 0.00 %	0.00 ± 0.00 %	0.00 ± 0.00 %
1,3-Butadiene	0.00 ± 0.00 %	0.00 ± 0.00 %	0.00 ± 0.00 %	0.00 ± 0.00 %	0.00 ± 0.00 %
1-Pentene	0.00 ± 0.00 %	0.00 ± 0.00 %	0.00 ± 0.00 %	0.00 ± 0.00 %	0.00 ± 0.00 %
3-Methyl-1-butene	**4.46 ± 0.13 %**	0.84 ± 0.03 %	0.63 ± 0.04 %	1.70 ± 0.10 %	1.87 ± 0.18 %
2-Methyl-1-butene	0.00 ± 0.00 %	0.00 ± 0.00 %	0.00 ± 0.00 %	0.00 ± 0.00 %	0.00 ± 0.00 %
***trans*-2-Pentene**	0.00 ± 0.00 %	0.00 ± 0.00 %	0.00 ± 0.00 %	0.00 ± 0.00 %	0.00 ± 0.00 %
***cis*-2-Pentene**	0.00 ± 0.00 %	0.00 ± 0.00 %	0.00 ± 0.00 %	0.00 ± 0.00 %	0.00 ± 0.00 %
2-Methyl-2-butene	**33.16 ± 0.10 %**	**8.86 ± 0.06 %**	**6.48 ± 0.03 %**	**6.26 ± 0.01 %**	**7.27 ± 0.04 %**
Alkenes (Biogenic)	**41.46 ± 0.66 %**	**47.48 ± 0.36 %**	**65.41 ± 0.28 %**	**40.69 ± 0.32 %**	**62.47 ± 0.85 %**

Isoprene	0.02 ± 0.01 %	0.05 ± 0.01 %	0.01 ± 0.01 %	0.03 ± 0.01 %	0.02 ± 0.01 %
***α*-Pinene**	22.07 ± 0.31 %	33.85 ± 0.10 %	61.42 ± 0.15 %	7.83 ± 0.09 %	30.36 ± 0.29 %
***β*-Pinene**	19.36 ± 0.34 %	13.58 ± 0.25 %	3.98 ± 0.12 %	32.83 ± 0.22 %	32.09 ± 0.55 %
Aromatics	**0.86 ± 0.10 %**	**0.14 ± 0.01 %**	**0.24 ± 0.05 %**	**0.85 ± 0.14 %**	**0.50 ± 0.10 %**
Benzene	0.00 ± 0.00 %	0.00 ± 0.00 %	0.00 ± 0.00 %	0.00 ± 0.00 %	0.00 ± 0.00 %
Toluene	0.00 ± 0.00 %	0.00 ± 0.00 %	0.00 ± 0.00 %	0.00 ± 0.00 %	0.00 ± 0.00 %
Ethylbenzene	0.00 ± 0.00 %	0.00 ± 0.00 %	0.00 ± 0.00 %	0.00 ± 0.00 %	0.00 ± 0.00 %
***m/p*-Xylene**	0.00 ± 0.00 %	0.00 ± 0.00 %	0.00 ± 0.00 %	0.00 ± 0.00 %	0.00 ± 0.00 %
***o*-Xylene**	0.00 ± 0.00 %	0.00 ± 0.00 %	0.00 ± 0.00 %	0.00 ± 0.00 %	0.00 ± 0.00 %
Styrene	0.00 ± 0.00 %	0.00 ± 0.00 %	0.00 ± 0.00 %	0.00 ± 0.00 %	0.00 ± 0.00 %
Isopropylbenzene	0.82 ± 0.10 %	0.09 ± 0.01 %	0.23 ± 0.05 %	0.85 ± 0.14 %	0.47 ± 0.10 %
***n*-Propylbenzene**	0.00 ± 0.00 %	0.00 ± 0.00 %	0.00 ± 0.00 %	0.00 ± 0.00 %	0.00 ± 0.00 %
***m*-Ethyltoluene**	0.00 ± 0.00 %	0.00 ± 0.00 %	0.00 ± 0.00 %	0.00 ± 0.00 %	0.00 ± 0.00 %
***p*-Ethyltoluene**	0.00 ± 0.00 %	0.00 ± 0.00 %	0.00 ± 0.00 %	0.00 ± 0.00 %	0.00 ± 0.00 %
***o*-Ethyltoluene**	0.00 ± 0.00 %	0.00 ± 0.00 %	0.00 ± 0.00 %	0.00 ± 0.00 %	0.00 ± 0.00 %
1,3,5-Trimethylbenzene	0.00 ± 0.00 %	0.00 ± 0.00 %	0.00 ± 0.00 %	0.00 ± 0.00 %	0.00 ± 0.00 %
1,2,4-Trimethylbenzene	0.00 ± 0.00 %	0.00 ± 0.00 %	0.00 ± 0.00 %	0.00 ± 0.00 %	0.00 ± 0.00 %
1,2,3-Trimethylbenzene	0.00 ± 0.00 %	0.00 ± 0.00 %	0.00 ± 0.00 %	0.00 ± 0.00 %	0.00 ± 0.00 %

Alkyne	**0.00 ± 0.00 %**	**0.00 ± 0.00 %**	**0.00 ± 0.00 %**	**0.00 ± 0.00 %**	**0.00 ± 0.00 %**
Ethyne	0.00 ± 0.00 %	0.00 ± 0.00 %	0.00 ± 0.00 %	0.00 ± 0.00 %	0.00 ± 0.00 %

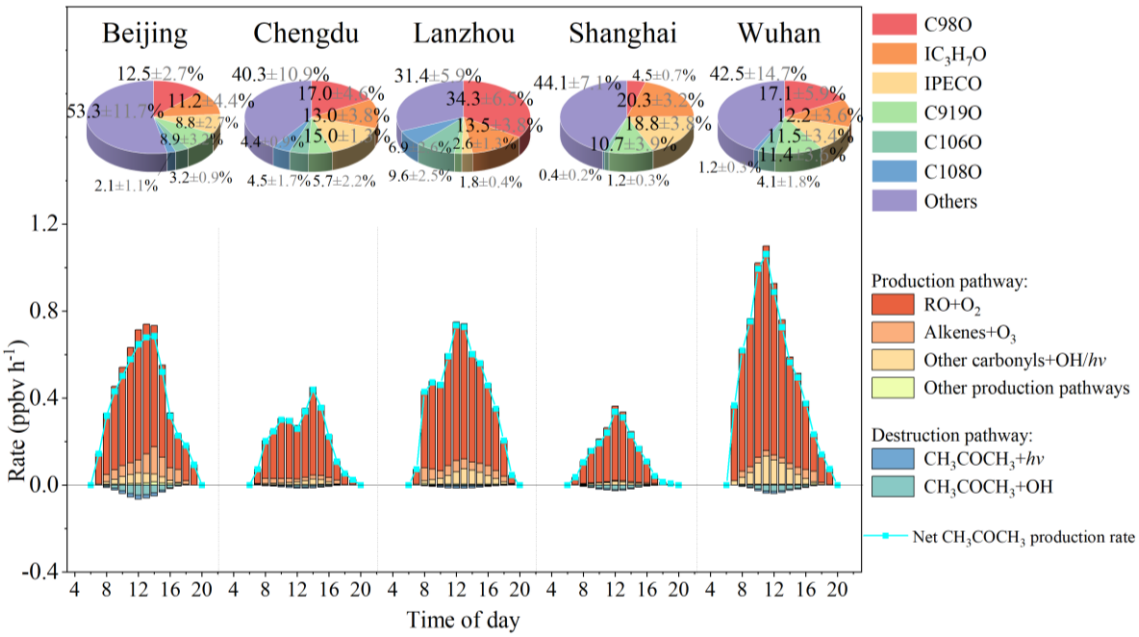

Figure 6.6. Diurnal variations of simulated production and destruction pathways of acetone (CH_3COCH_3). The pie charts illustrate the proportions of the main RO species contributing to the RO decomposition pathways for each city.

6.4 Impacts of carbonyls on radical cycling and O_3 formation

6.4.1 Impacts of carbonyls on reaction pathways

Figure 6.7 presents the major degradation pathways of VOCs to carbonyls and their respective contributions to radical and O_3 production in the five cities. Using Beijing as an example, formaldehyde destruction via OH oxidation and photolysis (as shown in Figure 6.3) directly contributed 31.8 ± 1.2 % to HO_2 production. In contrast, acetaldehyde and acetone mainly contribute to RO_2 production through OH oxidation. Specifically, acetaldehyde is oxidized to form peroxyacetyl radicals (PA, CH_3CO_3), making it the dominant source of PA radicals, with a contribution of 73.8 ± 2.2 % in Beijing. PA can further react with NO to produce CH_3O_2 radicals, accounting for 85.1 ± 0.4 % of CH_3O_2 formation. Consequently, acetaldehyde can be considered to indirectly contribute approximately 30 % to the combined pathway of PA and CH_3O_2 with NO. Furthermore, since CH_3O_2 is almost quantitatively converted to CH_3O radicals, acetaldehyde (62.2 ± 0.1 % of which originates from propene) also contributes about 26 % to formaldehyde formation via CH_3O decomposition, while its subsequent contributions to the HO_2 pathway via HCHO remain relatively minor (~1 %).

Beyond aldehydes, acetone is oxidized by OH to form $CH_3COCH_2O_2$ radicals. It reacts with NO to produce the corresponding RO radicals (CH_3COCH_2O), which can further thermally decompose to simultaneously generate PA and formaldehyde. This indicates that acetone can also be converted to formaldehyde and promote O_3 formation during its degradation. However, due to the low reaction rate of acetone with OH, these contributions are insignificant.

(a)

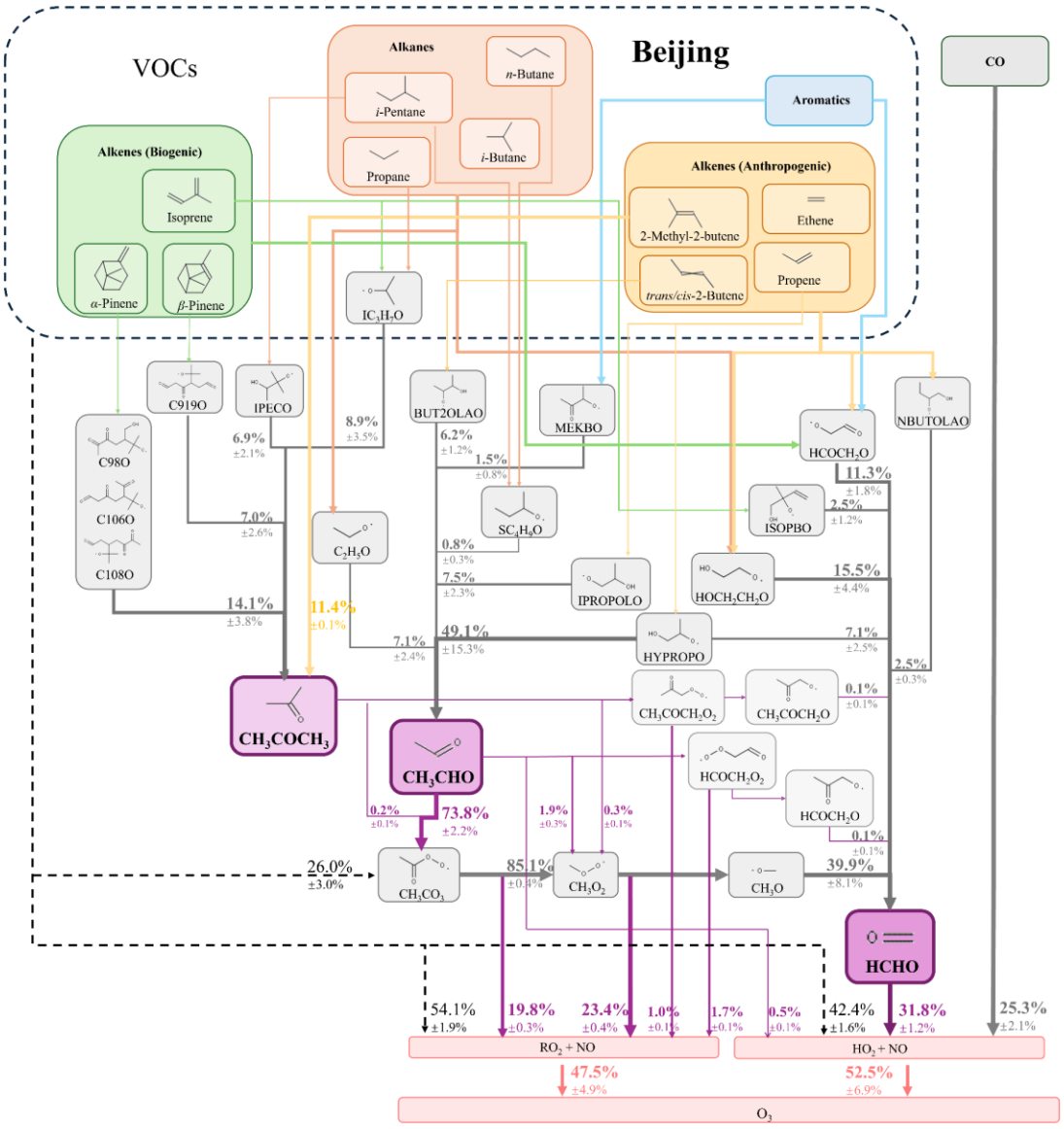
VOCs
Beijing
CO
Alkanes
n-Butane
i-Pentane
i-Butane
Propane
Aromatics
Alkenes (Biogenic)
Isoprene
α-Pinene
β-Pinene
Alkenes (Anthropogenic)
2-Methyl-2-butene
Ethene
trans/cis-2-Butene
Propene
IC4H7O
C919O
IPECO
BUT2OLAO
MEKBO
HCOCH2O
NBUTOLAO
C98O
C106O
C108O
8.9% ±3.5%
6.9% ±2.1%
6.2% ±1.2%
1.5% ±0.8%
11.3% ±1.8%
2.5% ±1.2%
7.0% ±2.6%
SC4H9O
ISOPBO
0.8% ±0.3%
C2H5O
7.5% ±2.3%
IPROPOLO
HOCH2CH2O
15.5% ±4.4%
14.1% ±3.8%
11.4% ±0.1%
7.1% ±2.4%
49.1% ±15.3%
HYPROPO
7.1% ±2.5%
2.5% ±0.3%
CH3COCH3
CH3COCH2O2
CH3COCH2O
0.1% ±0.1%
CH3CHO
HCOCH2O2
HCOCH2O
0.2% ±0.1%
73.8% ±2.2%
1.9% ±0.3%
0.3% ±0.1%
0.1% ±0.1%
26.0% ±3.0%
CH3CO3
85.1% ±0.4%
CH3O2
CH3O
39.9% ±8.1%
HCHO
54.1% ±1.9%
19.8% ±0.3%
23.4% ±0.4%
1.0% ±0.1%
1.7% ±0.1%
0.5% ±0.1%
42.4% ±1.6%
31.8% ±1.2%
25.3% ±2.1%
RO2 + NO
HO2 + NO
47.5% ±4.9%
52.5% ±6.9%
O3

(b)

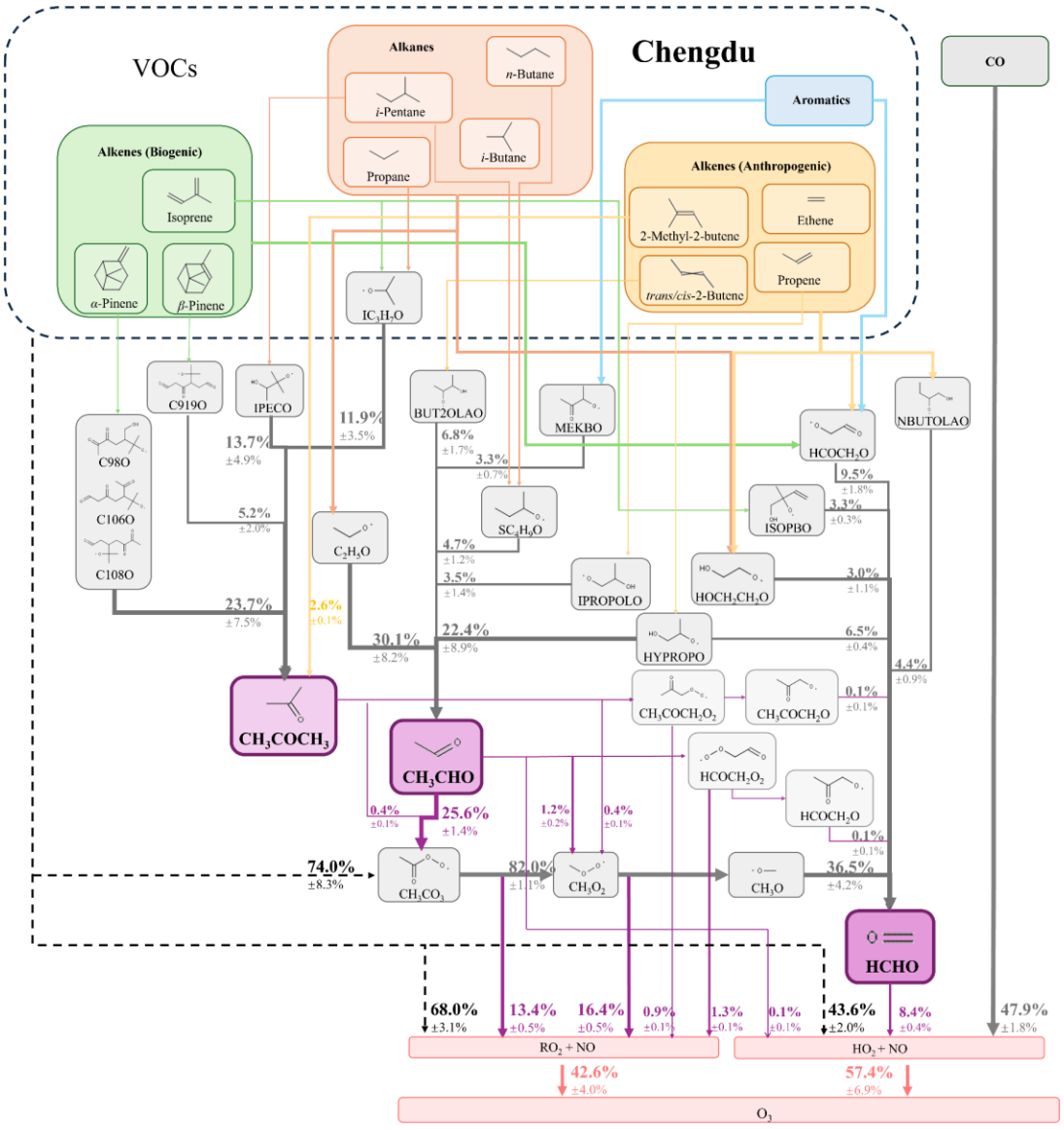
Chengdu
VOCs
Alkanes
n-Butane
i-Pentane
i-Butane
Propane
Aromatics
CO
Alkenes (Biogenic)
Isoprene
α-Pinene
β-Pinene
Alkenes (Anthropogenic)
2-Methyl-2-butene
Ethene
Propene
trans/cis-2-Butene
IC3H7O
C919O
IPECO
BUT2OLAO
MEKBO
HCOCH2O
NBUTOLAO
C98O
C106O
C108O
11.9% ±3.5%
13.7% ±4.9%
6.8% ±1.7%
3.3% ±0.7%
9.5% ±1.8%
3.3% ±0.3%
5.2% ±2.0%
SC4H9O
ISOPBO
C2H3O
4.7% ±1.2%
3.5% ±1.4%
IPROPOLO
HOCH2CH2O
3.0% ±1.1%
23.7% ±7.5%
2.6% ±0.1%
30.1% ±8.2%
22.4% ±8.9%
HYPROPO
6.5% ±0.4%
4.4% ±0.9%
CH3COCH3
CH3COCH2O2
CH3COCH2O
0.1% ±0.1%
CH3CHO
HCOCH2O2
HCOCH2O
0.1% ±0.1%
0.4% ±0.1%
25.6% ±1.4%
1.2% ±0.2%
0.4% ±0.1%
74.0% ±8.3%
CH3CO3
82.0% ±1.1%
CH3O2
CH3O
36.5% ±4.2%
HCHO
68.0% ±3.1%
13.4% ±0.5%
16.4% ±0.5%
0.9% ±0.1%
1.3% ±0.1%
0.1% ±0.1%
43.6% ±2.0%
8.4% ±0.4%
47.9% ±1.8%
RO2 + NO
HO2 + NO
42.6% ±4.0%
57.4% ±6.9%
O3

(c)

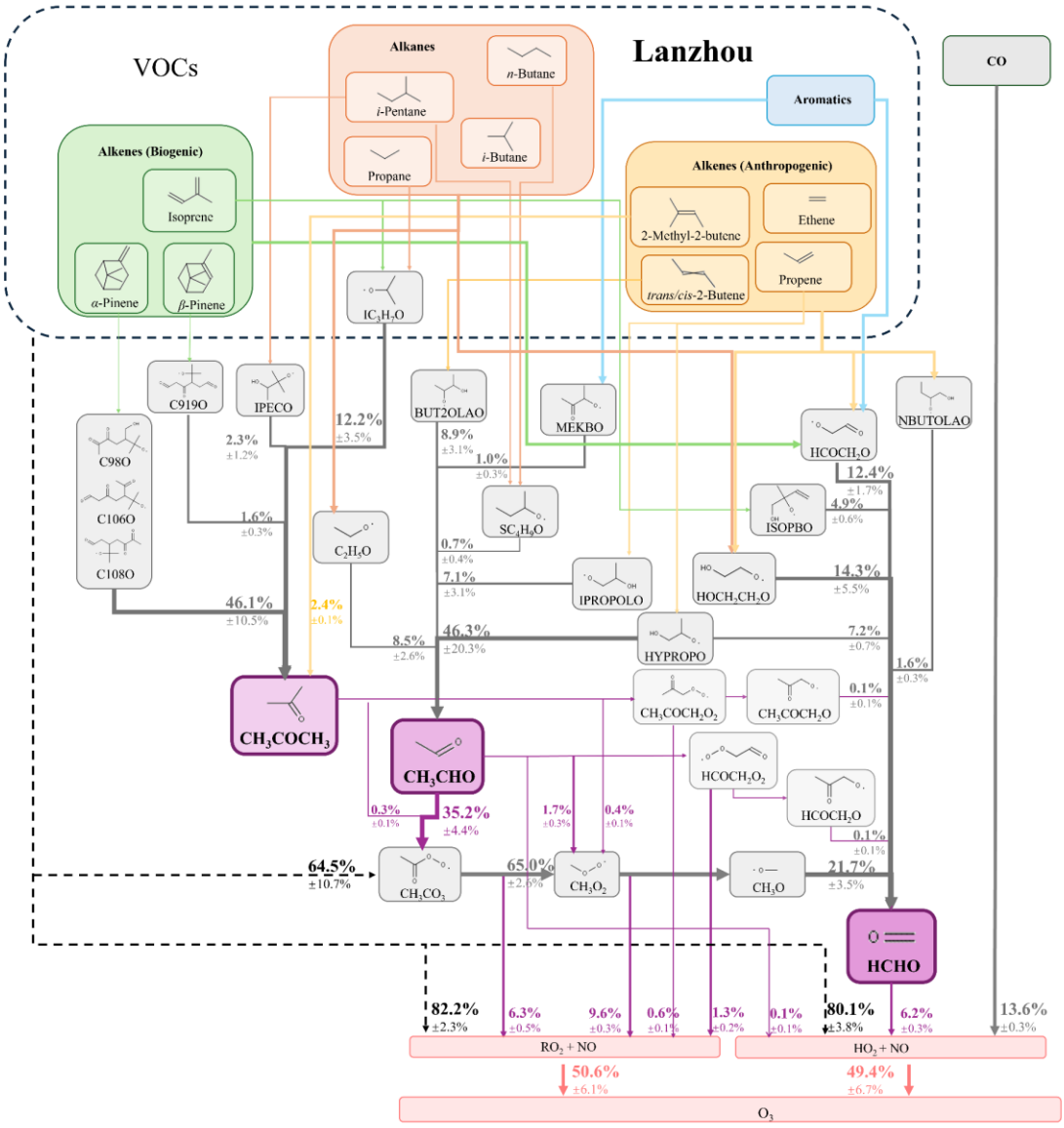
VOCs
Lanzhou
Alkanes
n-Butane
i-Pentane
i-Butane
Propane
Aromatics
CO
Alkenes (Biogenic)
Isoprene
α-Pinene
β-Pinene
Alkenes (Anthropogenic)
2-Methyl-2-butene
Ethene
trans/cis-2-Butene
Propene
IC3H7O
C919O
IPECO
BUT2OLAO
MEKBO
HCOCH2O
NBUTOLAO
C98O
C106O
C108O
12.2%
±3.5%
2.3%
±1.2%
8.9%
±3.1%
1.0%
±0.3%
12.4%
±1.7%
4.9%
±0.6%
ISOPBO
SC4H9O
C2H5O
1.6%
±0.3%
0.7%
±0.4%
7.1%
±3.1%
IPROPOLO
HOCH2CH2O
14.3%
±5.5%
46.1%
±10.5%
2.4%
±0.1%
8.5%
±2.6%
46.3%
±20.3%
HYPROPO
7.2%
±0.7%
1.6%
±0.3%
CH3COCH2O2
CH3COCH2O
0.1%
±0.1%
CH3COCH3
CH3CHO
HCOCH2O2
HCOCH2O
0.1%
±0.1%
0.3%
±0.1%
35.2%
±4.4%
1.7%
±0.3%
0.4%
±0.1%
64.5%
±10.7%
CH3CO3
65.0%
±2.5%
CH3O2
CH3O
21.7%
±3.5%
HCHO
82.2%
±2.3%
6.3%
±0.5%
9.6%
±0.3%
0.6%
±0.1%
1.3%
±0.2%
0.1%
±0.1%
80.1%
±3.8%
6.2%
±0.3%
13.6%
±0.3%
RO2 + NO
HO2 + NO
50.6%
±6.1%
49.4%
±6.7%
O3

(d)

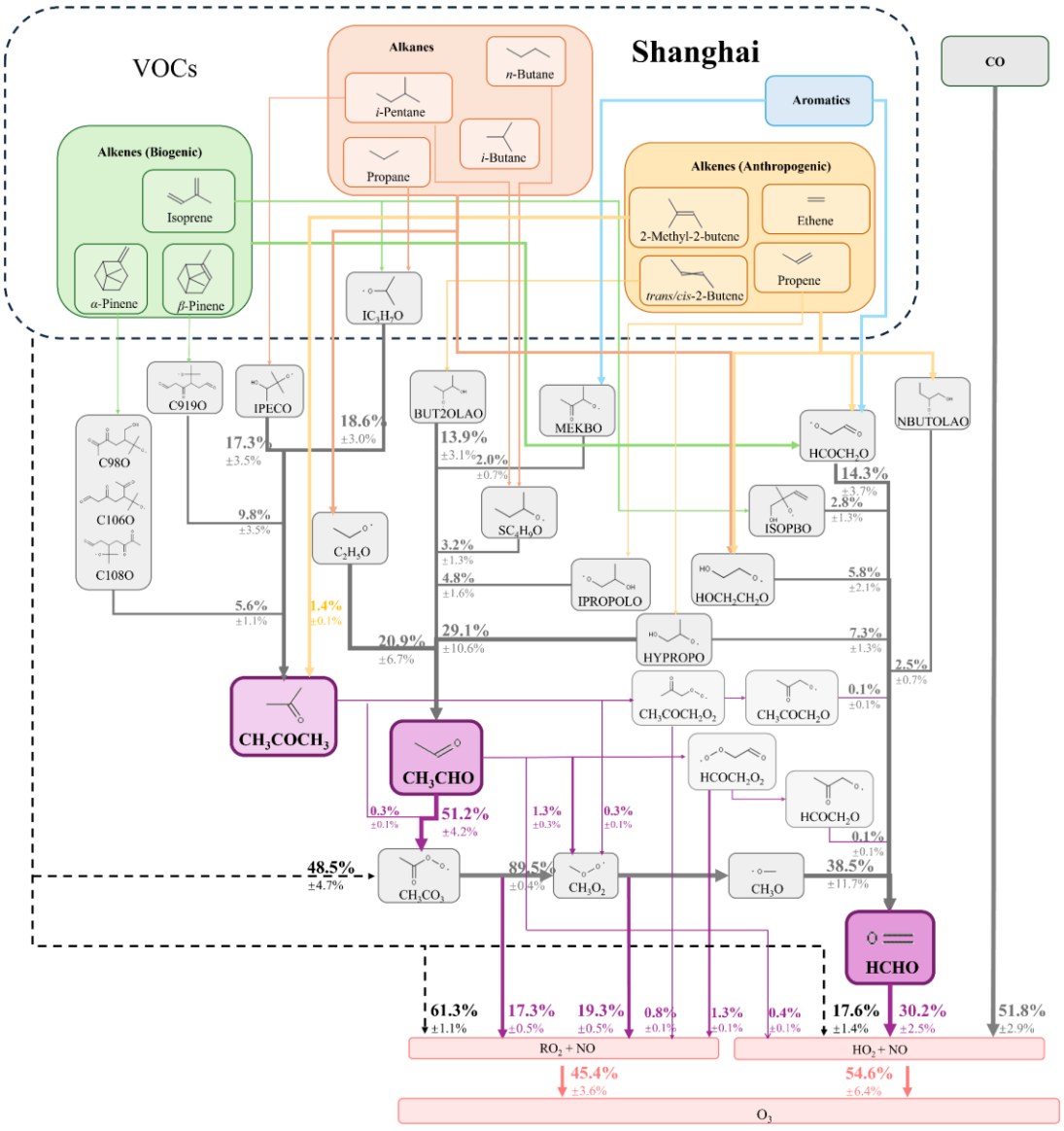
Shanghai
VOCs
Alkanes
n-Butane
i-Pentane
i-Butane
Propane
Aromatics
CO
Alkenes (Biogenic)
Isoprene
α-Pinene
β-Pinene
Alkenes (Anthropogenic)
2-Methyl-2-butene
Ethene
trans/cis-2-Butene
Propene
IC4H8O
C919O
IPECO
BUT2OLAO
MEKBO
HCOCH2O
NBUTOLAO
C98O
C106O
C108O
18.6% ±3.0%
17.3% ±3.5%
13.9% ±3.1%
2.0% ±0.7%
14.3% ±3.7%
2.8% ±1.3%
9.8% ±3.5%
C2H3O
SC4H9O
ISOPBO
3.2% ±1.3%
4.8% ±1.6%
IPROPOLO
HOCH2CH2O
5.8% ±2.1%
5.6% ±1.1%
1.4% ±0.1%
20.9% ±6.7%
29.1% ±10.6%
HYPROPO
7.3% ±1.3%
2.5% ±0.7%
CH3COCH3
CH3COCH2O2
CH3COCH2O
0.1% ±0.1%
CH3CHO
HCOCH2O2
HCOCH2O
0.1% ±0.1%
0.3% ±0.1%
51.2% ±4.2%
1.3% ±0.3%
0.3% ±0.1%
48.5% ±4.7%
CH3CO3
89.5% ±0.4%
CH3O2
CH3O
38.5% ±11.7%
HCHO
61.3% ±1.1%
17.3% ±0.5%
19.3% ±0.5%
0.8% ±0.1%
1.3% ±0.1%
0.4% ±0.1%
17.6% ±1.4%
30.2% ±2.5%
51.8% ±2.9%
RO2 + NO
HO2 + NO
45.4% ±3.6%
54.6% ±6.4%
O3

(e)

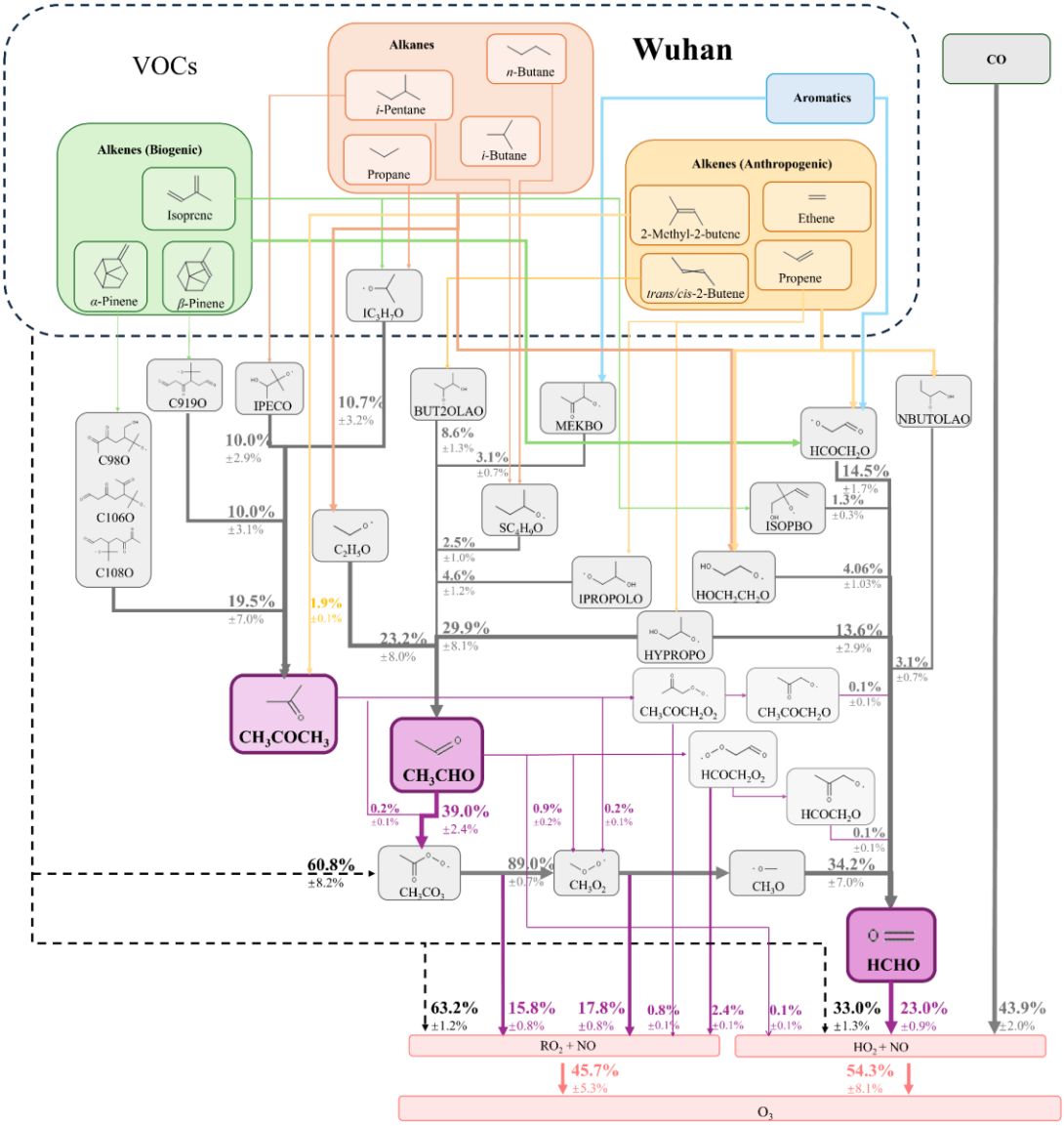

Figure 6.7. Degradation progresses from VOC to carbonyls and O_3 during peak hours (11:00–14:00LT) in (a) Beijing, (b) Chengdu, (c) Lanzhou, (d) Shanghai, and (e) Wuhan.

6.4.2 Impacts of carbonyls on radicals and O_3 formation

Summarizing the mechanistic diagrams for the five cities shown in Figure 6.7, Figure 6.8a presents the average contributions of the three carbonyls to peroxy radical formation, while Figure 6.8b displays their respective contributions to the O_3 production rate in each city. The specific proportions for each city are provided in Table 6.7. On average, formaldehyde accounted for 20.0 % of HO_2 production across the five cities. In Beijing, the influence of formaldehyde on HO_2 formation was similar to that in Shanghai (about 30 % each), followed by Wuhan (23.0 ± 0.9 %). In contrast, the contributions in Chengdu and Lanzhou were significantly lower (6–8 %). This limited influence in Chengdu and Lanzhou was primarily attributed to their low aldehyde concentrations, as well as the high contribution of alkenes in Lanzhou (X. F. Liu et al., 2021).

Regarding RO_2 formation, acetaldehyde contributed an average of 16 % across the five cities. In Beijing, RO_2 formation was strongly affected by acetaldehyde, with a contribution of 31.3 ± 0.8 %. In contrast, the contribution of acetaldehyde to RO_2 formation in Lanzhou was less than 10 %. In Shanghai and Wuhan, acetaldehyde accounted for 19.3 ± 0.9 % and 15.0 ± 1.0 % of RO_2 formation, respectively. In Chengdu and Lanzhou, acetaldehyde had a smaller contribution to RO_2 formation (5-9 %) compared to the other two cities ($p < 0.05$). The higher acetaldehyde concentration in Beijing (7.21 ± 0.08 ppbv), compared to the other cities (1–2 ppbv), led to its greater contribution to PA radicals. In Shanghai and Wuhan, the proportions of acetaldehyde among total VOCs were 7.3 % and 5.3 %, respectively, which were slightly higher than those in Chengdu (2.8 %) and Lanzhou (3.8 %). Finally, the contributions of acetone to RO_2 formation in all five cities were minimal, each less than 1 %. The results for Shanghai and Wuhan in this study are generally consistent with previous findings (J. L. Li et al., 2022; Pei Zeng et al., 2019; Zhang et al., 2021; J. Zhu et al., 2020), while the results for Beijing are lower than those reported in an earlier study, which found that carbonyls accounted for over 70 % in summertime Beijing (Yang et al., 2018).

By combining the proportions of the two peroxy radicals, the contribution of carbonyls to O_3 formation can be determined. As shown in Figure 6.8b, formaldehyde contributed 16.7 ± 0.6 %,

16.5 ± 1.4 %, and 12.5 ± 0.5 % to O_3 formation in Beijing, Shanghai, and Wuhan, respectively, while its contributions in Chengdu and Lanzhou were lower, at only 4.8 ± 0.2 % and 3.1 ± 0.2 %. Acetaldehyde made a significant contribution to O_3 formation in Beijing (15.1 ± 0.4 %) but had a more limited impact in the other four cities, with contributions ranging from 3 % to 4 % in Chengdu and Lanzhou, and from 6 % to 9 % in Shanghai and Wuhan. The contribution of acetone was less than 1 % in all five cities. Overall, the contribution of aldehydes to O_3 formation in these cities ranged from 6 % to 33 %. In Beijing, carbonyls accounted for 32.4 ± 1.0 % of O_3 formation, which is consistent with results reported for other cities (J. L. Li et al., 2022; X. F. Liu et al., 2021; Shen et al., 2021). The limited contributions of carbonyls in Chengdu and Lanzhou may be attributed to the significant influence of aromatics in Chengdu and the high contribution of alkenes in Lanzhou (X. F. Liu et al., 2021).

Table 6.7. Contribution of carbonyls to radicals and O_3 formation during peak hours (11:00–14:00 LT).

	Species	HO_2 formation	RO_2 formation	O_3 formation
Beijing	Formaldehyde	31.84 ± 1.17 %	/	16.71 ± 0.61 %
	Acetaldehyde	0.47 ± 0.05 %	31.29 ± 0.75 %	15.12 ± 0.38 %
	Acetone	/	1.15 ± 0.07 %	0.55 ± 0.03 %
Chengdu	Formaldehyde	8.39 ± 0.39 %	/	4.82 ± 0.22 %
	Acetaldehyde	0.14 ± 0.02 %	8.55 ± 0.56 %	3.72 ± 0.25 %
	Acetone	/	1.04 ± 0.07 %	0.44 ± 0.03 %
Lanzhou	Formaldehyde	6.18 ± 0.30 %	/	3.06 ± 0.15 %
	Acetaldehyde	0.14 ± 0.02 %	5.93 ± 0.63 %	3.07 ± 0.24 %
	Acetone	/	0.46 ± 0.03 %	0.32 ± 0.02 %
Shanghai	Formaldehyde	30.23 ± 2.48 %	/	16.52 ± 1.35 %
	Acetaldehyde	0.37 ± 0.07 %	19.33 ± 1.09 %	8.97 ± 0.53 %
	Acetone	/	0.92 ± 0.08 %	0.42 ± 0.03 %
Wuhan	Formaldehyde	23.04 ± 0.89 %	/	12.52 ± 0.48 %
	Acetaldehyde	0.89 ± 0.01 %	15.01 ± 0.66 %	6.93 ± 0.31 %
	Acetone	/	0.96 ± 0.05 %	0.44 ± 0.02 %

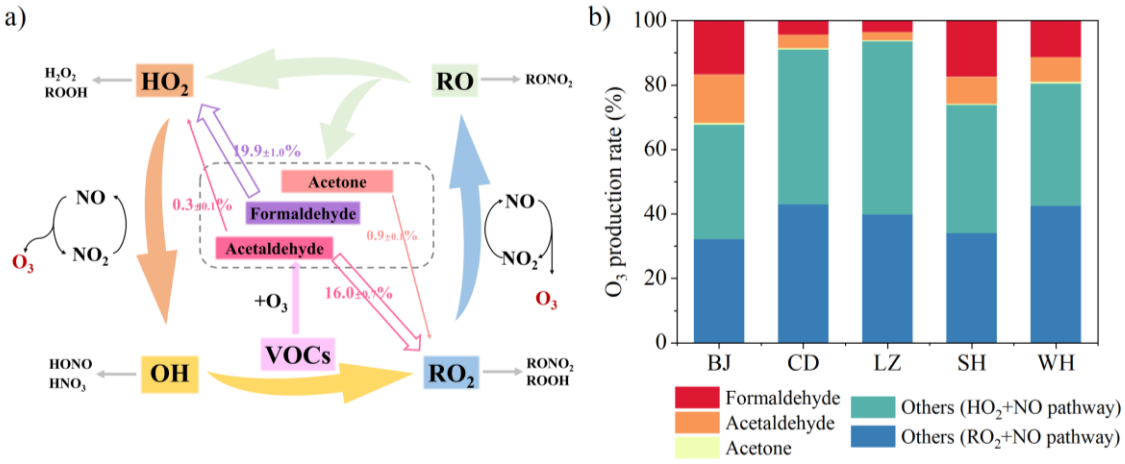

Figure 6.8. a) The average contribution of carbonyls to radical cycling during the peak hour (11:00–14:00LT) in five cities; b) The proportion of carbonyls contribution to O_3 formation during the peak hour (11:00–14:00LT) in Beijing (BJ), Chengdu (CD), Lanzhou (LZ), Shanghai (SH) and Wuhan (WH).

6.5 Policy recommendations for carbonyl control

6.5.1 Comparisons of the reduction ratio of VOCs/NO_x on carbonyls and O_3 formation

O_3 isopleth diagrams, also known as empirical kinetic modeling approach (EKMA) curves, were first developed by Dodge in 1977 and represent a classical method for assessing the nonlinear relationship of O_3 to its precursors under specific assumptions (Cui et al., 2021; Dodge, 1977; Ou et al., 2016). As carbonyl compounds exhibit a similar nonlinear relationship with their precursors, to inform science-based control strategies, O_3 and carbonyls isopleths were examined by plotting isopleths of their production rate as a function of VOCs and NO_x concentrations (X. F. Liu et al., 2021; Lyu et al., 2019; Zeng et al., 2022). In this study, different concentrations of O_3 precursors (i.e., VOCs and NO_x) were input into the model to simulate the formation of O_3 and carbonyls during peak periods. The base case scenario was determined by the concentrations of VOCs and NO_x measured during the carbonyl sampling period. Starting from this base case, both VOC and NO_x concentrations were systematically reduced in 10 % increments, ranging from 0 % (no reduction) to 100 % (full reduction) of their base values. This approach resulted in 11 levels for each precursor, forming an 11 × 11 matrix and yielding a total of 121 scenarios. Using the PBM-MCM model, we simulated these 121 scenarios and extracted the average production rates of O_3 and carbonyls at peak times for each scenario to generate the isopleths. In these isopleth diagrams, the base case is indicated by a black star in the upper right corner. The resulting isopleths are presented in Figure 6.9.

Because carbonyls and O_3 exhibit nonlinear relationships with their precursors, the feasibility of joint control strategies for these secondary pollutants can be evaluated. Figure 6.9 presents isopleth diagrams for the three carbonyls and O_3, based on sampling days in five cities. As shown, the positions of the base cases (marked with black stars) fall within the VOC-limited regime, indicating that reducing NO_x alone would increase the production of both carbonyls and O_3. Therefore, it is crucial to determine an appropriate VOC-to-NO_x reduction ratio to effectively prevent secondary pollutant formation. Typically, the minimum VOC/NO_x reduction ratio corresponds to the tangent of the contour line passing through the base case. In Figure 6.9d, the tangent to the contour line at the base case (shown in green) indicates a

VOC/NO_x reduction ratio of 0.8, suggesting that a higher reduction ratio of VOCs to NO_x is necessary to prevent an increase in O_3 production. In comparison, the minimum VOC/NO_x reduction ratios for the three carbonyls in Beijing ranged from 0.4 to 0.7 (Figure 6.9a–c), which are lower than that for O_3. Similar trends were observed in the other four cities, where the minimum VOC/NO_x ratios required for carbonyl control were also lower than those for O_3. This indicates that the VOC/NO_x reduction ratios necessary for effective O_3 control are also sufficient to suppress carbonyl formation. Thus, implementing O_3 reduction policies can simultaneously reduce carbonyl levels.

Compared to the O_3 isopleths, the lower VOC/NO_x ratios observed for the three carbonyls can be attributed to their flatter contour curves. Among these, the contour lines for formaldehyde most closely resemble those of O_3, likely because formaldehyde is produced from the degradation of nearly all VOC species. In contrast, the contour lines for acetaldehyde and acetone are noticeably flatter, which may be due to their more limited range of VOC precursors and their reduced involvement in photochemical reactions. The flatter isopleths for carbonyls indicate that O_3 control strategies are also effective in reducing carbonyl concentrations.

It is noteworthy that this evaluation approach is particularly well-suited for assessing control strategies aimed at locally formed secondary pollutants. This is because the isopleth plots presented in this study are based on the net production rates of carbonyls and O_3, rather than their ambient concentrations, which inherently incorporate all relevant formation and loss pathways for each species. Factors influencing the chemical lifetime of each species, such as dry deposition rates, photolysis, and reactions with OH radicals, are already considered in this modelling approach. Nevertheless, since the model focuses on local photochemical formation, it has limited capacity to account for the impact of secondary pollutants transported over regional scales. For example, acetone, which has a much longer lifetime compared to more reactive carbonyls (Atkinson, 2000; Carter, 1994; Sander et al., 2006; Seinfeld & Pandis, 2016), is likely to be more affected by regional transport. Therefore, caution should be exercised when applying this method to the evaluation of regional pollution control strategies.

(a) Beijing

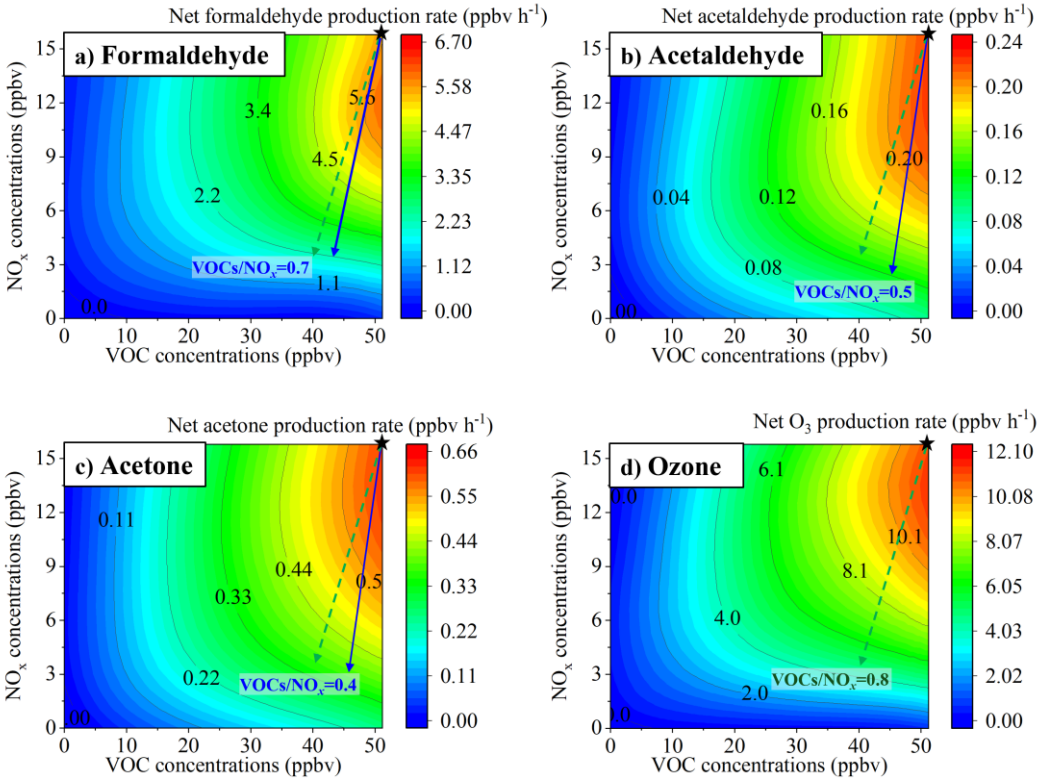
Net formaldehyde production rate (ppbv h-1)
a) Formaldehyde
3.4
5.6
4.5
2.2
VOCs/NOx=0.7
1.1
0.0
6.70
5.58
4.47
3.35
2.23
1.12
0.00
NOx concentrations (ppbv)
VOC concentrations (ppbv)
Net acetaldehyde production rate (ppbv h-1)
b) Acetaldehyde
0.16
0.20
0.04
0.12
0.08
VOCs/NOx=0.5
0.00
0.24
0.20
0.16
0.12
0.08
0.04
0.00
NOx concentrations (ppbv)
VOC concentrations (ppbv)
Net acetone production rate (ppbv h-1)
c) Acetone
0.11
0.44
0.5
0.33
0.22
VOCs/NOx=0.4
0.00
0.66
0.55
0.44
0.33
0.22
0.11
0.00
NOx concentrations (ppbv)
VOC concentrations (ppbv)
Net O3 production rate (ppbv h-1)
d) Ozone
6.1
0.0
10.1
8.1
4.0
2.0
VOCs/NOx=0.8
0.0
12.10
10.08
8.07
6.05
4.03
2.02
0.00
NOx concentrations (ppbv)
VOC concentrations (ppbv)

(b) Chengdu

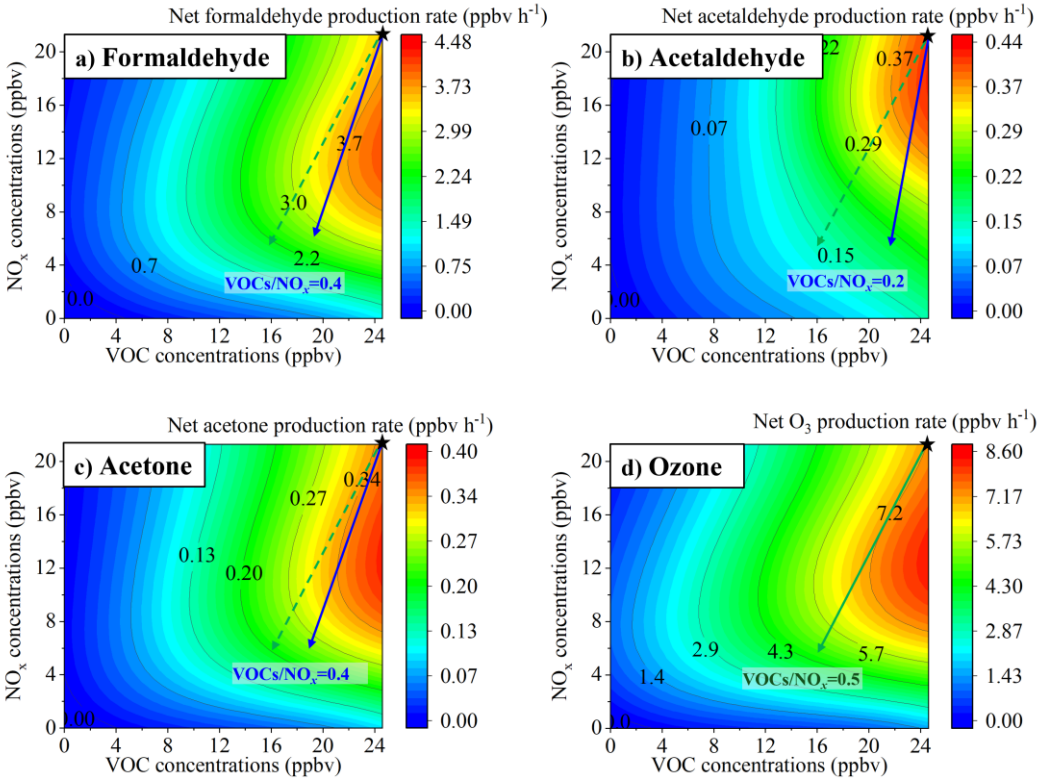

(c) Lanzhou

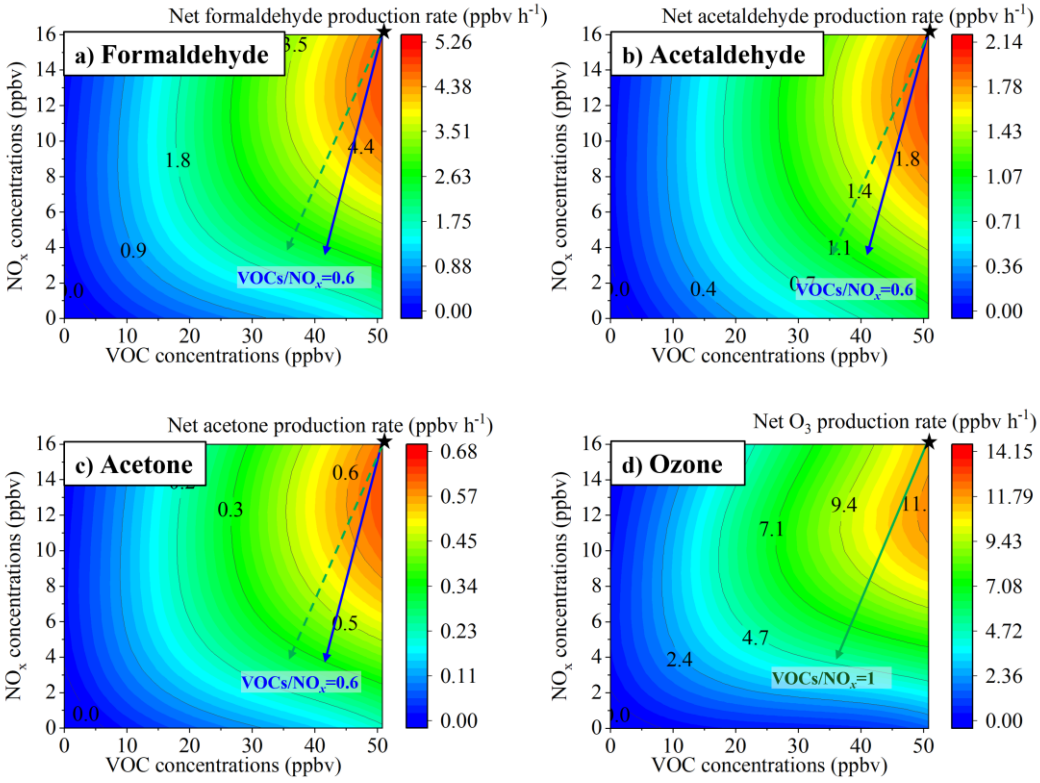

(d) Shanghai

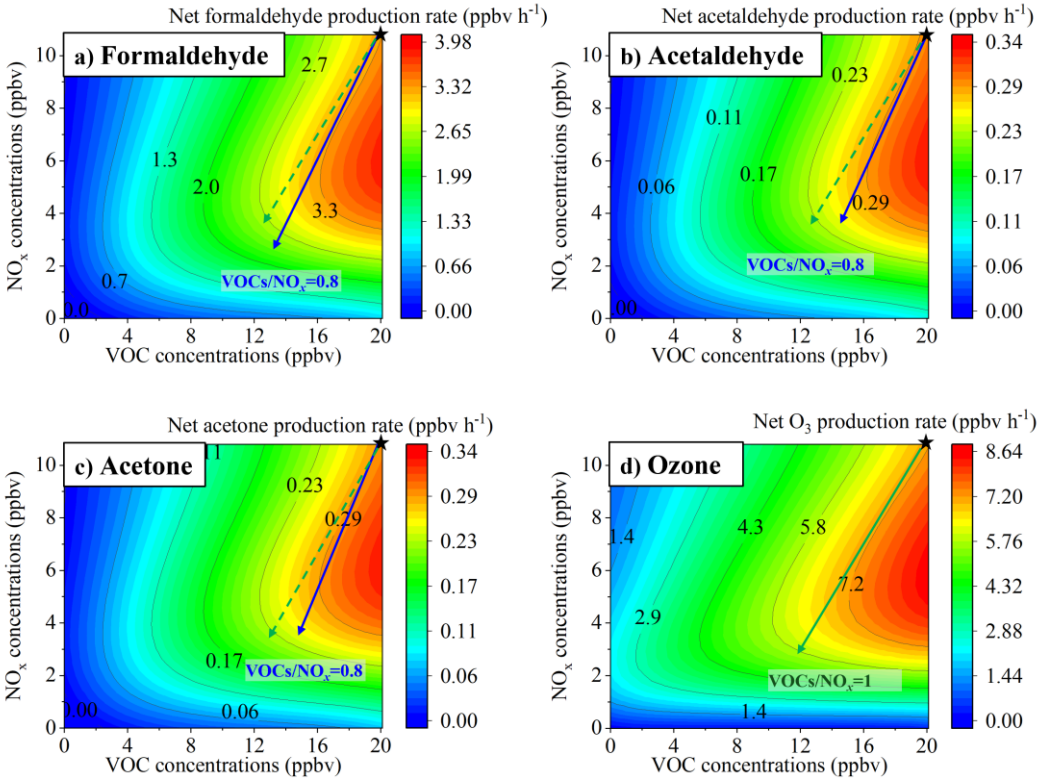

(e) Wuhan

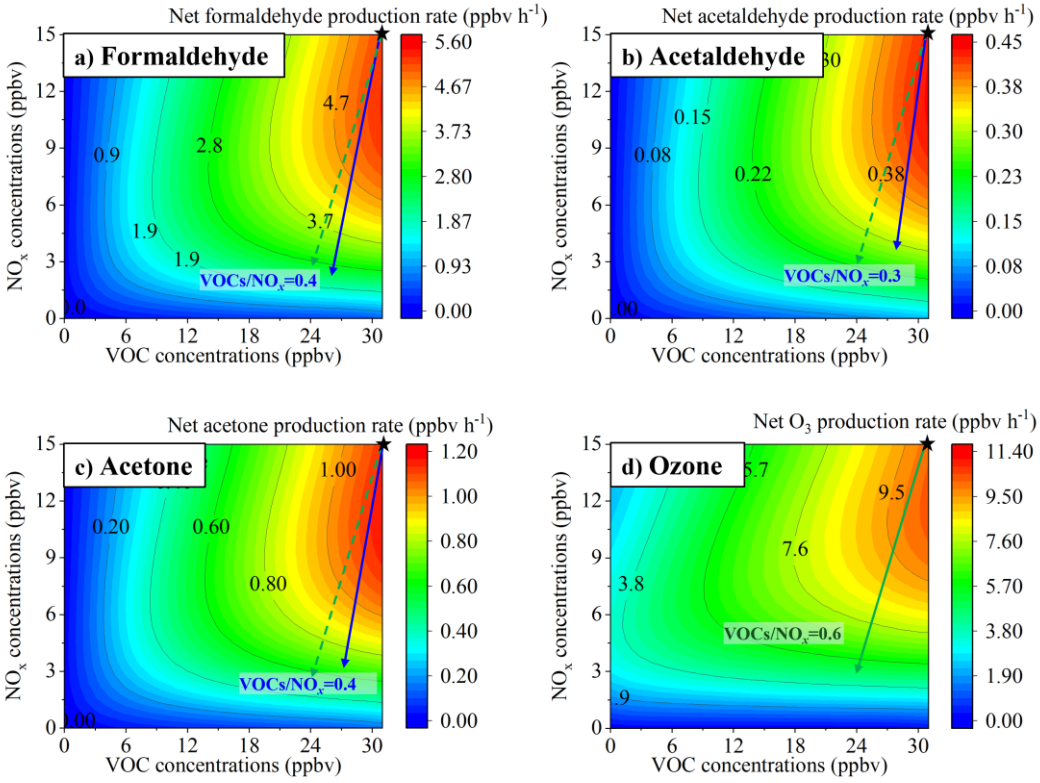

Figure 6.9. Simulated isopleths of a) formaldehyde, b) acetaldehyde, and c) acetone concentrations as a function of VOC and NO_x reduction rates during peak hours (11:00-14:00 LT) in (a) Beijing, (b) Chengdu, (c) Lanzhou, (d) Shanghai and (e) Wuhan. The black star represents the base case, while the purple dashed line indicates the most effective reduction strategy.

6.5.2 Estimation of primary and secondary sources of carbonyls

In the five cities, O_3 and 37 VOC species, including 14 alkanes, 13 alkenes, 1 alkyne, 6 aromatics, and 3 carbonyls, were input to the PMF model for source identification and quantification. The selection of the 37 VOC species and O_3 was based on their abundances and their roles as tracers. The source apportionment analysis using the PMF model identified seven sources, including diesel exhaust, gasoline exhaust, industrial emission, solvent usage, liquefied petroleum gas (LPG) usage, biogenic emission, and secondary formation. The source profiles are presented in Figure 6.10. To minimize uncertainty in the source apportionment results, all samples from Beijing (sample size: 43), Chengdu (42), Lanzhou (40), Shanghai (41), and Wuhan (33) were combined and input into the model for simulations, rather than conducting separate source apportionments for each city. The first factor, characterized by elevated levels of C_2–C_3 hydrocarbons (especially C_2–C_3 alkenes), C_6–C_{10} hydrocarbons, and benzene, was identified as diesel exhaust (X. F. Liu et al., 2021; Lyu et al., 2019). The second factor, marked by significant loadings of *i/n*-pentanes and C_6–C_{10} hydrocarbons, along with moderate amounts of C_2 hydrocarbons, was attributed to gasoline exhaust (Ho, 2009; Ling & Guo, 2014; Liu et al., 2008; Lyu et al., 2019; Wang et al., 2019; Yuan et al., 2024). The third factor, characterized by moderate to high levels of propane and *i/n*-butanes, represented Liquefied Petroleum Gas (LPG) usage (Guo, Ling, Cheung, Wang, et al., 2013; X. F. Liu et al., 2021; Lyu et al., 2019; Lyu et al., 2017). The fourth factor, defined by substantial amounts of 1,3-butadiene and styrene, as well as moderate loadings of ethyne and aromatics, was attributed to industrial emissions (Knighton et al., 2012; X. F. Liu et al., 2021). The fifth factor was associated with solvent usage, indicated by high levels of C_7–C_9 aromatics (Ling & Guo, 2014; Shao et al., 2016). The sixth factor was identified as biogenic emissions, dominated by isoprene and α/β-pinene (Cheng et al., 2018; Qian et al., 2019; Zhou et al., 2019). Finally, the seventh factor was attributed to secondary formation, characterized by high levels of carbonyls and O_3

(Li et al., 2010; Qian et al., 2019; Y. Xu et al., 2023). The source apportionment analysis using the PMF model identified seven sources: diesel exhaust, gasoline exhaust, industrial emissions, solvent usage, LPG usage, biogenic emissions, and secondary formation.

Since both gasoline and diesel exhaust are classified as vehicle emissions, they are considered as a single source in the following discussion. Table 6.8 presents the proportions of formaldehyde, acetaldehyde, and acetone attributed to these sources in five cities, as determined by the PMF model. Overall, formaldehyde and acetaldehyde in Beijing and Chengdu primarily originated from primary emission sources (54 %–67 %), whereas in the other three cities, secondary formation was the dominant source (54 %–66 %). In contrast, the contribution of secondary formation to acetone was less than 50 % in all cities, with primary emissions accounting for the majority (54 %–70 %). According to Table 6.8, formaldehyde and acetaldehyde were predominantly attributed to secondary formation in all five cities, with 5-city average contributions equal to or exceeding 50 %. Among the cities, Wuhan exhibited the highest contribution from secondary formation to formaldehyde (65.5 %), followed by Shanghai (63.2 %) and Lanzhou (55.5 %). In comparison, the proportion of secondary sources for formaldehyde in Beijing (43.8 %) and Chengdu (40.0 %) was slightly lower than the combined contribution from the five primary sources. Among primary sources, solvent usage was the largest contributor to formaldehyde, accounting for 16.5 % in Beijing and 17.6 % in Chengdu. Industrial emissions were notable contributors in Lanzhou (16.4 %), Shanghai (12.4 %), and Beijing (12.9 %). Biogenic emissions contributed approximately 10 % of the formaldehyde in all cities except Lanzhou. The source contributions for acetaldehyde were generally consistent with those for formaldehyde across all cities.

Acetone exhibited a different source distribution compared to the aldehydes. Although secondary formation remained the largest single contributor, its proportion did not exceed 50 % in any city, indicating that acetone is more strongly influenced by primary emissions. Among primary sources, acetone was mainly attributed to solvent usage in Chengdu (27.1 %), Beijing (22.4 %) and Shanghai (17.0 %). In Lanzhou, industrial emissions were the major source (20.1 %), highlighting the significance of local industrial activities for carbonyls. Additionally,

biogenic emissions had a notable impact on acetone in all five cities (averaging around 9 %), which is slightly higher than the contributions observed for the aldehydes.

Additionally, the proportions of primary and secondary sources for each city were compared with previous studies, as shown in Table 6.9. Overall, the findings are generally consistent with values reported in the literature. Table 6.9 presents the relative contributions of primary emissions and secondary formation to formaldehyde, acetaldehyde, and acetone in five cities, and also includes a comparison between the results of this study and those reported in previous literature. In Beijing and Chengdu, primary emissions contributed significantly to formaldehyde, accounting for 46.3 % and 47.8 %, respectively. In contrast, Lanzhou, Shanghai, and Wuhan exhibited higher contributions from secondary sources, at 55.5 %, 63.2 %, and 65.6 %, respectively. The contribution of biogenic emissions to formaldehyde in all cities was approximately 10 % except Lanzhou, which is lower than values reported in previous studies (Huang et al., 2020; C. Wang et al., 2017; Yuan et al., 2012). Acetaldehyde displayed similar primary and secondary source distribution characteristics to formaldehyde across the five cities, while acetone was mainly influenced by primary emissions. The PMF results for formaldehyde in Beijing and Chengdu are consistent with previous studies (Bao et al., 2022; Li et al., 2010; Qian et al., 2019), which also identified primary emissions as significant contributors. Similarly, the substantial contributions from secondary formation in Shanghai and Wuhan align with earlier findings (Wu et al., 2023; Z. Yang et al., 2019), and the importance of secondary sources in Lanzhou, Shanghai, and Wuhan has also been reported at urban sites in Guangzhou and industrial sites in Houston (Friedfeld et al., 2002; Ling et al., 2017). For acetaldehyde and acetone, the dominance of primary sources in Beijing and Chengdu is consistent with previous studies (Bao et al., 2022; Huang et al., 2020; Yuan et al., 2012).

Similar to PMF results, in Beijing and Chengdu, primary emissions by MLR model had higher contribution for formaldehyde and acetaldehyde compared to secondary formation, accounted for 47.5 % to 56.6 %, and Lanzhou, Shanghai and Wuhan were characterized by a higher contribution from secondary formation for formaldehyde and acetaldehyde, from 41.6 % to 64.7 %. In these cities, acetone had more balanced contributions between primary emissions,

secondary formation and background, around 30 %. In summary, carbonyls in Beijing and Chengdu were dominated by primary emissions, and Lanzhou, Shanghai and Wuhan showed higher secondary formation for formaldehyde and acetaldehyde and significant primary source for acetone.

The contributions of individual VOC species to the three carbonyls were quantified using PBM-MCM calculations (see Tables 6.3, 6.5, and 6.6). By combining the proportions of VOC species in various primary sources, as determined by the PMF model (see Figure 6.10), we further estimated the contributions of VOCs from each primary source to carbonyls, thereby enabling source apportionment of VOCs responsible for the secondary formation of carbonyls. It is noted that although the 37 VOC species used for source apportionment are fewer than those included in the MCM, these VOCs accounted for 82–90 % of formaldehyde, 95–98 % of acetaldehyde, and 93–96 % of acetone concentrations, thus largely covering the formation of carbonyl compounds. Figure 6.11 presents the proportions of formaldehyde, acetaldehyde, and acetone attributed to each source, as determined by the combined PMF and PBM-MCM results. When both primary and secondary contributions from each source to carbonyls are considered, vehicle emissions emerge as the dominant source of formaldehyde and acetaldehyde, contributing on average 37 % and 43 %, respectively, across the five cities. This increased contribution from vehicle emissions is primarily due to the high content of short-chain alkenes in this source, which significantly enhances the secondary formation of aldehydes. Propene, as a major precursor of acetaldehyde, further amplifies the contribution of vehicle emissions to acetaldehyde. These findings are consistent with previous understandings of anthropogenic sources of aldehydes and suggest that traffic-related sources should be prioritized in aldehyde control policies.

Additionally, the contributions from industrial emissions and solvent usage were comparable, each accounting for approximately 15–24 % of aldehydes. The increased total contribution from industrial sources is mainly due to the presence of a wide variety of alkenes and alkanes, which significantly contribute to secondary formation. Solvent usage, which is rich in aromatics, primarily enhances the secondary formation of formaldehyde. The contribution

from LPG usage also increased slightly, as the high content of C_3–C_4 alkanes in LPG has a limited effect on secondary formation.

It is also notable that the contribution from biogenic emissions increased significantly for formaldehyde and acetone, reaching 20 % and 27 %, respectively. This indicates that, even in densely populated urban areas, biogenic sources still make a substantial contribution to formaldehyde. For acetone, previous studies have focused primarily on its anthropogenic sources (Guo, Ling, Cheung, Wang, et al., 2013). However, our results highlight the importance of biogenic sources for acetone.

While our study quantifies the separate contributions of anthropogenic and biogenic sources to carbonyl formation, effective mitigation strategies must also consider their critical interaction, especially in urban environments. Recent studies have shown that the interaction between biogenic and anthropogenic emissions can lead to synergistic effects, resulting in higher levels of secondary pollutants than would be expected from either source alone (Gao et al., 2022; Li et al., 2018; Qu et al., 2013). This implies that controlling anthropogenic precursors serves a dual purpose: it not only reduces their direct impact but also mitigates their role in amplifying biogenic contributions. However, reductions in anthropogenic VOC or NO_x emissions may alter the non-linear relationship between secondary pollutants and their precursors. As a result, the synergistic effect on O_3 concentrations, for example, typically becomes more pronounced with decreasing anthropogenic VOC emissions, but tends to weaken with reductions in NO_x emissions (Gao et al., 2022). Therefore, accounting for this complex interaction is essential for designing effective and predictable pollution abatement strategies.

Table 6.8 Proportions of formaldehyde, acetaldehyde, and acetone from different sources in five cities.

City	Industrial emission	LPG usage	Vehicle emission	Solvent usage	Biogenic emission	Secondary formation
			Formaldehyde			
Beijing	12.91 %	7.85 %	9.11 %	16.46 %	9.88 %	43.79 %
Chengdu	5.31 %	9.85 %	15.00 %	17.64 %	12.23 %	39.97 %
Lanzhou	16.42 %	2.44 %	10.94 %	11.48 %	3.27 %	55.45 %
Shanghai	12.43 %	3.10 %	10.49 %	3.33 %	7.41 %	63.24 %
Wuhan	11.98 %	4.65 %	6.74 %	5.09 %	6.00 %	65.54 %
5-city average	**11.61 %**	**5.18 %**	**9.86 %**	**10.00 %**	**7.56 %**	**55.80 %**
			Acetaldehyde			
Beijing	12.71 %	7.27 %	11.53 %	16.43 %	6.15 %	45.91 %
Chengdu	7.30 %	9.01 %	17.72 %	23.18 %	9.28 %	33.51 %
Lanzhou	23.68 %	4.00 %	6.17 %	9.32 %	2.81 %	54.02 %
Shanghai	15.54 %	6.00 %	6.43 %	10.94 %	5.13 %	55.96 %
Wuhan	10.64 %	5.60 %	7.11 %	13.49 %	5.52 %	57.64 %
5-city average	**13.97 %**	**5.98 %**	**9.79 %**	**14.67 %**	**5.78 %**	**49.81 %**
			Acetone			
Beijing	12.81 %	10.85 %	9.61 %	22.40 %	11.90 %	32.43 %

Chengdu	10.51 %	8.97 %	10.47 %	27.12 %	12.13 %	30.80 %
Lanzhou	20.11 %	7.04 %	8.11 %	19.66 %	6.89 %	38.19 %
Shanghai	13.70 %	10.32 %	8.85 %	17.01 %	7.05 %	43.07 %
Wuhan	15.00 %	7.62 %	7.39 %	15.00 %	8.75 %	46.24 %
5-city average	**14.43 %**	**8.96 %**	**8.89 %**	**20.24 %**	**9.34 %**	**38.15 %**

Table 6.9. Proportions of primary emissions, secondary formation, biogenic emission and background of carbonyls in this study and previous studies.

Location	Primary emission	Secondary emission	Biogenic emission	Background	Method	Reference
			Formaldehyde			
Beijing-urban site	46.33 %	43.79 %	9.88 %	/	PMF	This study
Chengdu-urban site	47.80 %	39.97 %	12.23 %	/	PMF	This study
Lanzhou-urban site	41.28 %	55.45 %	3.27 %	/	PMF	This study
Shanghai-urban site	29.35 %	63.24 %	7.41 %	/	PMF	This study
Wuhan-urban site	28.46 %	65.54 %	6.00 %	/	PMF	This study
Beijing-urban site	48.39 %	45.27 %	/	6.34 %	MLR	This study
Chengdu-urban site	49.73 %	40.86 %	/	9.41 %	MLR	This study
Lanzhou-urban site	37.27 %	51.07 %	/	11.67 %	MLR	This study
Shanghai-urban site	30.57 %	53.79 %	/	15.65 %	MLR	This study
Wuhan-urban site	20.60 %	64.71 %	/	14.70 %	MLR	This study
Beijing-urban site	76 %	18 %	/	5 %	MLR	(Li et al., 2010)
Beijing-urban site	48 %	42 %	/	0 %	PMF	(Qian et al., 2019)

Beijing-urban site	22 %	28 %	36 %	15 %	PMF	(Yuan et al., 2012)
Beijing-urban site	10 %	23	42 %	25 %	Photochemical age-based parameterization method	(Huang et al., 2020)
Chengdu-urban site	66 %	34 %	/	0 %	MLR	(Bao et al., 2022)
Shanghai-urban site	30.4 %	56 %	/	12.7 %	MLR	(Wu et al., 2023)
Wuhan-urban site	17.5 %	67.2 %	/	15.2 %	MLR	(Z. Yang et al., 2019)
Nanjing-urban site	69.2 %	13.8 %	/	27.0 %	MLR	(Ma et al., 2016)
Zhejiang-urban site	18.5 %	34.9 %	/	46.7 %	MLR	(Wang et al., 2015)
Zhejiang-rural site	18 %	35 %	/	47 %	MLR	(Wang et al., 2015)
Guangzhou-urban site	47 %	53 %	/	/	PMF	(Ling et al., 2017)
Shenzhen-urban site	9 %	38 %	41 %	11 %	Photochemical age-based parameterization method	(C. Wang et al., 2017)
Tung Chung, Hong Kong -urban site	21.3 ± 8.5 %	30.4 ± 13.1 %	/	48.3 ± 9.4 %	MLR	(Lui et al., 2017)
Yuen Long, Hong Kong -urban site	39.8 ± 12.6 %	36.2 ± 15.8 %	/	24.0 ± 6.7 %	MLR	(Lui et al., 2017)
Hok Tsui, Hong Kong-background site	13.0 ± 7.3 %	52.5 ± 11.3 %	/	34.5 ± 11.3 %	MLR	(Lui et al., 2017)
Mt. Tai-mountain site	22 %	44 %	/	34 %	MLR	(Yang et al., 2017)
Houston-industrial site	36 %	64 %	/	/	MLR	(Friedfeld et al., 2002)

Mexico City-urban site	41 %	38 %	/	21 %	MLR	(Garcia et al., 2006)
			Acetaldehyde			
Beijing-urban site	47.94 %	45.91 %	6.15 %	/	PMF	This study
Chengdu-urban site	57.21 %	33.51 %	9.28 %	/	PMF	This study
Lanzhou-urban site	43.17 %	54.02 %	2.81 %	/	PMF	This study
Shanghai-urban site	38.91 %	55.96 %	5.13 %	/	PMF	This study
Wuhan-urban site	36.84 %	57.64 %	5.52 %	/	PMF	This study
Beijing-urban site	43.87 %	36.12 %	/	20.01 %	MLR	This study
Chengdu-urban site	46.33 %	30.94 %	/	22.73 %	MLR	This study
Lanzhou-urban site	35.12 %	47.60 %	/	17.28 %	MLR	This study
Shanghai-urban site	32.40 %	41.57 %	/	26.03 %	MLR	This study
Wuhan-urban site	30.26 %	50.90 %	/	18.84 %	MLR	This study
Beijing-urban site	46 %	30 %	16 %	8 %	PMF	(Yuan et al., 2012)
Beijing-urban site	13 %	23 %	44 %	20 %	Photochemical age-based parameterization method	(Huang et al., 2020)
Beijing-urban site	16 ± 11 %	48 ± 15 %	13 ± 6 %	22 ± 9 %	Photochemical age-based parameterization method	(Liu et al., 2009)
Chengdu-urban site	76 %	24 %	/	0 %	MLR	(Bao et al., 2022)
Zhejiang-urban site	69 %	23.2 %	/	7.8 %	MLR	(Wang et al., 2015)
Zhejiang-rural site	69 %	23 %	/	8 %	MLR	(Wang et al., 2015)
Hok Tsui, Hong Kong - background site	11.4 ± 0.6 %	27.1 ± 2.9 %	61.5 ± 0.4 %	0	Photochemical age-based	(Lyu et al., 2024)

					parameterization method	
Mt. Tai-mountain site	15 %	85 %	/	/	MLR	(Yang et al., 2017)
New England-urban site	9 %	51 %	13 %	26 %	Photochemical age-based parameterization method	(de Gouw et al., 2005)
			Acetone			
Beijing-urban site	55.67 %	32.43 %	11.90 %	/	PMF	This study
Chengdu-urban site	57.07 %	30.80 %	12.13 %	/	PMF	This study
Lanzhou-urban site	54.92 %	38.19 %	6.89 %	/	PMF	This study
Shanghai-urban site	49.88 %	43.07 %	7.05 %	/	PMF	This study
Wuhan-urban site	45.01 %	46.24 %	8.75 %	/	PMF	This study
Beijing-urban site	34.25 %	31.78 %	/	33.97 %	MLR	This study
Chengdu-urban site	38.64 %	30.91 %	/	30.45 %	MLR	This study
Lanzhou-urban site	34.95 %	32.79 %	/	32.26 %	MLR	This study
Shanghai-urban site	34.46 %	32.03 %	/	33.51 %	MLR	This study
Wuhan-urban site	32.11 %	29.05 %	/	38.84 %	MLR	This study
Beijing-urban site	38 %	5 %	9 %	47 %	PMF	(Yuan et al., 2012)
Beijing-urban site	16 %	18 %	28 %	38 %	Photochemical age-based parameterization method	(Huang et al., 2020)
Beijing-urban site	30 ± 8 %	9 ± 4 %	18 ± 8 %	43 ± 11 %	Photochemical age-based	(Liu et al., 2009)

					parameterization method	
Chengdu-urban site	70 %	30 %	/	0 %	MLR	(Bao et al., 2022)
Zhejiang-urban site	52.9 %	20.3 %	/	26.8 %	MLR	(Wang et al., 2015)
Zhejiang-rural site	53 %	20 %	/	27 %	MLR	(Wang et al., 2015)
Hok Tsui, Hong Kong - background site	17.9 ± 0.7 %	0	54.2 ± 0.4 %	27.9 ± 0.8 %	Photochemical age-based parameterization method	(Lyu et al., 2024)
Mt. Tai-mountain site	13 %	31 %	/	56 %	MLR	(Yang et al., 2017)
New England-urban site	25 %	16 %	13 %	46 %	Photochemical age-based parameterization method	(de Gouw et al., 2005)

(a) all five cities

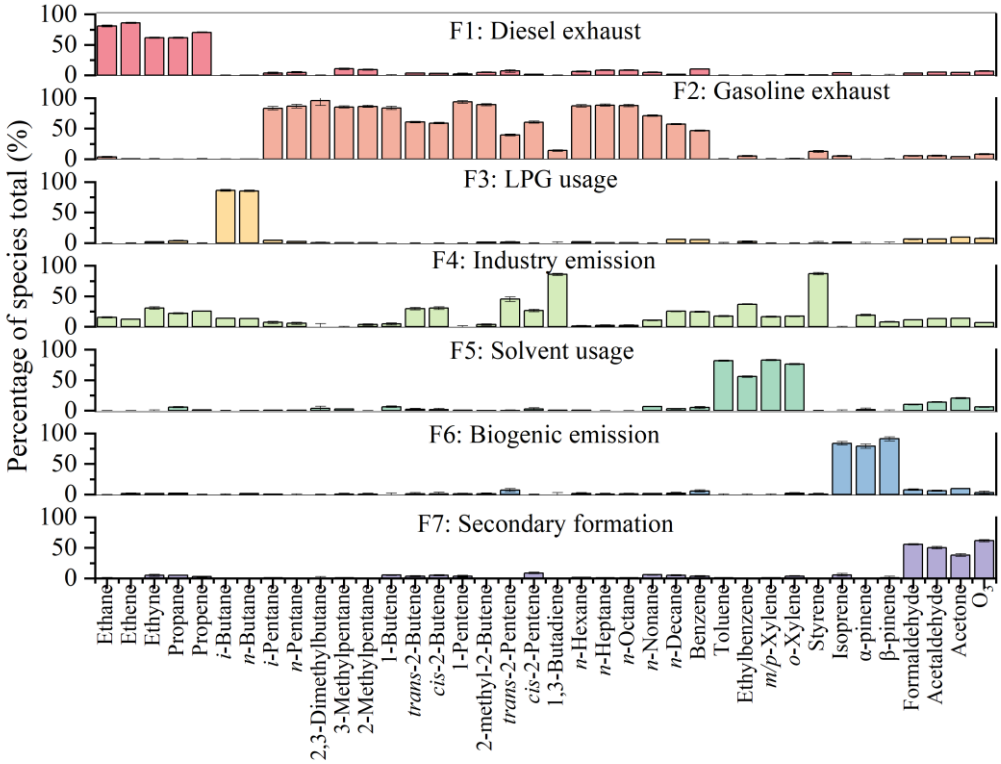

(b) Beijing

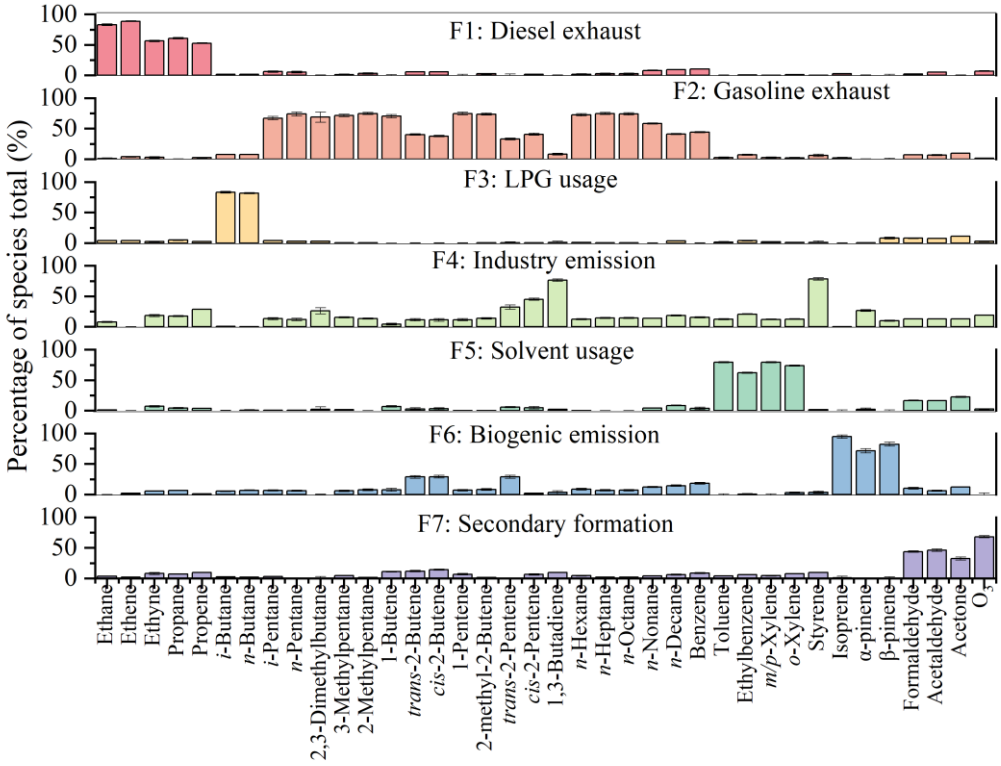

(c) Chengdu

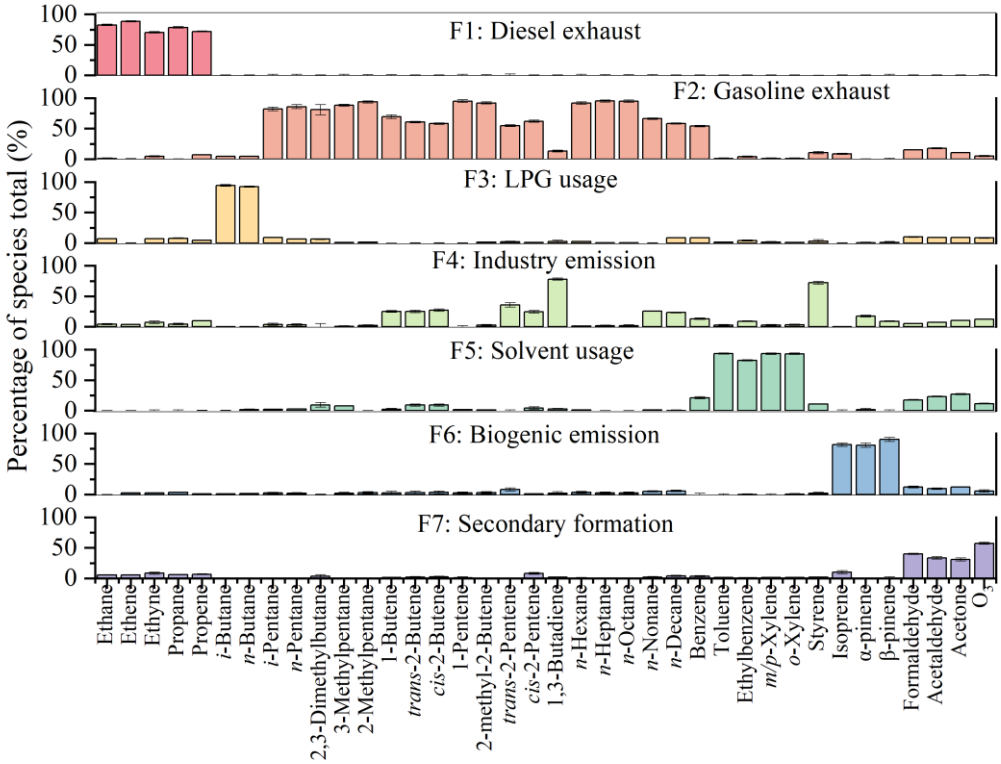
F1: Diesel exhaust
F2: Gasoline exhaust
F3: LPG usage
F4: Industry emission
F5: Solvent usage
F6: Biogenic emission
F7: Secondary formation
Percentage of species total (%)
100
50
0
Ethane
Ethene
Ethyne
Propane
Propene
i-Butane
n-Butane
i-Pentane
n-Pentane
2,3-Dimethylbutane
3-Methylpentane
2-Methylpentane
1-Butene
trans-2-Butene
cis-2-Butene
1-Pentene
2-methyl-2-Butene
trans-2-Pentene
cis-2-Pentene
1,3-Butadiene
n-Hexane
n-Heptane
n-Octane
n-Nonane
n-Decane
Benzene
Toluene
Ethylbenzene
m/p-Xylene
o-Xylene
Styrene
Isoprene
α-pinene
β-pinene
Formaldehyde
Acetaldehyde
Acetone
O3

(d) Lanzhou

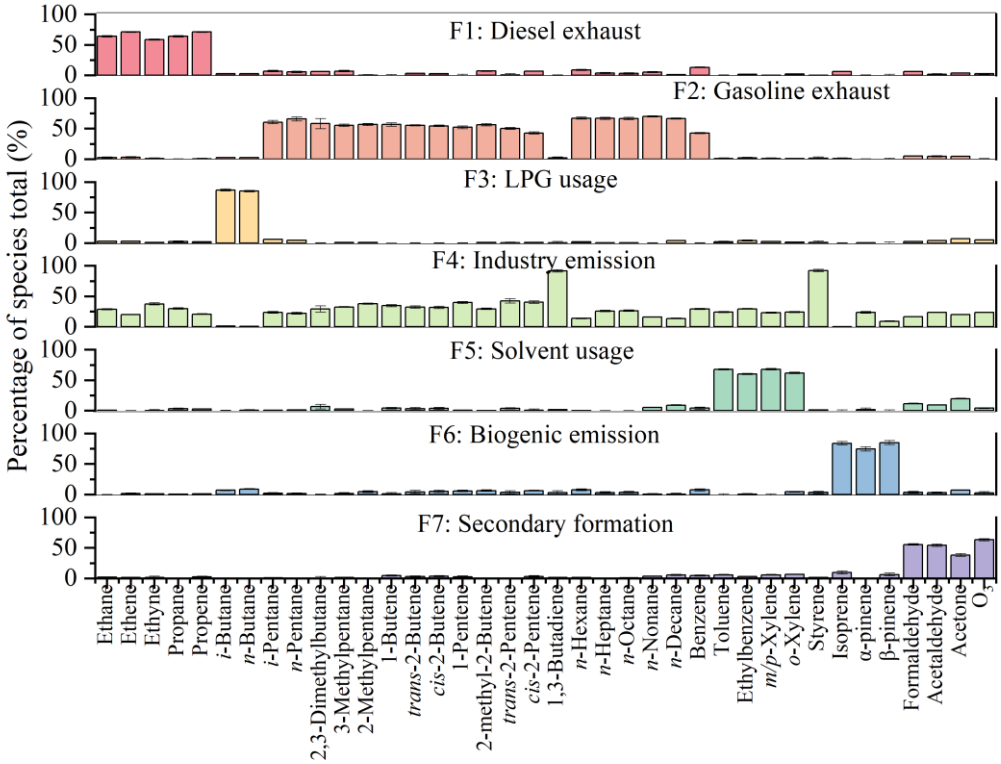

(e) Shanghai

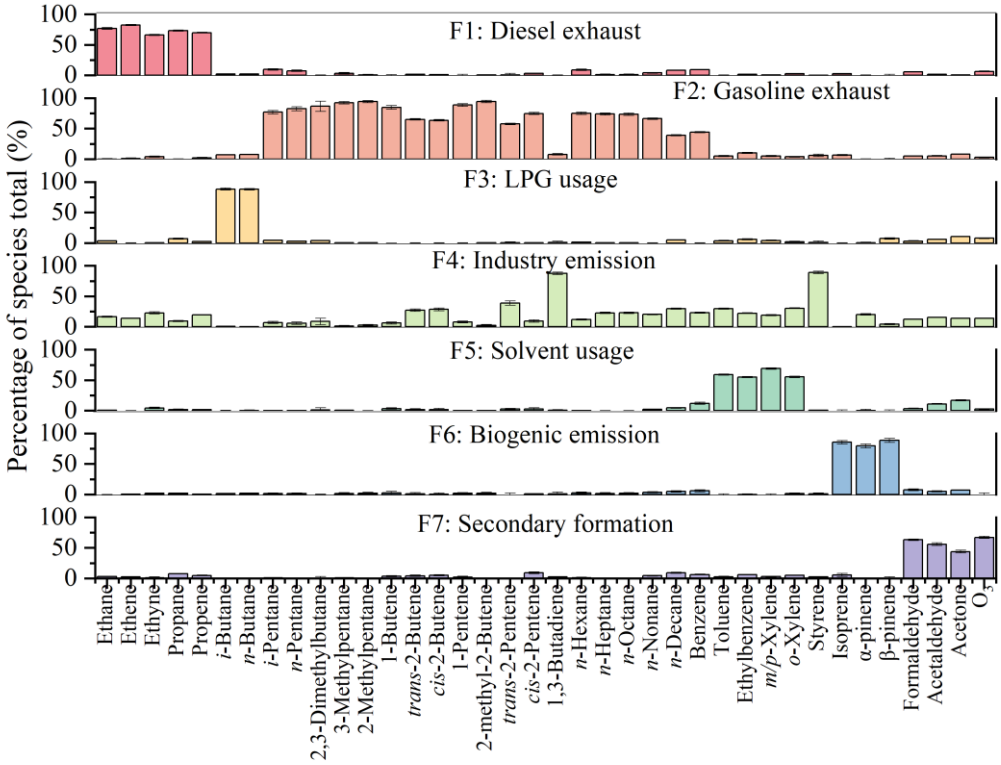

(f) Wuhan

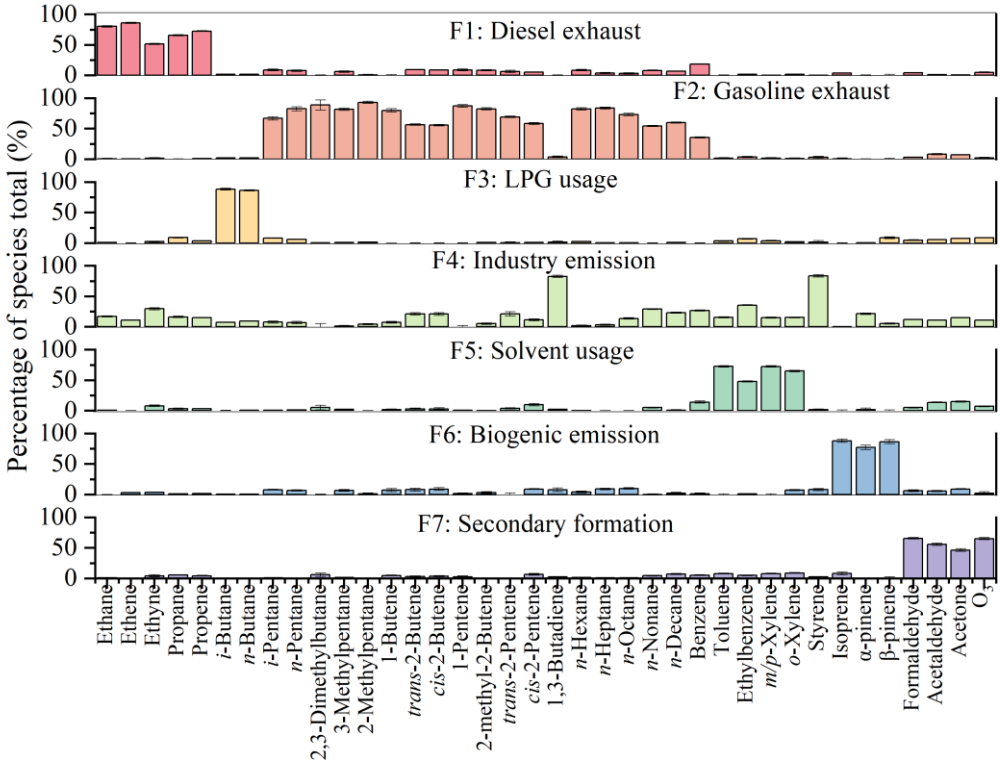

Figure 6.10. Average profile of the seven sources in (a) all five cities, (b) Beijing, (c) Chengdu, (d) Lanzhou, (e) Shanghai, (f) Wuhan extracted from PMF.

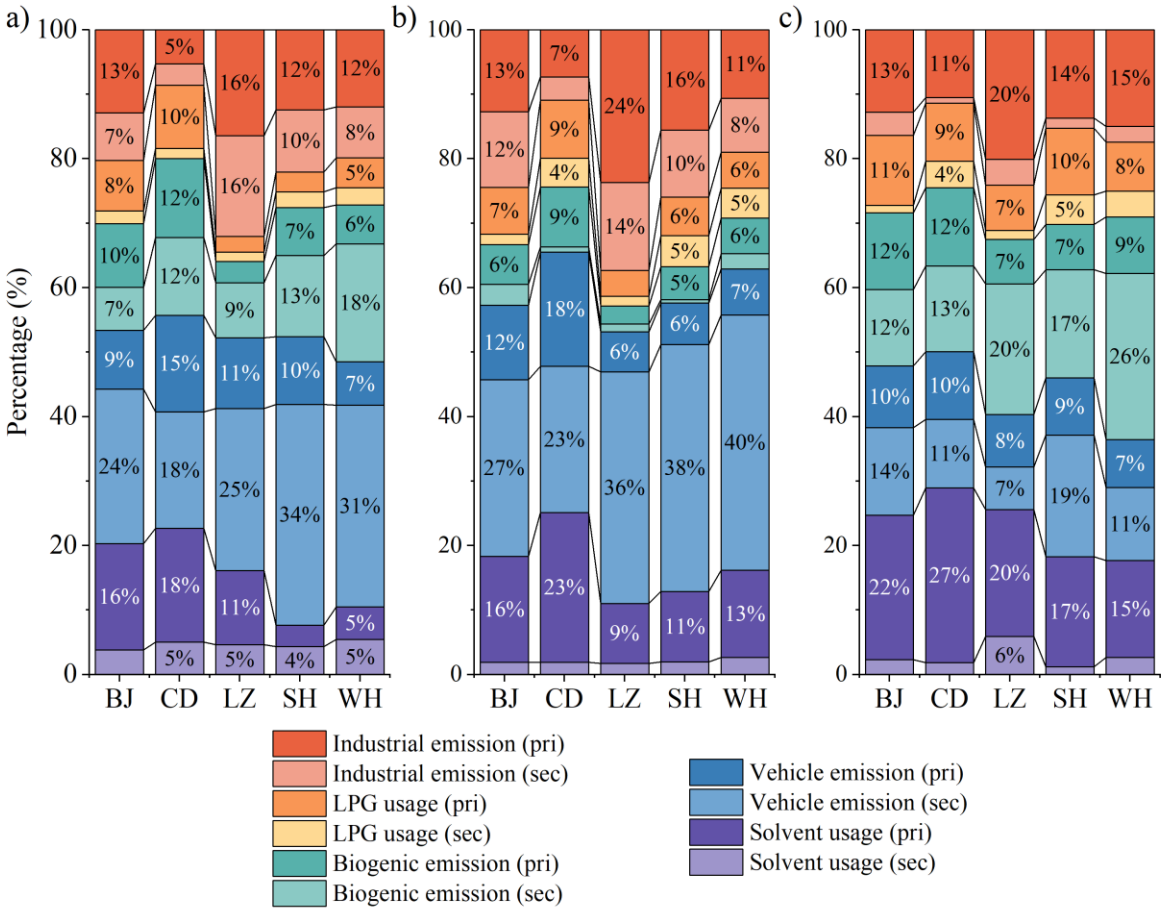

Figure 6.11. Contribution of primary and secondary sources to a) formaldehyde, b) acetaldehyde, and c) acetone in five cities.

6.6 Summary

This study investigated the formation mechanisms, sources, and atmospheric impacts of formaldehyde, acetaldehyde, and acetone in five Chinese cities by combining modeling and observational approaches. Although the data used are based on sampling conducted in 2018, the findings remain broadly relevant and provide valuable reference for understanding secondary pollution in China and other developing countries or regions. First, it is important to note that secondary O_3 pollution remains a significant challenge in China (Bao et al., 2022; Bao et al., 2025; Y. Li et al., 2023; Sun et al., 2023). Unlike primary particulate pollution, which is mainly driven by direct emissions and can be effectively controlled through emission reduction measures, secondary pollution is characterized by complex nonlinear relationships between secondary pollutants and their precursors. As a result, even when precursor emissions are reduced, the formation of secondary pollutants can persist.

While substantial progress has been made in reducing NO_x emissions in recent years, the reduction in VOC emissions has not kept pace, and the overall VOC concentration levels and speciation profiles have shown relatively minor changes (K. Li et al., 2019; Wu et al., 2022). As a result, the NO_x/VOC ratio has shifted, which can influence the efficiency of O_3 and secondary carbonyl formation, but the relative contributions of different VOC species and their chemical pathways remain largely consistent. Our study findings on the VOC contributions and chemical formation pathways of carbonyls therefore remain highly relevant. The detailed understanding of VOC oxidation to carbonyl formation, as elucidated in this study, continues to provide a scientific basis for targeted control strategies. Changes in the NO_x/VOC ratio can be further evaluated using isopleth diagrams to guide current and future management scenarios (Guo et al., 2023; Hua et al., 2024; L. Li et al., 2023).

Moreover, while the proportions of specific sources may have shifted over time, our multi-city comparison provides a valuable database of source contribution ranges that can serve as a reference for current and future research. These quantitative source profiles can inform policymakers about the likely impacts of changes in source composition and help prioritize control measures as emission patterns evolve. In summary, despite recent changes in emission

sources, our study insights into the chemical mechanisms and source contributions to carbonyl formation remain applicable and the isopleth can be adapted to current conditions for scenario analysis.

In summary, this study advances the understanding of carbonyl photochemistry and its relationship with O_3 pollution, providing a scientific basis for the development of more effective air pollution control strategies in China.

Chapter 7 Conclusions and suggestions for future study

7.1 Conclusions

This thesis addresses these issues through three main studies: (1) investigating the mechanisms of wintertime O_3 formation in Lanzhou, (2) analyzing long-term O_3 trends in Lanzhou, and (3) exploring the formation mechanisms and sources of secondary carbonyls across five major Chinese cities. Beyond summarizing the findings from these three research components, this work also provides new insights into the broader implications for air quality management and scientific understanding of O_3 and carbonyl pollution in China. The main findings are as follows:

1) Wintertime O_3 formation in Lanzhou

Field measurements conducted in Lanzhou during winter revealed that O_3 concentrations can reach exceptionally high levels, even under cold and low-light conditions. The results indicated that substantial emissions of alkenes from the petrochemical industry react with O_3 to form Criegee intermediates, generating significant amounts of RO_x radicals and thereby accelerating O3 production. Four alkenes, *trans/cis*-2-butene, propene, ethene, and *trans/cis*-2-pentene, were found to contribute over 80 % of O_3 formation. The study demonstrated that temperature changes had the minimal effect on alkene ozonolysis, which could proceed even in the absence of sunlight. These findings challenge the traditional view that strong solar radiation is necessary for high O_3 production and underscore the importance of dark reactions in wintertime photochemistry. The results also suggest that alkene ozonolysis can serve as a major source, rather than a sink, of O_3 in heavily industrialized regions. These results not only advance the mechanistic understanding of wintertime O_3 formation but also highlight the need to consider non-traditional photochemical pathways in air quality models and control strategies, especially for cities with significant petrochemical activity.

2) Long-term O_3 trends and radical chemistry in Lanzhou

This study systematically examined the long-term trends, chemical mechanisms, and source contributions of O_3 pollution in Lanzhou from 2013 to 2023, focusing on the summertime.

Results showed that, despite significant declines in $M_{2.5}$, CO, SO_2, and NO_2 due to emission controls, O_3 concentrations continued to rise, highlighting persistent O_3 pollution. While NO_2 and CO decreased steadily, VOC control was less effective. Model simulations revealed a shift from a VOC-limited to a VOC-NO_x co-limited regime, mainly due to NO_x reductions. Alkenes, especially ethene, propene, and *trans/cis*-2-butene, were the main VOC contributors, with vehicle emissions, petrochemical industry, and solvent use as key sources. These findings underscore the need for integrated O_3 control strategies targeting both NO_x and VOCs. **T**hese findings provide a scientific basis for refining O_3 pollution control policies in Lanzhou and may inform similar strategies in other cities facing persistent O_3 challenges. Moreover, the observed regime shift underscores the importance of dynamic, region-specific control strategies that adapt to changing precursor emission patterns and photochemical environments.

3) Photochemical characteristics and sources of carbonyls in five cities in China

The study also examined the formation mechanisms, sources, and atmospheric impacts of formaldehyde, acetaldehyde, and acetone in five Chinese megacities, including Lanzhou. These three carbonyls accounted for over 85 % of the total observed carbonyls, with the highest concentrations detected in Beijing and Wuhan. The main VOC precursors for carbonyl formation varied by city. In Lanzhou, alkenes were the dominant precursors, particularly for formaldehyde and acetaldehyde. In Beijing and Wuhan, vehicle-related alkenes such as propene played a key role, while in Chengdu, isoprene was especially important. The contribution of carbonyls to O_3 formation ranged from 6 % to 33 % across the cities. The study found that the VOC/NO_x reduction ratios required for effective carbonyl control were consistently lower than those for O_3, suggesting that current O_3 mitigation strategies can also help reduce carbonyl pollution. Both primary and secondary sources contributed to carbonyl levels, with vehicle emissions, industrial activities, solvent use, and biogenic sources all playing significant roles. These results emphasize the complexity of secondary pollution in urban China and demonstrate the value of coordinated control strategies that target both O_3 and carbonyls. The multi-city comparison also reveals regional differences in precursor sources and

photochemical regimes, providing important guidance for the design of tailored air quality management policies.

In summary, by integrating field measurements with advanced modelling, this work not only elucidates the chemical processes, temporal variations, long-term trends, and source contributions of VOC-driven O_3 pollution in northwestern Chinese industrial cities but also provides critical scientific evidence to support the development of more effective, regionally adaptive air quality management strategies. The findings contribute to a deeper understanding of the evolving challenges of O_3 and carbonyl pollution in China, and offer practical insights for policymakers seeking to achieve sustained improvements in urban air quality.

7.2 Suggestions for future study

Although this work has addressed several key questions regarding O_3 and carbonyl photochemistry, many areas remain that warrant further investigation. The following recommendations are proposed:

1) Long-term and multi-seasonal observations

The field campaigns in this study were limited in both duration and seasonal coverage. Future research should incorporate long-term, year-round measurements in Lanzhou and other major Chinese cities to more accurately capture seasonal and inter-annual variations in O_3 and carbonyl pollution. Additionally, expanding the study to include a broader range of cities, particularly those with diverse industrial activities and meteorological conditions, would improve the generalizability of the findings.

2) Regional and functional area comparisons

Future studies should examine the differences in O_3 and carbonyl formation mechanisms across various land-use types, such as industrial, residential, and traffic-dominated areas. Additionally, greater emphasis should be placed on understanding the regional impacts of VOCs and other precursors on O_3 and carbonyl formation.

3) Expansion of research on carbonyls and radical chemistry

This study primarily focused on a limited number of major carbonyls. Future research should include a broader spectrum of carbonyls, investigating both their primary and secondary sources, as well as their roles in O_3 production and radical chemistry.

By addressing these areas, future studies can further advance our understanding of O_3 and carbonyl pollution, thereby supporting the development of more effective air quality management strategies in China and beyond.

References

Acker, K., Möller, D., Wieprecht, W., Meixner, F. X., Bohn, B., Gilge, S.,…Berresheim, H. (2006). Strong daytime production of OH from HNO2 at a rural mountain site. *Geophysical Research Letters*, *33*(2). https://doi.org/10.1029/2005gl024643

Adame, J. A., & Sole, J. G. (2013). Surface ozone variations at a rural area in the northeast of the Iberian Peninsula. *Atmospheric Pollution Research*, *4*(2), 130-141. https://doi.org/10.5094/apr.2013.013

Ainsworth, E. A., Yendrek, C. R., Sitch, S., Collins, W. J., & Emberson, L. D. (2012). The Effects of Tropospheric Ozone on Net Primary Productivity and Implications for Climate Change. *Annual Review of Plant Biology, Vol 63*, *63*, 637-661. https://doi.org/10.1146/annurev-arplant-042110-103829

Alam, M. S., Rickard, A. R., Camredon, M., Wyche, K. P., Carr, T., Hornsby, K. E.,…Bloss, W. J. (2013). Radical product yields from the ozonolysis of short chain alkenes under atmospheric boundary layer conditions. *J Phys Chem A*, *117*(47), 12468-12483. https://doi.org/10.1021/jp408745h

Anderson, D. C., Nicely, J. M., Wolfe, G. M., Hanisco, T. F., Salawitch, R. J., Canty, T. P.,…Zeng, G. (2017). Formaldehyde in the Tropical Western Pacific: Chemical sources and sinks, convective transport, and representation in CAM-Chem and the CCMI models. *J Geophys Res Atmos*, *122*(20), 11201-11226. https://doi.org/10.1002/2016JD026121

Ariya, P. A., Sander, R., & Crutzen, P. J. (2000). Significance of HOx and peroxides production due to alkene ozonolysis during fall and winter: A modeling study. *Journal of Geophysical Research: Atmospheres*, *105*(D14), 17721-17738. https://doi.org/10.1029/2000jd900074

Ashmore, M. R. (2005). Assessing the future global impacts of ozone on vegetation. *Plant Cell and Environment*, *28*(8), 949-964. https://doi.org/10.1111/j.1365-3040.2005.01341.x

Atkinson, R. (2000). Atmospheric chemistry of VOCs and NOx. *Atmospheric Environment*, *34*(12-14), 2063-2101. https://doi.org/Doi 10.1016/S1352-2310(99)00460-4

Atkinson, R., Baulch, D. L., Cox, R. A., Crowley, J. N., Hampson, R. F., Hynes, R. G.,…Subcommittee, I. U. P. A. C. (2006). Evaluated kinetic and photochemical data for atmospheric chemistry: Volume II – gas phase reactions of organic species. *Atmos. Chem. Phys.*, *6*, 3625–4055.

Bao, J., Li, H., Wu, Z., Zhang, X., Zhang, H., Li, Y.,…Deng, L. (2022). Atmospheric carbonyls in a heavy ozone pollution episode at a metropolis in Southwest China: Characteristics, health risk assessment, sources analysis. *J Environ Sci (China)*, *113*, 40-54. https://doi.org/10.1016/j.jes.2021.05.029

Bao, J., Zhang, X., Wu, Z., Zhou, L., Qian, J., Tan, Q.,…Li, H. (2025). Atmospheric carbonyl compounds are crucial in regional ozone heavy pollution: insights from the Chengdu Plain Urban Agglomeration, China. *Atmospheric Chemistry and Physics*, *25*(3), 1899-1916. https://doi.org/10.5194/acp-25-1899-2025

Belan, B. D., & Savkin, D. E. (2019). The Role of Air Humidity in Variations in Near-Surface Ozone Concentration. *Atmospheric and Oceanic Optics*, *32*(5), 586-589. https://doi.org/10.1134/s1024856019050038

Bloomer, B. J., Stehr, J. W., Piety, C. A., Salawitch, R. J., & Dickerson, R. R. (2009). Observed relationships of ozone air pollution with temperature and emissions. *Geophysical Research Letters*, *36*(9). https://doi.org/10.1029/2009gl037308

Bureau, L. E. P. B. a. L. S. (2018). *Environmental Status Report of Lanzhou in 2017*. https://sthjj.lanzhou.gov.cn/art/2018/6/4/art_5758_480201.html

Cape, J. N. (2008). Surface ozone concentrations and ecosystem health: past trends and a guide to future projections. *Science of the Total Environment*, *400*(1-3), 257-269. https://doi.org/10.1016/j.scitotenv.2008.06.025

Cardelino, C. A., & Chameides, W. L. (1995). An observation-based model for analyzing ozone precursor relationships in the urban atmosphere. *J Air Waste Manag Assoc*, *45*(3), 161-180. https://doi.org/10.1080/10473289.1995.10467356

Carter, W. P. (1994). Development of ozone reactivity scales for volatile organic compounds. *Air & waste*, *44(7)*, 881-899.

Carter, W. P. (2000). *Implementation of the SAPRC-99 chemical mechanism into the Models-3 framework*.

Carter, W. P. (2010). Development of the SAPRC-07 chemical mechanism. *Atmospheric Environment*, *44*, 5324-5335.

Chameides, W. L., & Walker, J. C. (1973). A photochemical theory of tropospheric ozone. *Journal of Geophysical Research*, *78(36)*, 8751–8760.

Chameides, W. L., Yu, H., Liu, S. C., Bergin, M., Zhou, X., Mearns, L.,…Giorgi, F. (1999). Case study of the effects of atmospheric aerosols and regional haze on agriculture: An opportunity to enhance crop yields in China through emission controls? *Proceedings of the National Academy of Sciences of the United States of America*, *96*(24), 13626-13633. https://doi.org/10.1073/pnas.96.24.13626

Chang, K. L., Petropavlovskikh, I., Cooper, O. R., Schultz, M. G., Wang, T., Helmig, D., & Lewis, A. (2017). Regional trend analysis of surface ozone observations from monitoring networks in eastern North America, Europe and East Asia. *Elementa: Science of the Anthropocene*, *5*, 50.

Chen, S., Wang, H., Lu, K., Zeng, L., Hu, M., & Zhang, Y. (2020). The trend of surface ozone in Beijing from 2013 to 2019: Indications of the persisting strong atmospheric oxidation capacity. *Atmospheric Environment*, *242*. https://doi.org/10.1016/j.atmosenv.2020.117801

Chen, S. Y., Zhang, Q., McLellan, B., & Zhang, T. T. (2020). Review on the petroleum market in China: history, challenges and prospects. *Petroleum Science*, *17*(6), 1779-1794. https://doi.org/10.1007/s12182-020-00501-6

Chen, T., Xue, L., Zheng, P., Zhang, Y., Liu, Y., Sun, J.,…Wang, W. (2020). Volatile organic compounds and ozone air pollution in an oil production region in northern China. *Atmospheric Chemistry and Physics*, *20*(11), 7069-7086. https://doi.org/10.5194/acp-20-7069-2020

Chen, T., Zheng, P., Zhang, Y., Dong, C., Han, G., Li, H.,…Xue, L. (2022). Characteristics and formation mechanisms of atmospheric carbonyls in an oilfield region of northern

China. *Atmospheric Environment*, *274*. https://doi.org/10.1016/j.atmosenv.2022.118958

Chen, X., Wang, H., Liu, Y., Su, R., Wang, H., Lou, S., & Lu, K. (2019). Spatial characteristics of the nighttime oxidation capacity in the Yangtze River Delta, China. *Atmospheric Environment*, *208*, 150-157. https://doi.org/10.1016/j.atmosenv.2019.04.012

Chen, Z., Zhuang, Y., Xie, X., Chen, D., Cheng, N., Yang, L., & Li, R. (2019). Understanding long-term variations of meteorological influences on ground ozone concentrations in Beijing During 2006-2016. *Environmental Pollution*, *245*, 29-37. https://doi.org/10.1016/j.envpol.2018.10.117

Cheng, H., Guo, H., Wang, X., Saunders, S. M., Lam, S. H., Jiang, F.,…Ho, K. F. (2010). On the relationship between ozone and its precursors in the Pearl River Delta: application of an observation-based model (OBM). *Environ Sci Pollut Res Int*, *17*(3), 547-560. https://doi.org/10.1007/s11356-009-0247-9

Cheng, N., Jing, D., Gu, Z., Cai, X., Shi, Z., Li, S.,…Wang, Q. (2024). Observation-Based Ozone Formation Rules by Gradient Boosting Decision Trees Model in Typical Chemical Industrial Parks. *Atmosphere*, *15*(5). https://doi.org/10.3390/atmos15050600

Cheng, X., Li, H., Zhang, Y., Li, Y., Zhang, W., Wang, X.,…Lv, J. (2018). Atmospheric isoprene and monoterpenes in a typical urban area of Beijing: Pollution characterization, chemical reactivity and source identification. *J Environ Sci (China)*, *71*, 150-167. https://doi.org/10.1016/j.jes.2017.12.017

Chu, B., Ma, Q., Liu, J., Ma, J., Zhang, P., Chen, T.,…He, H. (2020). Air Pollutant Correlations in China: Secondary Air Pollutant Responses to NOx and SO2 Control. *Environmental Science & Technology Letters*, *7*(10), 695-700. https://doi.org/10.1021/acs.estlett.0c00403

Collins, W. J. (2003). Effect of stratosphere-troposphere exchange on the future tropospheric ozone trend. *Journal of Geophysical Research*, *108*(D12). https://doi.org/10.1029/2002jd002617

Colman, J. J., Swanson, A. L., Meinardi, S., Sive, B. C., Blake, D. R., & Rowland, F. S. (2001). Description of the analysis of a wide range of volatile organic compounds in whole air samples collected during PEM-Tropics A and B. *Anal. Chem.*, *73*, 3723-3731.

Crutzen, P. J. (1974). Photochemical reactions initiated by and influencing ozone in the unpolluted troposphere. *Tellus*, *26*, 47–57.

Cui, C., Zhu, Y., Yan, X., Zhang, X., Zhao, M., Mu, J.,…Li, H. (2025). Rapid formation of acetaldehyde and its influence on ozone formation in a petrochemical industrialized region. *J Environ Sci (China)*, *157*, 134-147. https://doi.org/10.1016/j.jes.2025.01.027

Cui, M., An, X., Xing, L., Li, G., Tang, G., He, J.,…Zhao, S. (2021). Simulated Sensitivity of Ozone Generation to Precursors in Beijing during a High O3 Episode. *Advances in Atmospheric Sciences*, *38*(7), 1223-1237. https://doi.org/10.1007/s00376-021-0270-4

Curtis, L., Rea, W., Smith-Willis, P., Fenyves, E., & Pan, Y. (2006). Adverse health effects of outdoor air pollutants. *Environ Int*, *32*(6), 815-830. https://doi.org/10.1016/j.envint.2006.03.012

Czader, B. H., Rappenglück, B., Percell, P., Byun, D. W., Ngan, F., & Kim, S. (2012). Modeling nitrous acid and its impact on ozone and hydroxyl radical during the Texas

Air Quality Study 2006. *Atmospheric Chemistry and Physics*, *12*(15), 6939-6951. https://doi.org/10.5194/acp-12-6939-2012

Dai, J., Zhang, K., Feng, Y., Yi, X., Li, R., Xue, J.,…Li, L. (2025). Significant influence of oxygenated volatile organic compounds on atmospheric chemistry: a case study in a typical industrial city in China. *Atmospheric Chemistry and Physics*, *25*(13), 7467-7484. https://doi.org/10.5194/acp-25-7467-2025

Dai, T., Wang, W., Ren, L., Chen, J., & Liu, H. (2010). Emissions of non-methane hydrocarbons from cars in China. *Science China Chemistry*, *53*(1), 263-272. https://doi.org/10.1007/s11426-010-0002-6

de Gouw, J. A., Middlebrook, A. M., Warneke, C., Goldan, P. D., Kuster, W. C., Roberts, J. M.,…Bates, T. S. (2005). Budget of organic carbon in a polluted atmosphere: Results from the New England Air Quality Study in 2002. *Journal of Geophysical Research: Atmospheres*, *110*(D16). https://doi.org/10.1029/2004jd005623

Ding, A. J., Fu, C. B., Yang, X. Q., Sun, J. N., Zheng, L. F., Xie, Y. N.,…Kulmala, M. (2013). Ozone and fine particle in the western Yangtze River Delta: an overview of 1 yr data at the SORPES station. *Atmospheric Chemistry and Physics*, *13*(11), 5813-5830. https://doi.org/10.5194/acp-13-5813-2013

Ding, A. J., Wang, T., Thouret, V., Cammas, J. P., & Nédélec, P. (2008). Tropospheric ozone climatology over Beijing: analysis of aircraft data from the MOZAIC program. *Atmospheric Chemistry and Physics*, *8(1)*, 1-13.

Dodge, M. C. (1977). *Combined use of modeling techniques and smog chamber data to derive ozone-precursor relationships.* (Vol. II). U.S. Environmental Protection Agency

Dong, J., Liu, Y., & Bao, H. (2021). Revalue associations of short-term exposure to air pollution with respiratory hospital admissions in Lanzhou, China after the control and treatment of current pollution. *Int J Hyg Environ Health*, *231*, 113658. https://doi.org/10.1016/j.ijheh.2020.113658

Du, T., Wang, M., Guan, X., Zhang, M., Zeng, H., Chang, Y.,…Tang, C. (2020). Characteristics and Formation Mechanisms of Winter Particulate Pollution in Lanzhou, Northwest China. *Journal of Geophysical Research: Atmospheres*, *125*(18). https://doi.org/10.1029/2020jd033369

Duan, J., Tan, J., Yang, L., Wu, S., & Hao, J. (2008). Concentration, sources and ozone formation potential of volatile organic compounds (VOCs) during ozone episode in Beijing. *Atmospheric Research*, *88*(1), 25-35. https://doi.org/10.1016/j.atmosres.2007.09.004

Edwards, P. M., Brown, S. S., Roberts, J. M., Ahmadov, R., Banta, R. M., deGouw, J. A.,…Zamora, R. (2014). High winter ozone pollution from carbonyl photolysis in an oil and gas basin. *Nature*, *514*(7522), 351-354. https://doi.org/10.1038/nature13767

Emberson, L. (2020). Effects of ozone on agriculture, forests and grasslands. *Philos Trans A Math Phys Eng Sci*, *378*(2183), 20190327. https://doi.org/10.1098/rsta.2019.0327

Emmerson, K. M., Carslaw, N., & Pilling, M. J. (2005). Urban Atmospheric Chemistry During the PUMA Campaign 2: Radical Budgets for OH, HO2 and RO2. *Journal of Atmospheric Chemistry*, *52*(2), 165-183. https://doi.org/10.1007/s10874-005-1323-2

Feister, U., & Warmbt, W. G. (1987). Long-term measurements of surface ozone in the German Democratic Republic. *J. Atmospheric Chemistry*, *5*, 1–21.

Feng, Z., Hu, E., Wang, X., Jiang, L., & Liu, X. (2015). Ground-level O3 pollution and its impacts on food crops in China: a review. *Environmental Pollution*, *199*, 42-48. https://doi.org/10.1016/j.envpol.2015.01.016

Field, R. A., Soltis, J., McCarthy, M. C., Murphy, S., & Montague, D. C. (2015). Influence of oil and gas field operations on spatial and temporal distributions of atmospheric non-methane hydrocarbons and their effect on ozone formation in winter. *Atmospheric Chemistry and Physics*, *15*(6), 3527-3542. https://doi.org/10.5194/acp-15-3527-2015

Filonchyk, M., & Yan, H. (2018). The characteristics of air pollutants during different seasons in the urban area of Lanzhou, Northwest China. *Environmental Earth Sciences*, *77*(22). https://doi.org/10.1007/s12665-018-7925-1

Friedfeld, S., Fraser, M., Ensor, K., Tribble, S., Rehle, D., Leleux, D., & Tittel, F. (2002). Statistical analysis of primary and secondary atmospheric formaldehyde. *Atmospheric Environment*, *36(30)*. https://doi.org/10.1016/S1352-2310(02)00558-7

Fu, X., Wang, T., Gao, J., Wang, P., Liu, Y., Wang, S.,…Xue, L. (2020). Persistent Heavy Winter Nitrate Pollution Driven by Increased Photochemical Oxidants in Northern China. *Environ Sci Technol*, *54*(7), 3881-3889. https://doi.org/10.1021/acs.est.9b07248

Fu, Y., Liao, H., & Yang, Y. (2019). Interannual and Decadal Changes in Tropospheric Ozone in China and the Associated Chemistry-Climate Interactions: A Review. *Advances in Atmospheric Sciences*, *36*(9), 975-993. https://doi.org/10.1007/s00376-019-8216-9

Fuhrer, J., Val Martin, M., Mills, G., Heald, C. L., Harmens, H., Hayes, F.,…Ashmore, M. R. (2016). Current and future ozone risks to global terrestrial biodiversity and ecosystem processes. *Ecol Evol*, *6*(24), 8785-8799. https://doi.org/10.1002/ece3.2568

Gao, M., Carmichael, G. R., Saide, P. E., Lu, Z., Yu, M., Streets, D. G., & Wang, Z. (2016). Response of winter fine particulate matter concentrations to emission

and meteorology changes in North China. *Atmospheric Chemistry and Physics*, *16*(18), 11837-11851. https://doi.org/10.5194/acp-16-11837-2016

Gao, M., Gao, J., Zhu, B., Kumar, R., Lu, X., Song, S.,…McElroy, M. B. (2020). Ozone pollution over China and India: seasonality and sources. *Atmospheric Chemistry and Physics*, *20*(7), 4399-4414. https://doi.org/10.5194/acp-20-4399-2020

Gao M., Wang F., Ding Y., Wu, Z., Xu, Y., & Lu, X. (2023). Large-scale climate patterns offer preseasonal hints on the co-occurrence of heat wave and O3 pollution in China. *Proceedings of the National Academy of Sciences*, *120(26)*. https://doi.org/10.1073/pnas.2218274120

Gao, W., Tie, X., Xu, J., Huang, R., Mao, X., Zhou, G., & Chang, L. (2017). Long-term trend of O(3) in a mega City (Shanghai), China: Characteristics, causes, and interactions with precursors. *Science of the Total Environment*, *603-604*, 425-433. https://doi.org/10.1016/j.scitotenv.2017.06.099

Gao, Y., Yan, F., Ma, M., Ding, A., Liao, H., Wang, S.,…Gao, H. (2022). Unveiling the dipole synergic effect of biogenic and anthropogenic emissions on ozone concentrations. *Science of the Total Environment*, *818*, 151722. https://doi.org/10.1016/j.scitotenv.2021.151722

Garcia, A. R., Volkamer, R., Molina, L. T., Molina, M. J., Samuelson, J., Mellqvist, J.,…Kolb, C. E. (2006). Separation of emitted and photochemical formaldehyde in Mexico City

using a statistical analysis and a new pair of gas-phase tracers. *Atmospheric Chemistry and Physics*, *6(12)*, 4545-4557. https://doi.org/10.5194/acp-6-4545-2006

Gery, M., Whitten, G., Killus, J., & Dodge, M. C. (1988). Development and testing of the CBM-IV for urban and regional modeling. *Atmosheric [sic] Sciences Research Laboratory.*

Gilman, J. B., Lerner, B. M., Kuster, W. C., & de Gouw, J. A. (2013). Source signature of volatile organic compounds from oil and natural gas operations in northeastern Colorado. *Environ Sci Technol*, *47*(3), 1297-1305. https://doi.org/10.1021/es304119a

Goliff, W. S., Stockwell, W. R., & Lawson, C. V. (2013). The regional atmospheric chemistry mechanism, version 2. *Atmospheric Environment*, *68*, 174-185.

Gong, C., & Liao, H. (2019). A typical weather pattern for ozone pollution events in North China. *Atmospheric Chemistry and Physics*, *19*(22), 13725-13740. https://doi.org/10.5194/acp-19-13725-2019

Gong, C., Liao, H., Zhang, L., Yue, X., Dang, R., & Yang, Y. (2020). Persistent ozone pollution episodes in North China exacerbated by regional transport. *Environmental Pollution*, *265*(Pt A), 115056. https://doi.org/10.1016/j.envpol.2020.115056

Gong, C., Yue, X., Liao, H., & Ma, Y. (2021). A humidity-based exposure index representing ozone damage effects on vegetation. *Environmental Research Letters*, *16*(4). https://doi.org/10.1088/1748-9326/abecbb

Government, G. P. P. s. (2013). Implementation Opinions of the People's Government of Gansu Province on Implementing the Action Plan for Air Pollution Prevention and Control of the State Council.

Guo, H., Jiang, F., Cheng, H. R., Simpson, I. J., Wang, X. M., Ding, A. J.,…Xie, M. (2009). Concurrent observations of air pollutants at two sites in the Pearl River Delta and the implication of regional transport. *Atmospheric Chemistry and Physics*, *9*(19), 7343-7360. https://doi.org/10.5194/acp-9-7343-2009, 2009

Guo, H., Ling, Z. H., Cheng, H. R., Simpson, I. J., Lyu, X. P., Wang, X. M.,…Blake, D. R. (2017). Tropospheric volatile organic compounds in China. *Science of the Total Environment*, *574*, 1021-1043. https://doi.org/10.1016/j.scitotenv.2016.09.116

Guo, H., Ling, Z. H., Cheung, K., Jiang, F., Wang, D. W., Simpson, I. J.,…Blake, D. R. (2013). Characterization of photochemical pollution at different elevations in mountainous areas in Hong Kong. *Atmospheric Chemistry and Physics*, *13*(8), 3881-3898. https://doi.org/10.5194/acp-13-3881-2013

Guo, H., Ling, Z. H., Cheung, K., Wang, D. W., Simpson, I. J., & Blake, D. R. (2013). Acetone in the atmosphere of Hong Kong: Abundance, sources and photochemical precursors. *Atmospheric Environment*, *65*, 80-88. https://doi.org/10.1016/j.atmosenv.2012.10.027

Guo, J., Zhang, X., Gao, Y., Wang, Z., Zhang, M., Xue, W.,…Wang, Z. (2023). Evolution of Ozone Pollution in China: What Track Will It Follow? *Environ Sci Technol*, *57*(1), 109-117. https://doi.org/10.1021/acs.est.2c08205

Guo, W., Chen, Q., Yang, Y., Zhang, Y., Liu, X., Zhang, R.,…Chen, M. (2022). Investigating the mechanism of morning ozone concentration peaks in a petrochemical industrial city. *Atmospheric Environment*, *270*. https://doi.org/10.1016/j.atmosenv.2021.118897

Guo, W., Yang, Y., Chen, Q., Zhu, Y., Zhang, Y., Zhang, Y.,…She, J. (2022). Chemical reactivity of volatile organic compounds and their effects on ozone formation in a

petrochemical industrial area of Lanzhou, Western China. *Science of the Total Environment*, *839*, 155901. https://doi.org/10.1016/j.scitotenv.2022.155901

Guo, X., Gong, D., Li, J., Mo, X., Ding, X., Chen, J.,…Wang, B. (2024). Comprehensive measurement of carbonyls in Lhasa, Tibetan Plateau: Implications for strong atmospheric oxidation capacity. *Science of the Total Environment*, *948*, 174626. https://doi.org/10.1016/j.scitotenv.2024.174626

Haagen-Smit, A. J. (1952). Chemistry and physiology of Los Angeles smog. *Industrial and Engineering Chemistry*, *44(6)*, 1342-1346.

Haman, C. L., Couzo, E., Flynn, J. H., Vizuete, W., Heffron, B., & Lefer, B. L. (2014). Relationship between boundary layer heights and growth rates with ground-level ozone in Houston, Texas. *Journal of Geophysical Research: Atmospheres*, *119*(10), 6230-6245. https://doi.org/10.1002/2013jd020473

Han, H., Liu, J., Shu, L., Wang, T., & Yuan, H. (2020). Local and synoptic meteorological influences on daily variability in summertime surface ozone in eastern China. *Atmospheric Chemistry and Physics*, *20*(1), 203-222. https://doi.org/10.5194/acp-20-203-2020

Han, Y., Gong, Z., Ye, J., Liu, P., McKinney, K. A., & Martin, S. T. (2019). Quantifying the Role of the Relative Humidity-Dependent Physical State of Organic Particulate Matter in the Uptake of Semivolatile Organic Molecules. *Environ Sci Technol*, *53*(22), 13209-13218. https://doi.org/10.1021/acs.est.9b05354

Han, Y., Huang, X., Wang, C., Zhu, B., & He, L. (2019). Characterizing oxygenated volatile organic compounds and their sources in rural atmospheres in China. *J Environ Sci (China)*, *81*, 148-155. https://doi.org/10.1016/j.jes.2019.01.017

Hao, J., Wu, Y., Fu, L., He, D., & He, K. (2001). Source contributions to ambient concentrations of CO and NOx in the urban area of Beijing. *Journal of Environmental Science and Health*, *36(2)*, 215-228.

Hatakeyama, S. (1994). Reactions of Criegee Intermediates in the Gas Phase. *Res. Chem. Intermed.*, *20*, 503-524. https://doi.org/10.1163/156856794X00432

He, J., Gong, S., Yu, Y., Yu, L., Wu, L., Mao, H.,…Li, R. (2017). Air pollution characteristics and their relation to meteorological conditions during 2014-2015 in major Chinese cities. *Environmental Pollution*, *223*, 484-496. https://doi.org/10.1016/j.envpol.2017.01.050

Heard, D. E. (2004). High levels of the hydroxyl radical in the winter urban troposphere. *Geophysical Research Letters*, *31*(18). https://doi.org/10.1029/2004gl020544

Henderson, B. H., Jeffries, H. E., Kim, B. U., & Vizuete, W. G. (2010). The influence of model resolution on ozone in industrial volatile organic compound plumes. *J Air Waste Manag Assoc*, *60*(9), 1105-1117. https://doi.org/10.3155/1047-3289.60.9.1105

Hendrick, F., Müller, J. F., Clémer, K., Wang, P., De Mazière, M., Fayt, C.,…Van Roozendael, M. (2014). Four years of ground-based MAX-DOAS observations of HONO and NO2 in the Beijing area. *Atmospheric Chemistry and Physics*, *14*(2), 765-781. https://doi.org/10.5194/acp-14-765-2014

Ho, K. a. L., SC and Ho, Wing Kei and Blake, DR and Cheng, Y and Li, Yok Sheung and Ho, Steven Sai Hang and Fung, K and Louie, PKK and Park, D. (2009). Vehicular emission

of volatile organic compounds (VOCs) from a tunnel study in Hong Kong. *9*, 7491–7504. https://doi.org/10.5194/acp-9-7491-2009

Ho, K. F., Ho, S. S., Dai, W. T., Cao, J. J., Huang, R. J., Tian, L., & Deng, W. J. (2014). Seasonal variations of monocarbonyl and dicarbonyl in urban and sub-urban sites of Xi'an, China. *Environ Monit Assess*, *186*(5), 2835-2849. https://doi.org/10.1007/s10661-013-3584-6

Ho, K. F., Ho, S. S. H., Huang, R. J., Dai, W. T., Cao, J. J., Tian, L., & Deng, W. J. (2015). Spatiotemporal distribution of carbonyl compounds in China. *Environmental Pollution*, *197*, 316-324. https://doi.org/10.1016/j.envpol.2014.11.014

Hu, F., Xie, P., Xu, J., Lv, Y., Zhang, Z., Zheng, J., & Tian, X. (2025). Long-term trends of ozone in the Yangtze River Delta, China: Spatiotemporal impacts of meteorological factors, local, and non-local emissions. *J Environ Sci (China)*, *156*, 408-420. https://doi.org/10.1016/j.jes.2024.07.017

Hua, J., Cui, Y., Guo, L., Li, H., Fan, J., Li, Y.,…Wang, X. (2023). Spatial characterization of HCHO and reapportionment of its secondary sources considering photochemical loss in Taiyuan, China. *Science of the Total Environment*, *865*, 161069. https://doi.org/10.1016/j.scitotenv.2022.161069

Hua, X., Wang, M., Yao, Z., Hao, R., & Wang, H. (2024). Characteristics and Sensitivity Analysis of Ozone Pollution in a Typical Inland City in China. *Atmosphere*, *15*(2). https://doi.org/10.3390/atmos15020160

Huang, Q. N., Cao, Z. Q., Xi, X. H., Li, X. W., Guo, H. D., & Wang, F. J. (2013). Comparison of Thermal Response of Extremely High Temperature in Jingjintang and Gtha Urban Agglomerations Based on Wrf Model. *2013 Ieee International Geoscience and Remote Sensing Symposium (Igarss)*, 3849-3852. https://doi.org/10.1109/Igarss.2013.6723671

Huang, X. F., Zhang, B., Xia, S. Y., Han, Y., Wang, C., Yu, G. H., & Feng, N. (2020). Sources of oxygenated volatile organic compounds (OVOCs) in urban atmospheres in North and South China. *Environmental Pollution*, *261*, 114152. https://doi.org/10.1016/j.envpol.2020.114152

Hui, L., Feng, X., Yuan, Q., Chen, Y., Xu, Y., Zheng, P.,…Wang, Z. (2023). Abundant oxygenated volatile organic compounds and their contribution to photochemical pollution in subtropical Hong Kong. *Environmental Pollution*, *335*, 122287. https://doi.org/10.1016/j.envpol.2023.122287

Hui, L. R., Liu, X. G., Tan, Q. W., Feng, M., An, J. L., Qu, Y.,…Jiang, M. Q. (2018). Characteristics, source apportionment and contribution of VOCs to ozone formation in Wuhan, Central China. *Atmospheric Environment*, *192*, 55-71. https://doi.org/10.1016/j.atmosenv.2018.08.042

Jacob, D. J. (1999). *Introduction to atmospheric chemistry*. Princeton university press.

Jacob, D. J., & Winner, D. A. (2009). Effect of climate change on air quality. *Atmospheric Environment*, *43*(1), 51-63. https://doi.org/10.1016/j.atmosenv.2008.09.051

Jenkin, M. E., Saunders, S. M., Wagner, V., and Pilling, M. J. (2003). Protocol for the development of the Master Chemical Mechanism, MCM v3 (Part B): tropospheric degradation of aromatic volatile organic compounds, . *Atmos. Chem. Phys.*, *3*(1), 181–193. https://doi.org/10.5194/acp-3-181-2003

Jenkin, M. E. a. S., Sandra M and Pilling, Michael J. (1997). The tropospheric degradation of volatile organic compounds: a protocol for mechanism development. *Atmospheric Environment*, *31*(1), 81--104. https://doi.org/10.1016/S1352-2310(96)00105-7

Jennifer, A. L. (1985). Tropospheric ozone: Seasonal behavior, trends, and anthropogenic influence. *Journal of Geophysical Research: Atmospheres*, *90*, 10463-10482. https://doi.org/10.1029/JD090iD06p10463

Jeong, J. I., & Park, R. J. (2013). Effects of the meteorological variability on regional air quality in East Asia. *Atmospheric Environment*, *69*, 46-55. https://doi.org/10.1016/j.atmosenv.2012.11.061

Jia, C., Mao, X., Huang, T., Liang, X., Wang, Y., Shen, Y.,…Gao, H. (2016). Non-methane hydrocarbons (NMHCs) and their contribution to ozone formation potential in a petrochemical industrialized city, Northwest China. *Atmospheric Research*, *169*, 225-236. https://doi.org/10.1016/j.atmosres.2015.10.006

Jia, C., Wang, Y., Li, Y., Huang, T., Mao, X., Mo, J.,…Ma, J. (2018). Oxidative Capacity and Radical Chemistry in a Semi-arid and Petrochemical-industrialized City, Northwest China. *Aerosol and Air Quality Research*, *18*(6), 1391-1404. https://doi.org/10.4209/aaqr.2017.11.0506

Jin, X., & Holloway, T. (2015). Spatial and temporal variability of ozone sensitivity over China observed from the Ozone Monitoring Instrument. *Journal of Geophysical Research: Atmospheres*, *120*(14), 7229-7246. https://doi.org/10.1002/2015jd023250

Johnson, C. E., Collins, W. J., Stevenson, D. S., & Derwent, R. G. (1999). Relative roles of climate and emissions changes on future tropospheric oxidant concentrations. *Journal of Geophysical Research: Atmospheres*, *104*(D15), 18631-18645. https://doi.org/10.1029/1999jd900204

Kavassalis, S. C., & Murphy, J. G. (2017). Understanding ozone-meteorology correlations: A role for dry deposition. *Geophysical Research Letters*, *44*(6), 2922-2931. https://doi.org/10.1002/2016gl071791

Kgabi, N. A. S., Ramotsamai M. (2012). Seasonal variations of tropospheric ozone concentrations. *Global journal of science frontier research chemistry*, *12*, 21-29.

Knighton, W. B., Herndon, S. C., Wood, E. C., Fortner, E. C., Onasch, T. B., Wormhoudt, J.,…Jones, M. (2012). Detecting Fugitive Emissions of 1,3-Butadiene and Styrene from a Petrochemical Facility: An Application of a Mobile Laboratory and a Modified Proton Transfer Reaction Mass Spectrometer. *Industrial & Engineering Chemistry Research*, *51*(39), 12706-12711. https://doi.org/10.1021/ie202794j

Lam, S. H. M., Saunders, S. M., Guo, H., Ling, Z. H., Jiang, F., Wang, X. M., & Wang, T. J. (2013). Modelling VOC source impacts on high ozone episode days observed at a mountain summit in Hong Kong under the influence of mountain-valley breezes. *Atmospheric Environment*, *81*, 166-176. https://doi.org/10.1016/j.atmosenv.2013.08.060

Lefohn, A. S., Shadwick, D., & Oltmans, S. J. (2008). Characterizing long-term changes in surface ozone levels in the United States (1980–2005). *Atmospheric Environment*, *42(35)*, 8252-8262.

Levy, H. (1971). Normal Atmosphere: Large Radical and Formaldehyde Concentrations Predicted. *Science*, *173(3992)*, 141-143.

Li, B., Ho, S. S. H., Qu, L., Gong, S., Ho, K. F., Zhao, D.,…Chan, C. S. (2021). Temporal and spatial discrepancies of VOCs in an industrial-dominant city in China during summertime. *Chemosphere*, *264*(Pt 2), 128536. https://doi.org/10.1016/j.chemosphere.2020.128536

Li, B., Lu, L., Shi, X., Ma, L., Jiang, J.-P., Yabo, S. D.,…Qi, H. (2023). Drivers of 2015–2021 trends in cold winter surface PM2.5 in the Harbin-Changchun megalopolis in China: Meteorology vs. anthropogenic emission. *Atmospheric Research*, *285*. https://doi.org/10.1016/j.atmosres.2023.106623

Li, C., Liu, Y., Cheng, B., Zhang, Y., Liu, X., Qu, Y.,…Feng, M. (2022). A comprehensive investigation on volatile organic compounds (VOCs) in 2018 in Beijing, China: Characteristics, sources and behaviours in response to O3 formation. *Science of the Total Environment*, *806*. https://doi.org/10.1016/j.scitotenv.2021.150247

Li, J., Mao, J., Min, K. E., Washenfelder, R. A., Brown, S. S., Kaiser, J.,…Horowitz, L. W. (2016). Observational constraints on glyoxal production from isoprene oxidation and its contribution to organic aerosol over the Southeast United States. *Journal of Geophysical Research: Atmospheres*, *121*(16), 9849-9861. https://doi.org/10.1002/2016jd025331

Li, J., Wang, Z., Chen, L., Lian, L., Li, Y., Zhao, L.,…Ma, J. (2020). WRF-Chem simulations of ozone pollution and control strategy in petrochemical industrialized and heavily polluted Lanzhou City, Northwestern China. *Science of the Total Environment*, *737*, 139835. https://doi.org/10.1016/j.scitotenv.2020.139835

Li, J. H., Deng, S. X., Tohti, A., Li, G. H., Yi, X. X., Lu, Z. Z.,…Zhang, S. (2022). Spatial characteristics of VOCs and their ozone and secondary organic aerosol formation potentials in autumn and winter in the Guanzhong Plain, China. *Environmental Research*, *211*. https://doi.org/10.1016/j.envres.2022.113036

Li, J. L., Xie, X. D., Li, L., Wang, X. Y., Wang, H. L., Jing, S. A.,…Hu, J. L. (2022). Fate of oxygenated volatile organic compounds in the Yangtze River Delta Region: source contributions and impacts on the atmospheric oxidation capacity. *Environmental science & technology*, *56(16)*, 11212-11224. https://doi.org/10.1021/acs.est.2c00038

Li, K., Jacob, D. J., Liao, H., Qiu, Y., Shen, L., Zhai, S.,…Kuk, S. K. (2021). Ozone pollution in the North China Plain spreading into the late-winter haze season. *Proc Natl Acad Sci U S A*, *118*(10). https://doi.org/10.1073/pnas.2015797118

Li, K., Jacob, D. J., Liao, H., Shen, L., Zhang, Q., & Bates, K. H. (2019). Anthropogenic drivers of 2013-2017 trends in summer surface ozone in China. *Proc Natl Acad Sci U S A*, *116*(2), 422-427. https://doi.org/10.1073/pnas.1812168116

Li, K., Jacob, D. J., Shen, L., Lu, X., De Smedt, I., & Liao, H. (2020). Increases in surface ozone pollution in China from 2013 to 2019: anthropogenic and meteorological influences. *Atmospheric Chemistry and Physics*, *20*(19), 11423-11433. https://doi.org/10.5194/acp-20-11423-2020

Li, L., An, J. Y., Shi, Y. Y., Zhou, M., Yan, R. S., Huang, C.,…Wu, J. (2016). Source apportionment of surface ozone in the Yangtze River Delta, China in the summer of

2013. *Atmospheric Environment*, *144*, 194-207. https://doi.org/10.1016/j.atmosenv.2016.08.076

Li, L., Chen, C. H., Huang, C., Huang, H. Y., Zhang, G. F., Wang, Y. J.,…Jang, C. J. (2012). Process analysis of regional ozone formation over the Yangtze River Delta, China using the Community Multi-scale Air Quality modeling system. *Atmospheric Chemistry and Physics*, *12*(22), 10971-10987. https://doi.org/10.5194/acp-12-10971-2012

Li, L., Zheng, Z., Xu, B., Wang, X., Bai, Z., Yang, W.,…Li, K. (2023). Investigation of O3-precursor relationship nearby oil fields of Shandong, China. *Atmospheric Environment*, *294*. https://doi.org/10.1016/j.atmosenv.2022.119471

Li, M., Shao, M., Li, L.-Y., Lu, S.-H., Chen, W.-T., & Wang, C. (2014). Quantifying the ambient formaldehyde sources utilizing tracers. *Chinese Chemical Letters*, *25*(11), 1489-1491. https://doi.org/10.1016/j.cclet.2014.07.001

Li, M., Yu, S., Chen, X., Li, Z., Zhang, Y., Wang, L.,…Seinfeld, J. H. (2021). Large scale control of surface ozone by relative humidity observed during warm seasons in China. *Environmental Chemistry Letters*, *19*(6), 3981-3989. https://doi.org/10.1007/s10311-021-01265-0

Li, M. Z., Huang, Y., & Han, M. D. (2019). How to Maintain a Sustainable Environment? A Spatial Evolution of Urban Atmospheric Pollution and Impact Factors in China. *Sustainability*, *11*(16). https://doi.org/ARTN 4376

10.3390/su11164376

Li, N., He, Q., Greenberg, J., Guenther, A., Li, J., Cao, J.,…Zhang, Q. (2018). Impacts of biogenic and anthropogenic emissions on summertime ozone formation in the Guanzhong Basin, China. *Atmospheric Chemistry and Physics*, *18*(10), 7489-7507. https://doi.org/10.5194/acp-18-7489-2018

Li, R., Cui, L., Li, J., Zhao, A., Fu, H., Wu, Y.,…Chen, J. (2017). Spatial and temporal variation of particulate matter and gaseous pollutants in China during 2014–2016. *Atmospheric Environment*, *161*, 235-246. https://doi.org/10.1016/j.atmosenv.2017.05.008

Li, W., Tong, S., Cao, J., Su, H., Zhang, W., Wang, L.,…Ge, M. (2021). Comparative observation of atmospheric nitrous acid (HONO) in Xi'an and Xianyang located in the GuanZhong basin of western China. *Environmental Pollution*, *289*, 117679. https://doi.org/10.1016/j.envpol.2021.117679

Li, X.-B., Yuan, B., Parrish, D. D., Chen, D., Song, Y., Yang, S.,…Shao, M. (2022). Long-term trend of ozone in southern China reveals future mitigation strategy for air pollution. *Atmospheric Environment*, *269*. https://doi.org/10.1016/j.atmosenv.2021.118869

Li, X. F., Zhang, Q. H., & Xue, H. W. (2017). The role of initial cloud condensation nuclei concentration in hail using the WRF NSSL 2-moment microphysics scheme. *Advances in Atmospheric Sciences*, *34*(9), 1106-1120. https://doi.org/10.1007/s00376-017-6237-9

Li, Y., Li, H., Zhang, X., Ji, Y., Gao, R., Wu, Z.,…Bai, H. (2023). Characteristics, sources and health risk assessment of atmospheric carbonyls during multiple ozone pollution episodes in urban Beijing: Insights into control strategies. *Science of the Total Environment*, *863*, 160769. https://doi.org/10.1016/j.scitotenv.2022.160769

Li, Y., Li, J., Yang, Z., Chen, T., Wang, J., Ma, J.,…Huang, T. (2022). The transition from a nitrogen oxides-limited regime to a volatile organic compounds-limited regime in the petrochemical industrialized Lanzhou City, China. *Atmospheric Research*, *269*. https://doi.org/10.1016/j.atmosres.2022.106035

Li, Y., Shao, M., Lu, S., Chang, C.-C., & Dasgupta, P. K. (2010). Variations and sources of ambient formaldehyde for the 2008 Beijing Olympic games. *Atmospheric Environment*, *44*(21-22), 2632-2639. https://doi.org/10.1016/j.atmosenv.2010.03.045

Li, Y., Wang, Y., He, Y., Cai, H., Wang, H., Yan, Z.,…Wang, B. (2025). Photochemical formation process of ozone and spatiotemporally targeted control strategies along the transport pathways in the Pearl River Delta region. *Journal of Environmental Sciences*. https://doi.org/https://doi.org/10.1016/j.jes.2025.05.032

Li, Y. J., Lee, B. P., Su, L., Fung, J. C. H., & Chan, C. K. (2015). Seasonal characteristics of fine particulate matter (PM) based on high-resolution time-of-flight aerosol mass spectrometric (HR-ToF-AMS) measurements at the HKUST Supersite in Hong Kong. *Atmospheric Chemistry and Physics*, *15*(1), 37-53. https://doi.org/10.5194/acp-15-37-2015

Lin, Y. C., Schwab, J. J., Demerjian, K. L., Bae, M. S., Chen, W. N., Sun, Y.,…Perry, J. (2012). Summertime formaldehyde observations in New York City: Ambient levels, sources and its contribution to HOx radicals. *Journal of Geophysical Research: Atmospheres*, *117*(D8). https://doi.org/10.1029/2011jd016504

Ling, Z. H., & Guo, H. (2014). Contribution of VOC sources to photochemical ozone formation and its control policy implication in Hong Kong. *Environmental Science & Policy*, *38*, 180-191. https://doi.org/10.1016/j.envsci.2013.12.004

Ling, Z. H., Guo, H., Lam, S. H. M., Saunders, S. M., & Wang, T. (2014). Atmospheric photochemical reactivity and ozone production at two sites in Hong Kong: Application of a Master Chemical Mechanism-photochemical box model. *Journal of Geophysical Research: Atmospheres*, *119*(17), 10567-10582. https://doi.org/10.1002/2014jd021794

Ling, Z. H., Zhao, J., Fan, S. J., & Wang, X. M. (2017). Sources of formaldehyde and their contributions to photochemical O(3) formation at an urban site in the Pearl River Delta, southern China. *Chemosphere*, *168*, 1293-1301. https://doi.org/10.1016/j.chemosphere.2016.11.140

Liu, C., Xin, Y., Zhang, C., Liu, J., Liu, P., He, X., & Mu, Y. (2023). Ambient volatile organic compounds in urban and industrial regions in Beijing: Characteristics, source apportionment, secondary transformation and health risk assessment. *Science of the Total Environment*, *855*, 158873. https://doi.org/10.1016/j.scitotenv.2022.158873

Liu, F., Beirle, S., Zhang, Q., van der, A. R., Zheng, B., Tong, D., & He, K. (2017). NO(x) emission trends over Chinese cities estimated from OMI observations during 2005 to 2015. *Atmospheric Chemistry and Physics*, *17*(15), 9261-9275. https://doi.org/10.5194/acp-17-9261-2017

Liu, H., Liu, S., Xue, B., Lv, Z., Meng, Z., Yang, X.,…He, K. (2018). Ground-level ozone pollution and its health impacts in China. *Atmospheric Environment*, *173*, 223-230. https://doi.org/10.1016/j.atmosenv.2017.11.014

Liu, H., Zhang, M., & Han, X. (2020). A review of surface ozone source apportionment in China. *Atmospheric and Oceanic Science Letters*, *13:5*, 470-484.

Liu, J., Ruan, Y., Wu, Q., Ma, Y., He, X., Li, L.,…Luo, B. (2020). Has the mortality risk declined after the improvement of air quality in an ex-heavily polluted Chinese city-Lanzhou? *Chemosphere*, *242*, 125196. https://doi.org/10.1016/j.chemosphere.2019.125196

Liu, J., Tuheti, A., Deng, S., Li, J., Li, Q., Huang, L., & Chen, J. (2024). Exploration of radical chemistry, precursor sensitivity and O3 control strategies in a provincial capital city, northwestern China. *Atmospheric Environment*, *338*. https://doi.org/10.1016/j.atmosenv.2024.120792

Liu, J., Wang, L., Li, M., Liao, Z., Sun, Y., Song, T.,…Kulmala, M. (2019). Quantifying the impact of synoptic circulation patterns on ozone variability in northern China from April to October 2013–2017. *Atmospheric Chemistry and Physics*, *19*(23), 14477-14492. https://doi.org/10.5194/acp-19-14477-2019

Liu, L., Ma, X., Wen, W., Sun, C., & Jiao, J. (2021). Characteristics and potential sources of wintertime air pollution in Linfen, China. *Environ Monit Assess*, *193*(5), 252. https://doi.org/10.1007/s10661-021-09036-8

Liu, N., Lin, W., Ma, J., Xu, W., & Xu, X. (2019). Seasonal variation in surface ozone and its regional characteristics at global atmosphere watch stations in China. *J Environ Sci (China)*, *77*, 291-302. https://doi.org/10.1016/j.jes.2018.08.009

Liu, Q., Gao, Y., Huang, W. W., Ling, Z. H., Wang, Z., & Wang, X. M. (2022). Carbonyl compounds in the atmosphere: A review of abundance, source and their contributions to O3 and SOA formation. *Atmospheric Research*, *274*. https://doi.org/ARTN 106184

10.1016/j.atmosres.2022.106184

Liu, S. C., Trainer, M., Fehsenfeld, F. C., Parrish, D. D., Williams, E. J., Fahey, D. W.,…Murphy, P. C. (1987). Ozone production in the rural troposphere and the implications for regional and global ozone distributions. *Journal of Geophysical Research: Atmospheres*, *92(D4)*, 4191-4207.

Liu, X. F., Guo, H., Zeng, L. W., Lyu, X., Wang, Y., Zeren, Y. Z.,…Zhang, G. (2021). Photochemical ozone pollution in five Chinese megacities in summer 2018. *Science of the Total Environment*, *801*. https://doi.org/10.1016/j.scitotenv.2021.149603

Liu, X. F., Lyu, X. P., Wang, Y., Jiang, F., & Guo, H. (2019). Intercomparison of O-3 formation and radical chemistry in the past decade at a suburban site in Hong Kong. *Atmospheric Chemistry and Physics*, *19*(7), 5127-5145. https://doi.org/10.5194/acp-19-5127-2019

Liu, Y., Shao, M., Kuster, W. C., Goldan, P. D., Li, X., Lu, S., & Gouw, J. A. D. (2009). Source identification of reactive hydrocarbons and oxygenated VOCs in the summertime in Beijing. *Environmental science & technology*, *43(1)*, 75-81. https://doi.org/10.1021/es801716n

Liu, Y., Shao, M., Lu, S., Chang, C.-C., Wang, J.-L., & Fu, L. (2008). Source apportionment of ambient volatile organic compounds in the Pearl River Delta, China: Part II. *Atmospheric Environment*, *42*(25), 6261-6274. https://doi.org/10.1016/j.atmosenv.2008.02.027

Liu, Y. H., Wang, H. L., Jing, S. G., Gao, Y. Q., Peng, Y. R., Lou, S. R.,…An, J. Y. (2019). Characteristics and sources of volatile organic compounds (VOCs) in Shanghai during

summer: Implications of regional transport. *Atmospheric Environment*, *215*. https://doi.org/ARTN 116902

10.1016/j.atmosenv.2019.116902

Liu, Z., Cui, Y., He, Q., Guo, L., Gao, X., Feng, Y.,…Wang, X. (2021). Seasonal Variations of Carbonyls and Their Contributions to the Ozone Formation in Urban Atmosphere of Taiyuan, China. *Atmosphere*, *12*(4). https://doi.org/10.3390/atmos12040510

Liu, Z., Wang, Y., Gu, D., Zhao, C., Huey, L. G., Stickel, R.,…Liu, S. C. (2012). Summertime photochemistry during CAREBeijing-2007: ROx budgets and O-3 formation. *Atmospheric Chemistry and Physics*, *12*(16), 7737-7752. https://doi.org/10.5194/acp-12-7737-2012

Louie, P. K. K., Ho, J. W. K., Tsang, R. C. W., Blake, D. R., Lau, A. K. H., Yu, J. Z.,…Zhong, L. (2013). VOCs and OVOCs distribution and control policy implications in Pearl River Delta region, China. *Atmospheric Environment*, *76*, 125-135. https://doi.org/10.1016/j.atmosenv.2012.08.058

Lu, H., Cai, Q. Y., Wen, S., Chi, Y., Guo, S., Sheng, G., & Fu, J. (2010). Seasonal and diurnal variations of carbonyl compounds in the urban atmosphere of Guangzhou, China. *Science of the Total Environment*, *408*(17), 3523-3529. https://doi.org/10.1016/j.scitotenv.2010.05.013

Lu, K., Guo, S., Tan, Z., Wang, H., Shang, D., Liu, Y.,…Zhang, Y. (2019). Exploring atmospheric free-radical chemistry in China: the self-cleansing capacity and the formation of secondary air pollution. *Natl Sci Rev*, *6*(3), 579-594. https://doi.org/10.1093/nsr/nwy073

Lu, Q., Zheng, J., Ye, S., Shen, X., Yuan, Z., & Yin, S. (2013). Emission trends and source characteristics of SO2, NOx, PM10 and VOCs in the Pearl River Delta region from 2000 to 2009. *Atmospheric Environment*, *76*, 11-20. https://doi.org/10.1016/j.atmosenv.2012.10.062

Lu, X., Chen, N., Wang, Y., Cao, W., Zhu, B., Yao, T.,…Lau, A. K. H. (2017). Radical budget and ozone chemistry during autumn in the atmosphere of an urban site in central China. *Journal of Geophysical Research: Atmospheres*, *122*(6), 3672-3685. https://doi.org/10.1002/2016jd025676

Lu, X., Zhang, L., Liu, X., Gao, M., Zhao, Y., & Shao, J. (2018). Lower tropospheric ozone over India and its linkage to the South Asian monsoon. *Atmospheric Chemistry and Physics*, *18*(5), 3101-3118. https://doi.org/10.5194/acp-18-3101-2018

Lu, X., Zhang, L., & Shen, L. (2019). Meteorology and Climate Influences on Tropospheric Ozone: a Review of Natural Sources, Chemistry, and Transport Patterns. *Current Pollution Reports*, *5*(4), 238-260. https://doi.org/10.1007/s40726-019-00118-3

Lu, X., Zhang, L., Wang, X. L., Gao, M., Li, K., Zhang, Y. Z.,…Zhang, Y. H. (2020). Rapid Increases in Warm-Season Surface Ozone and Resulting Health Impact in China Since 2013. *Environmental Science & Technology Letters*, *7*(4), 240-247. https://doi.org/10.1021/acs.estlett.0c00171

Luecken, D. J., Hutzell, W. T., Strum, M. L., & Pouliot, G. A. (2012). Regional sources of atmospheric formaldehyde and acetaldehyde, and implications for atmospheric

modeling. *Atmospheric Environment*, *47*, 477-490. https://doi.org/10.1016/j.atmosenv.2011.10.005

Lui, K. H., Ho, S. S. H., Louie, P. K. K., Chan, C. S., Lee, S. C., Hu, D.,…Ho, K. F. (2017). Seasonal behavior of carbonyls and source characterization of formaldehyde (HCHO) in ambient air. *Atmospheric Environment*, *152*, 51-60. https://doi.org/10.1016/j.atmosenv.2016.12.004

Lyu, X., Li, H., Lee, S. C., Xiong, E., Guo, H., Wang, T., & de Gouw, J. (2024). Significant Biogenic Source of Oxygenated Volatile Organic Compounds and the Impacts on Photochemistry at a Regional Background Site in South China. *Environ Sci Technol*, *58*(45), 20081-20090. https://doi.org/10.1021/acs.est.4c05656

Lyu, X. P., Chen, N., Guo, H., Zhang, W. H., Wang, N., Wang, Y., & Liu, M. (2016a). Ambient volatile organic compounds and their effect on ozone production in Wuhan, central China. *Science of the Total Environment*, *541*, 200-209. https://doi.org/10.1016/j.scitotenv.2015.09.093

Lyu, X. P., Chen, N., Guo, H., Zhang, W. H., Wang, N., Wang, Y., & Liu, M. (2016b). Ambient volatile organic compounds and their effect on ozone production in Wuhan, central China. *Science of the Total Environment*, *541*, 200-209. https://doi.org/10.1016/j.scitotenv.2015.09.093

Lyu, X. P., Chen, N., Guo, H., Zhang, W. H., Wang, N., Wang, Y., & Liu, M. (2016c). Ambient volatile organic compounds and their effect on ozone production in Wuhan, central China (vol 541, pg 200, 2016). *Science of the Total Environment*, *548*, 483-483. https://doi.org/10.1016/j.scitotenv.2016.01.168

Lyu, X. P., Wang, N., Guo, H., Xue, L. K., Jiang, F., Zeren, Y. Z.,…Zhou, Y. (2019). Causes of a continuous summertime O-3 pollution event in Jinan, a central city in the North China Plain. *Atmospheric Chemistry and Physics*, *19*(5), 3025-3042. https://doi.org/10.5194/acp-19-3025-2019

Lyu, X. P., Zeng, L. W., Guo, H., Simpson, I. J., Ling, Z. H., Wang, Y.,…Blake, D. R. (2017). Evaluation of the effectiveness of air pollution control measures in Hong Kong. *Environmental Pollution*, *220*, 87-94. https://doi.org/10.1016/j.envpol.2016.09.025

Ma, L., Fu, F., Li, Z., & Liu, P. (2012). Oil development in China: Current status and future trends. *Energy Policy*, *45*, 43-53. https://doi.org/10.1016/j.enpol.2012.01.023

Ma, R., Ban, J., Wang, Q., & Li, T. (2020). Statistical spatial-temporal modeling of ambient ozone exposure for environmental epidemiology studies: A review. *Science of the Total Environment*, *701*, 134463. https://doi.org/10.1016/j.scitotenv.2019.134463

Ma, T., Duan, F., He, K., Qin, Y., Tong, D., Geng, G.,…Ma, Y. (2019). Air pollution characteristics and their relationship with emissions and meteorology in the Yangtze River Delta region during 2014-2016. *J Environ Sci (China)*, *83*, 8-20. https://doi.org/10.1016/j.jes.2019.02.031

Ma, X., Tan, Z., Lu, K., Yang, X., Liu, Y., Li, S.,…Zhang, Y. (2019). Winter photochemistry in Beijing: Observation and model simulation of OH and HO(2) radicals at an urban site. *Science of the Total Environment*, *685*, 85-95. https://doi.org/10.1016/j.scitotenv.2019.05.329

Ma, Y., Diao, Y., Zhang, B., Wang, W., Ren, X., Yang, D.,…Zheng, J. (2016). Detection of formaldehyde emissions from an industrial zone in the Yangtze River Delta region of

China using a proton transfer reaction ion-drift chemical ionization mass spectrometer. *Atmospheric Measurement Techniques*, *9*(12), 6101-6116. https://doi.org/10.5194/amt-9-6101-2016

Maji, K. J., & Sarkar, C. (2020). Spatio-temporal variations and trends of major air pollutants in China during 2015-2018. *Environ Sci Pollut Res Int*, *27*(27), 33792-33808. https://doi.org/10.1007/s11356-020-09646-8

Maji, K. J., Ye, W. F., Arora, M., & Nagendra, S. M. S. (2019). Ozone pollution in Chinese cities: Assessment of seasonal variation, health effects and economic burden. *Environmental Pollution*, *247*, 792-801. https://doi.org/10.1016/j.envpol.2019.01.049

Manisalidis, I., Stavropoulou, E., Stavropoulos, A., & Bezirtzoglou, E. (2020). Environmental and Health Impacts of Air Pollution: A Review. *Front Public Health*, *8*, 14. https://doi.org/10.3389/fpubh.2020.00014

Mo, X., Gong, D., Liu, Y., Li, J., Zhao, Y., Zhao, W.,…Wang, B. (2023). Ground-based formaldehyde across the Pearl River Delta: A snapshot and meta-analysis study. *Atmospheric Environment*, *309*. https://doi.org/10.1016/j.atmosenv.2023.119935

Mo, Z., Huang, S., Yuan, B., Pei, C., Song, Q., Qi, J.,…Shao, M. (2022). Tower-based measurements of NMHCs and OVOCs in the Pearl River Delta: Vertical distribution, source analysis and chemical reactivity. *Environmental Pollution*, *292*(Pt B), 118454. https://doi.org/10.1016/j.envpol.2021.118454

Nussbaumer, C. M., Crowley, J. N., Schuladen, J., Williams, J., Hafermann, S., Reiffs, A.,…Fischer, H. (2021). Measurement report: Photochemical production and loss rates of formaldehyde and ozone across Europe. *Atmospheric Chemistry and Physics*, *21*(24), 18413-18432. https://doi.org/10.5194/acp-21-18413-2021

Oltmans, S., Schnell, R., Johnson, B., Pétron, G., Mefford, T., Neely, R.,…Pfister, G. (2014). Anatomy of wintertime ozone associated with oil and natural gas extraction activity in Wyoming and Utah. *Elementa: Science of the Anthropocene*, *2*. https://doi.org/10.12952/journal.elementa.000024

Oltmans, S. J., & Komhyr, W. D. (1986). Surface ozone distributions and variations from 1973–1984: Measurements at the NOAA Geophysical Monitoring for Climatic Change Baseline Observatories. *Journal of Geophysical Research: Atmospheres*, *91(D4)*, 5229-5236.

Oltmans, S. J., Lefohn, A. S., Shadwick, D., Harris, J. M., Scheel, H. E., Galbally, I.,…Kawasato, T. (2013). Recent tropospheric ozone changes – A pattern dominated by slow or no growth. *Atmospheric Environment*, *67*, 331-351. https://doi.org/10.1016/j.atmosenv.2012.10.057

Oltmans, S. J. a. L. I., Hiram. (1994). Surface ozone measurements from a global network. *Atmospheric Environment*, *28*(1), 9-24. https://doi.org/10.1016/1352-2310(94)90019-1

Osborn, D. L., & Taatjes, C. A. (2015). The physical chemistry of Criegee intermediates in the gas phase. *International Reviews in Physical Chemistry*, *34*(3), 309-360. https://doi.org/10.1080/0144235x.2015.1055676

Ou, J., Yuan, Z., Zheng, J., Huang, Z., Shao, M., Li, Z.,…Louie, P. K. (2016). Ambient Ozone Control in a Photochemically Active Region: Short-Term Despiking or Long-Term Attainment? *Environ Sci Technol*, *50*(11), 5720-5728. https://doi.org/10.1021/acs.est.6b00345

Paatero, P. (1997). Least squares formulation of robust non-negative factor analysis. *Chemometrics and Intelligent Laboratory Systems*, *37*(1), 23-35. https://doi.org/10.1016/S0169-7439(96)00044-5

Palmer, P. I., Abbot, D. S., Fu, T. M., Jacob, D. J., Chance, K., Kurosu, T. P.,…Sumner, A. L. (2006). Quantifying the seasonal and interannual variability of North American isoprene emissions using satellite observations of the formaldehyde column. *Journal of Geophysical Research: Atmospheres*, *111*(D12). https://doi.org/10.1029/2005jd006689

Panagi, M., Sommariva, R., Fleming, Z. L., Monks, P. S., Lu, G., Marais, E. A.,…Vande Hey, J. D. (2025). Daily evolution of VOCs in Beijing: chemistry, emissions, transport, and policy implications. *Atmospheric Pollution Research*. https://doi.org/10.1016/j.apr.2025.102783

Pang, X., & Mu, Y. (2006). Seasonal and diurnal variations of carbonyl compounds in Beijing ambient air. *Atmospheric Environment*, *40*(33), 6313-6320. https://doi.org/10.1016/j.atmosenv.2006.05.044

Parrish, D. D., Law, K. S., Staehelin, J., Derwent, R., Cooper, O. R., Tanimoto, H.,…Chan, E. (2012). Long-term changes in lower tropospheric baseline ozone concentrations at northern mid-latitudes. *Atmospheric Chemistry and Physics*, *12*(23), 11485-11504. https://doi.org/10.5194/acp-12-11485-2012

Pusede, S. E., Steiner, A. L., & Cohen, R. C. (2015). Temperature and recent trends in the chemistry of continental surface ozone. *Chem Rev*, *115*(10), 3898-3918. https://doi.org/10.1021/cr5006815

Qi, C., Wang, P., Yang, Y., Li, H., Zhang, H., Ren, L.,…Liao, H. (2024). Impacts of tropical cyclone–heat wave compound events on surface ozone in eastern China: comparison between the Yangtze River and Pearl River deltas. *Atmospheric Chemistry and Physics*, *24*(20), 11775-11789. https://doi.org/10.5194/acp-24-11775-2024

Qian, J., Liao, H., Yang, Y., Li, K., Chen, L., & Zhu, J. (2022). Meteorological influences on daily variation and trend of summertime surface ozone over years of 2015-2020: Quantification for cities in the Yangtze River Delta. *Science of the Total Environment*, *834*, 155107. https://doi.org/10.1016/j.scitotenv.2022.155107

Qian, X., Shen, H., & Chen, Z. (2019). Characterizing summer and winter carbonyl compounds in Beijing atmosphere. *Atmospheric Environment*, *214*. https://doi.org/10.1016/j.atmosenv.2019.116845

Qiao, W., Li, K., Yang, Z., Chen, L., & Liao, H. (2024). Implications of the extremely hot summer of 2022 on urban ozone control in China. *Atmospheric and Oceanic Science Letters*, *17*(6). https://doi.org/10.1016/j.aosl.2024.100470

Qu, H., Wang, Y., Zhang, R., Liu, X., Huey, L. G., Sjostedt, S.,…Zhang, Y. (2021). Chemical Production of Oxygenated Volatile Organic Compounds Strongly Enhances Boundary-Layer Oxidation Chemistry and Ozone Production. *Environ Sci Technol*, *55*(20), 13718-13727. https://doi.org/10.1021/acs.est.1c04489

Qu, K., Yan, Y., Wang, X., Jin, X., Vrekoussis, M., Kanakidou, M.,…Zhang, Y. (2024). The effect of cross-regional transport on ozone and particulate matter pollution in China: A review of methodology and current knowledge. *Science of the Total Environment*, *947*, 174196. https://doi.org/10.1016/j.scitotenv.2024.174196

Qu, Y., An, J., & Li, J. (2013). Synergistic impacts of anthropogenic and biogenic emissions on summer surface O3 in East Asia. *J Environ Sci (China)*, *25*(3), 520-530. https://doi.org/10.1016/s1001-0742(12)60069-2

Ran, L., Zhao, C., Geng, F., Tie, X., Tang, X., Peng, L.,…Guenther, A. (2009). Ozone photochemical production in urban Shanghai, China: Analysis based on ground level observations. *Journal of Geophysical Research: Atmospheres*, *114*(D15). https://doi.org/10.1029/2008jd010752

Ran, L., Zhao, C. S., Xu, W. Y., Lu, X. Q., Han, M., Lin, W. L.,…Chen, L. L. (2011). VOC reactivity and its effect on ozone production during the HaChi summer campaign. *Atmospheric Chemistry and Physics*, *11*(10), 4657-4667. https://doi.org/10.5194/acp-11-4657-2011

Rao, Z., Chen, Z., Liang, H., Huang, L., & Huang, D. (2016). Carbonyl compounds over urban Beijing: Concentrations on haze and non-haze days and effects on radical chemistry. *Atmospheric Environment*, *124*, 207-216. https://doi.org/10.1016/j.atmosenv.2015.06.050

Rosado-Reyes, C. M., & Francisco, J. S. (2007). Atmospheric oxidation pathways of propane and its by-products: Acetone, acetaldehyde, and propionaldehyde. *Journal of Geophysical Research: Atmospheres*, *112*(D14). https://doi.org/10.1029/2006jd007566

Rouvière, A., Brulfert, G., Baussand, P., & Chollet, J.-P. (2006). Monoterpene source emissions from Chamonix in the Alpine Valleys. *Atmospheric Environment*, *40*(19), 3613-3620. https://doi.org/10.1016/j.atmosenv.2005.09.058

Sander, S. P., Friedl, R. R., Golden, D. M., Kurylo, M. J., Moortgat, G. K., Wine, P. H.,…Keller-Rudek, H. (2006). *Chemical kinetics and photochemical data for use in atmospheric studies evaluation number 15*.

Saunders, S. M., Jenkin, M. E., Derwent, R. G., and Pilling, M. J. (2003). Protocol for the development of the Master Chemical Mechanism, MCM v3 (Part A): tropospheric degradation of non-aromatic volatile organic compounds. *Atmos. Chem. Phys.*, *3*(1), 161–180. https://doi.org/10.5194/acp-3-161-2003

Schnell, R. C., Oltmans, S. J., Neely, R. R., Endres, M. S., Molenar, J. V., & White, A. B. (2009). Rapid photochemical production of ozone at high concentrations in a rural site during winter. *Nature Geoscience*, *2*(2), 120-122. https://doi.org/10.1038/ngeo415

Seinfeld, J. H., & Pandis, S. N. (2016). *Atmospheric chemistry and physics: from air pollution to climate change*. John Wiley & Sons.

Shao, M., Lu, S., Liu, Y., Xie, X., Chang, C., Huang, S., & Chen, Z. (2009). Volatile organic compounds measured in summer in Beijing and their role in ground-level ozone formation. *Journal of Geophysical Research: Atmospheres*, *114*(D2). https://doi.org/10.1029/2008jd010863

Shao, P., An, J., Xin, J., Wu, F., Wang, J., Ji, D., & Wang, Y. (2016). Source apportionment of VOCs and the contribution to photochemical ozone formation during summer in the typical industrial area in the Yangtze River Delta, China. *Atmospheric Research*, *176-177*, 64-74. https://doi.org/10.1016/j.atmosres.2016.02.015

She, Y., Li, J., Lyu, X., Guo, H., Qin, M., Xie, X.,…Hu, J. (2024). Current status of model predictions of volatile organic compounds and impacts on surface ozone predictions during summer in China. *Atmospheric Chemistry and Physics*, *24*(1), 219-233. https://doi.org/10.5194/acp-24-219-2024

Shen, H., Liu, Y., Zhao, M., Li, J., Zhang, Y., Yang, J.,…Wang, W. (2021). Significance of carbonyl compounds to photochemical ozone formation in a coastal city (Shantou) in eastern China. *Science of the Total Environment*, *764*, 144031. https://doi.org/10.1016/j.scitotenv.2020.144031

Shen, L., Diao, Y., Zhao, T., Gu, X., & Shi, S. S. (2024). Meteorological influence on persistent O3 pollution events in Wuxi in the Yangtze River Delta, China. *Science of the Total Environment*, *917*, 170484. https://doi.org/10.1016/j.scitotenv.2024.170484

Shu, L., Wang, T., Han, H., Xie, M., Chen, P., Li, M., & Wu, H. (2020). Summertime ozone pollution in the Yangtze River Delta of eastern China during 2013-2017: Synoptic impacts and source apportionment. *Environmental Pollution*, *257*, 113631. https://doi.org/10.1016/j.envpol.2019.113631

Simon, H., Reff, A., Wells, B., Xing, J., & Frank, N. (2015). Ozone trends across the United States over a period of decreasing NOx and VOC emissions. *Environmental Science and Technology*, *49(1)*, 186-195.

Simpson, D., Arneth, A., Mills, G., Solberg, S., & Uddling, J. (2014). Ozone — the persistent menace: interactions with the N cycle and climate change. *Current Opinion in Environmental Sustainability*, *9-10*, 9-19. https://doi.org/10.1016/j.cosust.2014.07.008

Simpson, I. J., Blake, N. J., Barletta, B., Diskin, G. S., Fuelberg, H. E., Gorham, K.,…Blake, D. R. (2010). Characterization of trace gases measured over Alberta oil sands mining operations: 76 speciated C2-C10 volatile organic compounds (VOCs), CO2, CH4, CO, NO, NO2, NOy, O3 and SO2. *Atmospheric Chemistry and Physics*, *10*, 11931−11954.

Singh, A., Sarin, S. M., Shanmugam, P., Sharma, N., Attri, A. K., & Jain, V. K. (1997). Ozone distribution in the urban environment of Delhi during winter months,

Atmospheric Environment. *Atmospheric Environment*, *31*(20), 3421-3427. https://doi.org/10.1016/S1352-2310(97)00138-6

Slater, E. J., Whalley, L. K., Woodward-Massey, R., Ye, C., Lee, J. D., Squires, F.,…Heard, D. E. (2020). Elevated levels of OH observed in haze events during wintertime in central Beijing. *Atmospheric Chemistry and Physics*, *20*(23), 14847-14871. https://doi.org/10.5194/acp-20-14847-2020

Soares, A. R., & Silva, C. (2022). Review of Ground-Level Ozone Impact in Respiratory Health Deterioration for the Past Two Decades. *Atmosphere*, *13*(3). https://doi.org/10.3390/atmos13030434

Song, H., Zou, Q., & Lu, K. (2021). Parameterization and Application of Hydroperoxyl Radicals(HO₂) Heterogeneous Uptake Coefficient. *Progress in Chemistry*, *33*(7), 1175-1187. https://doi.org/10.7536/PC200749

Song, M., Tan, Q., Feng, M., Qu, Y., Liu, X., An, J., & Zhang, Y. (2018). Source Apportionment and Secondary Transformation of Atmospheric Nonmethane Hydrocarbons in Chengdu, Southwest China. *Journal of Geophysical Research: Atmospheres*, *123*(17), 9741-9763. https://doi.org/10.1029/2018jd028479

Steiner, A. L., Davis, A. J., Sillman, S., Owen, R. C., Michalak, A. M., & Fiore, A. M. (2010). Observed suppression of ozone formation at extremely high temperatures due to chemical and biophysical feedbacks. *Proc Natl Acad Sci U S A*, *107*(46), 19685-19690. https://doi.org/10.1073/pnas.1008336107

Steinfeld, J. I. (1998). Atmospheric Chemistry and Physics: From Air Pollution to Climate Change. *Environment: Science and Policy for Sustainable Development*, *40*(7), 26-26. https://doi.org/10.1080/00139157.1999.10544295

Stockwell, W. R., Kirchner, F., Kuhn, M., & Seefeld, S. (1997). A new mechanism for regional atmospheric chemistry modeling. *Journal of Geophysical Research: Atmospheres*, *102*, 25847-25879.

Su, H., Cheng, Y. F., Cheng, P., Zhang, Y. H., Dong, S., Zeng, L. M.,…Wiedensohler, A. (2008). Observation of nighttime nitrous acid (HONO) formation at a non-urban site during PRIDE-PRD2004 in China. *Atmospheric Environment*, *42*(25), 6219-6232. https://doi.org/10.1016/j.atmosenv.2008.04.006

Sun, J., He, Y., Ning, Y., Xue, Z., Wang, H., Zhang, Y.,…Chai, F. (2023). Pollution characteristics and sources of carbonyl compounds in a typical city of Fenwei Plain, Linfen, in summer. *Environmental Pollution*, *320*, 120913. https://doi.org/10.1016/j.envpol.2022.120913

Sun, J., Shen, Z., Zhang, Y., Dai, W., He, K., Xu, H.,…Cao, J. (2020). Profiles and Source Apportionment of Nonmethane Volatile Organic Compounds in Winter and Summer in Xi'an, China, based on the Hybrid Environmental Receptor Model. *Advances in Atmospheric Sciences*, *38*(1), 116-131. https://doi.org/10.1007/s00376-020-0153-0

Ta, W. Q., Wang, T., Xiao, H. L., Zhu, X. Y., & Xiao, Z. (2004). Gaseous and particulate air pollution in the Lanzhou Valley, China. *Science of the Total Environment*, *320*(2-3), 163-176. https://doi.org/10.1016/j.scitotenv.2003.08.026

Tan, Z., Hofzumahaus, A., Lu, K., Brown, S. S., Holland, F., Huey, L. G.,…Fuchs, H. (2020). No Evidence for a Significant Impact of Heterogeneous Chemistry on Radical Concentrations in the North China Plain in Summer 2014. *Environmental science & technology*, *54*(10), 5973-5979. https://doi.org/10.1021/acs.est.0c00525

Tan, Z., Lu, K., Jiang, M., Su, R., Wang, H., Lou, S.,…Zhang, Y. (2019). Daytime atmospheric oxidation capacity in four Chinese megacities during the photochemically polluted season: a case study based on box model simulation. *Atmospheric Chemistry and Physics*, *19*(6), 3493-3513. https://doi.org/10.5194/acp-19-3493-2019

Tan, Z., Rohrer, F., Lu, K., Ma, X., Bohn, B., Broch, S.,…Zhang, Y. (2018). Wintertime photochemistry in Beijing: observations of ROx radical concentrations in the North China Plain during the BEST-ONE campaign. *Atmospheric Chemistry and Physics*, *18*(16), 12391-12411. https://doi.org/10.5194/acp-18-12391-2018

Tan, Z. F., Lu, K. D., Jiang, M. Q., Su, R., Dong, H. B., Zeng, L. M.,…Zhang, Y. H. (2018). Exploring ozone pollution in Chengdu, southwestern China: A case study from radical chemistry to O-3-VOC-NOx sensitivity. *Science of the Total Environment*, *636*, 775-786. https://doi.org/10.1016/j.scitotenv.2018.04.286

Tang, X. Y., Tian, B. S., Chen, C. H., & Reng, Z. H. (1985). A study of photochemical smog pollution and its control at the Xigu district in Lanzhou city. *Chinese Journal of Environmental Science*, *5*, 1-11.

Tong, L., Zhang, H., Yu, J., He, M., Xu, N., Zhang, J.,…Xiao, H. (2017). Characteristics of surface ozone and nitrogen oxides at urban, suburban and rural sites in Ningbo, China. *Atmospheric Research*, *187*, 57-68. https://doi.org/10.1016/j.atmosres.2016.12.006

Tsai, D. H., Wang, J. L., Wang, C. H., & Chan, C. C. (2008). A study of ground-level ozone pollution, ozone precursors and subtropical meteorological conditions in central Taiwan. *J Environ Monit*, *10*(1), 109-118. https://doi.org/10.1039/b714479b

USEPA. (2017). *Positive Matrix Factorization Model for environmental data analyses*. https://doi.org/https://www.epa.gov/air-research/positive-matrix-factorization-model-environmental-data-analyses

Wang, C., Huang, X.-F., Han, Y., Zhu, B., & He, L.-Y. (2017). Sources and Potential Photochemical Roles of Formaldehyde in an Urban Atmosphere in South China. *Journal of Geophysical Research: Atmospheres*, *122*(21), 11,934-911,947. https://doi.org/10.1002/2017jd027266

Wang, F., Ho, S. S. H., Man, C. L., Qu, L., Wang, Z., Ning, Z., & Ho, K. F. (2024). Characteristics and sources of oxygenated VOCs in Hong Kong: Implications for ozone formation. *Science of the Total Environment*, *912*, 169156. https://doi.org/10.1016/j.scitotenv.2023.169156

Wang, G. Y., Jia, S. M., Li, R. H., Ma, S. R., Chen, X. F., Wu, Z. J.,…Niu, X. L. (2020). Seasonal variation characteristics of hydroxyl radical pollution and its potential formation mechanism during the daytime in Lanzhou. *Journal of Environmental Sciences*, *95*, 58-64. https://doi.org/10.1016/j.jes.2020.03.045

Wang, H., Ma, X., Tan, Z., Wang, H., Chen, X., Chen, S.,…Zhang, Y. (2022). Anthropogenic monoterpenes aggravating ozone pollution. *Natl Sci Rev*, *9*(9), nwac103. https://doi.org/10.1093/nsr/nwac103

Wang, M., Chen, W., Shao, M., Lu, S., Zeng, L., & Hu, M. (2015). Investigation of carbonyl compound sources at a rural site in the Yangtze River Delta region of China. *J Environ Sci (China)*, *28*, 128-136. https://doi.org/10.1016/j.jes.2014.12.001

Wang, M., Chen, X., Jiang, Z., He, T. L., Jones, D., Liu, J., & Shen, Y. (2024). Meteorological and anthropogenic drivers of surface ozone change in the North China Plain in 2015-2021. *Science of the Total Environment*, *906*, 167763. https://doi.org/10.1016/j.scitotenv.2023.167763

Wang, N., Ling, Z. H., Deng, X. J., Deng, T., Lyu, X. P., Li, T. Y.,…Chen, X. (2018). Source Contributions to PM2.5 under Unfavorable Weather Conditions in Guangzhou City, China. *Advances in Atmospheric Sciences*, *35*(9), 1145-1159. https://doi.org/10.1007/s00376-018-7212-9

Wang, P., Wang, T., & Ying, Q. (2020). Regional source apportionment of summertime ozone and its precursors in the megacities of Beijing and Shanghai using a source-oriented chemical transport model. *Atmospheric Environment*, *224*. https://doi.org/10.1016/j.atmosenv.2020.117337

Wang, S. W., Zhang, Q., Streets, D. G., He, K. B., Martin, R. V., Lamsal, L. N.,…Lu, Z. (2012). Growth in NOx emissions from power plants in China: bottom-up estimates and satellite observations. *Atmospheric Chemistry and Physics*, *12*(10), 4429-4447. https://doi.org/10.5194/acp-12-4429-2012

Wang, T., Xue, L. K., Brimblecombe, P., Lam, Y. F., Li, L., & Zhang, L. (2017). Ozone pollution in China: A review of concentrations, meteorological influences, chemical precursors, and effects. *Science of the Total Environment*, *575*, 1582-1596. https://doi.org/10.1016/j.scitotenv.2016.10.081

Wang, W., Fang, H., Zhang, Y., Ding, Y., Hua, F., Wu, T., & Yan, Y. (2023). Characterizing sources and ozone formations of summertime volatile organic compounds observed in a medium-sized city in Yangtze River Delta region. *Chemosphere*, *328*, 138609. https://doi.org/10.1016/j.chemosphere.2023.138609

Wang, W., Parrish, D. D., Wang, S., Bao, F., Ni, R., Li, X.,…Su, H. (2022). Long-term trend of ozone pollution in China during 2014–2020: distinct seasonal and spatial characteristics and ozone sensitivity. *Atmospheric Chemistry and Physics*, *22*(13), 8935-8949. https://doi.org/10.5194/acp-22-8935-2022

Wang, W., Yuan, B., Peng, Y., Su, H., Cheng, Y., Yang, S.,…Shao, M. (2022). Direct observations indicate photodegradable oxygenated volatile organic compounds (OVOCs) as larger contributors to radicals and ozone production in the atmosphere. *Atmospheric Chemistry and Physics*, *22*(6), 4117-4128. https://doi.org/10.5194/acp-22-4117-2022

Wang, X., Manning, W., Feng, Z., & Zhu, Y. (2007). Ground-level ozone in China: distribution and effects on crop yields. *Environmental Pollution*, *147*(2), 394-400. https://doi.org/10.1016/j.envpol.2006.05.006

Wang, X., Wang, H., Xue, L., Wang, T., Wang, L., Gu, R.,…Wang, W. (2017). Observations of N 2 O 5 and ClNO 2 at a polluted urban surface site in North China: High N 2 O 5 uptake coefficients and low ClNO 2 product yields. *Atmospheric Environment*, *156*, 125-134. https://doi.org/10.1016/j.atmosenv.2017.02.035

Wang, Y., Guo, H., Lyu, X. P., Zhang, L. Y., Zeren, Y. Z., Zou, S. C., & Ling, Z. H. (2019). Photochemical evolution of continental airmasses and their influence on ozone formation over the South China Sea. *Science of the Total Environment*, *673*, 424-434. https://doi.org/10.1016/j.scitotenv.2019.04.075

Wang, Y., Guo, H., Zou, S. C., Lyu, X. P., Ling, Z. H., Cheng, H. R., & Zeren, Y. Z. (2018). Surface O-3 photochemistry over the South China Sea: Application of a near-explicit chemical mechanism box model. *Environmental Pollution*, *234*, 155-166. https://doi.org/10.1016/j.envpol.2017.11.001

Wang, Y., Liu, T., Gong, D., Wang, H., Guo, H., Liao, M.,…Wang, B. (2023). Anthropogenic Pollutants Induce Changes in Peroxyacetyl Nitrate Formation Intensity and Pathways in a Mountainous Background Atmosphere in Southern China. *Environ Sci Technol*, *57*(15), 6253-6262. https://doi.org/10.1021/acs.est.2c02845

Wang, Y., Wang, H., Guo, H., Lyu, X. P., Cheng, H. R., Ling, Z. H.,…Blake, D. R. (2017). Long-term O-3-precursor relationships in Hong Kong: field observation and model simulation. *Atmospheric Chemistry and Physics*, *17*(18), 10919-10935. https://doi.org/10.5194/acp-17-10919-2017

Wang, Y., Yang, X., Wu, K., Mei, H., De Smedt, I., Wang, S.,…He, C. (2022). Long-term trends of ozone and precursors from 2013 to 2020 in a megacity (Chengdu), China: Evidence of changing emissions and chemistry. *Atmospheric Research*, *278*. https://doi.org/10.1016/j.atmosres.2022.106309

Wang, Z. B., Li, J. X., & Liang, L. W. (2020). Spatio-temporal evolution of ozone pollution and its influencing factors in the Beijing-Tianjin-Hebei Urban Agglomeration. *Environmental Pollution*, *256*, 113419. https://doi.org/10.1016/j.envpol.2019.113419

Weng, X., Forster, G. L., & Nowack, P. (2022). A machine learning approach to quantify meteorological drivers of ozone pollution in China from 2015 to 2019. *Atmospheric Chemistry and Physics*, *22*(12), 8385-8402. https://doi.org/10.5194/acp-22-8385-2022

Whaley, C. H., Strong, K., Jones, D. B. A., Walker, T. W., Jiang, Z., Henze, D. K.,…Fogal, P. F. (2015). Toronto area ozone: Long-term measurements and modeled sources of poor air quality events. *Journal of Geophysical Research: Atmospheres*, *120*(21). https://doi.org/10.1002/2014jd022984

Wolfe, G. M., Kaiser, J., Hanisco, T. F., Keutsch, F. N., de Gouw, J. A., Gilman, J. B.,…Warneke, C. (2016). Formaldehyde production from isoprene oxidation across NOx regimes. *Atmospheric Chemistry and Physics*, *16*(4), 2597-2610. https://doi.org/10.5194/acp-16-2597-2016

Worden, H. M., Bowman, K. W., Worden, J. R., Eldering, A., & Beer, R. (2008). Satellite measurements of the clear-sky greenhouse effect from tropospheric ozone. *Nature Geoscience*, *1*(5), 305-308. https://doi.org/10.1038/ngeo182

Wu, K., Wang, Y., Qiao, Y., Liu, Y., Wang, S., Yang, X.,…Lei, Y. (2022). Drivers of 2013-2020 ozone trends in the Sichuan Basin, China: Impacts of meteorology and precursor emission changes. *Environmental Pollution*, *300*, 118914. https://doi.org/10.1016/j.envpol.2022.118914

Wu, W., Xue, W., Lei, Y., & Wang, J. (2018). Sensitivity analysis of ozone in Beijing-Tianjin-Hebei (BTH) and its surrounding area using OMI satellite remote sensing data. *China Environmental Science*, *38(4)*, 1201-1208.

Wu, Y., Huo, J., Yang, G., Wang, Y., Wang, L., Wu, S.,…Wang, L. (2023). Measurement report: Production and loss of atmospheric formaldehyde at a suburban site of Shanghai in summertime. *Atmospheric Chemistry and Physics*, *23*(5), 2997-3014. https://doi.org/10.5194/acp-23-2997-2023

Wu, Y. L. (2019). *Characteristics and source apportionment of VOCs pollution in Lanzhou City* Lanzhou University].

Xu, J., Huang, X., Wang, N., Li, Y., & Ding, A. (2021). Understanding ozone pollution in the Yangtze River Delta of eastern China from the perspective of diurnal cycles. *Science of the Total Environment*, *752*, 141928. https://doi.org/10.1016/j.scitotenv.2020.141928

Xu, X., Zhang, H., Lin, W., Wang, Y., Xu, W., & Jia, S. (2018). First simultaneous measurements of peroxyacetyl nitrate (PAN) and ozone at Nam Co in the central Tibetan Plateau: impacts from the PBL evolution and transport processes. *Atmospheric Chemistry and Physics*, *18*(7), 5199-5217. https://doi.org/10.5194/acp-18-5199-2018

Xu, Y., Feng, X., Chen, Y., Zheng, P., Hui, L., Chen, Y.,…Wang, Z. (2023). Development of an enhanced method for atmospheric carbonyls and characterizing their roles in photochemistry in subtropical Hong Kong. *Science of the Total Environment*, *896*, 165135. https://doi.org/10.1016/j.scitotenv.2023.165135

Xu, Z., Zou, Q., Jin, L., Shen, Y., Shen, J., Xu, B.,…Wang, Z. (2023). Characteristics and sources of ambient Volatile Organic Compounds (VOCs) at a regional background site, YRD region, China: Significant influence of solvent evaporation during hot months. *Science of the Total Environment*, *857*(Pt 3), 159674. https://doi.org/10.1016/j.scitotenv.2022.159674

Xue, L. K., Gu, R. R., Wang, T., Wang, X. F., Saunders, S., Blake, D.,…Wang, W. X. (2016). Oxidative capacity and radical chemistry in the polluted atmosphere of Hong Kong and Pearl River Delta region: analysis of a severe photochemical smog episode. *Atmospheric Chemistry and Physics*, *16*(15), 9891-9903. https://doi.org/10.5194/acp-16-9891-2016

Xue, L. K., Wang, T., Gao, J., Ding, A. J., Zhou, X. H., Blake, D. R.,…Wang, W. X. (2014). Ground-level ozone in four Chinese cities: precursors, regional transport and heterogeneous processes. *Atmospheric Chemistry and Physics*, *14*(23), 13175-13188. https://doi.org/10.5194/acp-14-13175-2014

Xue, L. K., Wang, T., Louie, P. K. K., Luk, C. W. Y., Blake, D. R., & Xu, Z. (2014). Increasing External Effects Negate Local Efforts to Control Ozone Air Pollution: A Case Study of Hong Kong and Implications for Other Chinese Cities. *Environmental science & technology*, *48*(18), 10769-10775. https://doi.org/10.1021/es503278g

Yan, C., Wang, L., & Zhang, Q. (2021). Study on Coupled Relationship between Urban Air Quality and Land Use in Lanzhou, China. *Sustainability*, *13*(14). https://doi.org/10.3390/su13147724

Yan, D., Jin, Z., Zhou, Y., Li, M., Zhang, Z., Wang, T.,…Xie, M. (2024). Anthropogenically and meteorologically modulated summertime ozone trends and their health implications since China's clean air actions. *Environmental Pollution*, *343*, 123234. https://doi.org/10.1016/j.envpol.2023.123234

Yang, G., Liu, Y., & Li, X. (2020). Spatiotemporal distribution of ground-level ozone in China at a city level. *Sci Rep*, *10*(1), 7229. https://doi.org/10.1038/s41598-020-64111-3

Yang, J., Zeren, Y., Guo, H., Wang, Y., Lyu, X., Zhou, B.,…Zhang, G. (2024). Wintertime ozone surges: The critical role of alkene ozonolysis. *Environ Sci Ecotechnol*, *22*, 100477. https://doi.org/10.1016/j.ese.2024.100477

Yang, L., Luo, H., Yuan, Z., Zheng, J., Huang, Z., Li, C.,…Bian, Y. (2019). Quantitative impacts of meteorology and precursor emission changes on the long-term trend of ambient ozone over the Pearl River Delta, China, and implications for ozone control strategy. *Atmospheric Chemistry and Physics*, *19*(20), 12901-12916. https://doi.org/10.5194/acp-19-12901-2019

Yang, X., Lu, K., Ma, X., Gao, Y., Tan, Z., Wang, H.,…Zhang, Y. (2022). Radical chemistry in the Pearl River Delta: observations and modeling of OH and HO2 radicals in Shenzhen in 2018. *Atmospheric Chemistry and Physics*, *22*(18), 12525-12542. https://doi.org/10.5194/acp-22-12525-2022

Yang, X., Xue, L., Wang, T., Wang, X., Gao, J., Lee, S.,…Wang, W. (2018). Observations and Explicit Modeling of Summertime Carbonyl Formation in Beijing: Identification of Key Precursor Species and Their Impact on Atmospheric Oxidation Chemistry. *Journal of Geophysical Research: Atmospheres*, *123*(2), 1426-1440. https://doi.org/10.1002/2017jd027403

Yang, X., Xue, L., Yao, L., Li, Q., Wen, L., Zhu, Y.,…Wang, W. (2017). Carbonyl compounds at Mount Tai in the North China Plain: Characteristics, sources, and effects on ozone formation. *Atmospheric Research*, *196*, 53-61. https://doi.org/10.1016/j.atmosres.2017.06.005

Yang, X., Zhang, G., Hu, S., Wang, J., Zhang, P., Zhong, X., & Song, H. (2023). Summertime carbonyl compounds in an urban area in the North China Plain: Identification of sources, key precursors and their contribution to O(3) formation. *Environmental Pollution*, *331*(Pt 2), 121908. https://doi.org/10.1016/j.envpol.2023.121908

Yang, X., Zhang, G., Sun, Y., Zhu, L., Wei, X., Li, Z., & Zhong, X. (2020). Explicit modeling of background HCHO formation in southern China. *Atmospheric Research*, *240*. https://doi.org/10.1016/j.atmosres.2020.104941

Yang, Z., Cheng, H. R., Wang, Z. W., Peng, J., Zhu, J. X., Lyu, X. P., & Guo, H. (2019). Chemical characteristics of atmospheric carbonyl compounds and source identification of formaldehyde in Wuhan, Central China. *Atmospheric Research*, *228*, 95-106. https://doi.org/10.1016/j.atmosres.2019.05.020

Yarwood, G., Jung, J., Whitten, G. Z., Heo, G., Mellberg, J., & Estes, M. (2010). *Updates to the Carbon Bond mechanism for version 6 (CB6)* 9th Annual CMAS Conference, Chapel Hill, NC.,

Yarwood, G., & Rao, S. (2005). *Updates to the Carbon Bond Chemical Mechanism: CB05(Final report)*.

Yarwood, G., Whitten, G. Z., & Rao, S. (2005). Updates to the Carbon Bond 4 photochemical mechanism. *Environ. Int. Corp*, 565.

Yin, J., Gao, C. Y., Hong, J., Gao, Z., Li, Y., Li, X.,…Zhu, B. (2019). Surface Meteorological Conditions and Boundary Layer Height Variations During an Air Pollution Episode in Nanjing, China. *Journal of Geophysical Research: Atmospheres*, *124*(6), 3350-3364. https://doi.org/10.1029/2018jd029848

Yuan, B., Shao, M., de Gouw, J., Parrish, D. D., Lu, S., Wang, M.,…Hu, M. (2012). Volatile organic compounds (VOCs) in urban air: How chemistry affects the interpretation of positive matrix factorization (PMF) analysis. *Journal of Geophysical Research: Atmospheres*, *117*(D24). https://doi.org/10.1029/2012jd018236

Yuan, Q., Zhang, Z., Chen, Y., Hui, L., Wang, M., Xia, M.,…Lee, S. (2024). Origin and transformation of volatile organic compounds at a regional background site in Hong Kong: Varied photochemical processes from different source regions. *Science of the Total Environment*, *908*, 168316. https://doi.org/10.1016/j.scitotenv.2023.168316

Zeng, L. W., Yang, J., Guo, H., & Lyu, X. P. (2022). Impact of NO(x)reduction on long-term surface ozone pollution in roadside and suburban Hong Kong: Field measurements and model simulations. *Chemosphere*, *302*. https://doi.org/ARTN 134816

10.1016/j.chemosphere.2022.134816

Zeng, P., Lyu, X., Guo, H., Cheng, H., Wang, Z., Liu, X., & Zhang, W. (2019). Spatial variation of sources and photochemistry of formaldehyde in Wuhan, Central China. *Atmospheric Environment*, *214*. https://doi.org/10.1016/j.atmosenv.2019.116826

Zeng, P., Lyu, X. P., Guo, H., Cheng, H. R., Jiang, F., Pan, W. Z.,…Hu, Y. Q. (2018). Causes of ozone pollution in summer in Wuhan, Central China. *Environmental Pollution*, *241*, 852-861. https://doi.org/10.1016/j.envpol.2018.05.042

Zeng, P., Lyu, X. P., Guo, H., Cheng, H. R., Wang, Z. W., Liu, X. F., & Zhang, W. H. (2019). Spatial variation of sources and photochemistry, of formaldehyde in Wuhan, Central China. *Atmospheric Environment*, *214*. https://doi.org/ARTN 116826

10.1016/j.atmosenv.2019.116826

Zhan, J., Ma, W., Song, B., Wang, Z., Bao, X., Xie, H. B.,…Liu, Y. (2023). The contribution of industrial emissions to ozone pollution: identified using ozone formation path tracing approach. *NPJ Clim Atmos Sci*, *6*(1), 37. https://doi.org/10.1038/s41612-023-00366-7

Zhang, H., Wang, Y., Hu, J., Ying, Q., & Hu, X. M. (2015). Relationships between meteorological parameters and criteria air pollutants in three megacities in China. *Environmental Research*, *140*, 242-254. https://doi.org/10.1016/j.envres.2015.04.004

Zhang, J. J., Wei, Y., & Fang, Z. (2019). Ozone Pollution: A Major Health Hazard Worldwide. *Front Immunol*, *10*, 2518. https://doi.org/10.3389/fimmu.2019.02518

Zhang, K., Duan, Y., Huo, J., Huang, L., Wang, Y., Fu, Q.,…Li, L. (2021). Formation mechanism of HCHO pollution in the suburban Yangtze River Delta region, China: A box model study and policy implementations. *Atmospheric Environment*, *267*. https://doi.org/10.1016/j.atmosenv.2021.118755

Zhang, L., Wang, L., Ji, D., Xia, Z., Nan, P., Zhang, J.,…Hu, B. (2024). Explainable ensemble machine learning revealing the effect of meteorology and sources on ozone formation in megacity Hangzhou, China. *Science of the Total Environment*, *922*, 171295. https://doi.org/10.1016/j.scitotenv.2024.171295

Zhang, L., Wang, L., Liu, B., Tang, G., Liu, B., Li, X.,…Hu, B. (2023). Contrasting effects of clean air actions on surface ozone concentrations in different regions over Beijing from May to September 2013-2020. *Science of the Total Environment*, *903*, 166182. https://doi.org/10.1016/j.scitotenv.2023.166182

Zhang, Q., Yuan, B., Shao, M., Wang, X., Lu, S., Lu, K.,…Liu, S. C. (2014). Variations of ground-level O3 and its precursors in Beijing in summertime between 2005 and 2011. *Atmospheric Chemistry and Physics*, *14*(12), 6089-6101. https://doi.org/10.5194/acp-14-6089-2014

Zhang, W., Tong, S., Ge, M., An, J., Shi, Z., Hou, S.,…He, H. (2019). Variations and sources of nitrous acid (HONO) during a severe pollution episode in Beijing in winter 2016. *Science of the Total Environment*, *648*, 253-262. https://doi.org/10.1016/j.scitotenv.2018.08.133

Zhang, X., Tong, S., Jia, C., Zhang, W., Li, J., Wang, W.,…Ge, M. (2022). The Levels and Sources of Nitrous Acid (HONO) in Winter of Beijing and Sanmenxia. *Journal of Geophysical Research: Atmospheres*, *127*(10). https://doi.org/10.1029/2021jd036278

Zhang, X., Wu, Z., He, Z., Zhong, X., Bi, F., Li, Y.,…Wang, W. (2022). Spatiotemporal patterns and ozone sensitivity of gaseous carbonyls at eleven urban sites in southeastern China. *Science of the Total Environment*, *824*, 153719. https://doi.org/10.1016/j.scitotenv.2022.153719

Zhang, Y., Xue, L., Dong, C., Wang, T., Mellouki, A., Zhang, Q., & Wang, W. (2019). Gaseous carbonyls in China's atmosphere: Tempo-spatial distributions, sources, photochemical formation, and impact on air quality. *Atmospheric Environment*, *214*. https://doi.org/10.1016/j.atmosenv.2019.116863

Zhang, Z., Sun, Y., & Li, J. (2023). Characteristics and sources of VOCs in a coastal city in eastern China and the implications in secondary organic aerosol and O(3) formation. *Science of the Total Environment*, *887*, 164117. https://doi.org/10.1016/j.scitotenv.2023.164117

Zhang, Z., Wang, S., Wang, P., Zhu, S., Zhang, H., & Wang, S. (2024). Regional transport dominates air pollution events in all seasons in Beijing in 2020. *Atmospheric Environment*, *323*. https://doi.org/10.1016/j.atmosenv.2024.120395

Zhao, S., Yin, D., Yu, Y., Kang, S., Qin, D., & Dong, L. (2020). PM(2.5) and O(3) pollution during 2015-2019 over 367 Chinese cities: Spatiotemporal variations, meteorological and topographical impacts. *Environmental Pollution*, *264*, 114694. https://doi.org/10.1016/j.envpol.2020.114694

Zhao, S., Yu, Y., Li, J., Yin, D., Qi, S., & Qin, D. (2021). Response of particle number concentrations to the clean air action plan: lessons from the first long-term aerosol measurements in a typical urban valley in western China. *Atmospheric Chemistry and Physics*, *21*(19), 14959-14981. https://doi.org/10.5194/acp-21-14959-2021

Zheng, B., Tong, D., Li, M., Liu, F., Hong, C., Geng, G.,…Zhang, Q. (2018). Trends in China's anthropogenic emissions since 2010 as the consequence of clean air actions. *Atmospheric Chemistry and Physics*, *18*(19), 14095-14111. https://doi.org/10.5194/acp-18-14095-2018

Zheng, H., Kong, S., Seo, J., Yan, Y., Cheng, Y., Yao, L.,…Harrison, R. M. (2024). Achievements and challenges in improving air quality in China: Analysis of the long-term trends from 2014 to 2022. *Environ Int*, *183*, 108361. https://doi.org/10.1016/j.envint.2023.108361

Zheng, H., Kong, S., Xing, X., Mao, Y., Hu, T., Ding, Y.,…Qi, S. (2018). Monitoring of volatile organic compounds (VOCs) from an oil and gas station in northwest China for 1 year. *Atmospheric Chemistry and Physics*, *18*(7), 4567-4595. https://doi.org/10.5194/acp-18-4567-2018

Zheng, J., Zhong, L., Wang, T., Louie, P. K. K., & Li, Z. (2010). Ground-level ozone in the Pearl River Delta region: Analysis of data from a recently established regional air quality monitoring network. *Atmospheric Environment*, *44*(6), 814-823. https://doi.org/10.1016/j.atmosenv.2009.11.032

Zhou, X., Li, Z. Q., Zhang, T. J., Wang, F., Wang, F. T., Tao, Y.,…Huang, J. (2019). Volatile organic compounds in a typical petrochemical industrialized valley city of northwest China based on high-resolution PTR-MS measurements: Characterization, sources and chemical effects. *Science of the Total Environment*, *671*, 883-896. https://doi.org/10.1016/j.scitotenv.2019.03.283

Zhu, J., Wang, S., Wang, H., Jing, S., Lou, S., Saiz-Lopez, A., & Zhou, B. (2020). Observationally constrained modeling of atmospheric oxidation capacity and photochemical reactivity in Shanghai, China. *Atmospheric Chemistry and Physics*, *20*(3), 1217-1232. https://doi.org/10.5194/acp-20-1217-2020

Zhu, J. X., Cheng, H. R., Peng, J., Zeng, P., Wang, Z. W., Lyu, X. P., & Guo, H. (2020). O-3 photochemistry on O-3 episode days and non-O-3 episode days in Wuhan, Central China. *Atmospheric Environment*, *223*. https://doi.org/ARTN 117236